5-7-2016

Modifications To The Benzophenoxazine Architecture: Synthesis And Characterization

Vincent Martinez
vmartinez3@gsu.edu

MODIFICATIONS TO THE BENZOPHENOXAZINE ARCHITECTURE: SYNTHESIS AND CHARACTERIZATION

by

VINCENT JOHN MARTINEZ

Under the Direction of Professor Maged Henary

ABSTRACT

Nile red and Nile blue are intensely colored fluorescent dyes from the benzophenoxazine family. Modification of the donor amine with varying alkyl substituents was achieved with the principle aim being to investigate differences, both optical and physical, between dye scaffolds outfitted with secondary amines versus tertiary amines. These changes to the dyes' architectural framework gave holistic effects to the bulk molecule by modulating hydrophobicity, optical properties, and protein binding constants to human serum albumin.

INDEX WORDS: Benzophenoxazine, Dye, Nile red, Nile blue, Synthesis

MODIFICATIONS TO THE BENZOPHENOXAZINE ARCHITECTURE: SYNTHESIS AND CHARACTERIZATION

by

VINCENT JOHN MARTINEZ

A Thesis Submitted in Partial Fulfillment of the Requirements for the Degree of

Masters in Science

in the College of Arts and Sciences

Georgia State University

2016

MODIFICATIONS TO THE BENZOPHENOXAZINE ARCHITECTURE: SYNTHESIS AND CHARACTERIZATION

by

VINCENT JOHN MARTINEZ

Committee Chair: Maged Henary, PhD

Committee: Maged Henary, PhD

Peng Wang, PhD

Donald Hamelberg, PhD

Electronic Version Approved:

Office of Graduate Studies

College of Arts and Sciences

Georgia State University

May 2016

DEDICATION

I would like to dedicate this manuscript to my mother, Gara Martinez. I would not be where I am without her.

ACKNOWLEDGEMENTS

There have been so many people that have enabled me to pursue graduate training and that have helped me to resolve problems and focus my ideas. I would like to acknowledge my P.I., Dr. Maged Henary, for believing in my talent and for giving my research a direction. I would like to extend my personal thanks to our group's post-doctoral fellows both past and present, specifically Dr. Yunshan Wu and Dr. Konstantin Zyabrev. They were always very courteous and willing to extend a helping hand. Our team of talented graduate researchers has been an asset to my work. I would like to thank Eduardo Soriano, Carl Kananda, Matthew Laramie, Andrew Levitz, Eric Owens and Cory Holder for helping me to troubleshoot synthetic procedures or to debate mechanistic pathways. I would like to also thank our collaborators Eman Alsolmy and Dr. Gabor Patonay for doing excellent work and being great partners. The staff and faculty at Georgia State have been incredibly helpful. They have kindly taught and mentored me over the years. Lastly, I want to thank Amanda Mauldin for her patience. She has been instrumental in keeping me focused and her loving support has undoubtedly been essential to my success.

TABLE OF CONTENTS

ACKNOWLEDGEMENTS ..... **v**

LIST OF TABLES ..... **ix**

LIST OF FIGURES ..... **x**

1 INTRODUCTION **14**

1.1 Fluorescence Spectroscopy **15**

1.1.1 Fluorescence vs. Phosphorescence ***16***

1.1.2 Fluorescence Quenching ***18***

1.1.3 Resonance Energy Transfer ***19***

1.1.4 Fluorescence Anisotropy ***20***

1.1.5 Fluorescence Applications ***20***

1.2 Introduction to Nile Red and Nile blue Dyes **22**

1.3 Nomenclature of oxazines **23**

1.4 Photophysical Properties **24**

1.4.1 Solvatochromism ***26***

1.4.2 Thermochromism ***28***

1.4.3 FRET ***28***

1.4.4 Intersystem Crossing ***29***

1.5 Applications of Nile Red and Nile Blue **31**

1.5.1 Materials Science Applications ***31***

1.5.2 Biological Applications *33*

1.6 Synthesis of Nile Blue and Nile Red Analogues **37**

1.6.1 Dye Synthesis via a Nitroso intermediate *39*

1.6.2 Dye Synthesis via an Azo Intermediate *40*

1.6.3 Dye Derivatives with Conjugateable Groups *42*

1.6.4 Esters and Carboxylic Acids *43*

1.6.5 Primary Amines *45*

1.6.6 Azide-alkyne Huisgen Cycloaddition *48*

1.6.7 Halogenated *49*

1.6.8 Miscellaneous Syntheses *53*

1.7 Sensors **60**

1.7.1 Metal Sensors *60*

1.7.2 pH Sensors *61*

1.7.3 Biological Sensors *63*

2 SYNTHESIS, OPTICAL CHARACTERIZATION AND BINDING STUDIES OF NOVEL BENZO[A]PHENOXAZINE DYES **66**

2.1 Introduction **66**

2.2 Experimental Overview **68**

2.2.1 General *68*

2.2.2 Preparation of 3-amino-4-methylphenol *68*

2.2.3 Preparation of 3-(dialkylamino)phenols and 3-(alkylamino)phenols 69

2.2.4 Synthesis of nitrosylated intermediates 70

2.2.5 Synthesis of benzo[a]phenoxazinone and benzo[a]phenoxazinium perchlorate dyes 72

2.2.6 Spectroscopic studies of dyes 73

2.2.7 HSA binding interaction with Nile derivatives 74

2.3 Results and Discussion 76

2.3.1 Synthesis of Nile Red Analogues 84a-c and 85d-f. 76

2.3.2 Synthesis of Nile Blue Analogues 86a-f. 78

2.3.3 Proposed mechanism of dye formation. 79

2.3.4 Spectroscopic Properties of Nile red and Nile blue analogues. 80

3 CONCLUSIONS 92

4 EXPERIMENTAL 93

REFERENCES 103

APPENDICES 112

Appendix A — ^{1}H NMR, ^{13}C NMR, HRMS, and IR Spectra 112

LIST OF TABLES

Table 1.1 Photophysical properties of Nile blue analogues with differing chalcogen substitutions. 30

Table 1.2 Synthesis of benzo[*a*]phenoxazinium chlorides 65a-f by using the conventional heating method. 58

Table 1.3 Optimization reaction studies of nitrosophenol 27 with 1-amino-6-hydroxynaphthalene under microwave conditions 59

Table 1.4 Synthesis of benzo[*a*]phenoxazinium chlorides 65a-f by microwave irradiation at 90 °C. 59

Table 1.5 Reactions times and yields for the synthesis of dyes 66a-66g (Scheme 17) using conventional heating methods versus ultrasound (US). 60

Table 2.1 Optical properties of Nile red and Nile blue analogues 81

Table 2.2 HSA binding constants and clog*D* values of Nile red and Nile blue analogues. 91

LIST OF FIGURES

Figure 1.1— A Jablonski diagram showing the quantum processes related to the absorption and emission of photons..... 16

Figure 1.2 Structures of Nile red and Nile blue..... 23

Figure 1.3 Nomenclature of oxazines..... 24

Figure 1.4 A) Nile red in electronic ground state (planar); B) Nile red in in twisted excited state..... 26

Figure 1.5 Nile red conjugated to moiety with large TPA cross section. Excitation with 815 nm, 8 ns laser pulses gives near complete quenching of donor fluorescence with notable acceptor fluorescence..... 29

Figure 1.6 Benzo[*a*]phenoxazine analogues with different chalcogens substituted at the 7-position..... 30

Figure 1.7 Nile blue being reduced by alkaline phosphatase enzyme to yield a non-fluorescent product..... 35

Figure 1.8 Common postions for synthetic modification of Nile red and Nile blue. 38

Figure 1.9 General synthesis of Nile red and Nile blue analogues. 39

Figure 1.10 Synthesis of water soluble Nile blue analogues via arylazo intermediates. .. 42

Figure 1.11 Synthesis of bioconjugateable Nile red derivative with carboxylic acid handle. 44

Figure 1.12 Synthesis of amide coupled Nile red analogues to show proof of concept for bioconjugation. All dye—linker bonds are at the 2-position on Nile red. See Compound 19 on Figure 1.12 for complete structure of precursor. 45

Figure 1.13 Nile blue and Nile red analogues with primary amine handles attached to the chromophore via alkyl linkers at the 2- and 5-positions. 45

Figure 1.14 Synthesis of Nile blue analogues and labeling L-alanine, L-glycine, L-phenylalanine and L-glutamic acid (protected as methyl ester) with them. 46

Figure 1.15 Preparation of a Nile blue-IMC linked derivative with a hexanediamine linker. 47

Figure 1.16 Nile blue analogues with amide linked moieties. 48

Figure 1.17 Synthesis of propargylated Nile red and click to acpcPNA. 49

Figure 1.18 Synthesis of Nile red analogues with polyfluorinated ofefin substituent. 50

Figure 1.19 Synthesis of polyfluorinated Nile red analogues. 50

Figure 1.20 Synthesis of polyfluorinated Nile red analogues in higher yield. 51

Figure 1.21 Benzo[*a*]phenoxazinium chlorides with chlorinated terminals. 52

Figure 1.22 Synthesis of Nile red-based thiol sensors. A) Iodo sensor moiety is connected to 9-amino terminal via an ester linkage. B) Iodo sensor moiety is connected at 2-hydroxy position via an amide linkage. 53

Figure 1.23 Benzophenoxaziniums with julolidine moiety 54

Figure 1.24 Synthesis of Nile red FlAsH analogue. 55

Figure 1.25 Synthesis of Nile blue analogue with the oxygen replaced by selenium. 57

Figure 1.26 Benzo[*a*]phenoxazinium chlorides 65a-f synthesized via microwave irradiation. 58

Figure 1.27 Dyes prepared via sonication 60

Figure 1.28 Proposed mechanism for mercury-induced rearrangement. 61

Figure 1.29 Synthesis of Nile blue-based comonomer. 62

Figure 1.30 Synthesis of Nile blue morpholine (NBM) 64

Figure 1.31 Synthesis of hydrogen sulfide detecting benzo[a]phenoxazine systems..... 65

Figure 2.1 Nile blue and Nile red dyes; convenient positions for structural modification are at the 2-carbon and 9-amine. The 5-imine on Nile blue is also an option for modification. .. 67

Figure 2.2 Multi-route catalytic reduction of 4-methyl-3-nitrophenol to 3-amino-4-methylphenol..... 68

Figure 2.3 Synthesis of *N*-alkylated 3-aminophenols..... 69

Figure 2.4 Nitrosation of an *N*-alkylatedaminophenol. 70

Figure 2.5 Synthesis of Nile red and Nile blue derivatives 72

Figure 2.6 Proposed mechanism for the formation of Nile red via condensation of an aromatic nitroso compound with 1,6-dihydroxynaphthalene in catalytic amounts of acid. 79

Figure 2.7 A) Visible spectra of Nile red derivatives in 30 mM phosphate buffer. B) Visible spectra of NB derivatives in 30 mM phosphate buffer 83

Figure 2.8 Normalized absorbance and fluorescence of 86d in phosphate buffer..... 84

Figure 2.9 Fluorescence spectra of Nile red and Nile blue (5 μM) with HSA (5 μM) in 20 mM phosphate buffer pH = 7.2..... 85

Figure 2.10 Fluorescence spectra of Nile red derivatives (5 μM) with HSA (5 μM) in 20 mM phosphate buffer pH = 7.2..... 86

Figure 2.11 Fluorescence spectra of Nile blue derivatives (5 μM) with HSA (5 μM) in 20 mM phosphate buffer pH = 7.2..... 87

Figure 2.12 Binding interactions of Nile red derivatives observed with change in fluorescence vs. time. Binding interactions of Nile blue derivatives observed with change in fluorescence vs. time..... 88

Figure 2.13 Job's plots of 84b (A), 84c (B), 86b (C) and 86c (D) with HSA. Overall concentration is 4 μM in 20 mM phosphate buffer pH = 7.2. 89

1 INTRODUCTION

Color brings beauty to life. Everywhere we look, our eyes have evolved to see color. Whether it is the gorgeous shades of purple on a bougainvillea's flower or the striking red of a cardinal's plumage, color is ubiquitous in this world. But the utility of color is far deeper than pure aesthetics. Biologically, color is used as a signal. It can be a dire warning or a brash advertisement. The caterpillar of the monarch butterfly is a brilliant yellow, a caution to all birds who would dare to eat its poisonous flesh. The beautiful blue and iridescent feathers of the peacock are a signal to potential female mates that he is a male worthy of their attention. If one could see shorter wavelengths of light they would be privy to a world where flowers were not only beautiful but were tattooed with an array of ultraviolet runways. These are to attract bees much like the neon signs of the Vegas strip attract hordes of tourists and gamblers from across the desert vista.

A scientist might see color in a different light. Color is utility. Relationships have been devised that can use color to accurately measure a concentration of a chemical or to tag a biological molecule. What if a biologist wanted to clearly see an organelle deep in the interior of a cell? What if a surgeon wanted to visualize cancerous tissue for removal? What if an analytical chemist wanted to measure the amount of a toxic metal that was in a river or pond? Color can be generated and measured in all of these instances to offer relatively foolproof solutions to real world problems. The workhorse and primary tool for any chemist concerned with color is the dye.

A dye is simply any molecule that can absorb light. It can be differentiated from a pigment which is typically insoluble in most mediums and is of a much larger particle size. A dye can potentially undergo a number of different quantum processes when affected by light. It will always absorb light but some dyes can fluoresce or even phosphoresce. To the layman, the dif-

ference between these phenomena may seem subtle but that there is a complex array of quantum processes that result in these differing behaviors.

1.1 Fluorescence Spectroscopy

Fluorescence phenomena were first observed and documented by Sir Fredrich William Herschel in 1845. He was observing a solution of quinine and noticed that under "certain incidences of light" the solution gave off a "beautiful celestial blue color."[1] Since then, fluorescence has been studied extensively and is used in all facets of modern science and technology. There are biochemical applications of steady-state anisotropies, distance measuring using resonance energy transfer,[2] mutiphoton microscopy,[3] fluorescence sensing, DNA sequencing, fluorescence-lifetime imaging microscopy, single molecule detection, fluorescence correlation spectroscopy, and a plethora of other fluorescence dependent analytical techniques.

The best tool available for a qualitative description of fluorescence is the Jablonski diagram. The diagram (Figure 1.) clearly illustrates electron mobility between ground and excited energy states. It is most convenient for conveying all of the quantum processes responsible for observed optics. These include absorbance, fluorescence, and phosphorescence which are all dictated by excitation, relaxation, emission, internal conversion, phosphorescence, and intersystem crossing.

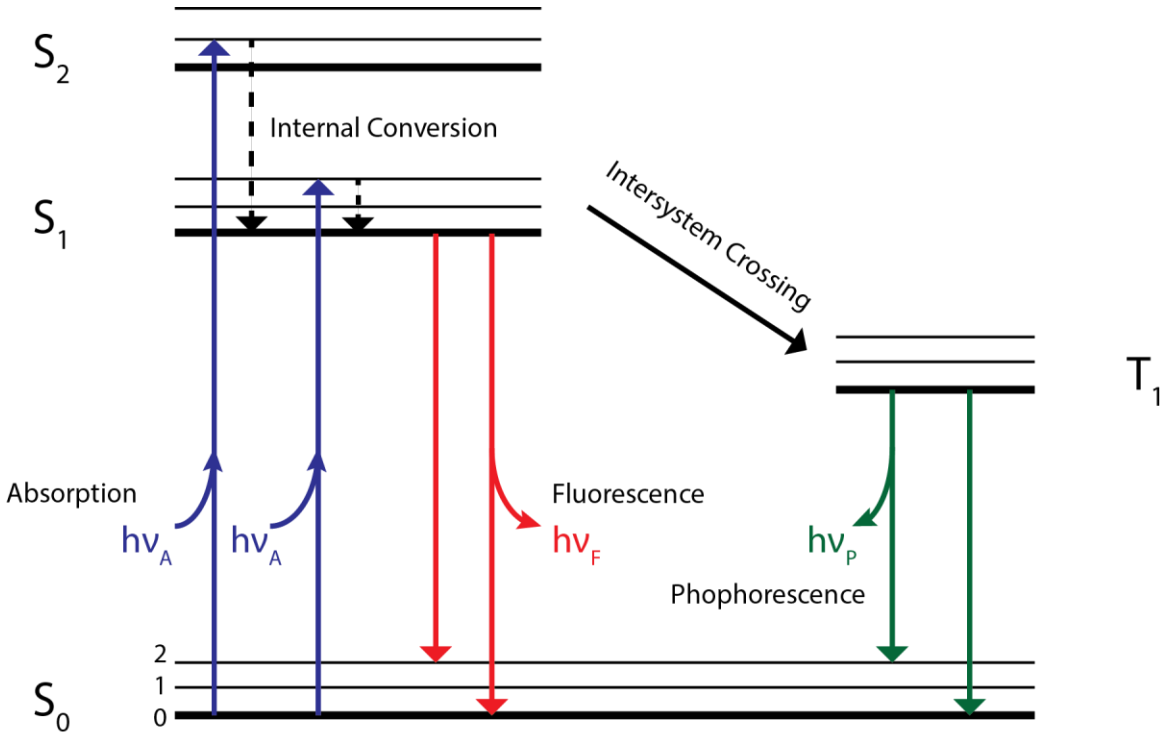

Figure 1.1— A Jablonski diagram showing the quantum processes related to the absorption and emission of photons

1.1.1 Fluorescence vs. Phosphorescence

Valence electrons are the most easily excitable electrons. In the ground energy state, these electrons are located in the highest occupied molecular orbital or HOMO. An absorption event occurs when an incident photon equal in energy to the energy gap between the lowest unoccupied molecular orbital (LUMO) and HOMO strikes the electron. The energy is nearly instantaneously absorbed (10^{-15} s) and the electron is excited across the energy gap from HOMO to LUMO. It should be noted that within individual electronic energy states, there exists a vast multitude of vibrational energy states and within these an even vaster array of rotational energy states. An excited electron will typically be excited to a vibrational state within an excited electronic state. This is called a vibronic transition being a combination of vibrational and electronic.

The electron will very quickly relax to the ground vibrational state within the excited electronic state and in so doing will give off energy as heat. This is known as internal conversion.[4] For fluorescence to occur there cannot be any overlap of vibrational states from S_0 to S_1. If there is overlap then the electron will continue to relax by generating heat. However, if there is no overlap, the only way for the electron to fully relax is to emit a photon of equal energy to the band gap between electronic energy levels. This phenomenon is known as fluorescence.

Fluorescence occurs rapidly, on the order of 10^{-8} s. This is still very slow compared to absorption processes. Fluorescence occurs from the relaxation of an electron that is in the singlet state. There are two states that the excited electron can occupy, the singlet state and the triplet state. A good way to understand triplet and singlet is to envision a helium atom. There are only two electrons and if one of them is excited then there are four possible spatial configurations that the electrons may find themselves. In one of the combinations, the electrons have opposite spin vectors making their net spin zero.[4] This is called the singlet state because there is a single orientation with a net spin vector of zero. The other state arises from the other three orientations hence the moniker triplet. If the spins are both aligned up then S = 1. If the spins are both aligned down then S = 1. If the spins are aligned in opposite directions but are parallel then they will have a net vector perpendicular to their axes of rotation. S = 1 in this instance as well.

In most cases it is highly unlikely for an excited electron to enter the triplet state. If such an event occurs, called intersystem crossing, relaxation becomes a forbidden transition. This is because the excited electron and the ground electron from the same ground state orbital will have the same spin vector. The Pauli Exclusion Principle states that no two electrons in the same atom can have the same four quantum numbers, these being n, l, m_l, and m_s. If relaxation were to occur from this triplet state then it would be in blatant violation of the Pauli Exclusion Principle.

After a time in the excited triplet state that is orders of magnitude longer than that of the excited singlet state (milliseconds to minutes) the electron will eventually be able to relax. Once again, if there is no overlap between electronic states by vibrational modes then relaxation will occur, not with the release of heat, but with the emission of a photon. An emission event of this sort is called phosphorescence and for the sake of brevity, it will not be discussed any further in this review.

1.1.2 Fluorescence Quenching

Quenching is a mode of action that results in a decrease in fluorescence intensity. There are many different types of quenching and each can give useful information about the fluorophore and how it interacts with its molecular environment. There is collisional (also called dynamic) quenching that occurs when electrons in the excited state lose energy from molecular collisions causing a loss of fluorescence. A well know collisional quencher is molecular oxygen which quenches almost all know fluorophores.[5] Reactions in the excited state, molecular rearrangements, different modes of energy transfer, and formation of a ground state complex can all result in quenching. Heavy atoms such as bromine and iodine can also act as quenchers when they are bound onto a fluorophore's pi system. These heavy atoms promote intersystem crossing of the excited electron to the triplet state. Due to relaxation times that are orders of magnitude longer in the triplet than in the singlet state, local quenching processes are far more pronounced. So even though the heavy halogens are promoting phosphorescence, they are indirectly causing quenching to occur.

The Stern-Volmer equation directly illustrates a decrease in fluorescence intensity and lifetime due to collisional quenching.

$$\frac{\tau_0}{\tau} = 1 + k_q \tau_0 [Q]$$

Equation 1.1 Stern-Volmer equation

Quenching can depopulate the excited state and is a rate process. This is what causes the decreased lifetime.

Static quenching is different from collisional quenching in that as soon as a photon is absorbed by the fluorophore it immediately relaxes without the emission of a photon. This is caused by the formation of a ground state complex with the fluorophore and the quencher. A convenient way to differentiate between dynamic and static quenching is to observe the absorbance spectrum of the molecule. If the quenching mode is dynamic than the absorbance spectrum will remain unperturbed since it is only the excited state electron that is perturbed. However, if the quenching mode is static then the formation of the ground state complex will affect the appearance of the absorbance spectrum.

1.1.3 Resonance Energy Transfer

One of the most novel uses of fluorescence is to measure distance. This can be done by a method called resonance energy transfer (RET.) Other accepted names are fluorescence resonance energy transfer or Förster resonance energy transfer (both called FRET.) FRET measures the distance between two dye molecules, termed the donor and the acceptor, by reporting on the amount of non-radiative energy transfer between them. This is done directly by measuring the total intensity and taking a ratio of the acceptor intensity to the total intensity[6]. The formula below gives the efficiency of energy transfer.

$$E = (1 + (\frac{R}{R_0})^6)^{-1}$$

Equation 1.2 Efficiency of energy transfer in FRET.

R is the inter-dye distance. R_0 is the Förster radius. RET measurements allow real time tracking of a single molecule's conformational dynamics[6]. RET is now even being used to probe the dynamics of individual DNA and RNA molecules[2].

1.1.4 Fluorescence Anisotropy

Isotropy is defined as having uniformity in all directions. Anisotropy, on the other hand, is the property of being directionally dependent. When a sample is excited with plane polarized light, the emitted photons also tend to be polarized in most cases. Anisotropy is the term used to describe the extent of polarization of the emitted photons from the sample[5]. There is a reason for this observed polarization. Analyte molecules that have their absorption-transition moments oriented parallel the electric vector of the incident light are more likely to be excited than those that are orthogonally oriented.

Steady state anisotropic measurements can be used to monitor protein binding. The anisotropy of the naked protein can be measured. Then it can be mixed with substrate and the anisotropy can be measured again. The difference in anisotropy is a strong indicator of binding and can be used to calculate the stoichiometry[5].

1.1.5 Fluorescence Applications

The field of fluorescence microscopy has experienced a renaissance over the last decade or two.[7] One of the most pronounced breakthroughs was the discovery of green fluorescent proteins (GFP) which were isolated from the jellyfish *Aequorea victoria*. The cDNA from these proteins can be concatenated with the DNA of target proteins. The new proteins will retain fluorescent properties while still maintaining the primary functions and cellular localizations of the native protein.[8] This has remarkable implications for using microscopy techniques to actually visualize the inner workings of living tissue in real time.

A classic technique that is arguably the cornerstone fluorescence microscopy technique is confocal scanning microscopy. Thin samples are easily excited with light and basic fluorescent microscopy techniques can be employed to great effect. However, whenever a thick sample is irradiated with light all areas are excited indiscriminately. A great deal of excited photons that are detected come from these out of focus fluorophores. Confocal microscopy seeks to rectify this issue by only allowing light to be detected that originates from the focal point.[9]

Out of focus light is eliminated by using optical sectioning. A large number of images are taken of each cross section of the surface of the object being observed. This is the scanning action described in the method name. A computer is then used to take all of the images and to reconstruct a three dimensional image of the object.[9]

Another technique that at one time was merely thought of as thought experiment by the famous German-American physicist Maria Goeppert-Mayer is two-photon microscopy.[7, 10] A major pitfall when attempting to image a biological system is that biological tissues scatter light.[11] Two-photon microscopy allows biologists to actually image this tissue by offering unprecedented optical penetration. Most traditional forms of fluorescence-based microscopy such as confocal microscopy use single-photon excitation. In order for two-photon excitation to occur, the lasers being employed must be incredibly fast. The limit set to where two photons are said to be arriving simultaneously is under five femtoseconds[11] and todays ultra-fast lasers can fire in femtosecond pulses. The energies of the two photons are summed and are simultaneously absorbed by the chromophore. Excitation and emission are not changed by this technique. This greatly enhances the efficiency of fluorescence microscopy where light intensities are sometime too low to cause a sizeable amount of excitation events. A key aspect in determining the efficiency of two-photon excitation is the multiphoton absorption cross-section. The light typically

used is in the near infrared which is deeply penetrating of tissue and is scattered far less than visible light.

Fiber-optic fluorescence imaging has recently received a boost in overall applicability from the development of a "photonic crystal fiber that can facilitate ultra-short pulse delivery for fiber-optic two-photon fluorescence imaging".[12] Fiber optics allows the user access to cell types that are not normally available to image, especially in vivo. These include tissue cavities and the insides of solid organs.[12] Due to the continuing shrinking of solid fiber optic parts, both optical and mechanical, and the use of deeply penetrating two-photon excitation techniques for microscopy, the use of fiber optics is now allowing unprecedented access into living organisms to view life as it happens.

1.2 Introduction to Nile Red and Nile blue Dyes

One of the earliest drivers for the formation of the modern chemical industry was the demand for synthetic dyes for the artificial coloring of fabrics. Small-molecule dyes have since found use in a wide range of industrial applications and cutting edge technologies. There are current needs being fulfilled in solar cells, *in vivo* imaging, photodynamic therapy, histological staining, metal sensing, organic light emitting diodes (OLED), and in laser pumping mediums.[13-30] Many of the popular chromophores such as carbocyanines, BODIPY, coumarin, squaraine, and rhodamine-based dyes are used across academic research, medicine and industry.[31-35] All dye architectures have their benefits and drawbacks related to photo/chemical stability, optical properties, solubility and synthetic access to analogues.

Benzophenoxazine dyes are often recognized in the literature for their intense colors and their lipophilic nature. Nile red and Nile blue are two fluorescent molecules belonging to this

benzophenoxazine family and historically, they have been used to dye clothing and stain lipids *in vitro*. Since their synthesis was first reported by Möhlau and Uhlmann in 1896, there have been ample papers published on the dyes' properties and uses.[36] Benzo[*a*]phenoxazines are analogous to benz[*a*]anthracene, also known as tetraphene, but with two heteroatoms, nitrogen and oxygen. This compact aromatic structure is noted for its strong fluorescence and stability.

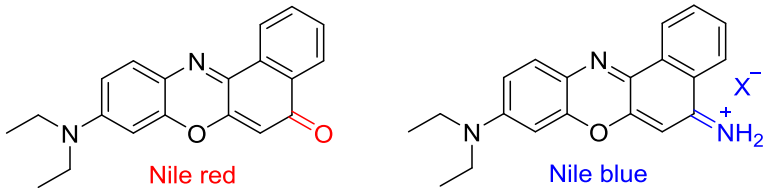

Figure 1.2 Structures of Nile red and Nile blue

Nile red has no formal charges and is intensely fluorescent with a high quantum yield in apolar media. However, in water, the dye is poorly soluble and does not show any fluorescence. Its chromophore is highly susceptible to changes in solvent polarity and dielectric constant giving this dye a wide solvatochromic range. Nile blue is a cationic dye and is thus more readily soluble in water than Nile red. It is highly sensitive to pH changes making it a useful pH probe. It has red shifted absorbance spectra compared to Nile red making it a viable candidate for biological imaging.

1.3 Nomenclature of oxazines

The name benzophenoxazine is derived from oxazine which corresponds to any heterocycle that contains both oxygen and nitrogen in a six-membered ring with two double bonds.[37] There are three possible isomers based on the position of the heteroatoms. They are 1,2-oxazine, 1,3-oxazine and 1,4-oxazine. Elongation of 1,4-oxazine by substituting two fused benzene rings along its only two C—C faces yields a phenoxazine with a similar linear shape to that of anthra-

cene. Further elongation of the conjugated system with another benzene ring fused along the *a*-*c* faces will give a benzophenoxazine. Nile red dyes are frequently referred to as benzo[*a*]phenoxazinones while Nile blue are called benzo[*a*]phenoxaziniums with a counter ion appended on as a suffix. These counter ions are typically halides but more exotic ions such as perchlorates are reported.

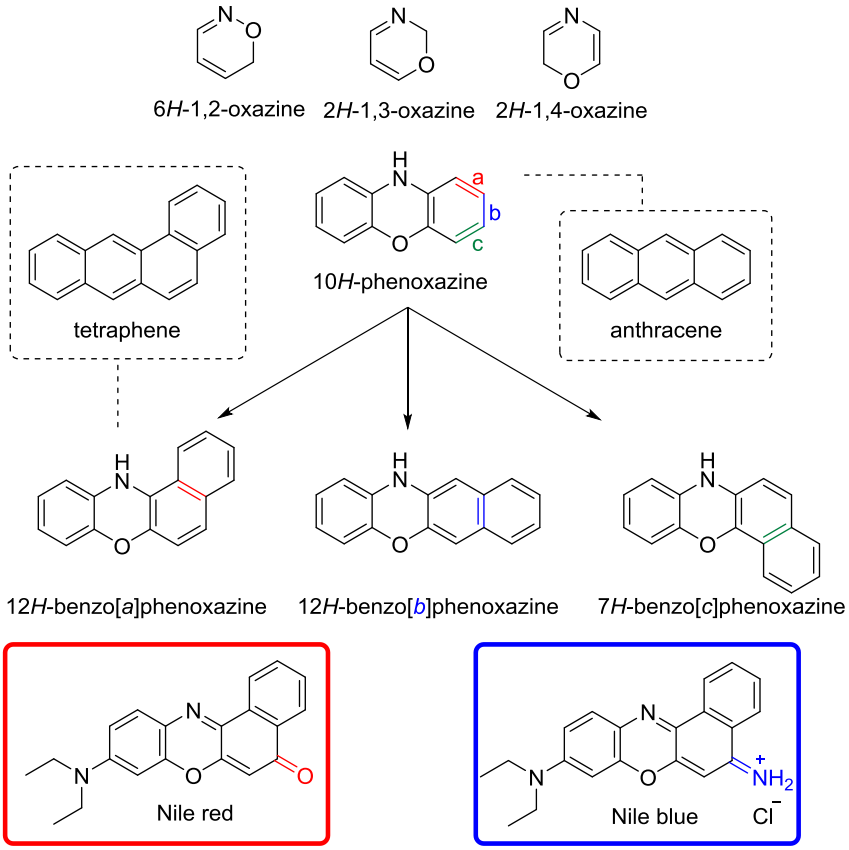

Figure 1.3 Nomenclature of oxazines

1.4 Photophysical Properties

Absorbance maxima are determined by the frequency of light required to excite an electron across a HOMO/LUMO band. The energy required for a π→π* transition is in the long UV through visible range wavelengths and can even extend into the near-infrared part of the spectrum. Benzo[*a*]phenoxazinones (Nile red) have absorption maxima at 550 nm in methanol while

benzo[a]phenoxaziniums (Nile blue) absorb at 630 nm. Why is there such a large difference between the two similar systems? The 80 nm difference can be accounted for in the strength of the two dyes' corresponding donor-acceptor systems.

Nile red is a neutral molecule with an amine donor and an oxo (carbonyl) acceptor. Intramolecular charge transfer must occur from a twisted excited state so as to attain overlap of the donor and acceptor molecular orbitals. Nile blue, which is cationic, has a much stronger acceptor in the form of the charged iminium group. This induces a strong net dipole across the molecule driving resonance. Because of this, the sp^2 character of the donor amine is more pronounced than in the neutral system and intramolecular charge transfer is more fluid. The physical implications of this are that the electronic band gaps for Nile blue-based dyes are smaller than those for Nile red-based dyes. Increased delocalization of electrons through intramolecular charge transfer processes will give a sizeable bathochromic shift.

In water, the photophysical behavior of Nile blue is most impacted by the acid form of the dye which can form H aggregates and do not fluoresce. It was found that small substitutional changes to the dye core had a measureable effect on acid/base equilibria with respect to the ability of the solvent's molecules to act as hydrogen bond acceptors. Alkyl groups substituted on the acceptor iminium cation can lend electron density to the N—H bond via inductive effects. This increases the strength of subsequently formed hydrogen bonds, thus decreasing the proton's acidity. The deprotonated dye species experience hypsochromic shifts of approximately 100 nm and are an order of magnitude less fluorescent than the acid forms.[38]

Emission spectra provide a window into the fine electronic band structure of a fluorophore and provide a glut of information regarding intermolecular interactions. Both benzo[a]phenoxazinones and benzo[a]phenoxaziniums are notable for their high fluorescence quan-

tum yields. The compact chromophore is held in a rigid conformation due to the multiple fused ring systems. Vibrational modes are highly restricted in these systems so the chances of thermal deactivation of the excited state are significantly diminished.

1.4.1 Solvatochromism

Steady-state spectral data has shown that a large change in dipole moment occurs upon excitation of Nile red.[39] This trait is caused by a process known as twisted intramolecular charge transfer (TICT). Nile red has an amino group at the 9-position which is substituted with two ethyl groups. This amine can rotate around the axis of the sigma bond appending it to the chromophore.

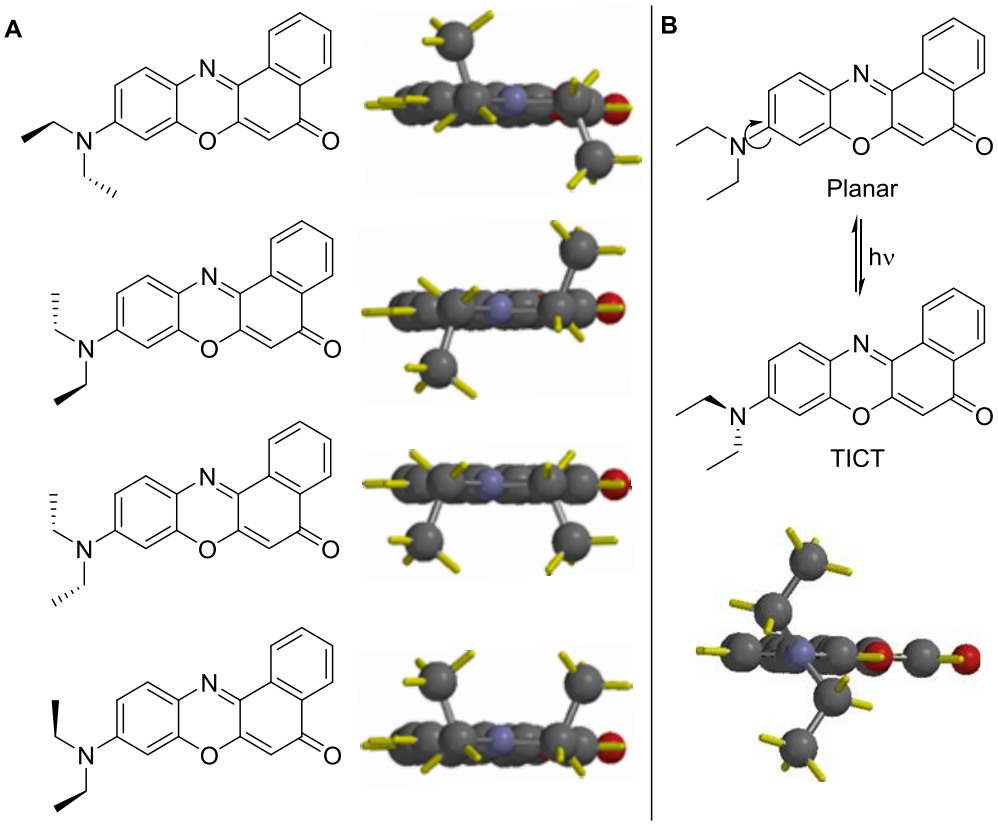

Figure 1.4 A) Nile red in electronic ground state (planar); B) Nile red in in twisted excited state.

It has been demonstrated by Adamo *et al*. that this bond rotation greatly increases the dipole moment across the entire molecule and that intramolecular charge transfer (ICT) is far more pronounced in this twisted state.[40] This is because the amine donor and oxo acceptor groups have overlap of their molecular orbitals. This hybridizes the donor/acceptor electronic states thus promoting ICT. Because the twisted excited state is so polar, it is best stabilized in polar solvents. In nonpolar media, TICT cannot occur because the Franck-Condon excited state cannot be stabilized due to its large dipole. There is nothing in the molecule's solvation sphere to stabilize such an excited state. Because of this, the molecule will maintain planarity even once excited. The trend is that increasing solvent polarity causes the absorption maximum to shift bathochromically while decreasing solvent polarity causes the absorption maximum to shift hypsochromically.[41] This is directly correlated to having a higher energy Franck-Condon excited state versus a lower energy one. Time-dependent density functional theory (TD-DFT) was used to computationally predict solvent effects on optical spectra for Nile red and Nile blue with results that closely mirrored the experimental data sets.[42, 43]

Nile red's TICT processes have been assessed in reverse micelles[44], Langmuir-Blodgett films[45], and faujasite zeolite[46] in order to understand how the dye's photophysical properties were affected once constrained onto a surface that would restrict its geometry. Quantum yield and other optical properties have also been assessed in solution with various organic bases.[47] The dye's powerful solvatochromism has been used to probe the partitioning of surfactants into aqueous and organic phases.[48] Studies have been done on solvent effects on Nile red using many approaches.[49, 50] Solvatochromism studies of Nile red and Nile blue in isotropic mediums versus anisotropic mediums were also conducted.[51]

1.4.2 Thermochromism

Thermochromism is a molecule's ability to undergo changes in its optical properties by varying the temperature. Perhaps the most notable example of this phenomenon is the commercial use of thermochromic inks by the Coors Brewing Company to print labels on their beer.[52]

Kawski *et al*. determined the excited state dipole moment of Nile red in several solvents. They used thermochromic shifts in optical spectra as a way of measuring these parameters. They cite a discrepancy in the literature saying that other researchers publishing in this field neglected to take into account the Onsager reaction field for a polarizable dipole. They claim that their method of measurement gives dipole values for the single isolated molecule irrespective of solvent properties and interactions.[53]

1.4.3 FRET

Förster resonance energy transfer (FRET) is a photophysical phenomenon whereby an excited state chromophore can excite a neighboring chromophore by through-space energy transfer. This is facilitated by overlap of the FRET donor emission band with the FRET acceptor absorption band in conjunction with the parallel spatial orientation of the donor's HOMO wave function with that of the acceptor's LUMO wave function. Within a short enough distance, known as the Förster distance, resonant energy transfer is accomplished vis-à-vis the FRET donor's excited-state polarization. Electron spin coupling at close range gives rise to the acceptor being able to "feel" the donor. As the donor's excited singlet state electron attempts to relax, the switch in polarization is felt by the spin coupled electron which then gains the kinetic energy needed to become promoted to an excited state. Chemists can utilize this process to attain a very small molecular ruler allowing measurements to be made on the Angstrom scale.[54]

Broumische *et al*. designed a bichromic FRET system with a large two-photon absorbing (TPA) cross-section. Irradiation of the of the donor segment with high intensity IR radiation will give two-photon absorption followed by resonance energy transfer to the Nile red acceptor.[55]

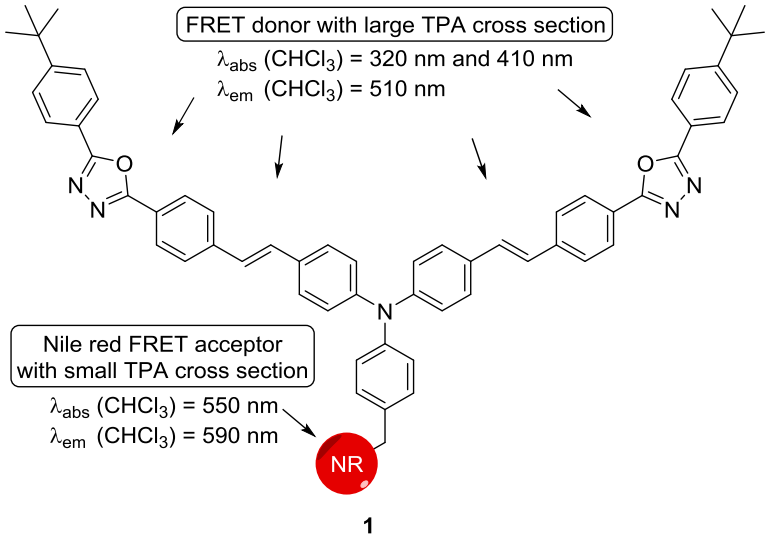

Figure 1.5 Nile red conjugated to moiety with large TPA cross section. Excitation with 815 nm, 8 ns laser pulses gives near complete quenching of donor fluorescence with notable acceptor fluorescence.

They followed up that paper with another publication showing multiphoton absorption by several dendritic structures followed by FRET to a Nile red acceptor.[56] This carries significant advantages by allowing an attractive UV-vis absorbing chromophore with a small TPA cross section to be excited by IR radiation which would otherwise not be feasible.

1.4.4 Intersystem Crossing

Heavy atoms have a long reported history of causing photophysical and photochemical intramolecular effects in organic molecules.[57, 58] Generation of singlet oxygen is promulgated by through-space energy transfer from neighboring electrons in the excited triplet state. Since the

heavy atom effect is efficient at generating large populations of excited triplet electrons, it is also quite effective at generating singlet oxygen.

Singlet oxygen is highly reactive and is utilized as a destructive agent in photodynamic therapy (PDT) whereby cancerous tissue is bombarded with high concentrations of singlet oxygen generated *in situ* by excitation of a PDT agent with light. Benzo[*a*]phenoxazines are poor candidates for PDT but derivatization with heavy halogens and chalcogens can yield more desirable candidates. Substitution of the oxazine's oxygen with a sulfur or a selenium shows a dramatic increase in singlet oxygen yields as shown in Table 1.1.

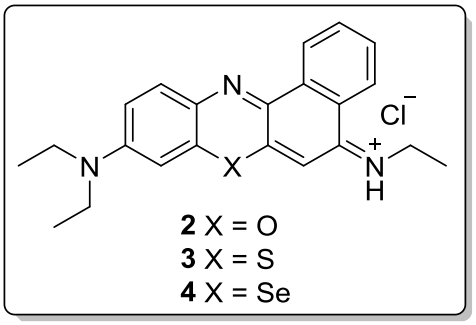

Figure 1.6 Benzo[*a*]phenoxazine analogues with different chalcogens substituted at the 7-position.

Dye	λ_{abs} (nm)[a]	λ_{em} (nm)[b]	Φ[c]	$^1O_2$[d]
2	632	660	0.27	0.003
3	654	693	0.21	0.03
4	661	703	0.03	0.78

[a] Absorption maximum in ethanol containing 0.1% acetic acid. [b] Fluorescence maximum in ethanol. [c] Absolute fluorescence quantum yield. [d] Absolute quantum yield for single oxygen formation.

Table 1.1 Photophysical properties of Nile blue analogues with differing chalcogen substitutions.

1.5 Applications of Nile Red and Nile Blue

Nile red and Nile blue have found many uses in industry and science since their original syntheses in the late 19th century. Their intense fluorescence and good photostability have made them attractive options as sensors, photosensitizers, and biological labels.

1.5.1 Materials Science Applications

1.5.1.1 Loading onto Inert Supports

Dyes incorporated into materials or onto surfaces can act as sensors for a variety of applications. Nile blue was infused with poly(*n*-butyl acrylate) microspheres to be used as a reflectometric ion sensor for potassium.[59] Nile red has been embedded in polystyrene films on a glass surface and adsorbed onto nanoclays to assess the hydrophobic loading abilities of these clays.[60, 61] It has been tested for dye-sensitized solar cells.[62] It has also been incorporated into graphene sheets for potential use as a biosensor or non-palladium fuel cell catalyst.[63] Nile blue, loaded into a silica sol gel matrix, was investigated for use in a solid state dye laser.[64]

Huang *et al*. wanted to study the electronic bands and transitions of Nile blue. They constructed Langmuir-Blodgett films with the dye embedded and then deposited these onto clay sheets. By changing the concentration of dye and the surface pressure, the group was able to form two types of adsorbed states. One state (type I) consisted of dyes stacked face to face and had an absorption maximum at 550 nm. This is very similar to the dye in solution with methanol. The other state (type II) consisted of the dyes stacked side-to-side with their long axes oriented perpendicular to the air/water surface. These had an absorption maximum of 590 nm.[65]

1.5.1.2 Nanoparticles

Nanoparticles have been a hot topic for many years. Gold nanoparticles are known for having massive Stokes shifts. Nile red can adsorb to their surface which will then weakly fluoresce due to FRET. Thiols in solution can compete with Nile red for adsorption sites giving a change in fluorescence and this is selective against amines, acids, alcohols, bovine serum albumin (BSA), and hemoglobin making it a useful detection method for thiol containing biomolecules.[66-70]

Gold nanoparticles doped into a polymer matrix containing Nile blue can have a direct effect on the dye's luminescence. Through surface plasmon coupling, luminescence can be enhanced by changing the distance of the dye molecules from the gold nanoparticles and by altering the charge on the gold nanoparticles. The excitation wavelength of the pumping laser source plays a strong role in this enhancement.[71] Nile red has recently been used in a polymer nanoparticle with a PEGylated exterior to selectively sense Fe^{3+} ions.[72]

1.5.1.3 Miscellaneous

Research during the early days of World War II was undertaken to search for acid/base indicators for use in non-aqueous media. The applications of such a dye could be for the detection of acid in essential war materials such as airplane fuels and lubricants. By 1966, this research had led to the investigation of Nile blue A as a good candidate for such detection. The anhydro form of the dye Nile blue is relatively basic since protonation results in a stable, cationic charge transfer platform. Nile blue was found to be well suited for titrations in apolar media.[73]

The EPA uses a variety of field tests for rapid detection and evaluation for a variety of toxins and contaminants in water and soil. Duan *et al*. were seeking to develop to a probe for the rapid detection of hypochlorite in water. Other probes and methods already exist for this applica-

tion but they wanted a method that used a cheap, commercially available fluorescent dye. They selected Nile blue A which had its fluorescence quenched in the presence of hypochlorite. The detection limit was very low (0.04 μmol/L) and appeared specific to hyprochlorite ions making detection facile for trace quantities of hypochlorite in water samples.[74]

1.5.2 Biological Applications

1.5.2.1 Biological Imaging

Nile red has been used historically as a histochemical stain to image lipid droplets in tissue.[75,76] Dioctyldecyldimethyl- ammonium bromide (DODAB) is a cationic lipid that composes some liposomes. By measuring the steady-state and time resolved anisotropy of Nile red, one can monitor the distribution of cholesterol in these DODAB vesicles. Fluorescence also reported useful information about the viscosity and polarity of local microenvironments within the vesicle.[77]

Nile blue also has an affinity for lipophilic molecules. Nile blue localizes in lysosomes and can subsequently be up taken by tumor cells.[78] Nile blue was investigated for use as a non-porphyrin photosensitizer.[79] Its effects were studied in human bladder carcinoma cells for use as an agent for photodynamic therapy (PDT).[80]

1.5.2.2 Biological Assays

Another common use for fluorescent dyes is in assays. Mild hypothermia (mHT) induced in tumor cells has been shown to increase the bioavailability of low molecular weight drugs due to a multitude of overlapping factors such as increased vascular permeability and tumor perfusion. The human epidermal growth factor receptor 2 (HER-2) overexpressed in breast cancer can be targeted effectively by a clinically approved antibody, Herceptin®. Escoffre *et al.* used a Nile

red assay to measure the formation of Herceptin® aggregates in order to assess the stability of the drug under mHT conditions.[81]

Nile blue was also used to study the efficacy of new drug release technology.[82] Mishra *et al*. investigated the binding of Nile blue to bile salts. Bile salts act of biosurfactants and are able to solvate a variety of hydrophobic biological chemical structures such as cholesterol and lipids. They have garnered interest as a potential drug delivery vehicle due to their low toxicity and biocompatibility.[83]

Kuramitz *et al*. developed a binding assay for protein-ligand interactions. They used spectroelectrochemical sensing which combines both optical spectroscopy and electrochemical techniques. With these two detection modes successfully integrated into a probe, the accuracy of measurements is increased due to the corroboration between the two data sets. They chose Nile blue as the optical label for the spectroscopic portion of their sensor.[84]

1.5.2.3 Biological Sensors

Due to the pH sensitivity of the Nile blue chromophore, it has been the subject of testing for use as a pH probe. Ma *et al*. used fluorescein isothiocyanate (FITC) and Nile blue chloride to construct a ratiometric pH sensitive probe. The FITC responds to small changes in pH. Increasing pH will cause the FITC emission signal at 515 nm to undergo a hyperchromic shift. Nile blue fluoresces at 670 nm and the signal stayed relatively constant through minor pH manipulations. This allowed the two emission spectra to be compared so as to determine the pH ratiometrically. FITC was chemically conjugated to the surface of carbon quantum dots. In order to keep Nile blue chloride from diffusing off of the surface, the quantum dots were coated in a sodium alginate hydrogel that would immobilize the dyes from "leaking". This sensor was tested for tracking the pH of the extracellular fluid between cancer cells in real time.[85]

Nile blue-based platforms for urea biosensors have been constructed.[86, 87] One such method involves a sensor design that was based on immobilizing a Nile blue chromoionophore and a urease enzyme in stacked sol-gel films. This method does not require chemical conjugation for analytical detection applications. The other method uses a kappa-carrageenan membrane that was doped with a Nile blue chromoionophore as an optode. Urease was physically attached to this structure for urea sensing.

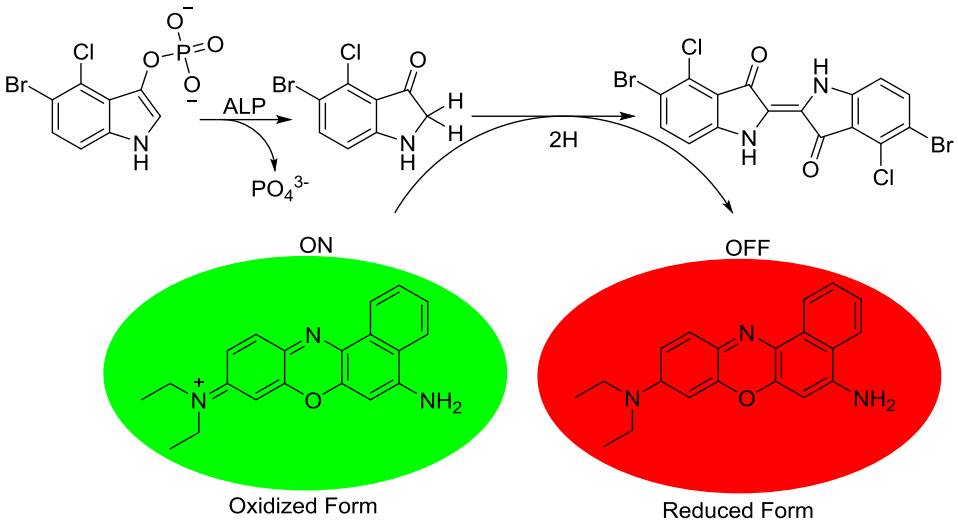

Figure 1.7 Nile blue being reduced by alkaline phosphatase enzyme to yield a non-fluorescent product.

Surface-enhanced Raman scattering (SERS) can be used to detect alkaline phosphatase. Nile blue A is Raman active and they used it to replace nitro blue tetrazolium which is more commonly used. The oxidized form is Raman active and it can be reduced by the ALP substrate product effectively turning off signal.[88]

1.5.2.4 DNA Applications

Nile blue binds to DNA. Mitra *et al*. looked at the binding of Nile blue with three different synthetic DNA oligonucleotides: $(CGCAAATTTGCG)_2$, $(GCGCGCGCGCGC)_2$, and $(ATATATATATAT)_2$. Using picosecond resolved fluorescence quenching and polarization analyzed anisotropy they were able to identify two modes of binding between the dye and DNA. Both modes were concentration dependent. Low DNA concentrations saw electrostatics play a large role in dye-DNA binding. At high concentrations of DNA, the preferred mode was intercalation of DNA by the dyes.[89]

Nile blue undergoes static quenching upon binding with DNA. This quenching is linear over a wide concentration range of nucleic acids and serves as the basis for a fluorescence quenching assay for the determination of concentrations of DNA and RNA down to $ng \bullet mL^{-1}$ levels.[90] There is also a protocol for the determination of DNA concentrations from the three-dimensional spectra of light scattering from Nile blue sulfate on DNA.[91] Studies of the binding of Nile blue sulfate to calf thymus DNA and fish sperm DNA showed through absorbance spectra that it was the H aggregates that were that were doing the binding; this process was enhanced in the presence of single stranded nucleic acids such as native yeast RNA and thermally denatured DNA.[92]

Since the dye has been shown to bind with DNA, a large amount of work has been done to expand the probe's utility with nucleotides. Staining/histology has historically been popular with benzo[a]phenoxazines. With respect to this history, a postelectrophoretic method for staining DNA with Nile blue in agarose and polyacrylamide gels was developed, adding yet another layer to the dyes histochemical applications.[93]

Another method for DNA detection involves glutathione (GSH)-capped CdTe quantum dots (QDs). They have intense fluorescence and surface binding (noncovalent) of Nile blue to the

QDs would quench fluorescence due to an electron transfer mechanism between the glutathione and Nile blue. If DNA is present in solution, the Nile blue will dissociate from the QDs and bind to DNA causing fluorescence to be restored. This is an on/off capability.[94] The interactions between oligonucleotides and Nile blue were investigated for the electrochemical detection of hepatitis C 3a virus.[95]

Nile blue sulfate was put into a DNA-based solid electrolyte for potential application in electrochromic devices such as smart windows.[96]

1.6 Synthesis of Nile Blue and Nile Red Analogues

Nile red was originally synthesized by boiling Nile blue in sulfuric acid, which would convert the iminium moiety to an oxo group as shown in Equation 2.[36] This harsh method is outdated and the most frequently reported synthetic protocols call for the use of a nitrosylated precursor instead.

Equation 2. Original method for synthesis of Nile red.

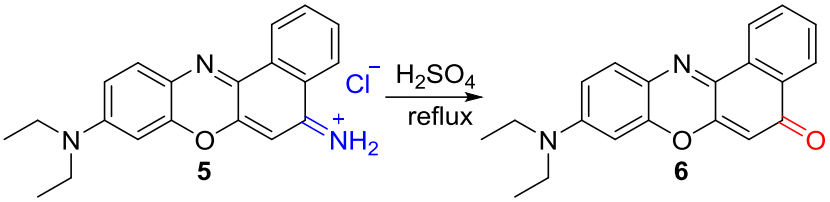

Synthetic access to analogues is limited primarily to two or three positions on the chromophore. On Nile blue they are the 2-position and the 5-and 9-amino/iminium groups. On Nile red they are the 2-position and 9-amino group (Figure 1.8.). The 2-position is frequently functionalized with a phenol. This can be conjugated to *n*-alkyl chains that are often capped with esters, acids, amines or halides. Many of these are reactive intermediates that can be used in some form of conjugation. Dye precursors contain a primary amine which can be successfully modified via

facile *N*,*N*-dialkylation reactions to form a large set of analogues. *N*-alkylation and Michael addition are also reported options for functionalization of the amines.

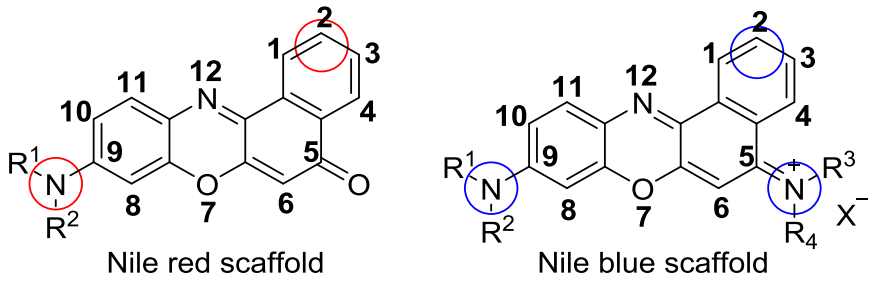

Figure 1.8 Common postions for synthetic modification of Nile red and Nile blue.

Other positions such as the 1, 3, 4, 6, and 8 carbons have been reported to be functionalized but these are typically unique cases without further synthetic development to expand analogue sets. The 10-position is sometimes substituted with a methyl group to aid in the formation of secondary amines at the 9-position by acting as a steric blocker to hinder overalkylation of the amine.

Nile blue is a charged, cationic species and can be prepared in condensation reactions where the anion is dependent on the acid used in its preparation. Chlorides are very common anions but perchlorates have much better solubility. This is because perchlorate is a weakly ligating anion due to extensive delocalization of its anionic charge. This trait coupled with its large size gives the ion very low charge density causing it to have weak associations with its neighboring cations.[97]

1.6.1 Dye Synthesis via a Nitroso intermediate

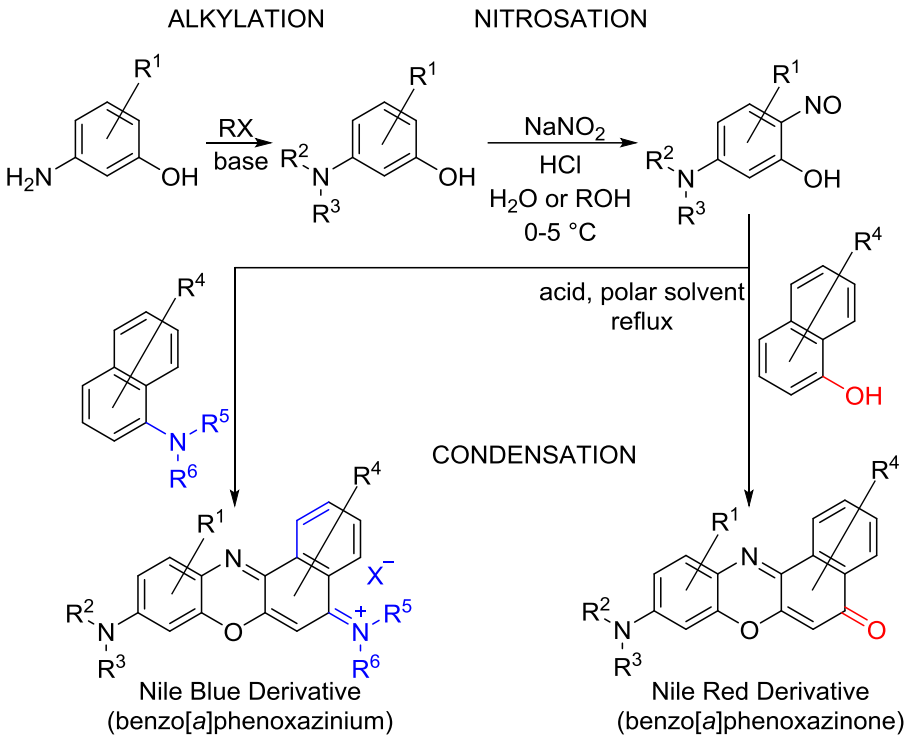

Figure 1.9 General synthesis of Nile red and Nile blue analogues.

The most common method reported for preparing these Nile red and Nile blue dyes starts with alkylating an aminophenol. The primary amine at the 3-position is a good nucleophile and will rapidly attack most alkyl halides. It can also undergo a Michael-like addition with acrylic acid to gain propionic acid substituents. Alkylation this way is seldom clean due to the formation of multiple alkylated products. Column chromotography is almost always required to isolate the desired compounds.

Nitrosylating an *N*,*N*-dialkylated-3-amino phenol is the next step. This is done by dissolving the substituted aminophenol in a polar solvent, usually a low molecular weight alcohol, with hydrochloric acid added. Sodium nitrite, dissolved in water, is very carefully dripped into the solution. The whole reaction is kept on an ice bath to prevent a runaway exotherm.

Under the acidic conditions, the nitrite anion is dehydrated rapidly to form the nitrosonium cation, a potent electrophilic species. The amine, being the most nucleophilic functionality present in solution, will attack the nitrosonium cation forming a nitrosamine. However, the nitroso group will not remain at this locale as it is always directed to the position ortho to the phenol and para to the amine by undergoing Fischer-Hepp rearrangement upon heating.[98] The final product is an HCl salt. These aromatic nitroso groups are very reactive. Heating of a nitrosylated aminophenol under acidic conditions with hydroxynaphthalene or aminonaphthalene will yield Nile red and Nile blue, respectively, via an acid-catalyzed condensation reaction. The whole synthetic process is outlined in Figure 1.9.

Nile blue and Nile red exhibit intense fluorescence so their main utility comes from being able to label, detect and track things. The major problem with these dye systems is that they suffer from a lack of water solubility. This is of paramount concern for any biological applications whether *in vitro* or *in vivo*. They also lack good handles for bioconjugation.

There have been several approaches to these problems. Water solubility can be remedied by incorporating sulfonic and carboxylic acids, hydroxyl groups, or even polyethylene glycol (PEG).[99-102] All of these water soluble analogues have larger fluorescence quantum yields in aqueous media than their insoluble cousins and they are all prepared from nitrosylated aromatics as shown in Figure 1.9.

1.6.2 Dye Synthesis via an Azo Intermediate

Ho *et al*. synthesized a series of water soluble Nile blue analogues for use in the detection of enzymatic activities. As sulfonate groups were added to the dye, fluorescence intensity increased noticeably in water.[103] This is one of the few instances where a nitroso compound was not used as a dye precursor. The reasoning behind using an azo intermediate lies in the fact that

that sulfonated nitrosoanilines perform poorly in the final dye reaction. Direct sulfonation of the dye is not desirable either as there are multiple aryl positions that are vulnerable to substitution. This greatly complicates the purification process and yields will suffer.

The azo method starts with *p*-nitroaniline which is converted into the diazonium salt **12** in nitrous acid. The diazonium salt is further reacted *in situ* with either **a**, **b**, or **c** in Figure 1.10 which will then constitute either the western or eastern portions of the final dye. The product is an arylazo compound which can then be condensed with either aminonaphthalene or a 3-aminophenol derivative in the presence of perchloric acid to yield a Nile blue analogue.

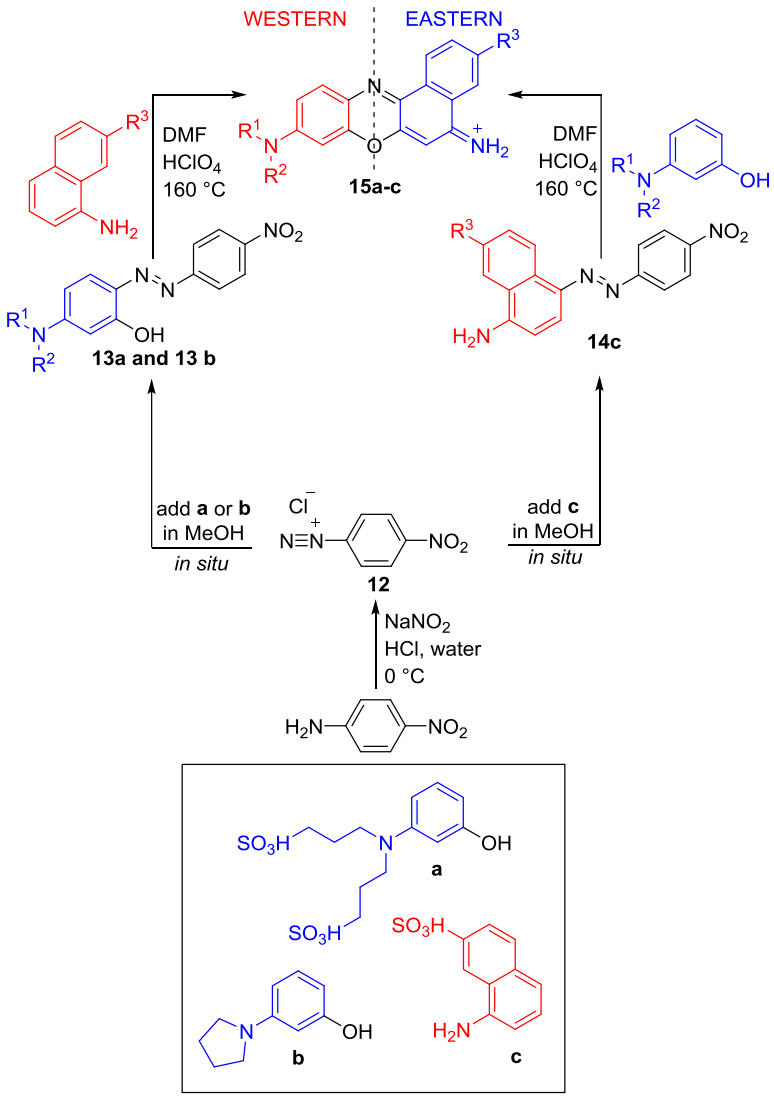

Figure 1.10 Synthesis of water soluble Nile blue analogues via arylazo intermediates.

1.6.3 Dye Derivatives with Conjugateable Groups

Organic dyes are typically flat and hydrophobic compounds. They possess few of the traits that one would find in a typical molecule that would be deemed drug like. This generally makes them poor candidates for the selective targeting of biological systems. However, conjugating a dye to bioactive compounds known to penetrate or target specific sites can be invaluable for imparting bioselectivity to a fluorophore. Targets can be lit up with some predictability. Nile red and Nile

blue can both be modified to have functional groups that act as handles. These handles can easily be conjugated to a substrate by one of several well-known methods.

1.6.4 Esters and Carboxylic Acids

Carboxylic acids are convenient functional groups for bioorthogonal conjugation so it would be pertinent to incorporate this functionality onto the dye backbone. Substitution with alkyl-capped esters is generally the first step to preparing the acid and this has been accomplished on a vast array of Nile blue and Nile red analogues.[38, 101, 102] Many successful attempts have already been made to incorporate an alkyl-capped carboxylic acid at the 5-amino and 9-amino position for Nile blue and the 9-amino position for Nile red.[38, 99, 100, 104]

A hydroxyl handle is easily achieved at the 2-position via condensation of the nitrosylated 3-aminophenol with 1-amino-6-hydroxynaphthalene or 1,6-dihydroxynaphthalene for Nile blue or Nile red respectively as shown in Figure 1.9. Substitution at this position is facile with an alkyl linker that has an ester endcap. This can be achieved in two ways. The first method involves alkylating **16** at the 2-hydroxy position with an ester-capped alkyl halide under basic conditions to give **17**. Treatment of the ester with pig liver esterase (PLE) at a pH of 7 will deprotect and give the acid. This has a lower overall yield than the second method as is shown in Figure 1.11.

The second method uses a similar alkyl halide but it is capped with a benzyl ester instead of an ethyl ester. The benzyl group is cleaved with the boron trifluoride dimethylsulfide adduct. This gives a 74% yield versus 62% for the PLE deprotection of the ethyl ester.[105, 106] If a methyl ester is used, deprotection with potassium trimethylsilanolate (TMSOK) will give very high yields (92%) of the acid.

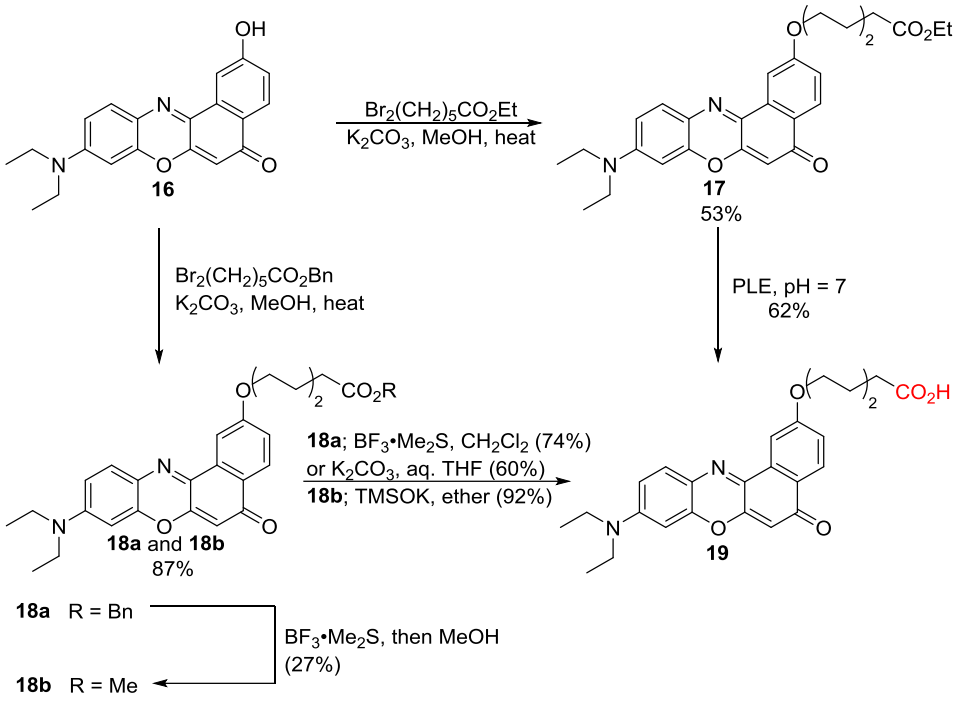

Figure 1.11 Synthesis of bioconjugateable Nile red derivative with carboxylic acid handle.

N-hydroxysuccinimide (NHS) and *N*-cyclohexyl-*N*‘-(2-morpholinoethyl)carbodiimide methyl-*p*-toluenesulfonate (morpho CDI) will react with a naked acid to form an NHS ester. Morpho CDI is a carbodiimide salt. The carbodiimides are very effective at forming amide bonds between acids and amines and will condense the naked acid with the NHS. Linkage to a primary amine is facile and as proof of concept, Briggs *et al*. used allylamine and 3-phenyl-1-aminopropane to form amide links to the dye as is shown in Figure 1.12.[105] 4-Dimethylaminopyridine, known as DMAP, is a very strong organic base that will catalyze this reaction.

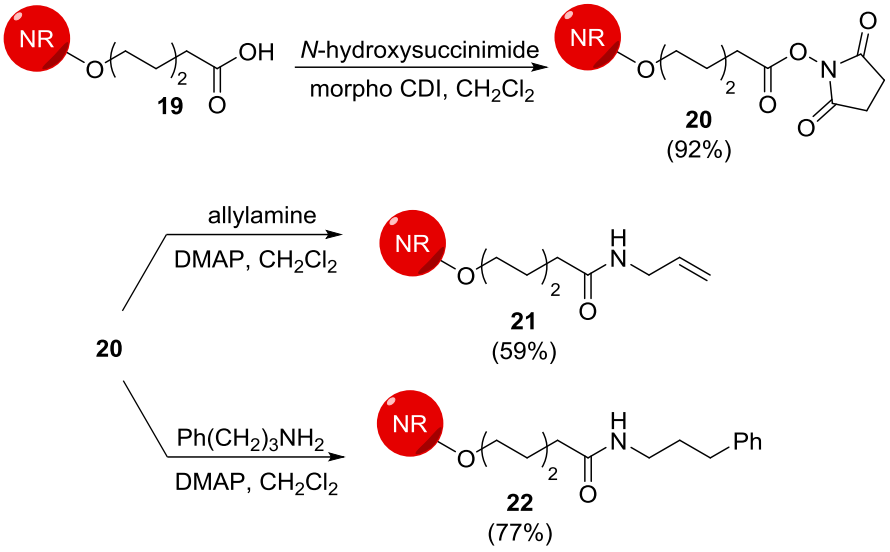

Figure 1.12 Synthesis of amide coupled Nile red analogues to show proof of concept for bioconjugation. All dye—linker bonds are at the 2-position on Nile red. See Compound 19 on Figure 1.12 for complete structure of precursor.

1.6.5 Primary Amines

Just as acids can be used as handles to couple dyes to primary amines, the reverse is also true. Many Nile blue and Nile red derivatives have been prepared with primary amines covalently attached to sp^3 carbons.[101, 102, 107-109] These are convenient functional groups for coupling and will readily react with a carboxylic acid that has been activated by a carbodiimide.

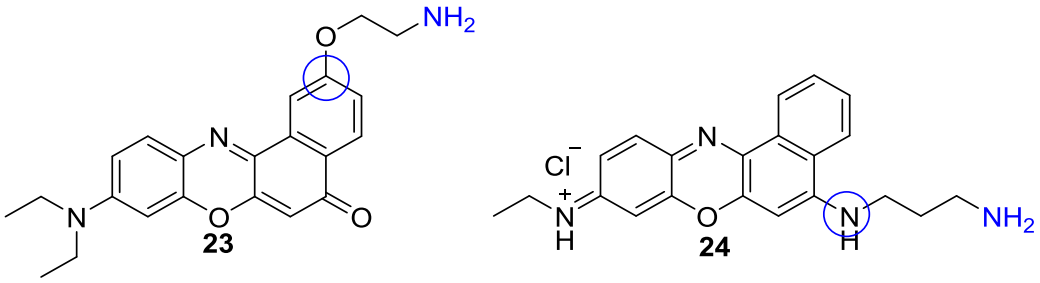

Figure 1.13 Nile blue and Nile red analogues with primary amine handles attached to the chromophore via alkyl linkers at the 2- and 5-positions.

A convenient method for stapling peptides to each other or onto various structures is through DCC/HObt coupling. Mild conditions allow an amide linkage to be formed between a carboxylic acid and a primary amine. It has been demonstrated that the technique can be used to append short peptides onto Nile blue. This can be done to a dye precursor before the final condensation reaction to form the dye or it can be achieved directly to the dye itself in good yield.

As shown by Frade *at al*., DCC coupling can be done to the naphthalene precursor and then condensed to form the dye. Nile blue is also stable enough to undergo DCC coupling with amino acids directly to the dye core. They successfully conjugated the dyes to several amino acids via amide and ester linkages.[110, 111]

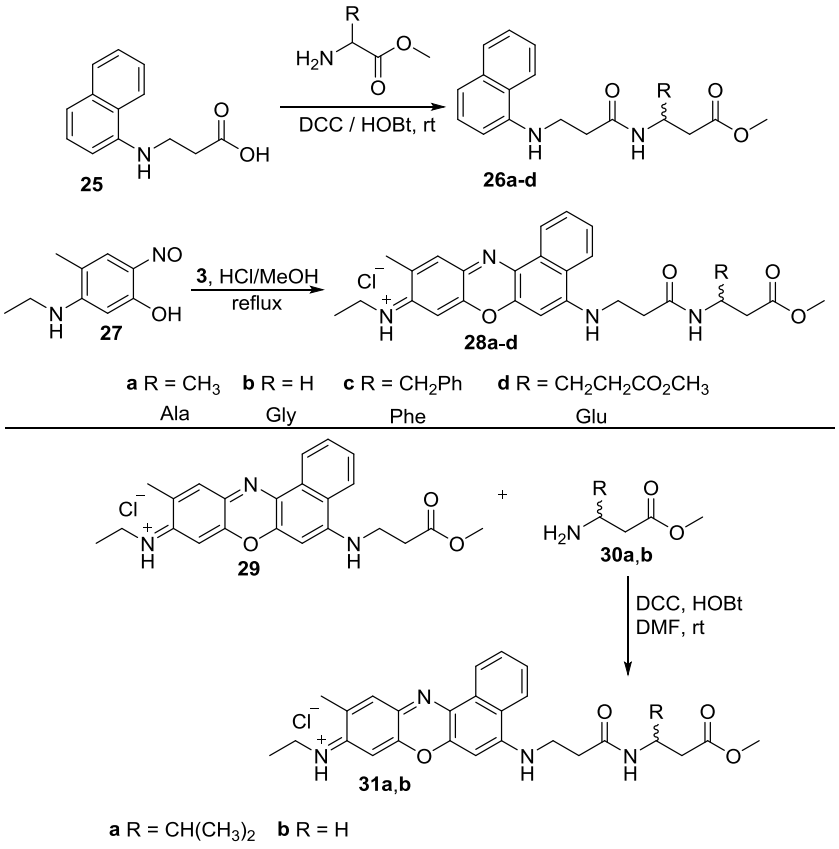

Figure 1.14 Synthesis of Nile blue analogues and labeling L-alanine, L-glycine, L-phenylalanine and L-glutamic acid (protected as methyl ester) with them.

The technique of coupling an amine to an acid has been used to append substrates onto Nile blue for selective targeting. Cyclooxygenase-2 (COX-2) is an enzyme that is overexpressed in tumor cells.[112-117] Wang *et a*l. designed a Nile blue-based NIR probe that has the indomethacin (IMC) moiety conjugated to it via a hexanediamine linker.[109] This was achieved similarly to the stapled peptides using HOBt. The long linker was used so as to allow the IMC group to fully insert into the COX-2 active site which accumulates in the Golgi of tumor cells. IMC has been shown to bind very tightly and selectively to COX-2. The probe allows for effective NIR imaging of tumors and could have *in vivo* applications.

Preparation of the IMC-linked Nile blue derivative started with the electrophilic aromatic substitution of hexanediamine onto bromonaphthalene as shown in Figure 1.15 to afford compound **33**. Condensation of this compound with the nitrosylated aminophenol shown will give the dye **34**. This reaction was discussed in detail in section 4.1. Dye **34** can be directly coupled to IMC using 1-ethyl-3-(3-dimethylaminopropyl)carbodiimide (EDCl) and HOBt to yield **35**.

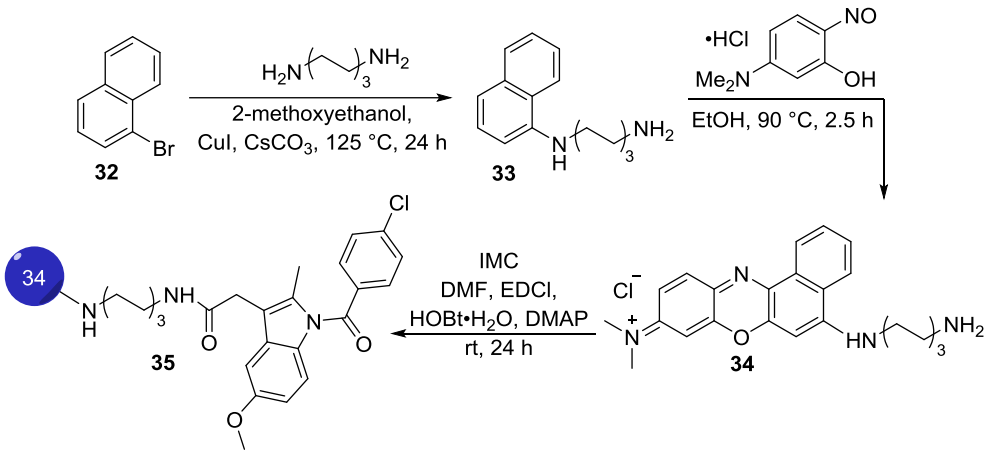

Figure 1.15 Preparation of a Nile blue-IMC linked derivative with a hexanediamine linker.

Frade *et al*. reported the synthesis of Nile blue analogues with a series of interesting structures such as pyrene, p-toluenesulfonamide, and an azo moiety.[108] All of these were coupled to a diamine linker extending from the 5-amino position using DCC/HObt. This illustrates further synthetic utility of the method for appending a diverse set of functionalities to Nile blue.

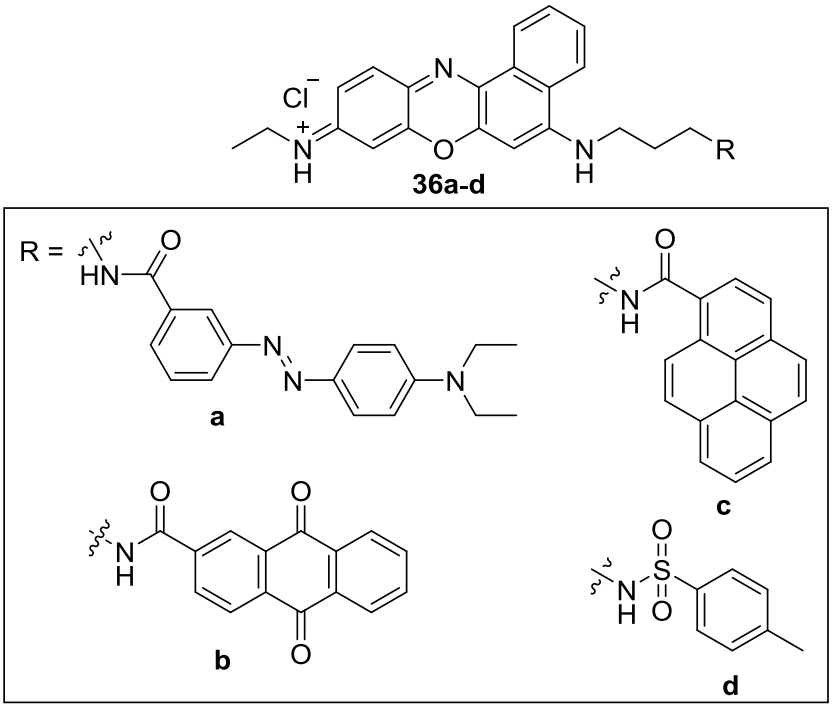

Figure 1.16 Nile blue analogues with amide linked moieties.

1.6.6 Azide-alkyne Huisgen Cycloaddition

Vilaivan *et al*. used click chemistry to conjugate a Nile red label to pyrrolidinyl peptide nucleic acid (PNA).[118] This was done in order to probe the local environment of PNA-DNA duplexes by utilizing Nile red's solvatochromic properties.

2-hydroxy Nile red (**16**) will undergo a simple S_N2 reaction with propargyl bromide in the presence of a mild base such as potassium carbonate in a polar aprotic solvent to give **37** as shown in Figure 1.17. This primary alkyne will undergo a copper-catalyzed "click" reac-

tion with an azide. PNA can have such a group appended on via an alkyl linker and then it can be "clicked" together with the alkyne on **37** to give the Nile red linked PNA (**38**).

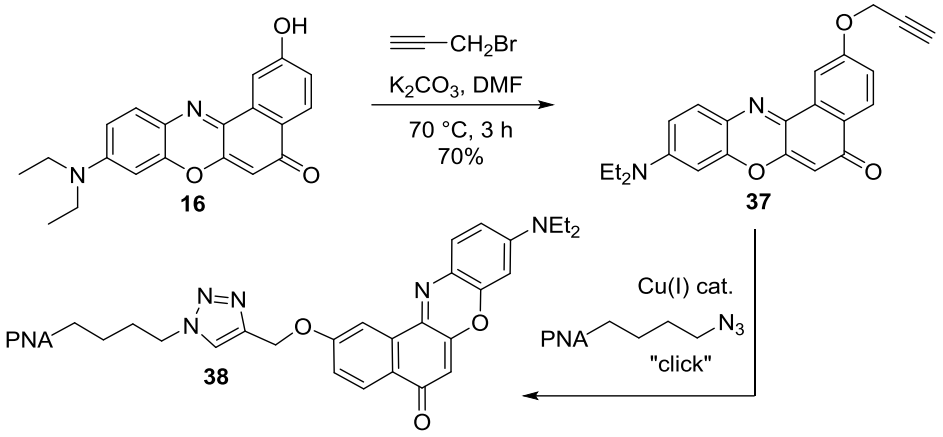

Figure 1.17 Synthesis of propargylated Nile red and click to acpcPNA.

1.6.7 Halogenated

1.6.7.1 Fluorinated Nile Red Derivatives

Halogens can have many marked effects when incorporated into dye structures. With the exception of fluorine, they make great leaving groups and the heavier ones, namely bromine and iodine, are adept at promoting intersystem crossing of the excited singlet state into the excited triplet state. Fluorine itself is a remarkable atom when substituted for hydrogen on drugable molecules. Its small size makes it a great mimic of hydrogen and its very strong electronegativity can allow it to impart unique effects on a drug without significantly changing its molecular footprint. Park *et al*. synthesized a series of Nile red analogues with two different polyfluorinated olefin moieties at the 2- and 3- hydroxyl positions. Their series included *N*,*N*-diethyl as well as *N*,*N*-dibutyl substituents at the 9-amino position and *n*-butoxyl / *t*-butoxyl substitutions (not shown) at the 6-position. Only one product is shown for the sake of brevity.[119]

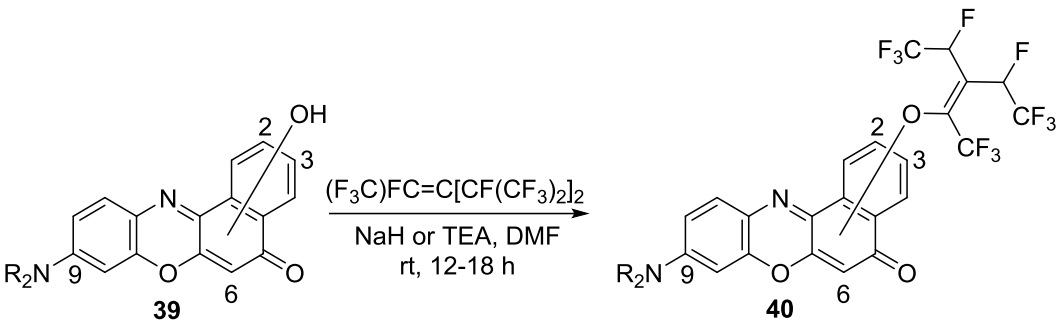

Figure 1.18 Synthesis of Nile red analogues with polyfluorinated ofefin substituent.

Gerasimova *et al*. reported the synthesis of a polyfluorinated Nile red analogue through an *N*-oxide intermediate as shown in Figure 1.19. They started with octafluoronaphthalene and condensed it with 3-(*N*,*N*-diethylamino)phenol. The product was obtained in a modest yield of 24%. The following step used sodium nitrite and acidic condtions followed by oxidation with O_2 gas to generate the *N*-oxide. It was in this step that the yield was abysmally poor with a reported yield of 3%. The final step involved the reduction of the *N*-oxide with zinc under acidic conditions. The overall yield after three steps was a synthetically useless 0.5%.[120]

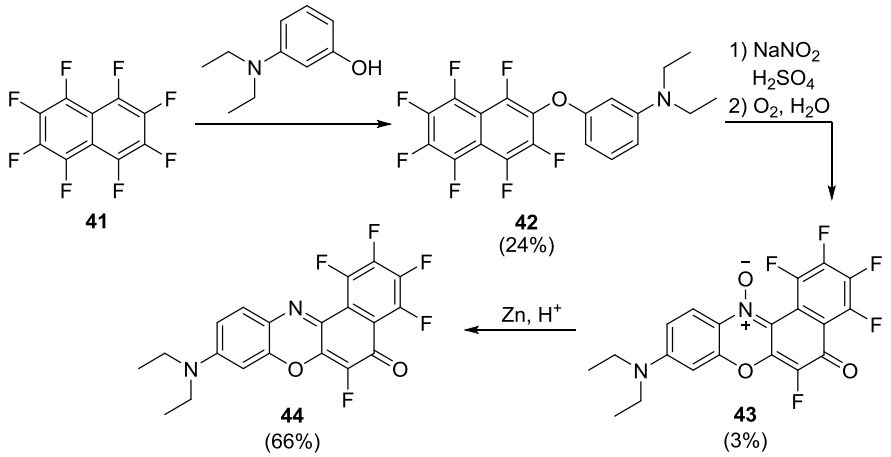

Figure 1.19 Synthesis of polyfluorinated Nile red analogues.

Ektova *et al*. sought to improve the yield of Gerasimova's method and found a different set of conditions that gave the same product in two steps as opposed to three as shown in Figure

1.20.[121] Instead of starting with a completely fluorinated naphthalene, they opted to use the heptafluorinated analogue with a hydroxyl group at the 1-position. This was condensed directly with an already nitrosylated diethylaminophenol in dioxane. Products included both the *N*-oxide (in 37% yield as opposed to 3%) as well as a fully formed benzo[*a*]phenoxazinone dye. Reduction of the pot with zinc under acidic conditions converted remaining *N*-oxide to final dye and had a yield of 90%. Overal yield went from 0.5% to a much more acceptable 55%.

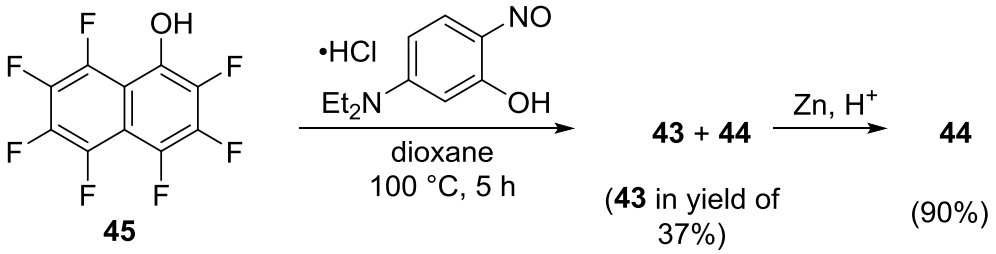

Figure 1.20 Synthesis of polyfluorinated Nile red analogues in higher yield.

1.6.7.2 Chlorinated Nile Blue Derivatives

The literature reports the preparation of some benzo[*a*]phenoxazinium dyes with chlorinated terminals.[122] The syntheses of these compounds is relatively trivial and be accomplished as outlined by the general synthetic method shown in Scheme 1. Of most interest in the synthesis is the use of 1-bromo-3-chloropropane during the alkylation step. Bromine, being a better leaving group will have faster reaction kinetics than the chlorine terminal giving the corresponding chloropropyl substituents off of the amine. These are useful for conjugation to other molecules via simple S_N2 chemistry.

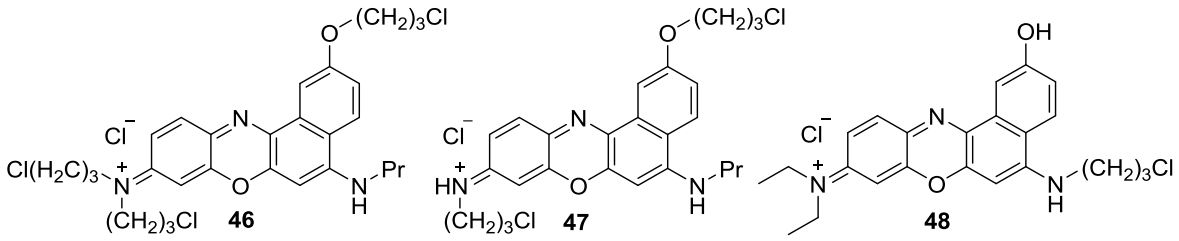

Figure 1.21 Benzo[*a*]phenoxazinium chlorides with chlorinated terminals.

1.6.7.3 Iodinated Nile Red Derivatives

Sherman *et al*. prepared Nile red analogues with iodo substituents for sensing thiols. Nucleophilic thiolate anions will attack the carbon vicinal to iodine in a facile S_N2 reaction.[123] These dyes were created with the thiol-reactive iodine moeity extending off an alyl linker that was either attached via an oxygen at the dye's 2-position or from the nitrogen at the 5-amino position as shown in Figure 1.22.

Dye **49** contains a primary alcohol that caps an alkyl substituted off of the 5-amino position. Stirring of **49** with iodoacetic anhydride in the presence of a strong organic base such as DMAP will give the substition product **50** where the iodo-containing moiety is attached via an ester linkage.

To get the substition off of the 2-position the 2-hydroxy Nile red (**16**) is used. Refluxing of **16** in DMF with *N*-bromoethylphthalimide and potassium carbonate will give dye **51**. Addition of methylamine in MeOH to **51** followed by reflux will afford **52**. The final reaction proceeds with **52** and iodoacetic anhydride in methyline chloride. No further base was added. This afforded dye **53** where the iodine-containing substituent was attached to the linker via an amide.

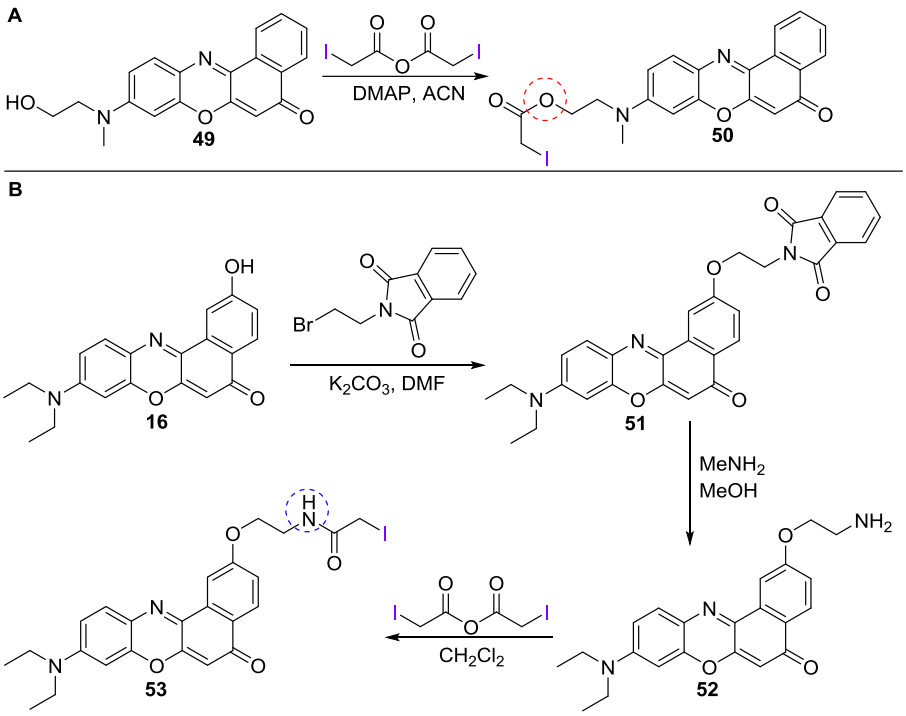

Figure 1.22 Synthesis of Nile red-based thiol sensors. A) Iodo sensor moiety is connected to 9-amino terminal via an ester linkage. B) Iodo sensor moiety is connected at 2-hydroxy position via an amide linkage.

1.6.8 Miscellaneous Syntheses

1.6.8.1 Bridged Naphthoxazinium Dyes

Kanitz and Hartmann prepared a novel set of benzo[*a*]phenoxazinium (and one phenoxazinium) salts. Naphthoxazinium salts are vulnerable to hydrolysis. By incorporating bridged systems either on the amine or on the naphthalene, it was hypothesized that hydrolysis could be prevented or at the very least, reduced. They incorporated a julolidine functionality where normally there is an *N*,*N*-dialkylated amine at the 9-position. One derivative contained a nitrogen heteroatom at the 4-position while another had sulfonamide group appended as a ring fused at the 4-carbon and 5-iminium nitrogen. They also prepared an alkylene-bridged benzophenoxazinium.[124] These are all highly novel and ineresting structures in the benzo[*a*]phenoxazine literature.

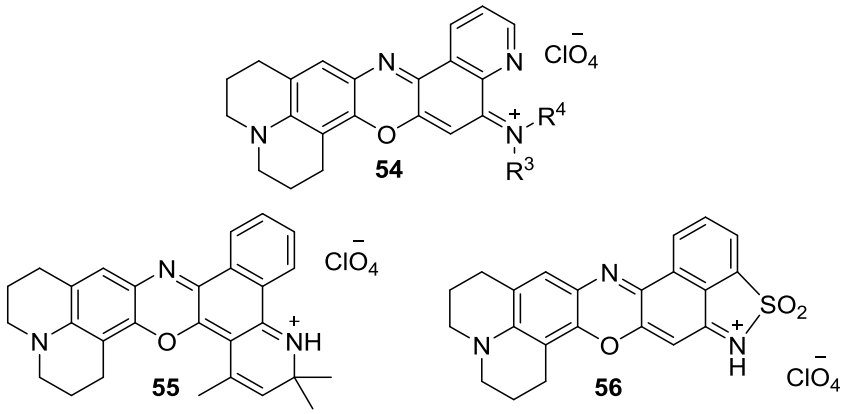

Figure 1.23 Benzophenoxaziniums with julolidine moiety

1.6.8.2 Metalation of a benzo[a]phenoxazinone

Many dyes can chelate metals or have chelating appendages that will cause a dye to undergo optical shifts upon capture of a metal ion. Direct metalation of dyes is much rarer. The only examples of this in the literature were benzo[*a*]phenoxazines metalated directly with mercury (**58**).[125, 126]

Mercuration of the Nile red core proved useful for synthesizing so-called FlAsH dyes (**60**) which use biarsenical ligands to selectively bind to cysteine as shown in Figure 1.24. Since Nile red reports on the local polar environment, they were able to use these dyes to monitor conformational changes in recombinant proteins in live cells upon addition of Ca^{2+}.[125] Further work by Adams *et al*. used biarsenical motif to monitor the formation of tetracysteine *in vitro* and *in vivo*.[127]

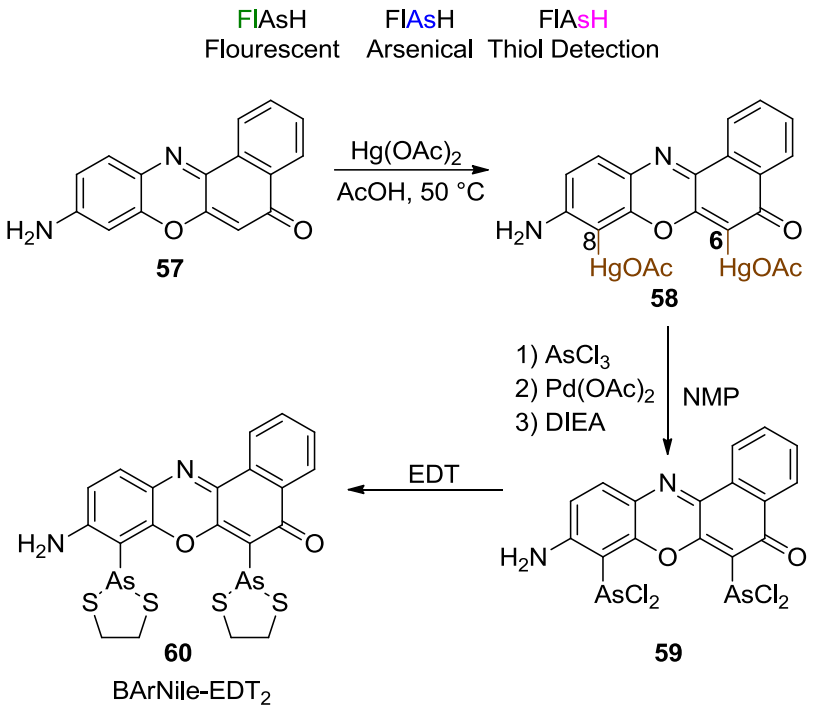

Figure 1.24 Synthesis of Nile red FlAsH analogue.

1.6.8.3 Conversion of oxo to dicyanomethylidine

Changing a carbonyl to either a cyano or dicyanomethylidene has been reported to shift absorbance wavelength bathochromically.[128, 129] For Nile red, this was an attractive option to modulate the scaffold for NIR applications. However, fluorescence no longer occurred even though the λ_{max} shifted from 550 nm to 643 nm.[105] Modification of the 5-oxo group was achieved using malononitrile, titanium tetrachloride and pyridine to afford **61** which has a dicyanomethylidine substituent in place of Nile red's carbonyl. This is shown in Equation 3.

Equation 3 Synthesis of Nile red analogue where the 5-oxo position has been substituted with a methylene dicyano moiety

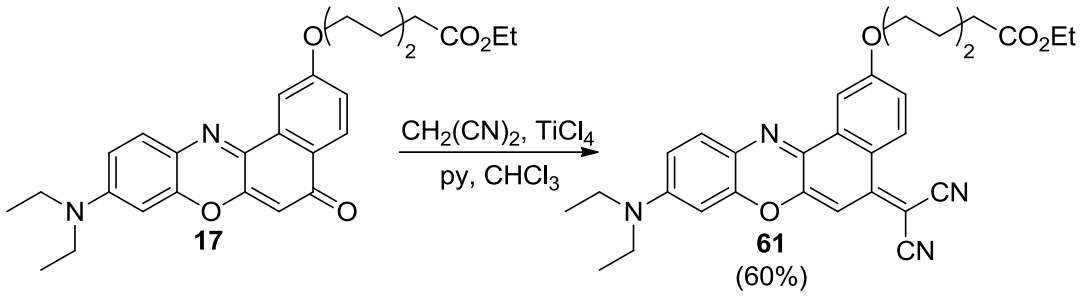

1.6.8.4 Replacement of 7-oxygen with a selenium atom

Foley *et al.* synthesized a short series of Nile blue analogues with varied chalcogen substitution (oxygen, sulfur and selenium) at the 7-position. They then ran a comparative analysis of all three as PDT agents against various bacterial strains to assess antibacterial efficacy. As expected, the selenium analogue outperformed the other candidates due to high triplet quantum yields.[130] The data for this experiment was shown previously in Table 1.1.

As shown in Figure 1.25, synthesis started with *N*,*N*-diethyl-3-iodoaniline being mixed with magnesium turnings in dry ether to form the Grignard reagent. Dry selenium powder was added and allowed to react thoroughly. Then air was bubbled through the flask to give the diselenide product **63**. Nitrosation of **63** was achieved the normal way as described in Scheme 1 to give **64** followed by condensation with *N*-ethylnaphthalen-1-amine to give the final selenium dye **4**.

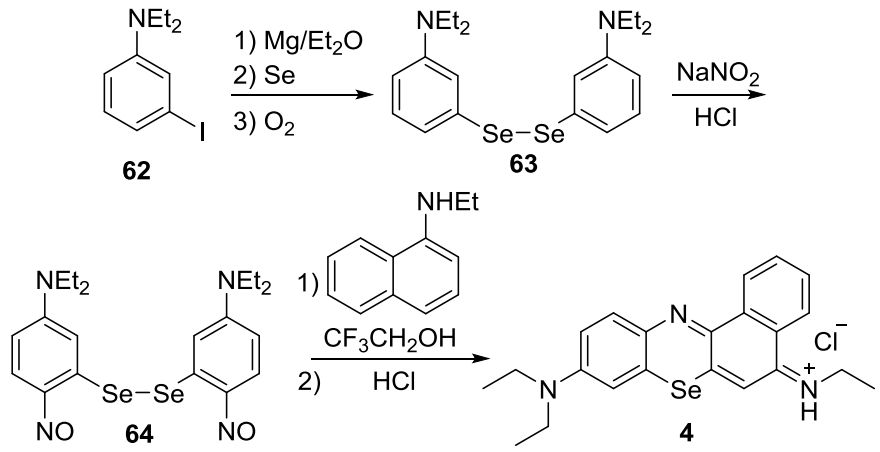

Figure 1.25 Synthesis of Nile blue analogue with the oxygen replaced by selenium.

1.6.8.5 Microwave-assisted synthesis

Microwave heating allows for the rapid increase in temperature of a polar, bulk solvent. Since this kind of heating is caused by rapid polarization of the medium from the oscillating electromagnetic wave, the heat generated is generally uniform and the onset of high temperatures is fast. Conventional heating methods are slow due to a reliance on convection and thermal energy transfer through a glass reaction vessel. This makes the microwave an attractive option for rapidly completing reactions on a smaller scale.

Firmino *et al*. synthesized a series of Nile blue derivatives using conventional heating methods as shown in Figure 1.26. They then optimized the microwave synthesis of a model compound before proceeding with using the best conditions for the subsequent synthesis of their dye series. The best solvent was ethanol and high yields were achieved in three minutes or less of μwave irradiation.[107]

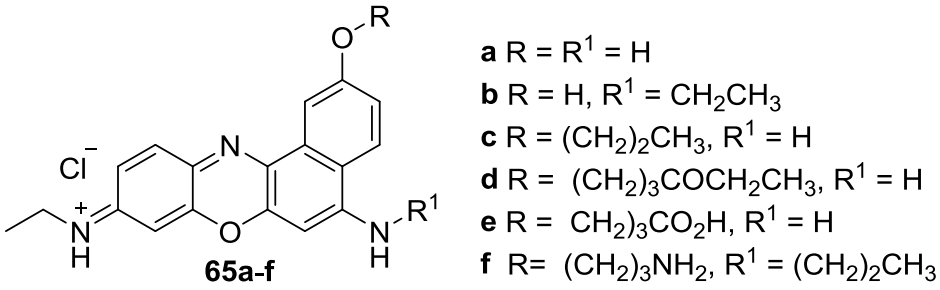

Figure 1.26 Benzo[*a*]phenoxazinium chlorides 65a-f synthesized via microwave irradiation.

Reaction times using conventional heating were varied from as short as nine minutes to as long 280 minutes (over 4½ hours) as is shown in Table 1.2.

Compound	Solvent	Temp. [°C]	Time [min]	Yield [%][a]
65a	EtOH	65	9	96
65b	EtOH	65	280	89
65c	EtOH	65	50	77
65d	EtOH	65	155	34
65e	DMF	70	60	66
65f	EtOH	65	120	60

[a] Isolated yield.

Table 1.2 Synthesis of benzo[*a*]phenoxazinium chlorides **65a-f** by using the conventional heating method.

For the microwave reaction solvent had to be optimized using a model system. Firmino used **65a** as their model dye and irradiation with microwaves gave the best results—highest yields and shortest times—in ethanol as shown in Table 1.3.

Solvent	Temp. [°C]	Time [min]	Yield [%][a]
None [b]	90	10	NR
MeCN	90/120	8/40	59
DMF	90	5	41
EtOH	90	3	97
EtOH	90	1	68
H_2O	90	—	NR

[a] Isolated yield; NR: no reaction. [b] Solvent-free (silica support).

Table 1.3 Optimization reaction studies of nitrosophenol 27 with 1-amino-6-hydroxynaphthalene under microwave conditions

Using their previously established microwave conditions, all of their Nile blue analogues (**65a-f**) were synthesized again in three minutes or less with the lowest yield being 75% as shown in Table 1.4. These are remarkably efficient results and researchers hoping to synthesize phenoxazine dyes in the future would be wise to incorporate microwave synthesis into their protocols.

Compound	Solvent	Time [min]	Yield [%][a]
65a	EtOH	3	97
65b	EtOH	1.3	93
65c	EtOH	1.3	90
65d	EtOH	2	86
65e	DMF	—	NR
65f	EtOH	2.5	75

Table 1.4 Synthesis of benzo[*a*]phenoxazinium chlorides **65a-f** by microwave irradiation at 90 °C.

1.6.8.6 Ultrasonic Synthesis

Sonication of a sample is another method of achieving rapid energy transfer into a reaction vessel. Pulses of ultrasonic radiation can generate large mechanical loads onto a molecule and in some cases can be strong enough to overcome the activation energy barrier required to initiate a reaction.

Ragu *et al*. reported synthesizing a series of Nile blue derivatives using ultrasound as shown in Figure 1.27.[131] Reaction times for dye formation were three times faster (**66b**, **66c**, **66f**) up to as high as seven times faster (**66g**) as seen in Table 1.5. Even on the low end of reaction speed, the rates were still significantly higher. Product yields were barely affected except for **66b** which showed a large increase in yield from 53% to 93%. For their conventional methods, they re-fluxed the reagents in ethanol/HCl.

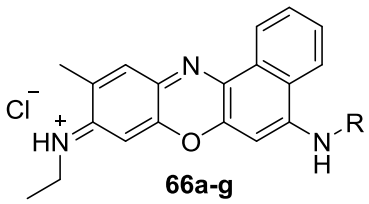

66a-g

a: R = $CH_2CH_2CH(CH3)_2$
b: R = $CH_2CH_2(C_6H_{11})$
c: R = $CH_2CH_2(C_6H_5)$
d: R = $CH_2CH_2CH_2COOH$
e: R = $CH_2CH_2CH_2COOEt$
f : R = $CH_2CH_2CH_2OH$
g: R = H

Figure 1.27 Dyes prepared via sonication

Dye	Reaction Time (min)		Yield (%)	
	Conventional	US	Conventional	US
6a	480	90	96	90
6b	290	90	53	93
6c	270	90	78	91
6d	480	105	75	91
6e	450	300	40	NR
6f	180	64	97	95
6g	540	75	80	86

Table 1.5 Reactions times and yields for the synthesis of dyes 66a-66g (Scheme 17) using conventional heating methods versus ultrasound (US).

1.7 Sensors

1.7.1 Metal Sensors

Hu *et al*. developed a Nile blue-based chemodosimeter for Hg^{2+} ions in aqueous solution. The Nile blue sensor undergoes a hypsochromic shift from 650 nm to 576 nm and has its fluo-

rescence quenched in the presence of Hg^{2+} ions.[132] The authors claim that the mercury-induced intramolecular reaction is what caused the quenching and that it was not complexation of the mercury ion with the chromophore. We dispute this claim as there is nothing about structure **68** that suggests it would not fluoresce. We propose that mercury is both causing the reaction and complexing with product to quench fluorescence and more evidence is needed to substantiate the authors' claims.

As shown in Figure 1.28, compound **67** will capture the Hg^{2+} ion with the sulfur atom. This activates the carbon vicinal to the sulfur for intramolecular nucleophilic attack from the 5-amino group. This intermediate will rearrange forming a five-membered ring and subsequently elimi-nates the sulfur-mercury complex to give **68**.

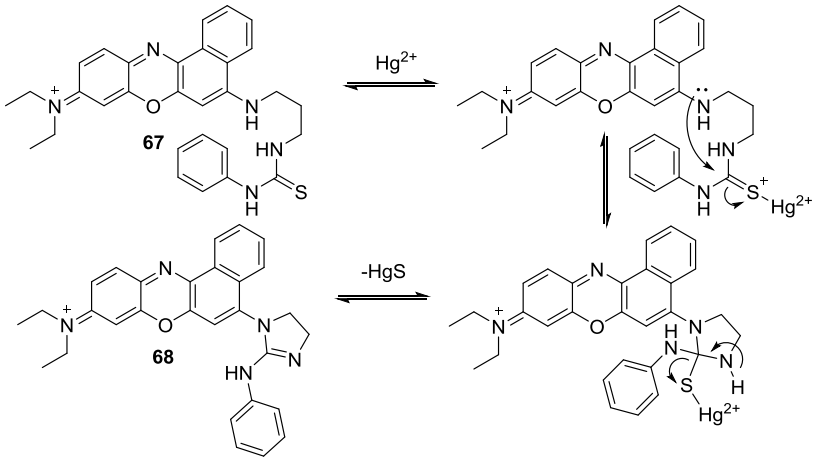

Figure 1.28 Proposed mechanism for mercury-induced rearrangement.

1.7.2 pH Sensors

Madsen *et al*. developed a Nile blue-based pH sensor for *in vivo* imaging.[133] They cited an issue in the literature with a lack of effective probes for monitoring the pH in the interstitial fluid between cancer cells. Most probes would penetrate into the cell and report on the pH of in-tracellular fluid. They developed Nile blue labeled PMPC-PDPA diblock copolymers that would self-assemble into vesicles.

Nile blue is protonated at the 5-amino position. Deprotonation of this position in base will generate a neutral dye that has significantly different optical properties than its charged counterpart. This is because the charged iminium acceptor is changed to an amino donor. Without a donor-acceptor system, the ICT transfer band increases in energy giving a large hypsochromic shift.

As shown in Figure 1.29, Nile blue is mixed with methacrylic anhydride and triethylamine (TEA). TEA will deprotonated the 5-imino group, converting it into a nucleophile. This will attack the anhydride and eliminate the ester. Workup in dilute hydrochloric acid will regenerate the dye as the HCl salt **69** (the Nile blue methacrylamide or NBM). Dye **70** was created under identical conditions and workup but used a carbamate instead of an anhydride to give a urea linkage. This is the Nile blue 2-methacryloyloxyethyl carbamate or NBC.

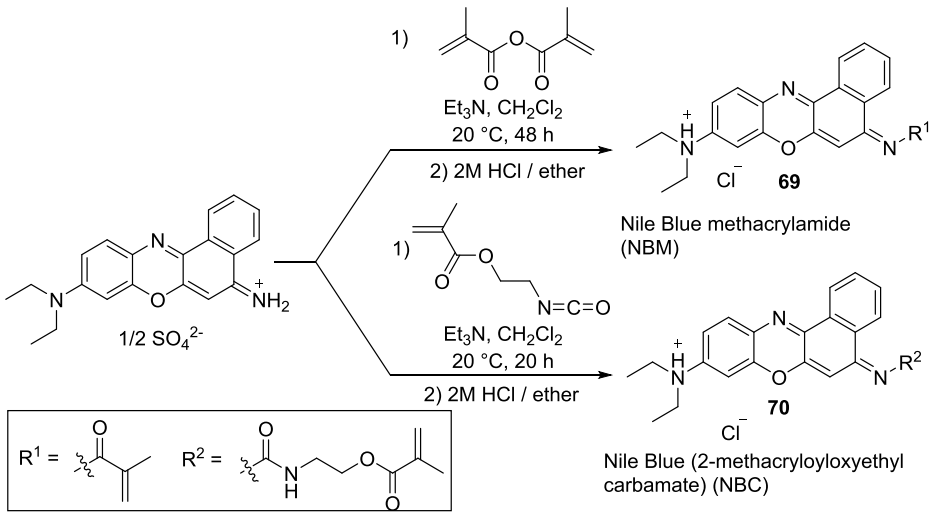

Figure 1.29 Synthesis of Nile blue-based comonomer.

The PMPC-PDPA diblock copolymers were generated with a bromine on the terminal to function as a leaving group. As seen in Equation 4, Nile blue, NBM and NBC will all attack and substitute at this position to become fully conjugated to the polymer (**72**).

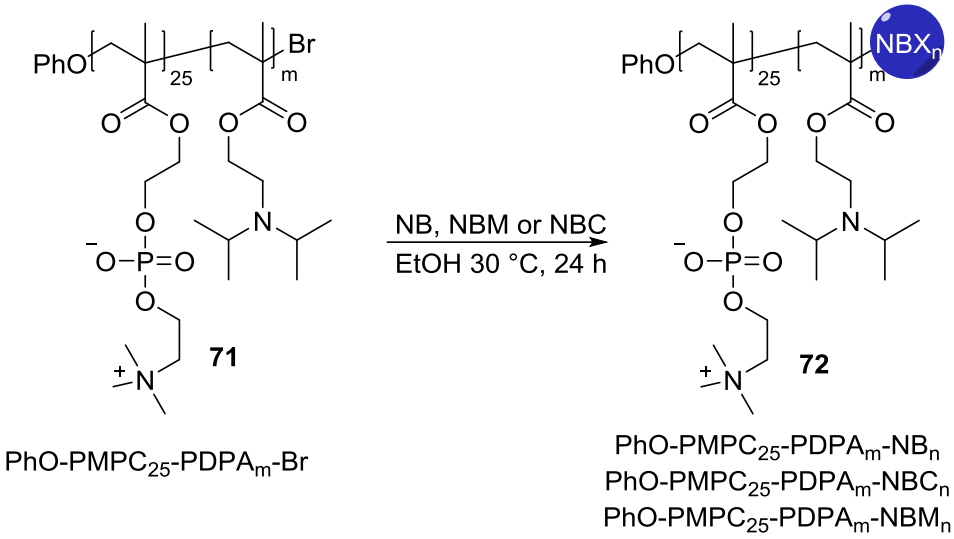

Equation 4 Synthesis of PMPC-PDPA diblock copolymers terminated with either Nile blue (NB) alone containing a Nile blue-based comonomer (either NBM or NBC).

1.7.3 Biological Sensors

1.7.3.1 Lysotracker

A Nile blue sensor with a morpholine substituent (NBM) was prepared by Fan *et al*. using the general synthetic method described in Figure 1.9.[134] The morpholine acted as the targetable group that allowed the dye to bind to lysosomes. The morpholine substitent was substituted onto 1-aminonaphthalene using 4-(2-chloroethyl)morpholine and cesium carbonate as the base as shown in Figure 1.30.

Nile blue was chosen as an alternative to other probes due to its NIR absorption and emission profile, high extinction coefficient/quantum yield, and good stability against photobleaching. It was demonstrated that NBM was a viable lysotracker by using it to observe morphological changes to lysosomes during cell apoptosis as well as the production of lysosomes during cell division.

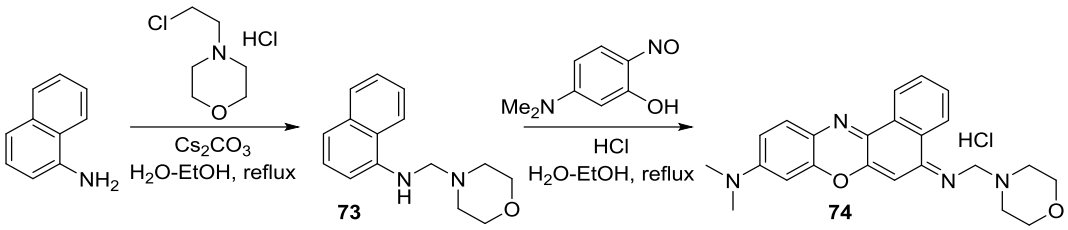

Figure 1.30 Synthesis of Nile blue morpholine (NBM)

1.7.3.2 Hydrogen Sulfide Sensor

Another method for sensing hydrogen sulfide was investigated by Liu *et al.* They utilized a 2,4-dinitrobenzene moiety by conjugating it to the dye scaffold (either Nile red or Nile blue) in order to quench fluorescence. In the presence of hydrogen sulfide, the group is cleaved resulting in a return of fluorescence.[135] The use of the 2,4-dinitrophenyl ether for sulfide sensing is relatively new to the chemical literature and had not been applied to a benzo[*a*]phenoxazine architecture.[136,137,138]

As shown in Figure 1.31, the nitroso salt can be condensed with either an aminonaphthalene or a hydroxynapththalene as originally described in Scheme 1 to give dyes **75** or **77** respectively. Refluxing these dyes in DMF with 1-bromo-2,4-dinitrobenzene and potassium carbonate will cause the substitution of the dinitrophenyl group at the 3-hydroxy position. This quenching moiety is susceptible to attack from hydrogen sulfide.

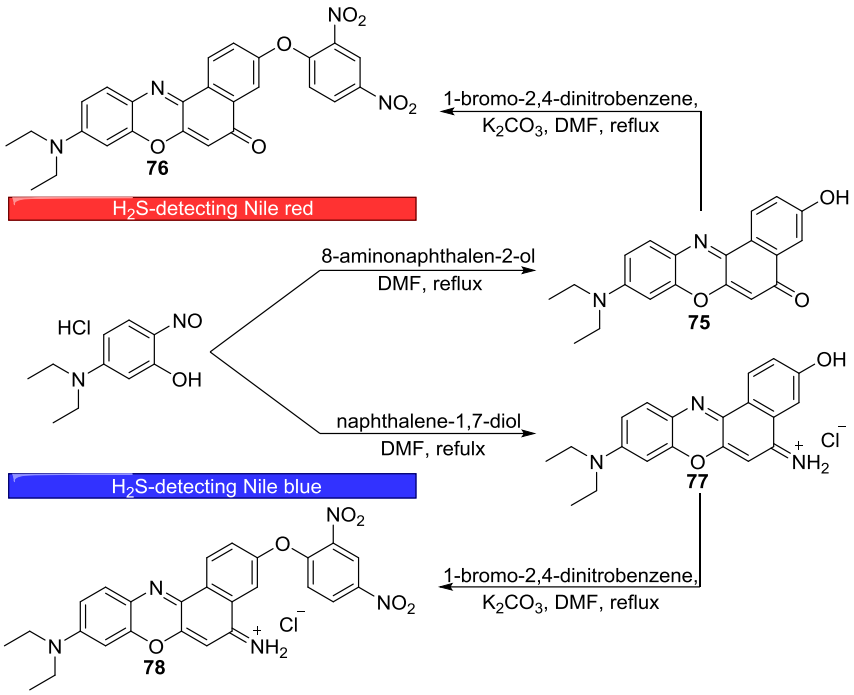

Figure 1.31 Synthesis of hydrogen sulfide detecting benzo[*a*]phenoxazine systems.

2 SYNTHESIS, OPTICAL CHARACTERIZATION AND BINDING STUDIES OF NOVEL BENZO[A]PHENOXAZINE DYES

2.1 Introduction

Popular dye structural motifs such as the BODIPY, squaraine, rhodamine and carbocyanine fluorophores have been explored exhaustively for their ability to act as visual reporters for a large variety of chemical processes and cross-platform applications.[31-33, 35]. Another classic dye structure, the benzophenoxazine, has attracted considerable interest in recent years. Benzophenoxazine dyes consist of a chemically robust, polycyclic aromatic core and are typically characterized by strong absorption of visible light and high fluorescence quantum yields in apolar media.

In the benzophenoxazine family of dyes, Nile red and Nile blue are popular due to their high fluorescence quantum yields and optical sensitivity to their local solvent environment. These compounds were first synthesized in 1896 by Möhlau and Uhlmann and have since been appropriated for a variety of histological applications.[36, 75, 76, 106]

Nile red is a powerful solvatochromic and thermochromic reporter. It is highly lipophilic and as such it is poorly soluble in water. To rectify this problem, work has been done to append water soluble moieties to the dye scaffold. Solubilizing the dye in aqueous media causes optical spectra to undergo a 100 nm bathochromic shift into the near infrared spectrum.[39, 139] Nile blue, is a cationic dye with much better water solubility than Nile red. It is highly susceptible to changes in pH and this makes it a great pH reporter. Nile blue has an iminium functional group that acts as a potent electron acceptor. Subsequent intramolecular charge transfer through the chromophore's D-π-A system results in an 80 nm bathochromic shift in absorbance compared to Nile red.

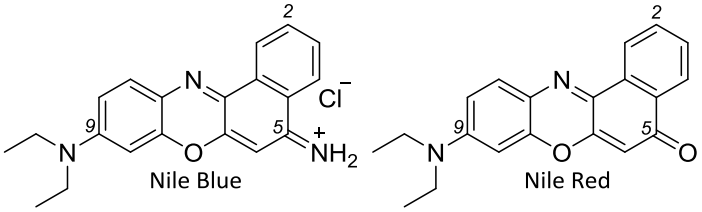

Figure 2.1 Nile blue and Nile red dyes; convenient positions for structural modification are at the 2-carbon and 9-amine. The 5-imine on Nile blue is also an option for modification.

Since both the Nile red and Nile blue dye scaffolds have biologically useful NIR absorption bands when solvated in aqueous media, they could potentially be used for a variety of imaging applications. An imaging agent that offered inspiration for this project was oxazine-4, an amino-phenoxazineiminium dye containing secondary amino substituents. It showed a remarkable ability to target and bind to nerves.[29] Benzo[*a*]phenoxazine dyes contain one more fused benzene ring than phenoxazine systems. By mimicking the secondary amine from oxazine-4, perhaps another nerve-binding agent can be constructed?

Before *in vivo* work can be started, a comparative study of optical properties and protein—ligand affinities between Nile red and Nile blue derivatives must be undertaken. It was the aim of this study to synthesize analogous sets of Nile red and Nile blue derivatives with both tertiary and secondary amino substituents at the 9-position. Hydrophobicity was modified by appending alkyl groups of different sizes to the amine. Optical properties were investigated to understand how amino substituents modulate the chromophore. Human serum albumin (HSA), the most abundant transport protein in the blood was chosen as a model biological system. HSA—dye binding affinities were investigated and compared against calculated distribution coefficient values (log*D*) to find viable dye candidates for *in vivo* applications.[†]

[†] Analytical work with HSA was conducted by our collaborator Eman Alsolmy from the Patonay group.

2.2 Experimental Overview

2.2.1 General

All starting reagents used were obtained commercially from major chemical suppliers and were not purified before use. All ^{1}H NMR and ^{13}C NMR data were obtained on a Bruker Avance 400 spectrometer. HRMS data were obtained on a Waters Micromass Q-TOF mass spectrometer coupled with a Waters 2695 HPLC. Fatty acid free human serum albumin (≥ 96% purity) was obtained from Sigma-Aldrich (St. Louis, MO). DMSO was obtained from Acros Organics (99.9%) (Belgium) and methanol was obtained from Sigma-Aldrich (≥ 99.9%) (St. Louis, MO). Sodium phosphate monobasic and sodium phosphate dibasic were obtained from Aldrich Chemical Company (Milwaukee, WI). Absorbance spectra were acquired using a Cary 3G UV-visible spectrophotometer (Varian Inc., Palo Alto, CA) interfaced to a PC. Fluorescence spectra were achieved using a K2 Spectrofluorometer (ISS Inc., Champaign, IL) interfaced to a PC. Excitation was achieved using a Xenon Arc lamp, model PS 300-1, (ILC Technology Inc., Sunnyvale, CA). Spectroscopic studies were performed in disposable plastic cuvettes and binding studies were performed in quartz cuvettes, both with a path length of 1 cm. Nanopure water was obtained using an ELGA Purelab Classic water purification system.

2.2.2 Preparation of 3-amino-4-methylphenol

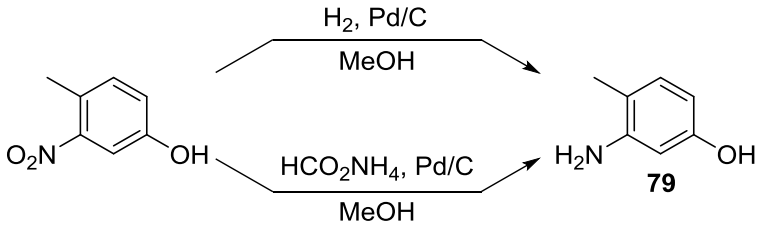

Figure 2.2 Multi-route catalytic reduction of 4-methyl-3-nitrophenol to 3-amino-4-methylphenol.

4-Methyl-3-nitrophenol (15 g, 98 mmol) was dissolved in 50 mL of MeOH. A catalytic amount of palladium on carbon was added. The flask was degassed and then put under hydrogen atmosphere three separate times to ensure the removal of oxygen. The reaction was run at room temperature for four days with hydrogen supplied via balloon. The balloon was changed several times over the course of the reaction. The reaction was followed by TLC until completion. Product (**79**) was filtered over a Celite pad in a Buchner funnel to remove catalyst. The filtrate was concentrated on a rotary evaporator to recover the product (95% yield.) No further purification was needed. A second route was also used for further synthesis of compound **79** as shown in Figure 2.2. Ammonium formate with palladium on carbon will transfer hydrogen to the molecule being reduced. This is most effective if refluxed in MeOH but care must be taken to keep the condensers clean. Ammonium formate will sublime and then deposit in the base of the condenser. This can cause blockage which, with the constant evolution of hydrogen gas, can cause dangerous complications if not taken care of promptly.

2.2.3 Preparation of 3-(dialkylamino)phenols and 3-(alkylamino)phenols

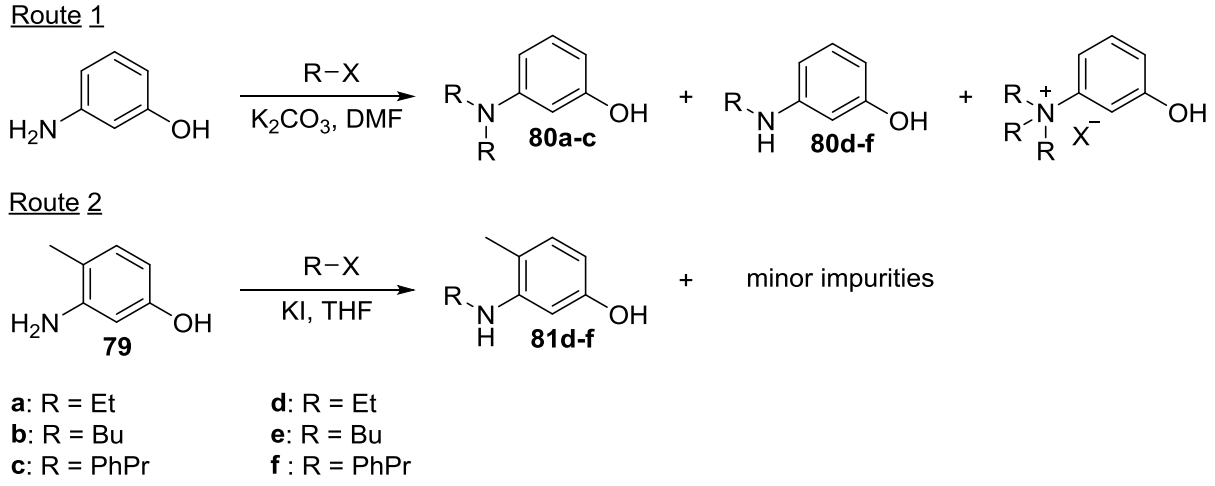

Figure 2.3 Synthesis of *N*-alkylated 3-aminophenols

All of the alkylated 3-aminophenols (**80a-f**), with the exception of the 4-methyl substituted ones, were prepared by first dissolving 3-aminophenol in DMF. Stoichiometric amounts of finely powdered K_2CO_3 were added (1:1 for mono-substitution, 2:1 for di-substitution) and the system was mixed rapidly and heated to 50 °C. The alkyl halides were all liquids and were added dropwise. Reactions were monitored by TLC until completion. Compounds **81d-f** were prepared in a similar manner but using dry THF as the solvent and using KI as a catalyst instead of base. Iodide is weakly nucleophilic and can act as a catalyst. Very little of the dialkylated products were formed using this procedure.

Reaction workup proceeded by first removing all solvent under reduced pressure. The products, which were all oils, were then taken up in DCM and filtered to remove salts. The reaction mixtures were all purified using column chromatography on normal phase silica and eluting with various compositions of EtOAc/Hexanes.

2.2.4 Synthesis of nitrosylated intermediates

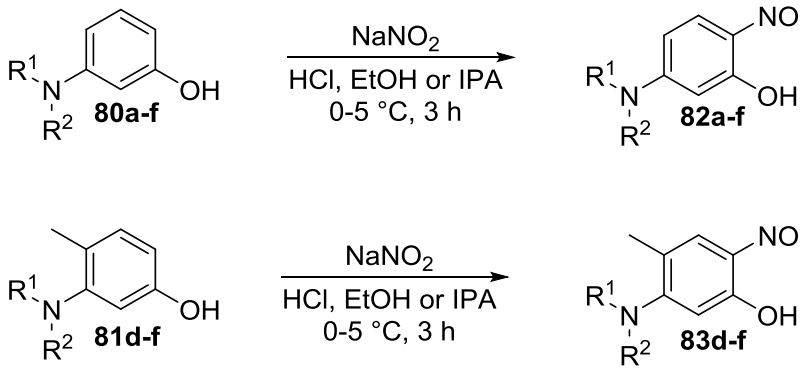

Figure 2.4 Nitrosation of an *N*-alkylatedaminophenol.

All nitrosation reactions were conducted in the same manner as shown in Figure 2.4. An alkylated aminophenol was dissolved in EtOH or IPA and a molar excess of HCl was added. The entire system was cooled on an ice bath. Sodium nitrite (1.2 mol. eq.) was dissolved in 2 mL of DI water and very carefully added dropwise to the reaction flask over 15-20 min. The reaction was allowed to stir for an additional 2-3 h on the ice bath.

Solvent was removed under reduced pressure and the reaction residues were taken up in EtOH and filtered to remove inorganic salts. Nitroso products are unstable and were dried used in the next step without further purification. They were stored in a refrigerator when not being used.

2.2.5 Synthesis of benzo[a]phenoxazinone and benzo[a]phenoxazinium perchlorate dyes

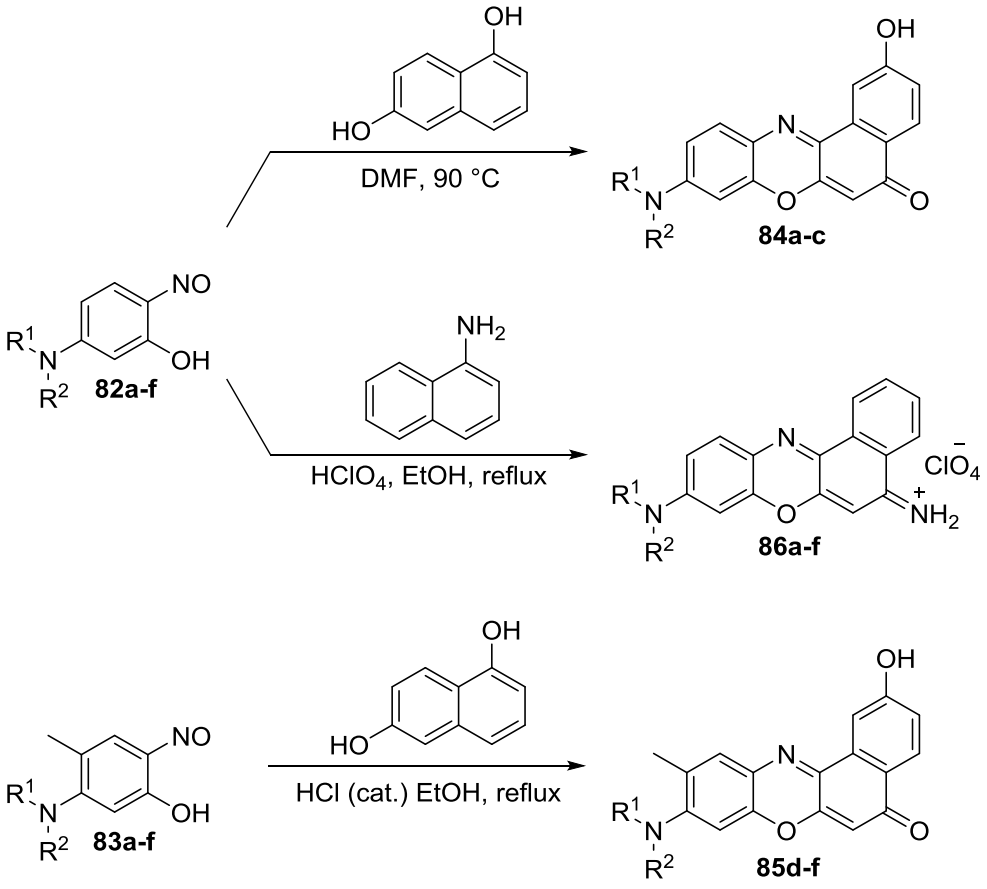

Figure 2.5 Synthesis of Nile red and Nile blue derivatives

Dialkylated Nile red derivatives (**84a-c**) were prepared by dissolving the nitrosylated precursor in DMF with 1,6-dihydroxynapthlene in 1:1 stoichiometric ratios. The solutions were heated to 90 °C for several hours. Dye formation was confirmed visually and the reactions were halted when UV-Vis spectra showed only the dye peak at 550 nm and the nitroso peak at 400 nm had completely disappeared. Monoalkylated Nile red derivatives (**85d-f**) were prepared the same way except using ethanol instead of DMF as a solvent and adding catalytic amounts of HCl. All

Nile blue derivatives (**86a-f**) could be prepared by refluxing the nitroso and aminonaphthalene precursors in ethanol with perchloric acid.

2.2.6 Spectroscopic studies of dyes

2.2.6.1 Determination of molar absorptivity

Serial dilutions of each dye were prepared in DMSO and methanol with concentrations ranging from 0.2×10^{-5} – 1.60×10^{-5} M. It was achievable to determine the molar absorptivity values in 20 mM phosphate buffer pH 7.2 for some monoalkylated dyes specifically **86a** and **86b** in the same concentration range. All working solutions in methanol and phosphate buffer contained only 1.6% (v/v) DMSO to facilitate dye dissolution. The maximum wavelength of absorption (λ_{Abs}) of each dye was determined. The molar absorptivity values of each dye were determined using Beer's law. Duplicate absorbance measurements were obtained, and the average molar attenuation values were reported.

2.2.6.2 Determination of quantum yield

Serial dilutions of each dye were prepared in DMSO and methanol with concentrations ranging from 0.2×10^{-6} – 1.60×10^{-6} M, at concentrations diluted tenfold more than the absorbance measurements in which the absorbance values were below 0.1 units to avoid inner filter effects or self-quenching. Quantum yields values were determined in 20 mM phosphate buffer at pH 7.2 for some monoalkylated dyes, particularly Nile blue derivatives **86d** and **86e** in the same concentration range. All working solutions in methanol and phosphate buffer contained only 1.6% (v/v) DMSO to facilitate dye dissolution. The relative method was used to determine quantum yield values for all dyes using Nile blue as a standard and applying the equation:

$$\Phi_S = \Phi_S \left[\frac{\text{Slope}_S}{\text{Slope}_{STD}}\right]\left[\frac{\eta^2{}_{STD}}{\eta^2{}_{STD}}\right]$$

Where Φ_S and Φ_{STD} are the quantum yield of the sample and the standard, slope $_S$ and slope $_{STD}$ are the slopes of plotting the area under the emission curve as a function of the absorbance value at excited wavelength of the sample and the standard. η_S and η_{STD} are the refractive index of solvent of the sample and the standard. Duplicate measurements were obtained, and the average quantum yield values were reported. All solutions in DMSO were excited at 580 nm and in methanol and phosphate buffer were excited at 560 nm. The excitation wavelengths were chosen to ensure the full integration of emission peaks, especially for the monoalkylated derivatives since they are blue shifted compared to dialkylated derivatives.

2.2.7 HSA binding interaction with Nile derivatives

The initial investigation of binding interactions between HSA and the dye involves using fluorescence spectroscopy to monitor a fixed concentration of the dye itself in buffer first. Then the same concentration of the dye is mixed with a similar concentration of the protein assuming 1:1 stoichiometry in buffer. The dye concentration is determined by which the absorbance value should be below 0.1 units to avoid inner filter effects or self-quenching. Using fluorescence spectroscopy allows for observing any changes that might occur in the maximum wavelength of emission (bathchromic or hypsochromic shift) or in fluorescence intensity (hyperchromic or hypochromic shift) after interactions between the dye and the protein. For Nile blue derivatives, 2.0×10^{-6} of the dye in 20 mM phosphate buffer pH 7.2 was recorded first. Then, 2.0×10^{-6} of the dye with 2.0×10^{-6} of HSA in 20 mM phosphate buffer pH 7.2 was recorded. To confirm the HSA—dye binding ratio, Job's method was used to identify the stoichiometry as discussed in the following section.

2.2.7.1 Determination HSA-dye stoichiometry using Job's method

Job's method or the method of continuous variation is used to determine the stoichiometry of the predominant complex when multiple interactions can occur. This method includes varying the number of moles for the protein and the dye whereas the total concentration of the solution remains constant. Fluorescence spectroscopy can be used to identify this predominant complex which is corresponding to maximum fluorescence intensity as a function of the mole fraction of HSA. Thus, variation of the number of HSA moles resulted in a maximum mole fraction of 0.50 for the dialkylated dyes (NB, **86a**, **86b**, and **86c**) complexes, which corresponded to 1:1 stoichiometry of HSA—dye complex. For the monoalkylated dyes, Job' method provides another evidence that these dyes did not bind to HSA. The total concentration of HSA—dye complex was 4.0×10^{-6} M.

2.2.7.2 Effect of time on HSA—Dye complex

The effect of time on solution containing 2.0×10^{-6} M of dye and 2.0×10^{-6} M of HSA was studied in 20 mM phosphate buffer pH 7.2. The reaction was monitored by recording the fluorescence intensity every 5 minutes for 30 minutes at room temperature.

2.2.7.3 Determination binding constant using Scatchard plot

The HSA binding interaction with NB, 8**6a**, 8**6b** and 8**6c** were studied by titrating a fixed concentration of dye (2.0×10^{-6} M) with different micromolar concentrations of HSA in 20 mM phosphate buffer pH 7.2. All working solutions contained only 1% (v/v) DMSO to facilitate dye dissolution and more importantly to avoid HSA denaturation. The HSA—dye complex was vortexed for 30 seconds and then left five minutes to allow enough time for it to reach equilibrium. Duplicate measurements were obtained, and the average binding constant values were reported. To determine the binding constant of the HSA—dye complex, the complex formation was evalu-

ated using Scatchard's method. The concentrations of the different reaction species were measured at equilibrium. Applying the equation,

$$\text{Dye} + \text{HSA} \rightleftharpoons \text{Dye—HSA}$$

and assuming 1:1 reaction stoichiometry

$$K = \frac{[\text{Dye—HSA}]}{[\text{Dye}][\text{Dye}]}$$

the binding constant (K) is determined from the linear fit of the data of the fluorimetric titration of a fixed concentration of dye with HSA according to equation:

$$\frac{1}{\Delta F} = \frac{1}{k[\text{Dye}]} + \left(\frac{1}{k[\text{Dye}]K}\right)\frac{1}{[\text{HSA}]}$$

Where ΔF represents the change in emission intensity of the HSA—dye complex, k is a constant dependent on the quantum efficiency of the process and the instrumentation. A plot of the reciprocal of ΔF versus the reciprocal of HSA concentration gives a straight line relationship that intersects the x-axis. The binding constant is calculated by dividing the intercept by the slope of the line.

2.3 Results and Discussion

2.3.1 Synthesis of Nile Red Analogues 84a-c and 85d-f.

The syntheses of the Nile red analogues **84a-c** and **85d-f** are illustrated in Figure 2.5. The starting materials used for the synthesis depended on the degree that the 9-amino position was to be substituted. For the tertiary amine-containing dyes, the first reaction was an alkylation of 3-aminophenol. Alkylating agents used were iodobutane and 1-bromo-3-phenylpropane. 3-(*N*,*N*-diethylamino)phenol was available commercially. Alkylations were conducted in DMF at 70 °C in 2:2:1 molar equivalents of potassium carbonate, alkylating agent, and 3-aminophenol respec-

tively. After TLC showed full consumption of the starting reagents, workup of the mixture consisted of first removing all solvent under reduced pressure. The oily residues were then taken up in ethanol, filtered to remove salts, and then loaded onto silica for purification. All of these alkylated aminophenols were purified on columns using normal phase silica and ethyl acetate/hexanes solvent systems.

The next step was nitrosation of the alkylated amino phenols para to the amino position via Fischer-Hepp rearrangement.[98, 140] The starting material was dissolved in ethanol and concentrated HCl was added carefully. The system was then cooled on an ice bath. Sodium nitrite (1.2 mol. eq.) was dissolved in water and added slowly over 20-30 min. The reaction was kept stirring and cold for 3 hours afterwards. Solvent was then removed under reduced pressure until all water was pulled off with special care taken not to heat the system over 50 °C. Overheating would decompose the nitroso compound and the contents of the flask would turn first green, then blue. It is most likely that the nitroso salts react with each other at elevated temperatures to form some sort of azo dye. The compound was then taken up in ethanol and filtered to remove salts. Solvent was removed again under reduced pressure to yield solid, yellow nitroso hydrochloride salts.

Dye formation was achieved via a condensation reaction between the nitroso salts and 1,6-dihydroxynaphthalene in a 1:1 mole ratio. Reactants were heated to 90 °C in DMF until UV-Vis showed the disappearance of the nitroso peak (~400 nm). DMF was then removed under reduced pressure and the dye was taken up in a small volume of ethanol. Solubility of the dyes was sparing in this solvent. Vacuum filtration of the mixture gave spectroscopically clean dyes that needed no further purification.

Synthesis of Nile red analogues with a secondary amine presented a different challenge because alkylation of 3-aminophenol would be driven to higher degrees of substitution forming ter-

tiary and quaternary amines/ammonium salts. To combat this, 4-methyl-3-aminophenol was used where the methyl group would act as a steric blocker, slowing down kinetics for subsequent, unwanted alkylations. This compound was prohibitively expensive so 3-nitroaminophenol was purchased and then reduced to the corresponding amine using palladium on carbon and hydrogen gas.

In order to further protect the amine, alkylations were conducted in THF using catalytic amounts of potassium iodide and one molar equivalent of alkylating agent to aminophenol. Workup and purification as well as nitrosation were conducted in the same fashion as previously stated.

Dye formation was achieved as previously stated except that ethanol was used instead of DMF and catalytic amounts of HCl were added. The reaction mixture was refluxed until complete as verified by UV-Vis spectroscopy. Workup and purification were the same as for the previous dyes.

2.3.2 Synthesis of Nile Blue Analogues 86a-f.

Compounds **82a-f** described previously were used to make **86a-f**. Condensation of 1-aminonaphthalene with **82a-f** were carried out in ethanol and slight molar excess of perchloric acid in a sealed tube at 90 °C. Compounds **86a-f** are only slightly soluble in cold ethanol and can simply be filtered to yield a product of high purity.

2.3.3 Proposed mechanism of dye formation.

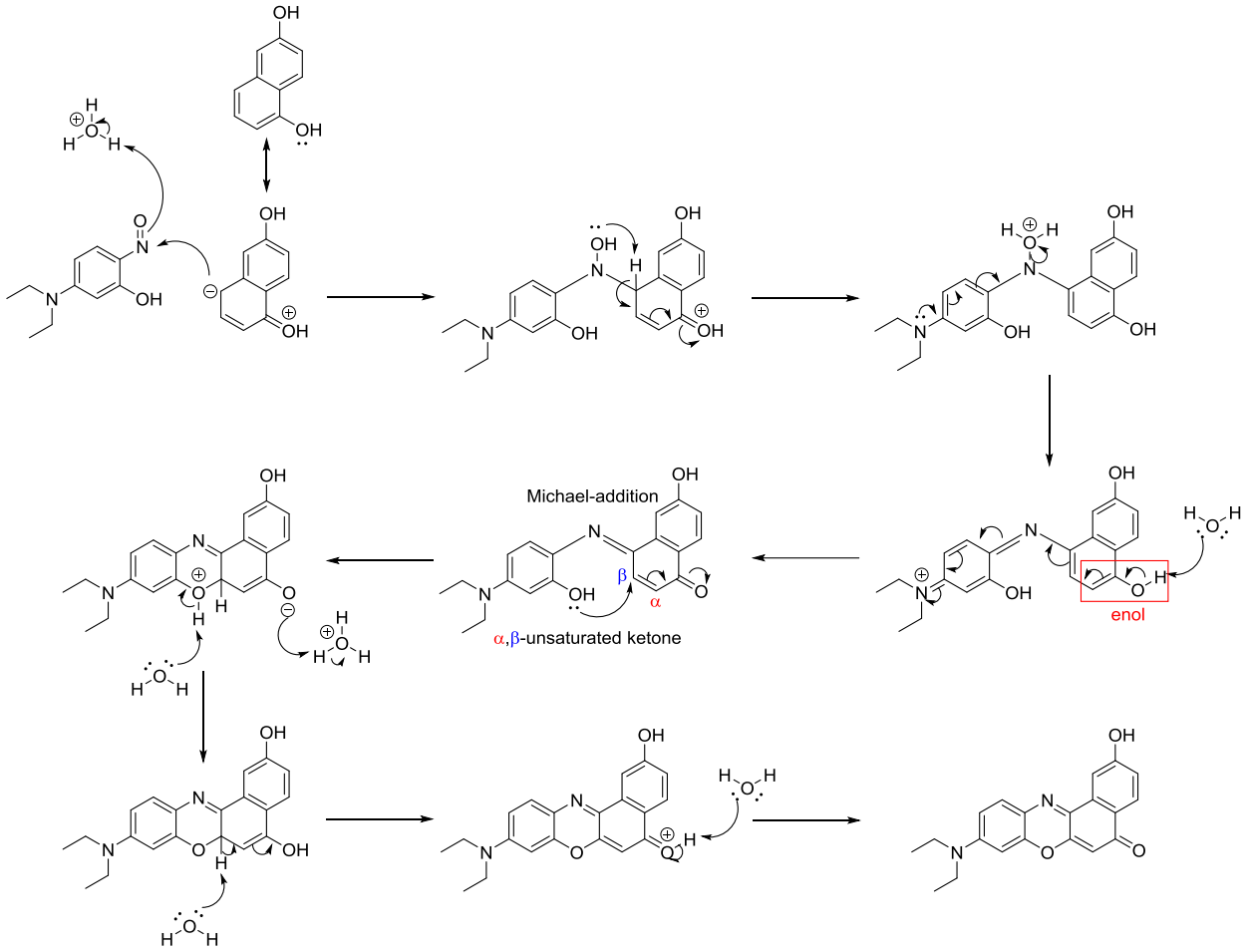

Figure 2.6 Proposed mechanism for the formation of Nile red via condensation of an aromatic nitroso compound with 1,6-dihydroxynaphthalene in catalytic amounts of acid.

Dye formation is the product of an acid-catalyzed condensation reaction between a nitroso precursor and 1,6-dihydroxynaphthalene or 1-aminonaphthalene. A mechanism for this reaction has been proposed. The first step is nucleophilic attack by the carbon para to the 1-hydroxy position on the dihydroxynaphthalene to the nitrogen on the nitroso group. The oxygen on the nitroso group resembles a carbonyl with its double bond and should make the nitrogen more electrophilic. After the attack, the electrons in the double bond will move to the oxygen and will readily receive a proton from an acid.

The resulting intermediate is no longer aromatic and is carrying a positive charge on the 1-hydroxy position. Intramolecular proton transfer from the previously nucleophilic carbon to the *N*-hydroxyl group will allow restoration of aromaticity. The diethylamine will donate electrons into the conjugated system causing water to leave what had been the nitroso nitrogen.

The enol on the right side of the molecule can be deprotonated by water and will tautomerize to a ketone. The cascading electron push will neutralize the positive charge on the diethylamine. The ketone is very similar to an α,β-unsaturated system and should cause the β carbon to act as a Michael acceptor. The Michael donor will be the phenolic oxygen on the adjacent aromatic ring. The lone pair on this oxygen will attack the electron deficient β carbon and then be deprotonated by water.

The enolate that formed on the right side of the molecule will pick up a proton from acid. This will set up the electronics to favor deprotonation by water at the β carbon where the oxygen had previously attacked. As the electrons push towards the enol, the oxygen will gain a positive charge allowing for water to act as a base and abstract a proton from this position. This step will complete the formation of the neutral dye molecule (for Nile red).

2.3.4 Spectroscopic Properties of Nile red and Nile blue analogues.

The optical properties of all Nile red and Nile blue derivatives were conducted in both DMSO and MeOH. In DMSO, monosubstitution at the 9-amino position of the benzo[*a*]phenoxazinone dye scaffold showed several noticeable trends. Absorbance shifted by 3-6 nm hypsochromically and emission by 8-9 nm hypsochromically when going from a tertiary amine to a secondary amine for Nile red derivatives. Stokes shift reduced by 3-7 nm while the quantum yield showed almost no difference using both standards (R6G and RB). Since the disubstituted dyes had an extra alky substituent, it would have more vibrational and rotational modes. These extra modes,

when summed across the entire molecule, should be responsible for greater loss of energy from S_1 via internal conversion and this is apparent because the disubstituted Nile red analogues have larger Stokes shifts.

dye	λ_{abs} (nm)	ε ($M^{-1}cm^{-1}$)	λ_{em} (nm)	Φ_f*	fwhm (nm)	solvent
NR	552	40,300	633	0.42	62	DMSO
	554	39,100	631	0.28	61	MeOH
84a	546	32,500	627	0.43	62	DMSO
	548	33,900	628	0.29	61	MeOH
84b	548	37,600	630	0.45	63	DMSO
	551	39,000	632	0.26	62	MeOH
84c	546	38,100	629	0.43	64	DMSO
	549	40,500	630	0.25	63	MeOH
85d	543	23,400	619	0.47	60	DMSO
	542	23,000	616	0.39	57	MeOH
85e	543	45,200	620	0.44	60	DMSO
	544	42,200	617	0.37	56	MeOH
85f	542	32,000	621	0.45	60	DMSO
	544	32,400	618	0.39	57	MeOH
NB	636	67,100	669	0.30	49	DMSO
	625	80,800	655	0.26	52	MeOH
86a	636	70,000	671	0.27	49	DMSO
	625	77,600	655	0.25	52	MeOH
86b	639	67,800	674	0.24	50	DMSO
	629	78,600	660	0.21	52	MeOH
86c	638	69,000	674	0.29	50	DMSO
	628	74,700	660	0.27	53	MeOH
86d	622	56,000	648	0.70	46	DMSO
	610	65,300	633	0.87	46	MeOH
86e	624	61,600	649	0.65	46	DMSO
	612	69,300	634	0.80	46	MeOH
86f	623	68,200	649	0.69	47	DMSO
	611	72,700	634	0.79	48	MeOH

* Φ_f-R6G = 0.95 and Φ_f-RB = 0.70 in EtOH

Table 2.1 Optical properties of Nile red and Nile blue analogues

In MeOH, monosubstitution at the 9-amino position of the dye scaffold showed similar trends to the dyes with disubstitution of the 9-amino position, but they diverged very strongly in quantum yield. Absorbance shifted by ~5 nm hypsochromically and emission by 12-14 nm hypsochromically when going from a tertiary amine to a secondary amine. Stokes shift reduced by 6-8 nm while quantum yield showed a marked increase by 10-13% across the board for derivatives with secondary amines.

Nile blue derivatives showed similar optical trends to Nile red with a few notable exceptions. Monosubstitued varieties of Nile blue had very high quantum yields and these increased significantly when measured in MeOHas opposed to DMSO. This is the opposite as was observed for Nile red derivatives. Here we see a polar, protic solvent increasing fluorescence output. Why is that? One proposed reason is that Nile blue has many more hydrogen bond donors than Nile red does. Perhaps a hydrogen bond matrix formed between dye and solvent can work to increase the local viscosity. This will of course have the expected outcome of increasing fluorescence quantum yields.

Now that optical properties had been determined in organic media, our attention was turned to how the dyes responded in aqueous, buffered environments as shown in Figure 2.8

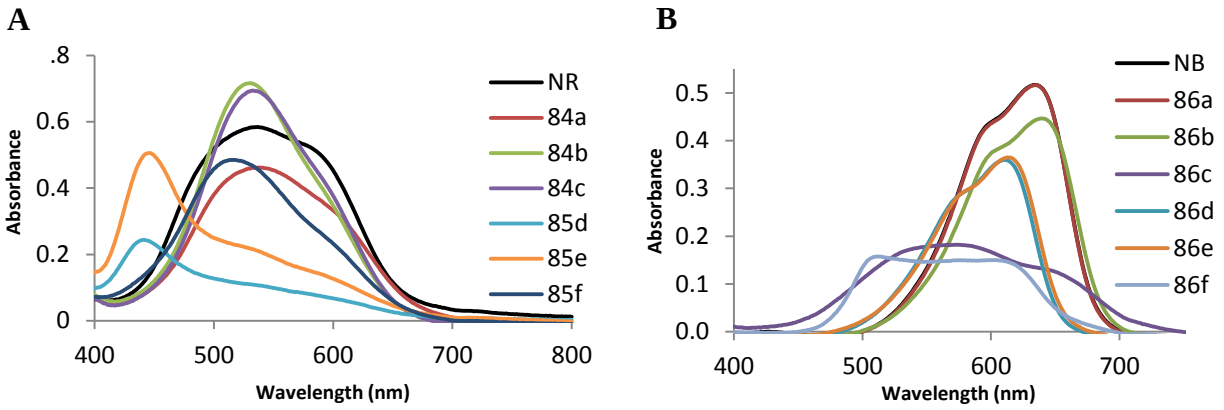

Figure 2.7 A) Visible spectra of Nile red derivatives in 30 mM phosphate buffer. B) Visible spectra of NB derivatives in 30 mM phosphate buffer

The Nile red analogues were dissolved in 30 mM phosphate buffer (pH = 7.2) to make 30 μM stock solutions. The absorbance spectra of each of the dyes showed differing λ_{max} as well as varying absorption profiles. This was interesting because λ_{max} was largely unchanged in MeOH and DMSO from dye to dye. It suggested that the pK_a of each dye species can be substantially modified by its substituents and degree of substitution. Nile red and dye **84a** had the same broad shape but had slightly different absorption intensities. **84a** only has an extra hydroxyl group from Nile red so they can be expected to be similar. **84b** and **84c** were practically identical in both line shape and intensity in their respective UV-Vis spectra. Both the butyl and phenylpropyl substituents were very hydrophobic and both dyes contained tertiary amines so similar effects were not surprising. **85d** and **85e** which have *N*-ethyl and *N*-butyl substitutions, respectively, both gave a yellow color with **85e** having weaker intensity.

Dyes that contained tertiary amines had very little perturbation of λ_{max} and minor differences in absorption intensity. If the dyes had a secondary amine then the immediate effect was to have a hypsochromic shift. The ethyl and butyl containing monsubstituted dyes shifted hypsochromical-

ly by approximately 100 nm. This was in opposition to **85f** with a phenylpropyl group, which had a 20 nm hypsochromic shift.

A hypsochromic shift is indicative of a less conjugated system or if the donor/acceptor pair was modified to have a weaker push/pull effect across the conjugated pi system. Protonation of the secondary amine would give the molecule not one, but two effective acceptor moieties. Without the donor, excitation of the dye with light would require greater energies. It can be concluded that the monosubstituted dyes were being protonated effectively in buffer and that their pK_as were subsequently higher than their analogous disubstituted analogues which had optical properties that were relatively unperturbed in buffer solution. Increasing substitution on an amine will increase its basicity.[141] What is remarkable about this data is that it would appear that the less substituted amines were more basic than their tertiary counterparts.

The Nile blue derivatives showed less differentiation than Nile red dyes but the very hydrophobic **86c** and **86f** had very flat, broad absorption profiles. This is almost certainly due to poor solubility and aggregation.

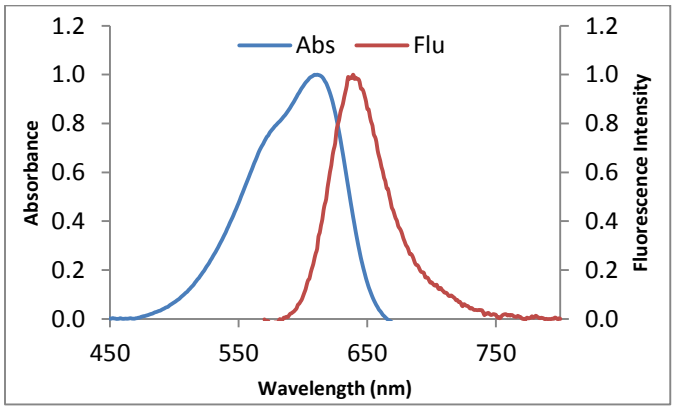

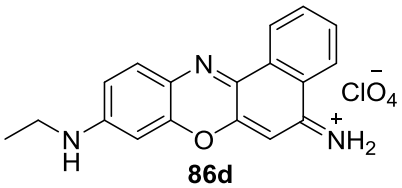

86d

Figure 2.8 Normalized absorbance and fluorescence of **86d** in phosphate buffer

86d and **86e** showed nearly identical absorbance/fluorescence wavelengths in phosphate buffer. They were chosen from the Nile blue derivatives for having superior absorption in buffer. A

small shoulder present at 577 nm on the absorbance spectra (Figure 2.9) is absent from the fluorescence spectra. This is most likely an H aggregate band.

Now that dye performance and behavior in buffered aqueous media had been assessed, the project moved forward into investigating how the dyes would behave in a model biological system. Human serum albumin (HSA) was chosen as that system.

HSA is the most common protein found in human blood plasma. Because of how ubiquitous it is in the blood and because of its physiological mobility, it acts as a transporter for an astounding variety of small molecules.[142] Whether or not a drug candidate binds to HSA and the strength of said binding interaction can have a pronounced effect on drug efficacy, retention/clearance, and toxicity.[143]

A series of binding studies were done to see how the Nile red analogues bound to HSA. Fluorescence spectroscopy was used to determine binding constants. Nile red has a very low quantum yield in water. This is mostly due to aggregation caused by poor solubility.

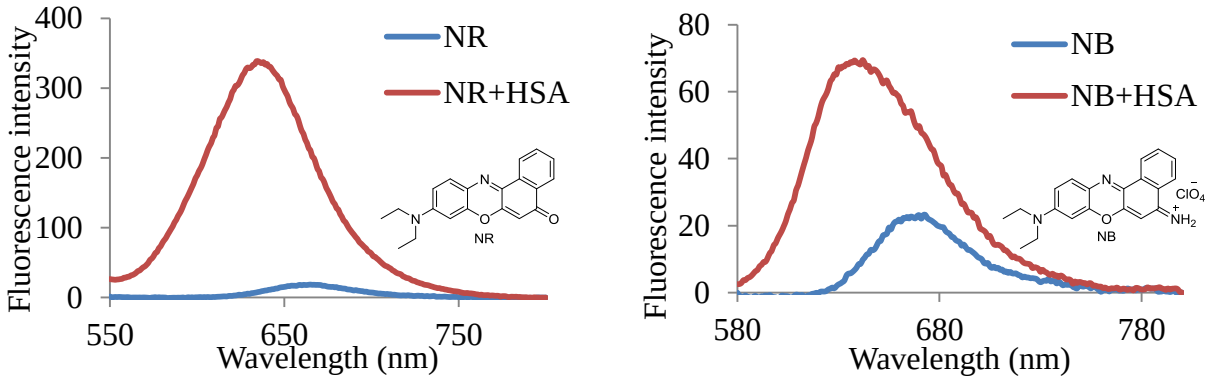

Figure 2.9 Fluorescence spectra of Nile red and Nile blue (5 μM) with HSA (5 μM) in 20 mM phosphate buffer pH = 7.2

As shown in Figure 2.9, Both Nile red and Nile blue showed significant increases in fluorescence upon binding to HSA. The dyes are very hydrophobic and flat so that they will tend to pi

stack and aggregate. The dyes should be prone to binding at hydrophobic sites on protein surfaces and grooves. Such binding would break up aggregates giving a large increase in observed fluorescence. Fluorescence increase could also be due to immobilization of dye molecules and restriction of rotation. Dyes in solution are constantly tumbling and there are many degrees of movement that deactivate the excited state. Immobilized on a protein, there are far less degrees of movement/rotation and the excited state is less likely to be perturbed. Now the binding of the Nile red and Nile blue derivatives had to be assessed.

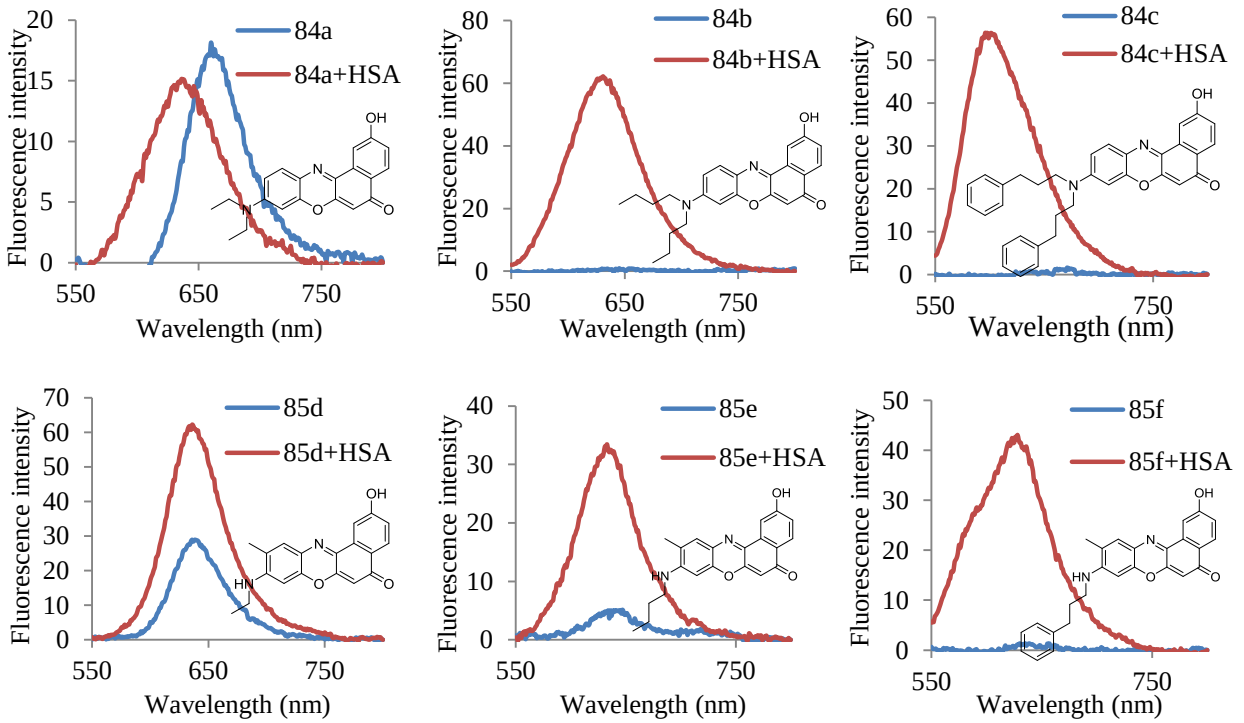

Figure 2.10 Fluorescence spectra of Nile red derivatives (5 μM) with HSA (5 μM) in 20 mM phosphate buffer pH = 7.2

The largest increase in fluorescence intensity was actually observed on Nile red with a 350 fold increase in Figure 2.9. Dye **84a** decreased in fluorescence intensity and had a hypsochromic shift. This wavelength shift in and of itself could prove somewhat useful. **85d** performed poorly because baseline fluorescence from the unbound dye was already present and the binding in-

crease was not substantially greater. **84b**, **84c**, and **85f** all showed very little baseline fluorescence with large increases in fluorescence intensity upon binding with HSA as shown in Figure 2.10.

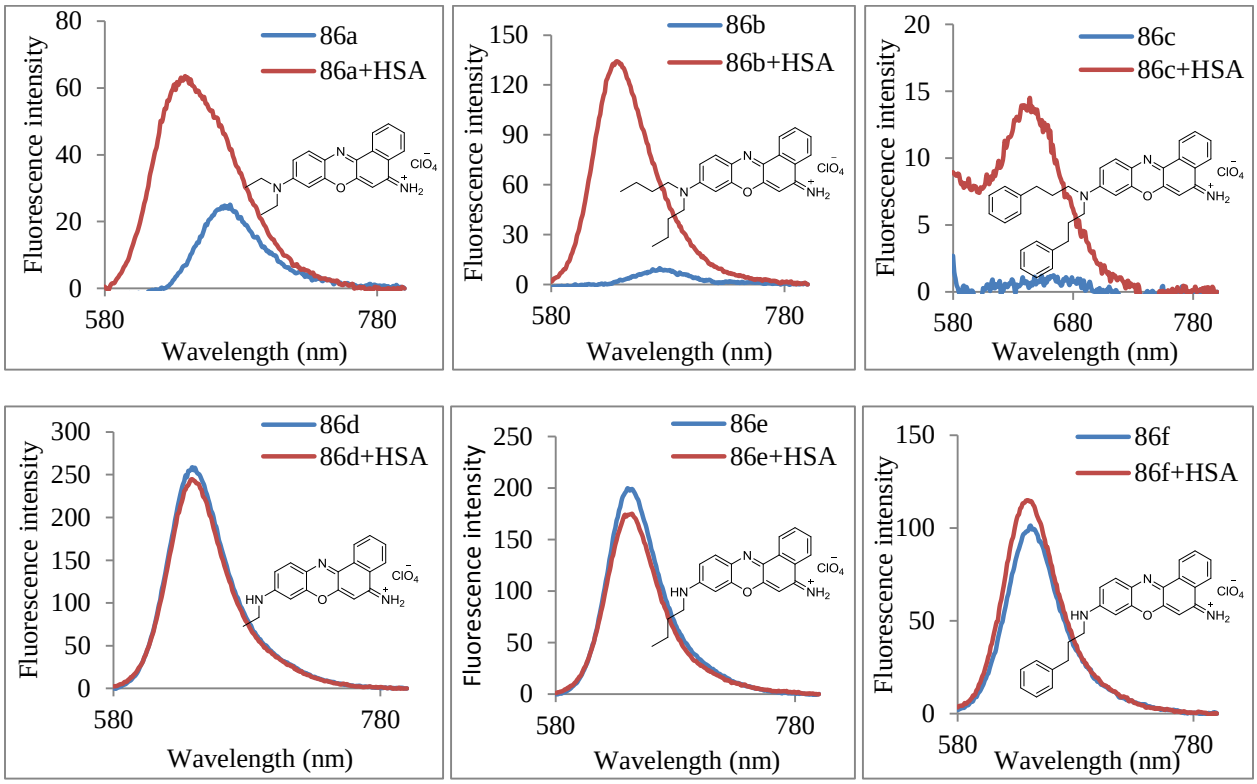

Figure 2.11 Fluorescence spectra of Nile blue derivatives (5 μM) with HSA (5 μM) in 20 mM phosphate buffer pH = 7.2

Nile blue derivatives behaved quite differently with HSA than their Nile red counterparts. Only the disubstitued dyes (**86a-c**) showed any kind of fluorescence increase upon addition to HSA as seen in Figure 2.11. This would indicate that monosubstituted dyes **86d-f** do not bind HSA. Of the disubstituted dyes, **86b** and **86c** had the greatest relative fluorescence increase from unbound versus bound. However, **86c** had a low overall fluorescence intensity, especially compared to **86b** which would appear to be the best dye.

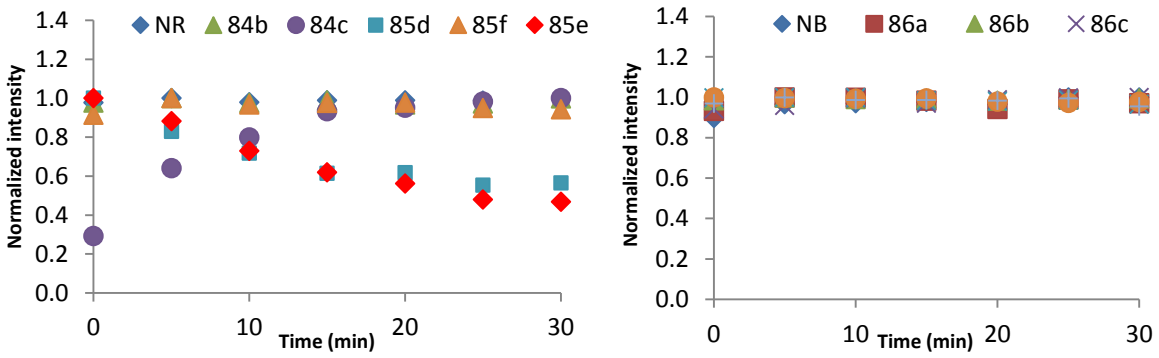

Figure 2.12 Binding interactions of Nile red derivatives observed with change in fluorescence vs. time. Binding interactions of Nile blue derivatives observed with change in fluorescence vs. time.

Nile red, **84b**, **85d**, **85e**, and 85**f** all had fast binding interactions that gave high fluorescence intensity as shown in Figure 2.12. Nile red, **84b**, and **85f** maintained the same intensities for 30 minutes. **85d** and **85e** lost intensity over time suggesting decomposition or dissociation from the dye—HSA complex. **84c** showed increased binding over time as fluorescence intensity gradually increased, reaching its maximum after 20 minutes.

The next step was to determine the stoichiometry of the dye—HSA complex. This was achieved using Job's method. Dye and HSA were mixed together at a fixed overall concentration. The mole fraction of the dye versus the HSA would be changed but the solution would be maintained at a constant concentration. The effect of this is that as dye binds to HSA, fluorescence increases. At high concentrations of dye, fluorescence will be low because there will not be enough protein in solution to bind all of it. As dye concentration decreases and protein concentration increases the fluorescence should increase. Eventually there will be more protein than dye to bind it. The mole fraction at which the apex of fluorescence intensity is reached is indicative of dye—protein binding stoichiometry.

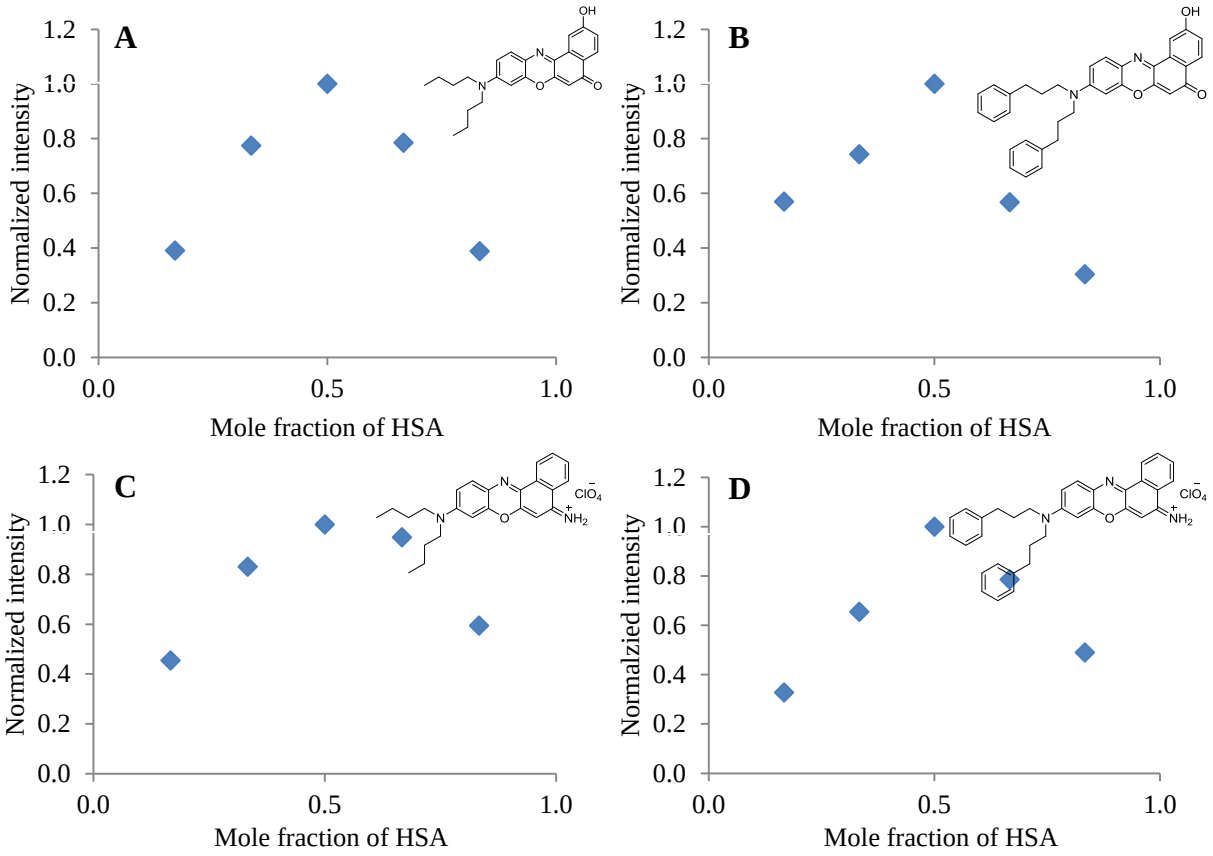

Figure 2.13 Job's plots of **84b** (A), **84c** (B), **86b** (C) and **86c** (D) with HSA. Overall concentration is 4 μM in 20 mM phosphate buffer pH = 7.2.

Out of all of the Nile red/blue derivatives, those shown in Figure 2.13 gave the best shapes for a Job's plot which is that of an arrow. Monosubstituted Nile blue dyes gave completely linear Job's plots suggesting that they did not bind at all to HSA. All of the plots shown showed maximum fluorescence at a mole fraction of 0.5 meaning that dye—HSA binding stoichiometry is 1:1.

Calculating log*D* values and their implications. The calculated distribution coefficient (log*D*) is a useful bioavailability predictor and its calculation is trivial using modern software. Chemaxon has log*D* calculator plugin in Marvin that is convenient to use. The calculated partition coefficient (log*P*) is the ratio of the concentration of a compound in *n*-octanol vs. water. It is

a parameter that clearly indicates the hydrophobicity of the target compound and can be used to screen molecules for biocompatibility before wasting resources on actual biological testing. The reason log*D* is preferred over log*P* is because it is more accurate as it takes into account both ionized and un-ionized forms of the target molecule while log*P* is much more one-dimensional, taking into account only the un-ionized form.

Low log*D* values indicate a molecule that is very hydrophilic. These molecules will typically be poor binders to transport proteins and can be rapidly removed via renal clearance. A log*D* value that is high is indicative of hydrophobicity. These compounds are prone to aggregate and/or bind irreversibly to proteins. They can persist in the body and this can cause toxic side effects and poor clearance.

The log*D* values of all of the dyes are displayed in Table 2.2. Compounds **84c** and **86c** were the most hydrophobic with log*D* values exceeding 4. Compounds **84b**, **85f**, and **86b** were within the 2-4 log*D* value range while **84a**, **85d**, **85e**, **86a**, **86d**, **86e**, and **86f** were less than 2.

Binding constants were determined using Scatchard's method. The values did not correspond with any linearity or regularity to logD values. This is a good indication that hydrophobicity is not the sole determinant in binding affinity between the dyes and the protein.

Dye	K (M^{-1})	clogD (pH =7.4)
NR	1.10×10^{5}	3.83
84a	—	1.59
84b	7.64×10^{4}	3.31
84c	1.58×10^{4}	5.75
85d	1.97×10^{6}	0.55
85e	6.55×10^{4}	1.42
85f	3.62×10^{4}	2.63
NB[a]	$2.63\text{x}10^{4}$	0.60
86a	$2.30\text{x}10^{4}$	0.60
86b	$3.56\text{x}10^{4}$	2.53
86c	$347\text{x}10^{5}$	4.80
86d	—	-0.40
86e	—	0.57
86f	—	1.71

[a]Nile blue chloride salt

Table 2.2 HSA binding constants and clog*D* values of Nile red and Nile blue analogues.

3 CONCLUSIONS

A series of Nile red and Nile blue derivatives with increasing lipophilicity were synthesized. Alkylation of the 9-amino position was controlled to give dyes with either tertiary amines or secondary amines. Dyes with tertiary amines had higher extinction coeffients and larger Stokes shifts than dye with secondary amines. However, the secondary amine-containing dyes had noticeably larger quantum yields. Nile red with one ethyl substituent at the 9-amino position had the highest binding affinity to HSA out of all dye candidates. Nile blue differed with disubstituted candidates binding strongly and their monosubstituted counterparts hardly binding at all. The largest fluorescence increase from dye binding to HSA was observed with compound **86b** which is a Nile blue derivative containing a tertiary amine with two butyl groups

4 EXPERIMENTAL

4-methyl-3-aminophenol. The starting reagent, 4-methyl-3-nitrophenol (15 g) was dissolved put into a 250 mL round bottom flask and dissolved in 50 mL of MeOH. A catalytic amount of palladium on carbon was added. The flask was degassed and then put under hydrogen atmosphere three separate times to ensure the removal of oxygen. The reaction was run for four days with hydrogen supplied via balloon. The balloon was changed several times over the course of the reaction. The reaction was followed by TLC until completion. Product was filtered over a Celite pad in a glass sintered funnel to remove catalyst. The pad was washed with ethyl acetate and the filtrate was concentrated on a rotary evaporator to recover the product (91% yield.) No purification was needed. ^{1}H NMR (400 MHz, DMSO-d_6) **δ** 8.61 (s, 1H), 6.65 (d, 1H, J = Hz), 6.05 (d, 1H, J = 4Hz), 5.89 (q, 1H, J = Hz), 4.64 (s, 2H), 1.92 (s, 3H); ^{13}C NMR (100 MHz, DMSO-d_6) **δ** 155.58, 146.69, 129.71, 111.20, 102.85, 100.61, 16.02

3-(dibutylamino)phenol. Iodobutane (4.17 mL, 3.67 mol) was combined with 3-amino phenol (2.00 g, 1.83 mol) in a 100 mL round bottom flask. Two equivalents of potassium carbonate were dissolved in a water/isopropanol solution which was then added to the reaction flask. The mixture was refluxed at 70 °C for 2 h. 55% yield.

3-(bis(3-phenylpropyl)amino)phenol. 3-aminophenol (2.00 g) was dissolved in DMF along with 5.06 g of K_2CO_3. The mixture was sonicated and allowed to mix for 15 minutes. Two molar equivalents (with respect to 3-aminophenol) of 1-bromo-3-phenylpropane (3.56 mL) were added dropwise at room temperature. The mixture was left to stir at room temperature for an additional 15 min and then was gradually heated to a maximum temperature of 70 °C over the course of two hours. TLC confirmed that all the starting material had been consumed but that three products had formed. The products were separated via regular phase column chromatog-

raphy eluting first with 1:1 v/v of Hexanes/DCM. This was increased to 100% DCM to finish the separation. The middle spot was confirmed by spectroscopic analysis of the eluting products to be the desired compound. 88% yield. ^{1}H NMR (400 MHz, $CDCl_3$) **δ** 8.86 (s, 2H), 7.28 (m, 6H), 6.81 (t, 1H, J = 4Hz), 5.96 (m, 3H), 5.46 (s, 1H), 2.93 (s, 2H), 2.66 (t, 2H, J = 4Hz), 1.82 (t, 2H, J = 4Hz); ^{13}C NMR (100 MHz, $CDCl_3$) **δ** 157.63, 149.82, 141.42, 128.90, 127.77, 127.76, 125.18, 103.01, 102.48, 98.28, 41.87, 32.23, 30.04.

3-(ethylamino)phenol. 3-aminophenol (4.00 g, 36.7 mmol), potassium carbonate (5.07 g, 36.7 mmol), and ethyl iodide (2.95 mL, 36.7 mmol) were combined in a flask with 20 mL of DMF. The reaction mixture was stirred and heated for 2 h at 100 °C. It was then concentrated under reduced pressure to remove all DMF. The residual oil was loaded onto a regular phase column and eluted with a 1:4 EtOAc/Hexanes mobile phase which was removed under reduced pressure. The product was a light brown oil and was recovered with a 51% yield. ^{1}H NMR (400 MHz, DMSO-d_6) **δ** 1.13 (t, 3H, J =8Hz), 2.96 (q, 2H, J = 8Hz), 5.99 (m, 3H), 6.83 (t, 1H, J = 8Hz); ^{13}C NMR (100 MHz, DMSO-d_6) **δ** 14.36, 37.35, 98.89, 103.09, 103.59, 129.37, 150.18, 158.10.

3-(butylamino)phenol. ^{1}H NMR (400 MHz, $CDCl_3$) **δ** 7.002 (t, 1H, J = Hz), 6.194 (dd, 2H, J = Hz), 6.081 (s, 1H, J = Hz), 3.062 (t, 2H, J = 7.2 Hz), 1.579 (quin, 2H, J = 7.2 Hz), 1.407 (sex, 2H, J = 7.2 Hz), 0.944 (t, 3H, J = 7.2 Hz); ^{13}C NMR (100 MHz, $CDCl_3$) **δ** 156.73, 150.10, 130.17, 105.99, 104.26, 99.64, 43.74, 31.58, 20.29, 13.92; m.p. 59-60 °C

3-((3-phenylpropyl)amino)phenol. ^{1}H NMR (400 MHz, $CDCl_3$) **δ** 8.895 (s, 1H), 7.308-7.163 (m, 5H), 6.836 (t, 1H, J = 8.0 Hz), 6.024-5.963 (m, 3H), 5.464 (s, 1H), 2.959-2.948 (m, 2H), 2.672 (t, 2H, J = 7.6 Hz), 1.829 (quin, 2H, J = 7.6 Hz); ^{13}C NMR (100 MHz, $CDCl_3$) **δ**

158.64, 150.82, 142.41, 129.91, 128.77, 128.74, 126.16, 104.01, 103.50, 99.30, 42.88, 33.23, 31.04; m.p. 101-103 °C

3-(ethylamino)-4-methylphenol. Compound **79** (3.85 g, 31.26 mmol) and iodoethane (0.5 mL, 6.25 mmol) were dissolved in anhydrous THF. A catalytic amount of KI (0.05 mol eq.) was added to the mixture. The reaction mixture was heated 50 °C for 5 h. TLC eluting with 4:1 hexanes/EtOAc showed only two spots. The top spot was the desired product and the bottom spot was the starting material which had been used in excess. The product was purified by normal phase column chromatography eluting with same mobile phase used in the TLC analysis. The product was a yellow oil. A solid was obtained by placing the product under high vacuum for several hours. The crystals were off white. Percent yield was 53% off of the column. ^{1}H NMR (400 MHz, DMSO-d_6) **δ** 1.18 (t, 3H, J = 8Hz), 1.95 (s, 3H), 3.02 (t, 2H, J = 8Hz), 4.50 (s, 1H), 5.92 (d, 1H, J = 8Hz), 5.97 (s, 1H), 6.70 (d, 1H, J = 8Hz), 8.71 (s, 1H); ^{13}C NMR (100 MHz, DMSO-d_6) **δ** 14.38, 16.69, 37.42, 97.01, 102.11, 112.11, 129.93, 147.32, 156.46; m.p. 88-90 °C.

3-(butylamino)-4-methylphenol. Compound **79** (7.39 g, 60 mmol) and iodobutane (1.39 mL, 13.6 mmol) were dissolved in anhydrous THF. A catalytic amount of KI (0.05 mol eq.) was added to the mixture. The reaction mixture was heated 50 °C for 24 h. TLC eluting with 4:1 hexanes/EtOAc showed only two spots. The top spot was the desired product and the bottom spot was the starting material which had been used in excess. The product was purified by normal phase column chromatography eluting with same mobile phase used in the TLC analysis. The product was a yellow oil with an orange tinge. A solid was obtained by placing the product under high vacuum for several hours. The crystals were off white. ^{1}H NMR (400 MHz, $CDCl_3$) **δ** 1.00 (t, 3H, J = 8Hz), 1.47 (sex, 2H, J = 8 Hz), 1.67 (quin, 2H, J = 8Hz), 2.08 (s, 3H), 3.14 (t, 2H, J =

8Hz), 6.12 (d, 1H, J = 4Hz), 6.16 (s, 1H), 6.90 (d, 1H, J = 8Hz); ^{13}C NMR (100 MHz, $CDCl_3$) **δ** 13.83, 16.51, 20.24, 31.44, 43.71, 98.06, 103.33, 114.12, 130.47, 147.32, 155.12; MS (ESI): 179.6 (M^+); m.p. 47-49 °C.

4-methyl-3-((3-phenylpropyl)amino)phenol. Compound **79** (40 mmol) and 1-bromo-3-phenylpropane (1.23 mL, 8.1 mmol) were dissolved in anhydrous THF. The molar ratio of **79** to alkyl halide was 5:1. A catalytic amount of KI was added (0.5 molar eq.) The reaction mixture was heated to 45 °C for 48 h. TLC showed that some alkyl halide still remained but the reaction was halted at this time. The crude mixture was concentrated under reduced pressure and purified via normal phase chromatography eluting with 4:1 hexanes/EtOAc to get the product off of the column. Starting material **79** was easily recovered by then eluting with 100% EtOAc. The product was concentrated under reduced pressure to yield a viscous, yellow oil. The addition of 0.75 mL of $CDCl_3$ caused the oil to immediately crystallize. The crystal were further dried under vacuum and appeared an off white color. ^{1}H NMR (400 MHz, $CDCl_3$) **δ** 1.95 (t, 2H, J = 8Hz), 2.02 (s, 3H), 2.74 (d, 2H, J = 8Hz), 3.14 (t, 2H, J = 4Hz), 6.08 (d, 1H, J = 4Hz), 6.10 (s, 1H), 6.83 (d, 1H, J = 4Hz), 7.28 (m, 5H); ^{13}C NMR (100 MHz, $CDCl_3$) **δ** 15.03, 29.76, 32.13, 42.20, 96.40, 101.72, 112.56, 116.43, 124.87, 127.46, 129.43, 141.38, 146.55, 155.39; MS (ESI): 241.4 (M^+); m.p. 95-96 °C.

5-(diethylamino)-2-nitrosophenol hydrochloride. A solution of 3-(diethylamino)phenol (1.07 g, 6.48 mmol) was prepared by dissolving it in HCl (8 mL, 32%) and 20 g of ice. The solution was kept at 0-5 °C. A solution of sodium nitrite (0.4471 g, 6.48 mmol) and DI water (6 mL) was added drop wise to previous solution for 1 h at 0-5 °C. The resulting brown slurry was stirred for 2 h at 0-5 °C. The slurry was filtered and the filtrate was collected and dried under re-

duced pressure. Due to the unstable nature of reported nitroso compounds the product was used without any further purification.[100]

5-(dibutylamino)-2-nitrosophenol. Compound **80b** was dissolved in 10 mL of isopropanol. HCl (8 ml, 32%) was added to the solution along with 20 g of ice. The solution was kept on an ice bath, stirring for the remainder of the reaction to maintain a temperature at 0-5 °C. Over a period of 1 h, an 8 mL of solution of sodium nitrite (0.4471 g) was added drop wise by an addition funnel. The mixture was left to stir for 2 h at low temperature. An orange precipitate was collect by vacuum filtration, dried, and then used without any further purification to avoid decomposition.

5-(bis(3-phenylpropyl)amino)-2-nitrosophenol. Compound **80c** was dissolved in 15 mL of EtOH . HCl (8 ml, 32%) was added to the solution. The solution was kept on an ice bath, stirring for the remainder of the reaction to maintain a temperature at 0-5 °C. Over a period of 1 h, an 8 mL of solution of sodium nitrite (0.4471 g) was added drop wise by an addition funnel. The mixture was left to stir for 2 h at low temperature. There was not any precipitate due to the organic solvent added for solubility issues. The reaction mixture was decanted into another round bottom flask and was put on a rotovap. All solvent was removed under reduced pressure at approximately 60 °C. This left a yellow-orange residue tinged with brown impurities. DCM was added to the mixture to dissolved the impurities. The flask was placed into a sonicator where the impurities went into solution and the precipitate formed a globular pellet in the center. The pellet was scooped out and washed with 5 mL of DCM. No further purification was carried out due to cited instability of the nitroso compound; 46% yield

5-(butylamino)-4-methyl-2-nitrosophenol. Compound **81e** (1.87 g, 10.42 mmol) was dissolved in 25 mL of EtOH. The solution was cooled to 0 °C on an ice bath. Sodium nitrite (800

mg, 11.59 mmol) was dissolved in 6 mL of D.I. water and was added to the reaction mixture drop wise over the course of an hour. The reaction mixture was left to stir for an addition 2 h on ice. The product was concentrated under reduced pressure to remove all traces of water. It was then dissolved in the minimum amount of ethanol and filtered to remove salts. The product was concentrated again and was used in the next step without further purification. Product was obtained with 94% yield. ^{1}H NMR (400 MHz, DMSO-d_6) **δ** 0.90 (t, 3H, J = 8Hz), 1.34 (sex, 2H, J = 8.0Hz), 1.62 (quin, 2H, J = 8.0Hz), 2.20 (s, 3H), 3.53 (t, 2H, J = 8Hz), 6.58 (s, 1H), 7.36 (s, 1H), 10.47 (s, 1H); ^{13}C NMR (100 MHz, DMSO-d_6) **δ** 13.07, 16.97, 19.06, 29.64, 43.94, 95.26, 120.05, 130.71, 144.29, 162.77, 166.70; m.p. 156-158 °C.

4-methyl-2-nitroso-5-((3-phenylpropyl)amino)phenol. Compound **81f** (659 mg, 2.73 mmol) was dissolved in 25 mL of EtOH. The solution was cooled to 0 °C on an ice bath. Sodium nitrite (207 mg, 3 mmol) was dissolved in 2 mL of D.I. water and was added to the reaction mixture drop wise over the course of an hour. The reaction mixture was left to stir for an addition 2 h on ice. The product was concentrated under reduced pressure to remove all traces of water. It was then dissolved in the minimum amount of ethanol and filtered to remove salts. The product was concentrated again and was used in the next step without further purification. MS (ESI): 270.2 (M^+); λ_{max}= 355 nm (MeOH).

9-(diethylamino)-2-hydroxy-5H-benzo[*a*]phenoxazin-5-one. Compound **82a** (0.771 g, 3.97 mmol) was mixed with 1,6-dihydroxynaphthalene in DMF and then refluxed at 70 °C for 2 h to afford the product. The reaction mixture was dried by rotary evaporation and the product was crystallized from MeOH/ether. Product was then purified by normal phase chromatography eluting with 1% MeOH in DCM. 60% yield. ^{1}H NMR (400 MHz, DMSO-d_6) **δ** 10.49 (s, 1H), 7.96 (d, 1H, J = 8.0 Hz), 7.87 (s, 1H), 7.54 (d, 1H, J = 12.0 Hz), 7.09 (d, 1H, J = 8.0 Hz), 6.78

(d, 1H, J = 8.0), 6.13 s, 1H), 1.15 (t, 6H, J = 8.0 Hz); ^{13}C NMR (100 MHz, DMSO-d_6) **δ** 181.12, 160.04, 151.07, 150.15, 145.85, 138.02, 133.20, 130.28, 126.94, 123.31, 117.80, 109.41, 107.55, 103.48, 95.42, 43.89, 11.89; MS (ESI): 336 (M^+); λ_{max}=548 nm (MeOH); m.p. >230 °C

9-(dibutylamino)-2-hydroxy-5*H*-benzo[*a*]phenoxazin-5-one. Compound **82b** was mixed with 1,6-dihydroxynaphthalene in DMF and then refluxed at 70 °C for 2 h to afford the product. Solvent was removed under reduced pressure and the residue was purified via regular phase column chromatography eluting with 1% MeOH in DCM. The product was still slightly impure. Washing the product with 1 mL of EtOAc and then decanting off the liquid left a green solid once dry. 52% yield. ^{1}H NMR (400 MHz, $CDCl_3$) **δ** 8.26 (d, 1H, J = 8Hz), 7.59 (d, 1H, J = 8Hz), 7.15 (d, 1H, J =8Hz), 6.66 (d, 1H, J = 8Hz), 6.46 (s, 1H), 6.34 (s, 1H), 6.34 (s, 1H), 5.66 (m, 1H), 3.41 (t, 4H, J = 8Hz), 1.66 (t, 4H, J = 8Hz), 1.44 (q, 4H, J = 8Hz), 1.03 (t, 6H, J = 8Hz); MS (ESI): 390 (M^+); m.p. 224-226 °C

9-(butylamino)-2-hydroxy-10-methyl-5*H*-benzo[*a*]phenoxazin-5-one. 41% yield. ^{1}H NMR (400 MHz, DMSO-d_6) **δ** 0.94 (t, 3H, J = 8Hz), 1.40 (sex, 2H, J = 8Hz), 1.61 (quin, 2H, J = 8Hz), 2.21 (s, 3H), 3.30 (t, 2H, J = 8Hz), 6.36 (s, 1H), 6.63 (s, 1H), 7.135 (dd, 1H), 7.47 (s, 1H), 7.90 (d, 1H, J = 8Hz), 8.00 (d, 1H, J = 8Hz)

2-hydroxy-10-methyl-9-((3-phenylpropyl)amino)-5*H*-benzo[*a*]phenoxazin-5-one. 28% yield. ^{1}H NMR (400 MHz, DMSO-d_6) **δ** 1.94 (quin, 2H, J = 8Hz), 2.20 (s, 3H), 2.71 (t, 2H, J = 8Hz), 3.32 (t, 2H, J = 8Hz), 6.32 (s, 1H), 6.59 (s, 1H), 7.135 (dd, 1H), 7.18-7.33 (m, 5H), 7.47 (s, 1H), 7.92 (d, 1H, J = 4Hz), 8.01 (d, 1H, J = 8Hz);

3-(ethylamino)phenol. 3-aminophenol (4.00 g, 36.7 mmol), potassium carbonate (5.07 g, 36.7 mmol), and ethyl iodide (2.95 mL, 36.7 mmol) were combined in a flask with 20 mL of DMF. The reaction mixture was stirred and heated for 2 h at 100 °C. It was then concentrated

under reduced pressure to remove all DMF. The residual oil was loaded onto a regular phase column and eluted with a 1:4 EtOAc/Hexanes mobile phase which was removed under reduced pressure. The product was a light brown oil and was recovered with a 51% yield. ^{1}H NMR (400 MHz, DMSO-d_6) **δ** 1.13 (t, 3H, J =8Hz), 2.96 (q, 2H, J = 8Hz), 5.99 (m, 3H), 6.83 (t, 1H, J = 8Hz); ^{13}C NMR (100 MHz, DMSO-d_6) **δ** 14.36, 37.35, 98.89, 103.09, 103.59, 129.37, 150.18, 158.10.

9-(diethylamino)-5H-benzo[a]phenoxazin-5-iminium perchlorate. 60% yield; ^{1}H NMR (400 MHz, DMSO-d_6) **δ** 9.814 (s, 1H), 9.752 (s, 1H), 8.748, (d, 1H, J = 8.0 Hz), 8.425 (d, 1H, J = 8.0 Hz), 7.968 (t, 1H, J = 8.0 Hz), 7.858 (t, 1H, J = 8.0 Hz), 7.799 (d, 1H, J = 10.0 Hz), 7.230 (d, 1H, J = 10.0 Hz), 6.960 (s, 1H), 6.797 (s, 1H), 3.655 (q, 4H, J = 7.2 Hz), 1.236 (t, 6H, J = 7.2 Hz); ^{13}C NMR (100 MHz, DMSO-d_6) **δ** 161.19, 153.93, 151.35, 148.07, 133.69, 132.91, 132.85, 131.66, 129.97, 129.57, 124.47, 124.32, 122.89, 115.44, 96.91, 96.21, 45.84, 13.07; λ_{max} = 626 nm (MeOH); m.p. 285-287 °C

9-(dibutylamino)-5H-benzo[a]phenoxazin-5-iminium perchlorate. 34% yield. ^{1}H NMR (400 MHz, DMSO-d_6) **δ** 9.776 (s, 2H), 8.688 (d, 1H, J = 8 Hz), 8.385 (d, 1H, J = 8 Hz), 7.926 (t, 1H, J = 7.6 Hz), 7.817 (t, 1H, J = 7.6 Hz), 7.727 (d, 1H, J = 9.2), 7.151(d, 1H, J = 8.8 Hz), 6.862 (s, 1H), 6.743 (s, 1H), 3.540 (t, 4H, J = 7.2 Hz), 1.584 (quin, 4H, J = 7.2 Hz), 1.391 (sex, 4H, J = 7.2 Hz), 0.954 (t, 6H, J = 7.2 Hz); ^{13}C NMR (100 MHz, DMSO-d_6) **δ** 161.30, 154.26, 151.44, 148.06, 133.97, 132.86, 131.76, 130.01, 129.55, 124.54, 124.40, 123.07, 115.49, 97.06, 96.39, 51.38, 29.65, 19.96, 14.27;

9-(bis(3-phenylpropyl)amino)-5H-benzo[a]phenoxazin-5-iminium perchlorate. 29% yield; ^{1}H NMR (400 MHz, DMSO-d_6) **δ** 9.906 (s, 1H), 9.832 (s, 1H), 8.762 (d, 1H, J = 8.0 Hz), 8.449 (d, 1H, J = 8.4 Hz), 7.974 (t, 1H, J = 8.0 Hz), 7.866 (t, 1H, J = 7.6 Hz), 7.772 (d, 1H, J =

9.2 Hz), 7.346-7.213 (m, 10H), 7.151 (d, 1H, J = 8.0 Hz), 6.824 (s, 1H), 6.812 (s, 1H), 3.619-3.584 (m, 4H), 2.717-2.679 (m, 4H), 1.945-1.912 (m, 4H); ^{13}C NMR (100 MHz, DMSO-d_6) **δ** 161.47, 154.18, 151.60, 148.00, 141.71, 134.27, 133.00, 132.77, 131.79, 130.15, 129.52, 128.89, 128.75, 126.46, 124.60, 124.48, 123.06, 115.40, 97.07, 96.46, 51.07, 32.57, 29.19;λ_{max}= 628 nm (MeOH); m.p. 218-220 °C

9-(ethylamino)-5H-benzo[a]phenoxazin-5-iminium perchlorate. 20% yield; ^{1}H NMR (400 MHz, DMSO-d_6) **δ** 8.596 (d, 1H, J = 8.0 Hz), 8.316, (d, 1H, J = 8.0 Hz), 7.876 (t, 1H, J = 7.2 Hz), 7.770 (t, 1H, J = 7.2 Hz), 7.623 (d, 1H, J = 8.8 Hz), 6.965 (d, 1H, J = 8.8 Hz), 6.63 (s, 1H), 6.652 (s, 1H), 3.311-3.294 (m, 2H), 1.250 (t, 3H, J = 7.2 Hz); ^{13}C NMR (100 MHz, DMSO-d_6) **δ** 160.82, 156.37, 151.08, 133.00, 132.66, 131.58, 130.10, 129.79, 124.36, 124.18, 122.82, 96.66, 38.29, 14.19; λ_{max} = 610 nm (MeOH); m.p. 198-200 °C

9-(butylamino)-5H-benzo[a]phenoxazin-5-iminium perchlorate. 12% yield. ^{1}H NMR (400 MHz, DMSO-d_6) **δ** 9.641 (s, 2H), 8.661 (d, 1H, J = Hz), 8.468 (s, 1H), 8.368 (d, 1H, J = Hz), 7.909 (t, 1H, J = Hz), 7.798 (t, 1H, J = Hz), 7.678 (d, 1H, J = Hz), 7.031 (d, 1H, J = Hz), 6.736 (s, 2H), 3.291 (m, 2H), 1.607 (m, 2H), 1.420 (m, 2H), 0.959 (m, 3H); ^{13}C NMR (100 MHz, DMSO-d_6) **δ** 160.85, 156.65, 151.22, 133.06, 132.69, 131.70, 130.23, 129.82, 124.43, 124.25, 122.90, 96.70, 43.23, 30.74, 20.14, 14.13;

9-((3-phenylpropyl)amino)-5H-benzo[a]phenoxazin-5-iminium perchlorate. 12% yield. ^{1}H NMR (400 MHz, DMSO-d_6) **δ** 9.714 (s, 2H), 8.788 (d, 1H, J = Hz), 8.552 (s, 1H), 8.454 (d, 1H, J = Hz), 7.982 (t, 1H, J = Hz), 7.872 (t, 1H, J = Hz), 7.798 (d, 1H, J = Hz), 7.321-7.217 (m, 5H), 7.106 (d, 1H, J = Hz), 6.832 (s, 2H), 2.736 (m, 2H), 1.950 (m, 2H); ^{13}C NMR (100 MHz, DMSO-d_6) **δ** 161.10, 156.63, 151.55, 141.78, 133.51, 132.89, 131.87, 130.30,

130.02, 128.86, 128.79, 126.42, 124.55, 124.42, 123.06, 96.83, 43.01, 32.87, 30.44; λ_{max} = 616 nm (MeOH)

REFERENCES

1. Herschel, J. F. W., On a Case of Superficial Colour presented by a homogenous liquid internally colourless. *Philosophical Transactions of the Royal Society of London* **1845**, 135, 143-145.
2. Sabanayagam, C. R.; Eid, J. S.; Meller, A., Using fluorescence resonance energy transfer to measure distances along individual DNA molecules: corrections due to nonideal transfer. *The Journal of chemical physics* **2005**, 122, 061103.
3. Zipfel, W. R.; Williams, R. M.; Webb, W. W., Nonlinear magic: multiphoton microscopy in the biosciences. *Nature biotechnology* **2003**, 21, 1369-77.
4. Engel, T.; Hehre, W. J., *Quantum chemistry and spectroscopy*. Pearson/Benjamin Cummings: San Francisco, 2006; p xiv, 489 p.
5. Lakowicz, J. R., *Principles of Fluorescence Spectroscopy*. 3rd ed.; 2007.
6. Roy, R.; Hohng, S.; Ha, T., A practical guide to single-molecule FRET. *Nat Methods* **2008**, 5, 507-16.
7. Yuste, R., Fluorescence microscopy today. *Nature methods* **2005**, 2, 902-4.
8. Miyawaki, A.; Llopis, J.; Heim, R.; McCaffery, J. M.; Adams, J. A.; Ikura, M.; Tsien, R. Y., Fluorescent indicators for Ca2+ based on green fluorescent proteins and calmodulin. *Nature* **1997**, 388, 882-7.
9. Conchello, J. A.; Lichtman, J. W., Optical sectioning microscopy. *Nature methods* **2005**, 2, 920-31.
10. Göppert-Mayer, M., Über Elementarakte mit zwei Quantemsprüngen. *Annalen der Physik* **1931**, 401, 273-294.
11. Helmchen, F.; Denk, W., Deep tissue two-photon microscopy. *Nature methods* **2005**, 2, 932-40.
12. Flusberg, B. A.; Cocker, E. D.; Piyawattanametha, W.; Jung, J. C.; Cheung, E. L.; Schnitzer, M. J., Fiber-optic fluorescence imaging. *Nature methods* **2005**, 2, 941-50.
13. Hagfeldt, A.; Boschloo, G.; Sun, L. C.; Kloo, L.; Pettersson, H., Dye-Sensitized Solar Cells. *Chemical Reviews* **2010**, 110, 6595-6663.
14. Hyun, H.; Park, M. H.; Owens, E. A.; Wada, H.; Henary, M.; Handgraaf, H. J. M.; Vahrmeijer, A. L.; Frangioni, J. V.; Choi, H. S., Structure-inherent targeting of near-infrared fluorophores for parathyroid and thyroid gland imaging. *Nat Med* **2015**, 21, 104-U9.
15. Ormond, A. B.; Freeman, H. S., Dye Sensitizers for Photodynamic Therapy. *Materials* **2013**, 6, 817-840.
16. Veuthey, T.; Herrera, G.; Dodero, V. I., Dyes and stains: from molecular structure to histological application. *Front Biosci-Landmrk* **2014**, 19, 91-112.
17. Carter, K. P.; Young, A. M.; Palmer, A. E., Fluorescent Sensors for Measuring Metal Ions in Living Systems. *Chemical Reviews* **2014**, 114, 4564-4601.
18. Swanson, S. A.; Wallraff, G. M.; Chen, J. P.; Zhang, W. J.; Bozano, L. D.; Carter, K. R.; Salem, J. R.; Villa, R.; Scott, J. C., Stable and efficient fluorescent red and green dyes for external and internal conversion of blue OLED emission. *Chem Mater* **2003**, 15, 2305-2312.
19. Chenais, S.; Forget, S., Recent advances in solid-state organic lasers. *Polym Int* **2012**, 61, 390-406.
20. Ashitate, Y.; Hyun, H.; Kim, S. H.; Lee, J. H.; Henary, M.; Frangioni, J. V.; Choi, H. S., Simultaneous mapping of pan and sentinel lymph nodes for real-time image-guided surgery. *Theranostics* **2014**, 4, 693-700.

21. Ashitate, Y.; Kim, S. H.; Tanaka, E.; Henary, M.; Choi, H. S.; Frangioni, J. V.; Flaumenhaft, R., Two-wavelength near-infrared fluorescence for the quantitation of drug antiplatelet effects in large animal model systems. *J Vasc Surg* **2012**, 56, 171-80.
22. Choi, H. S.; Gibbs, S. L.; Lee, J. H.; Kim, S. H.; Ashitate, Y.; Liu, F.; Hyun, H.; Park, G.; Xie, Y.; Bae, S.; Henary, M.; Frangioni, J. V., Targeted zwitterionic near-infrared fluorophores for improved optical imaging. *Nature biotechnology* **2013**, 31, 148-53.
23. Hyun, H.; Henary, M.; Gao, T.; Narayana, L.; Owens, E. A.; Lee, J. H.; Park, G.; Wada, H.; Ashitate, Y.; Frangioni, J. V.; Choi, H. S., 700-nm Zwitterionic Near-Infrared Fluorophores for Dual-Channel Image-Guided Surgery. *Mol Imaging Biol* **2016**, 18, 52-61.
24. Hyun, H.; Owens, E. A.; Wada, H.; Levitz, A.; Park, G.; Park, M. H.; Frangioni, J. V.; Henary, M.; Choi, H. S., Cartilage-Specific Near-Infrared Fluorophores for Biomedical Imaging. *Angewandte Chemie* **2015**, 54, 8648-52.
25. Hyun, H.; Park, M. H.; Owens, E. A.; Wada, H.; Henary, M.; Handgraaf, H. J.; Vahrmeijer, A. L.; Frangioni, J. V.; Choi, H. S., Structure-inherent targeting of near-infrared fluorophores for parathyroid and thyroid gland imaging. *Nat Med* **2015**, 21, 192-7.
26. Hyun, H.; Wada, H.; Bao, K.; Gravier, J.; Yadav, Y.; Laramie, M.; Henary, M.; Frangioni, J. V.; Choi, H. S., Phosphonated near-infrared fluorophores for biomedical imaging of bone. *Angewandte Chemie* **2014**, 53, 10668-72.
27. Njiojob, C. N.; Owens, E. A.; Narayana, L.; Hyun, H.; Choi, H. S.; Henary, M., Tailored near-infrared contrast agents for image guided surgery. *J Med Chem* **2015**, 58, 2845-54.
28. Owens, E. A.; Lee, S.; Choi, J.; Henary, M.; Choi, H. S., NIR fluorescent small molecules for intraoperative imaging. *Wiley Interdiscip Rev Nanomed Nanobiotechnol* **2015**, 7, 828-38.
29. Park, M. H.; Hyun, H.; Ashitate, Y.; Wada, H.; Park, G.; Lee, J. H.; Njiojob, C.; Henary, M.; Frangioni, J. V.; Choi, H. S., Prototype nerve-specific near-infrared fluorophores. *Theranostics* **2014**, 4, 823-33.
30. Wada, H.; Hyun, H.; Vargas, C.; Gravier, J.; Park, G.; Gioux, S.; Frangioni, J. V.; Henary, M.; Choi, H. S., Pancreas-targeted NIR fluorophores for dual-channel image-guided abdominal surgery. *Theranostics* **2015**, 5, 1-11.
31. Beija, M.; Afonso, C. A. M.; Martinho, J. M. G., Synthesis and applications of Rhodamine derivatives as fluorescent probes. *Chemical Society reviews* **2009**, 38, 2410-2433.
32. Doja, M. Q., The Cyanine Dyes. *Chemical Reviews* **1932**, 11, 273-321.
33. Boens, N.; Leen, V.; Dehaen, W., Fluorescent indicators based on BODIPY. *Chemical Society reviews* **2012**, 41, 1130-1172.
34. Wang, T.; Zhao, Y. X.; Shi, M. Q.; Wu, F. P., The synthesis of novel coumarin dyes and the study of their photoreaction properties. *Dyes and Pigments* **2007**, 75, 104-110.
35. Hu, L.; Yan, Z. Q.; Xu, H. Y., Advances in synthesis and application of near-infrared absorbing squaraine dyes. *Rsc Adv* **2013**, 3, 7667-7676.
36. Möhlau, R.; Uhlmann, K., Zur Kenntniss der Chinazin- und Oxazinfarbstoffe. *Annalen der Chemie* **1895**, 289, 90-128.
37. Gilchrist, T. L., *Heterocyclic Chemistry*. 3rd ed.; Pearson Education Limited: Harlow, Essex, England, 1997; p xvi, 414 p.
38. Frade, V. H. J.; Goncalves, M. S. A. T.; Coutinho, P. J. G.; Moura, J. C. V. P., Synthesis and spectral properties of long-wavelength fluorescent dyes. *J Photoch Photobio A* **2007**, 185, 220-230.

39. Golini, C. M.; Williams, B. W.; Foresman, J. B., Further Solvatochromic, Thermochromic, and Theoretical Studies on Nile Red. *Journal of Fluorescence* **1998**, 8, 395-404.
40. Guido, C. A.; Mennucci, B.; Jacquemin, D.; Adamo, C., Planar vs. twisted intramolecular charge transfer mechanism in Nile Red: new hints from theory. *Physical Chemistry Chemical Physics* **2010**, 12, 8016-8023.
41. Reichardt, C., Solvatchromic Dyes as Solvent Polarity Indicators. *Chemical Reviews* **1994**, 94, 2319-2358.
42. Fleming, S.; Mills, A.; Tuttle, T., Predicting the UV-vis spectra of oxazine dyes. *Beilstein journal of organic chemistry* **2011**, 7, 432-41.
43. Owen Tuck, P.; Christopher Mawhinney, R.; Rappon, M., An ab initio and TD-DFT study of solvent effect contributions to the electronic spectrum of Nile Red. *Physical Chemistry Chemical Physics* **2009**, 11, 4471-4480.
44. Datta, A.; Mandal, D.; Pal, S. K.; Bhattacharyya, K., Intramolecular Charge Transfer Processes in Confined Systems. Nile Red in Reverse Micelles†. *The Journal of Physical Chemistry B* **1997**, 101, 10221-10225.
45. Dutta, A. K.; Kamada, K.; Ohta, K., Langmuir-Blodgett films of nile red: A steady-state and time-resolved fluorescence study. *Chem Phys Lett* **1996**, 258, 369-375.
46. Sarkar, N.; Das, K.; Nath, D. N.; Bhattacharyya, K., Twisted Charge Transfer Process of Nile Red in Homogeneous Solution and in Faujasite Zeolite. *Langmuir* **1994**, 10, 326-329.
47. Sebok-Nagy, K.; Miskolczy, Z.; Biczok, L., Interaction of 2-hydroxy-substituted Nile red fluorescent probe with organic nitrogen compounds. *Photochem Photobiol* **2005**, 81, 1212-8.
48. Hungerford, G.; Castanheira, E. M. S.; Oliveira, M. E. C. D. R.; Miguel, M. D.; Burrows, H., Monitoring ternary systems of C12E5/water/tetradecane via the fluorescence of solvatochromic probes. *Journal of Physical Chemistry B* **2002**, 106, 4061-4069.
49. Moog, R. S.; Kim, D. D.; Oberle, J. J.; Ostrowski, S. G., Solvent effects on electronic transitions of highly dipolar dyes: A comparison of three approaches. *J Phys Chem A* **2004**, 108, 9294-9301.
50. Boldrini, B.; Cavalli, E.; Painelli, A.; Terenziani, F., Polar Dyes in Solution: A Joint Experimental and Theoretical Study of Absorption and Emission Band Shapes. *The Journal of Physical Chemistry A* **2002**, 106, 6286-6294.
51. Tajalli, H.; Gilani, A. G.; Zakerhamidi, M. S.; Tajalli, P., The photophysical properties of Nile red and Nile blue in ordered anisotropic media. *Dyes and Pigments* **2008**, 78, 15-24.
52. LaGuardia, W.; LaGuardia, D. Temperature-Indicating Container. US 20070053406, 2007.
53. Kawski, A.; Kuklinski, B.; Bojarski, P., Photophysical properties and thermochromic shifts of electronic spectra of Nile Red in selected solvents. Excited states dipole moments. *Chem Phys* **2009**, 359, 58-64.
54. Yuan, L.; Lin, W. Y.; Zheng, K. B.; Zhu, S. S., FRET-Based Small-Molecule Fluorescent Probes: Rational Design and Bioimaging Applications. *Accounts Chem Res* **2013**, 46, 1462-1473.
55. Brousmiche, D. W.; Serin, J. M.; Frechet, J. M. J.; He, G. S.; Lin, T. C.; Chung, S. J.; Prasad, P. N., Fluorescence resonance energy transfer in a novel two-photon absorbing system. *Journal of the American Chemical Society* **2003**, 125, 1448-1449.
56. Brousmiche, D. W.; Serin, J. M.; Frechet, J. M. J.; He, G. S.; Lin, T. C.; Chung, S. J.; Prasad, P. N.; Kannan, R.; Tan, L. S., Fluorescence resonance energy transfer in novel

multiphoton absorbing dendritic structures. *Journal of Physical Chemistry B* **2004**, 108, 8592-8600.
57. Koziar, J. C.; Cowan, D. O., Photochemical heavy-atom effects. *Accounts Chem Res* **1978**, 11, 334-341.
58. Gastilovich, E. A.; Serov, S. A.; Korol'kova, N. V.; Klimenko, V. G., Heavy atom effect on photophysical deactivation of molecular triplet states. *Opt Spectrosc+* **2000**, 88, 313-315.
59. Yew, P. L.; Heng, L. Y., A reflectometric ion sensor for potassium based on acrylic microspheres. *Sensor Actuat B-Chem* **2014**, 191, 719-726.
60. Kim, H. H.; Song, N. W.; Park, T. S.; Yoon, M., Laser scanning confocal microscope (LSCM)-fluorescence spectral properties of Nile Red embedded in polystyrene film of different thickness. *Chem Phys Lett* **2006**, 432, 200-204.
61. Felbeck, T.; Behnke, T.; Hoffmann, K.; Grabolle, M.; Lezhnina, M. M.; Kynast, U. H.; Resch-Genger, U., Nile-Red-Nanoclay Hybrids: Red Emissive Optical Probes for Use in Aqueous Dispersion. *Langmuir* **2013**, 29, 11489-11497.
62. Siami, E.; Sabzi, R. E.; Rasouli, F.; Kheiri, F., Nile Blue and Nickel Organometallic Dyes Applied in Dye-sensitized Solar Cells. *Portugaliae electrochimica acta* **2015**, 33, 23-33.
63. Shervedani, R. K.; Amini, A., Preparation of graphene/nile blue nanocomposite: Application for oxygen reduction reaction and biosensing. *Electrochim Acta* **2015**, 173, 354-363.
64. Al-Maliki, F. J., Energy transfer studies in binary laser dye mixtures in organically modified silicates. *Eur Phys J D* **2014**, 68.
65. Huang, M.; He, S.; Liu, W.; Yao, Y.; Miao, S., Spectral Inspections on Molecular Configurations of Nile Blue A Adsorbed on the Elementary Clay Sheets. *The journal of physical chemistry. B* **2015**, 119, 13302-8.
66. Lee, K. H.; Chen, S. J.; Jeng, J. Y.; Cheng, Y. C.; Shiea, J. T.; Chang, H. T., Fluorescence and interactions with thiol compounds of Nile Red-adsorbed gold nanoparticles. *J Colloid Interface Sci* **2007**, 307, 340-8.
67. Chen, S. J.; Chang, H. T., Nile red-adsorbed gold nanoparticles for selective determination of thiols based on energy transfer and aggregation. *Analytical chemistry* **2004**, 76, 3727-3734.
68. Tseng, W. L.; Lee, K. H.; Chang, H. T., Using nile red-adsorbed gold nanoparticles to locate glutathione within erythrocytes. *Langmuir* **2005**, 21, 10676-83.
69. Huang, Y. F.; Chang, H. T., Nile Red-adsorbed gold nanoparticle matrixes for determining aminothiols through surface-assisted laser desorption/ionization mass spectrometry. *Analytical chemistry* **2006**, 78, 1485-93.
70. Han, W. T.; Liao, S. Z.; Zhang, C. H.; Ding, H. Z.; Wu, Z. Y.; Shen, G. L.; Yu, R. Q., Highly Sensitive Fluorometric Assay Method for Acetylcholinesterase Inhibitor Based on Nile Red-Adsorbed Gold Nanoparticles. *Chinese J Chem* **2013**, 31, 1072-1078.
71. Chubinidze, K.; Partsvania, B.; Sulaberidze, T.; Khuskivadze, A.; Davitashvili, E.; Koshoridze, N., Luminescence enhancement in nanocomposite consisting of polyvinyl alcohol incorporated gold nanoparticles and Nile blue 690 perchlorate. *Appl Opt* **2014**, 53, 7177-81.
72. Wei, R.; Wei, Z.; Sun, L.; Zhang, J. Z.; Liu, J.; Ge, X.; Shi, L., Nile Red Derivative-Modified Nanostructure for Upconversion Luminescence Sensing and Intracellular Detection of Fe(3+) and MR Imaging. *ACS Appl Mater Interfaces* **2016**, 8, 400-10.
73. Davis, M. M.; Helzer, H. B., Titrimetric and Equilibrium Studies Using Indicators Related to Nile Blue A. *Analytical chemistry* **1966**, 38, 451-461.

74. Duan, R. L.; Li, C. Y.; Liu, S. P.; Liu, Z. F.; Li, Y. F.; Zhu, J. H.; Hu, X. L., A selective fluorescence quenching method for the determination of trace hypochlorite in water samples with nile blue A. *J Taiwan Inst Chem E* **2015**, 50, 43-48.
75. Fowler, S. D.; Greenspan, P., Application of Nile red, a fluorescent hydrophobic probe, for the detection of neutral lipid deposits in tissue sections: comparison with oil red O. *The journal of histochemistry and cytochemistry : official journal of the Histochemistry Society* **1985**, 33, 833-6.
76. Greenspan, P.; Mayer, E. P.; Fowler, S. D., Nile red: a selective fluorescent stain for intracellular lipid droplets. *The Journal of cell biology* **1985**, 100, 965-73.
77. Hungerford, G.; Castanheira, E. M.; Baptista, A. L.; Coutinho, P. J.; Oliveira, M. E., Domain formation in DODAB-cholesterol mixed systems monitored via Nile Red anisotropy. *J Fluoresc* **2005**, 15, 835-40.
78. Lin, C. W.; Shulok, J. R.; Kirley, S. D.; Cincotta, L.; Foley, J. W., Lysosomal localization and mechanism of uptake of Nile blue photosensitizers in tumor cells. *Cancer Res* **1991**, 51, 2710-9.
79. Wainwright, M., Non-porphyrin photosensitizers in biomedicine. *Chemical Society reviews* **1996**, 25, 351-360.
80. Lin, C. W.; Shulok, J. R.; Wong, Y. K.; Schanbacher, C. F.; Cincotta, L.; Foley, J. W., Photosensitization, uptake, and retention of phenoxazine Nile blue derivatives in human bladder carcinoma cells. *Cancer Res* **1991**, 51, 1109-16.
81. Escoffre, J.-M.; Deckers, R.; Sasaki, N.; Bos, C.; Moonen, C., In *Radiology and Oncology*; 2015; Vol. 49, p 41.
82. Vimalarasa, R.; Foot, P. J. S.; Calabrese, G., Evaluation of a Smart Polymer Nanosphere for Potential Use in Anticancer Drug Delivery. *Polymers & Polymer Composites* **2014**, 22, 753-762.
83. Mishra, S. S.; Subuddhi, U., Spectroscopic investigation of interaction of Nile Blue A, a potent photosensitizer, with bile salts in aqueous medium. *J Photochem Photobiol B* **2014**, 141, 67-75.
84. Kuramitz, H.; Piruska, A.; Halsall, H. B.; Seliskar, C. J.; Heineman, W. R., Simultaneous multiselective spectroelectrochemical sensing of the interaction between protein and its ligand using the redox dye Nile blue as a label. *Analytical chemistry* **2008**, 80, 9642-8.
85. Ma, J.; Ding, C.; Zhou, J.; Tian, Y., 2D ratiometric fluorescent pH sensor for tracking of cells proliferation and metabolism. *Biosens Bioelectron* **2015**, 70, 202-8.
86. Alqasaimeh, M. S.; Heng, L. Y.; Ahmad, M., A urea biosensor from stacked sol-gel films with immobilized nile blue chromoionophore and urease enzyme. *Sensors-Basel* **2007**, 7, 2251-2262.
87. Esmaeili, C.; Heng, L. Y.; Ling, T. L., Nile Blue chromoionophore-doped kappa-carrageenan for a novel reflectometric urea biosensor. *Sensors and Actuators B: Chemical* **2015**, 221, 969-977.
88. Dong, J.; Li, Y.; Zhang, M.; Li, z.; Yan, T.; Qian, W., Ultrasensitive surface-enhanced Raman scattering detection of alkaline phosphatase. *Analytical Methods* **2014**, 6, 9168-9172.
89. Mitra, R. K.; Sinha, S. S.; Maiti, S.; Pal, S. K., Sequence dependent ultrafast electron transfer of nile blue in oligonucleotides. *J Fluoresc* **2009**, 19, 353-61.
90. Chen, Q. Y.; Li, D. H.; Zhao, Y.; Yang, H. H.; Zhu, Q. Z.; Xu, J. G., Interaction of a novel red-region fluorescent probe, Nile blue, with DNA and its application to nucleic acids assay. *Analyst* **1999**, 124, 901-6.

91. Huang, C. Z.; Li, Y. F.; Hu, X. L.; Li, N. B., Three-dimensional spectra of the long-range assembly of Nile Blue sulfate on the molecular surface of DNA and determination of DNA by light-scattering. *Analytica Chimica Acta* **1999**, 395, 187-197.
92. Huang, C. Z.; Li, Y. F.; Zhang, D. J.; Ao, X. P., Spectrophotometric study on the supramolecular interactions of nile blue sulphate with nucleic acids. *Talanta* **1999**, 49, 495-503.
93. Yang, Y. I.; Hong, H. Y.; Lee, I. S.; Bai, D. G.; Yoo, G. S.; Choi, J. K., Detection of DNA using a visible dye, Nile blue, in electrophoresed gels. *Anal Biochem* **2000**, 280, 322-4.
94. Shen, Y.; Liu, S.; Kong, L.; Tan, X.; He, Y.; Yang, J., Detection of DNA using an "off-on" switch of a regenerating biosensor based on an electron transfer mechanism from glutathione-capped CdTe quantum dots to nile blue. *Analyst* **2014**, 139, 5858-67.
95. Alipour, E.; Allaf, F.; Mahmoudi-Badiki, T., Investigation of specific interactions between Nile blue and single type oligonucleotides and its application in electrochemical detection of hepatitis C 3a virus. *J Solid State Electrochem* **2015**, 1-10.
96. Mindroiu, M.; Zgarian, R. G.; Kajzar, F.; Rau, I.; De Oliveira, H. C. L.; Pawlicka, A.; Tihan, G. T., DNA-based membranes for potential applications. *Ionics* **2015**, 21, 1381-1390.
97. Urbansky, E. T., Perchlorate Chemistry: Implications for Analysis and Remediation. *Bioremediation Journal* **1998**, 2, 81-95.
98. Williams, D. L. H., The Mechanism of the Fischer-Hepp Rearrangement of Aromatic N-Nitroso-Amines. *Tetrahedron* **1975**, 31, 1343-1349.
99. Jose, J.; Ueno, Y.; Burgess, K., Water-soluble Nile Blue derivatives: syntheses and photophysical properties. *Chemistry* **2009**, 15, 418-23.
100. Jose, J.; Burgess, K., Syntheses and properties of water-soluble Nile Red derivatives. *Journal of Organic Chemistry* **2006**, 71, 7835-7839.
101. Raju, B. R.; Garcia, A. M. F.; Costa, A. L. S.; Coutinho, P. J. G.; Gonçalves, M. S. T., Synthesis of new benzo[a]phenoxazinium probes possessing carboxylic ester, hydroxyl and amino functional groups: Photophysical studies in dry ethanol and conjugation with CdTe quantum dots. *Dyes and Pigments* **2014**, 110, 203-213.
102. Long, J.; Wang, Y. M.; Matsuura, T.; Meng, J. B., Synthesis and fluorescence properties of novel benzo[a]phenoxazin-5-one derivatives. *J Heterocyclic Chem* **1999**, 36, 895-899.
103. Ho, N.-h.; Weissleder, R.; Tung, C.-H., Development of water-soluble far-red fluorogenic dyes for enzyme sensing. *Tetrahedron* **2006**, 62, 578-585.
104. Frade, V. H. J.; Goncalves, M. S. T.; Moura, J. C. V. P., Synthesis and fluorescence properties of side-chain carboxylated 5,9-diaminobenzo[a]phenoxazinium salts. *Tetrahedron Lett* **2005**, 46, 4949-4952.
105. Briggs, M. S. J.; Bruce, I.; Miller, J. N., Synthesis of functionalised fluorescent dyes and their coupling to amines and amino acids. *Journal of the Chemical Society, Perkin Transactions 1* **1997**, 7, 1051-1058.
106. Jose, J.; Loudet, A.; Ueno, Y.; Barhoumi, R.; Burghardt, R. C.; Burgess, K., Intracellular imaging of organelles with new water-soluble benzophenoxazine dyes. *Organic & biomolecular chemistry* **2010**, 8, 2052-9.
107. Firmino, A.; Firmino, A. D. G.; Raju, B. R.; Gonçalves, M. S. T., Microwave Synthesis of Water-Soluble 2-, 5- and 9-Substituted Benzo[a]phenoxazinium Chlorides in Comparison with Conventional Heating. *European journal of organic chemistry* **2013**, 2013, 1506-1514.
108. Frade, V. H. J.; Sousa, M. J.; Moura, J. C. V. P.; Goncalves, M. S. T., Synthesis, characterisation and antimicrobial activity of new benzo[a] phenoxazine based fluorophores. *Tetrahedron Lett* **2007**, 48, 8347-8352.

109. Wang, B.; Fan, J.; Wang, X.; Zhu, H.; Wang, J.; Mu, H.; Peng, X., A Nile blue based infrared fluorescent probe: imaging tumors that over-express cyclooxygenase-2. *Chem Commun (Camb)* **2015**, 51, 792-5.
110. Frade, V. H. J.; Coutinho, P. J. G.; Moura, J. C. V. P.; Goncalves, M. S. T., Functionalised benzo[a]phenoxazine dyes as long-wavelength fluorescent probes for amino acids. *Tetrahedron* **2007**, 63, 1654-1663.
111. Frade, V. H. J.; Barros, S. A.; Moura, J. C. V. P.; Goncalves, M. S. T., Fluorescence derivatisation of amino acids in short and long-wavelengths. *Tetrahedron Lett* **2007**, 48, 3403-3407.
112. Denkert, C.; Winzer, K. J.; Muller, B. M.; Weichert, W.; Pest, S.; Kobel, M.; Kristiansen, G.; Reles, A.; Siegert, A.; Guski, H.; Hauptmann, S., Elevated expression of cyclooxygenase-2 is a negative prognostic factor for disease free survival and overall survival in patients with breast carcinoma. *Cancer* **2003**, 97, 2978-87.
113. Uddin, M. J.; Crews, B. C.; Blobaum, A. L.; Kingsley, P. J.; Gorden, D. L.; McIntyre, J. O.; Matrisian, L. M.; Subbaramaiah, K.; Dannenberg, A. J.; Piston, D. W.; Marnett, L. J., Selective visualization of cyclooxygenase-2 in inflammation and cancer by targeted fluorescent imaging agents. *Cancer Res* **2010**, 70, 3618-27.
114. Gautam, R.; Jachak, S. M.; Kumar, V.; Mohan, C. G., Synthesis, biological evaluation and molecular docking studies of stellatin derivatives as cyclooxygenase (COX-1, COX-2) inhibitors and anti-inflammatory agents. *Bioorg Med Chem Lett* **2011**, 21, 1612-6.
115. Vitale, P.; Tacconelli, S.; Perrone, M. G.; Malerba, P.; Simone, L.; Scilimati, A.; Lavecchia, A.; Dovizio, M.; Marcantoni, E.; Bruno, A.; Patrignani, P., Synthesis, pharmacological characterization, and docking analysis of a novel family of diarylisoxazoles as highly selective cyclooxygenase-1 (COX-1) inhibitors. *J Med Chem* **2013**, 56, 4277-99.
116. Zhang, H.; Fan, J.; Wang, J.; Zhang, S.; Dou, B.; Peng, X., An off-on COX-2-specific fluorescent probe: targeting the Golgi apparatus of cancer cells. *J Am Chem Soc* **2013**, 135, 11663-9.
117. Uddin, M. J.; Crews, B. C.; Ghebreselasie, K.; Marnett, L. J., Design, synthesis, and structure-activity relationship studies of fluorescent inhibitors of cycloxygenase-2 as targeted optical imaging agents. *Bioconjugate chemistry* **2013**, 24, 712-23.
118. Yotapan, N.; Charoenpakdee, C.; Wathanathavorn, P.; Ditmangklo, B.; Wagenknecht, H. A.; Vilaivan, T., Synthesis and optical properties of pyrrolidinyl peptide nucleic acid carrying a clicked Nile red label. *Beilstein journal of organic chemistry* **2014**, 10, 2166-74.
119. Park, S. Y.; Kubota, Y.; Funabiki, K.; Shiro, M.; Matsui, M., Near-infrared solid-state fluorescent naphthooxazine dyes attached with bulky dibutylamino and perfluoroalkenyloxy groups at 6-and 9-positions. *Tetrahedron Lett* **2009**, 50, 1131-1135.
120. Gerasimova, T.; Kolchina, E.; Kargapolova, I.; Fokin, E., Synthesis of fluorinated 7-(diethylamino)phenoxazin-3-ones and 9-(diethylamino)-5H-benzo[a]phenoxazin-5-ones. *Russ J Org Chem+* **1997**, 33, 735-739.
121. Ektova, L. V.; Berezhnaya, V. N., Improved synthesis of 9-diethylamino-1,2,3,4,6-pentafluoro-5H-benzo[a]phenoxazin-5-one. *Russ J Org Chem+* **2013**, 49, 1094-1095.
122. Firmino, A.; Goncalves, M. S. A. T., In *International Electronic Conference on Synthetic Organic Chemistry* 2011, pp a42/1-a42/6.
123. Sherman, D. B.; Pitner, J. B.; Ambroise, A.; Thomas, K. J., Synthesis of thiol-reactive, long-wavelength fluorescent phenoxazine derivatives for biosensor applications. *Bioconjugate chemistry* **2006**, 17, 387-392.

124. Kanitz, A.; Hartmann, H., Preparation and characterization of bridged naphthoxazinium salts. *European Journal of Organic Chemistry* **1999**, 923-930.
125. Nakanishi, J.; Nakajima, T.; Sato, M.; Ozawa, T.; Tohda, K.; Umezawa, Y., Imaging of conformational changes of proteins with a new environment/sensitive fluorescent probe designed for site specific labeling of recombinant proteins in live cells. *Analytical chemistry* **2001**, 73, 2920-2928.
126. Lee, H.; Choi, M. G.; Yu, H. Y.; Ahn, S.; Chang, S. K., Selective Mercuration of 2-Hydroxy Nile Red and Its Application towards Chemodosimetric Hg2+-selective Signaling. *B Korean Chem Soc* **2010**, 31, 3539-3542.
127. Adams, S. R.; Campbell, R. E.; Gross, L. A.; Martin, B. R.; Walkup, G. K.; Yao, Y.; Llopis, J.; Tsien, R. Y., New biarsenical ligands and tetracysteine motifs for protein labeling in vitro and in vivo: synthesis and biological applications. *J Am Chem Soc* **2002**, 124, 6063-76.
128. Heo, J.; Lim, C. K.; Whang, D. R.; Shin, J.; Jeong, S. Y.; Park, S. Y.; Kwon, I. C.; Kim, S., Self-deprotonation and colorization of 1,3-bis(dicyanomethylidene)indan in polar media: a facile route to a minimal polymethine dye for NIR fluorescence imaging. *Chemistry* **2012**, 18, 8699-704.
129. Janowska, I.; Zakrzewski, J.; Nakatani, K.; Delaire, J. A.; Palusiak, M.; Walak, M.; Scholl, H., Ferrocenyl D-pi-A chromophores containing 3-dicyanomethylidene-1-indanone and 1,3-bis(dicyanomethylidene)indane acceptor groups. *J Organomet Chem* **2003**, 675, 35-41.
130. Foley, J. W.; Song, X. Z.; Demidova, T. N.; Jalil, F.; Hamblin, M. R., Synthesis and properties of benzo[a] phenoxazinium chalcogen analogues as novel broad-spectrum antimicrobial photosensitizers. (vol 49, pg 5291, 2006). *Journal of Medicinal Chemistry* **2006**, 49, 7252-7252.
131. Raju, B. R.; Sampaio, D. M. F.; Silva, M. M.; Coutinho, P. J. G.; Goncalves, M. S. T., Ultrasound promoted synthesis of Nile Blue derivatives. *Ultrason Sonochem* **2014**, 21, 360-366.
132. Hu, M. M.; Yin, J. H.; Li, Y. H.; Zhao, X. F., Development of a Nile-Blue Based Chemodosimeter for Hg2+ in Aqueous Solution and its Application in Biological Imaging. *Journal of Fluorescence* **2015**, 25, 403-408.
133. Madsen, J.; Canton, I.; Warren, N. J.; Themistou, E.; Blanazs, A.; Ustbas, B.; Tian, X.; Pearson, R.; Battaglia, G.; Lewis, A. L., Nile Blue-Based Nanosized pH Sensors for Simultaneous Far-Red and Near-Infrared Live Bioimaging. *Journal of the American Chemical Society* **2013**, 135, 14863-14870.
134. Fan, J. L.; Dong, H. J.; Hu, M. M.; Wang, J. Y.; Zhang, H.; Zhu, H.; Sun, W.; Peng, X. J., Fluorescence imaging lysosomal changes during cell division and apoptosis observed using Nile Blue based near-infrared emission. *Chem Commun* **2014**, 50, 882-884.
135. Liu, X.-D.; Fan, C.; Sun, R.; Xu, Y.-J.; Ge, J.-F., Nile-red and Nile-blue-based near-infrared fluorescent probes for in-cellulo imaging of hydrogen sulfide. *Analytical and bioanalytical chemistry* **2014**, 406, 7059-7070.
136. Wang, J.; Lin, W.; Li, W., Three-channel fluorescent sensing via organic white light-emitting dyes for detection of hydrogen sulfide in living cells. *Biomaterials* **2013**, 34, 7429-7436.
137. Liu, H.-Y.; Zhao, M.; Qiao, Q.-L.; Lang, H.-J.; Xu, J.-Z.; Xu, Z.-C., Fluorescein-derived fluorescent probe for cellular hydrogen sulfide imaging. *Chinese Chemical Letters* **2014**, 25, 1060-1064.
138. Liu, T.; Zhang, X.; Qiao, Q.; Zou, C.; Feng, L.; Cui, J.; Xu, Z., A two-photon fluorescent probe for imaging hydrogen sulfide in living cells. *Dyes and Pigments* **2013**, 99, 537-542.

139. Deye, J. F.; Berger, T. A.; Anderson, A. G., Nile Red as a solvatochromic dye for measuring solvent strength in normal liquids and mixtures of normal liquids with supercritical and near critical fluids. *Analytical chemistry* **1990**, 62, 615-622.
140. Neber, P. W.; Rauscher, H., Mechanism of the O. Fischer-Hepp rearrangement of nitrosoamines. *Justus Liebigs Annalen der Chemie* **1942**, 550, 182-95.
141. McMurry, J., *Organic chemistry*. 7e. ed.; Thomson Brooks/Cole: Belmont, CA, 2008; p xxiv, 1224, 56, 38 p.
142. He, X. M.; Carter, D. C., Atomic structure and chemistry of human serum albumin. *Nature* **1992**, 358, 209-15.
143. Yang, F.; Zhang, Y.; Liang, H., Interactive association of drugs binding to human serum albumin. *Int J Mol Sci* **2014**, 15, 3580-95.
144. Jose, J.; Burgess, K., Benzophenoxazine-based fluorescent dyes for labeling biomolecules. *Tetrahedron* **2006**, 62, 11021-11037.

APPENDICES

Appendix A — ^{1}H NMR, ^{13}C NMR, HRMS, and IR Spectra

All ^{1}H NMR and ^{13}C NMR spectra were obtained using a 400 MHz Bruker Avance spectrometer and were processed using the Topspin program. All NMR spectra were post processed for this thesis using Mestrenova Lite. High resolution mass spectra were taken using either a Waters Q-TOF micro (ESI-Q-TOF) mass spectrometer provided at the Georgia State University Mass Spectrometry Facility or from a Waters Micromass LCT TOF ES+ Premier Mass Spectrometer.

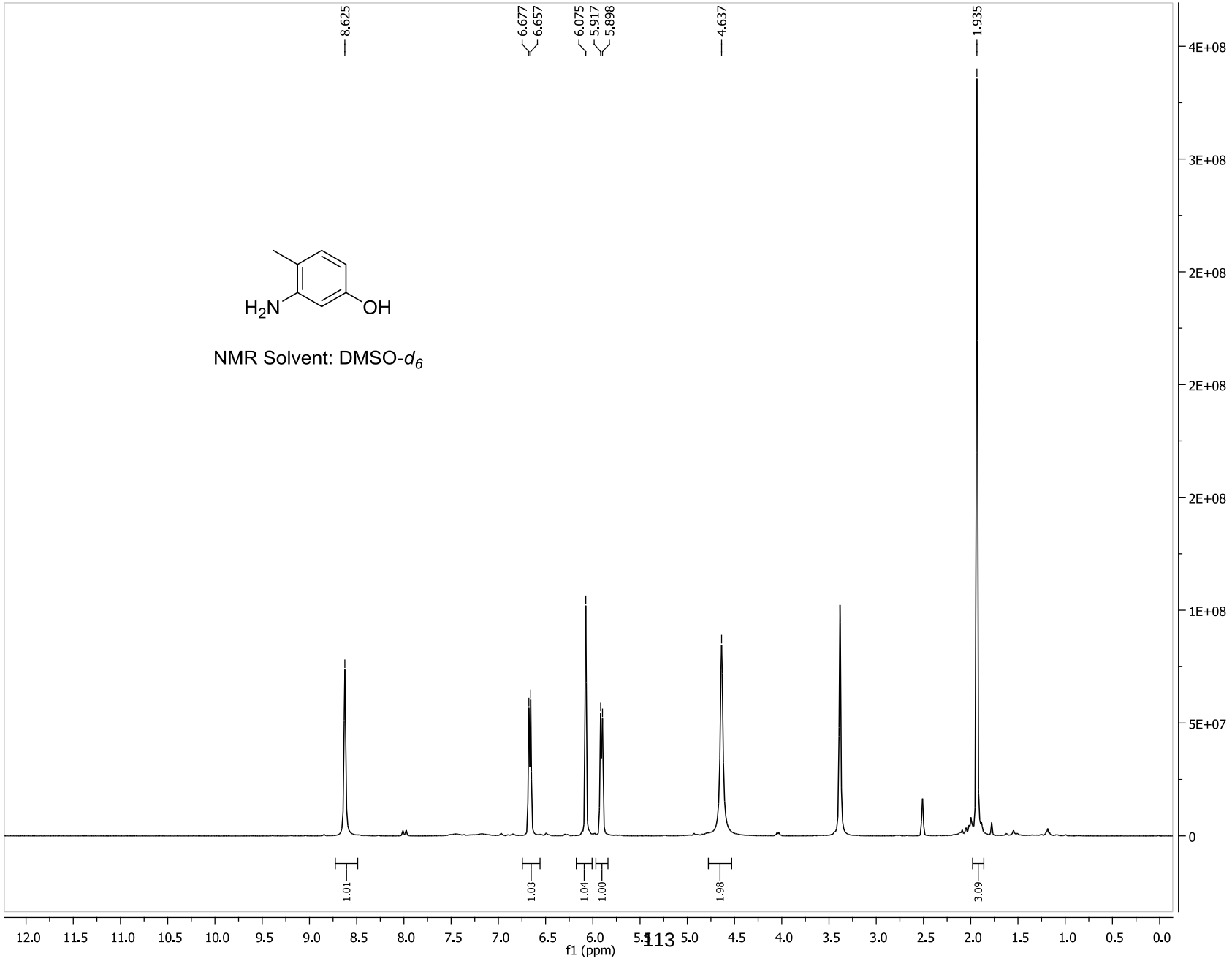
8.625
6.677
6.657
6.075
5.917
5.898
4.637
1.935
H2N
OH
NMR Solvent: DMSO-d6
4E+08
3E+08
2E+08
2E+08
2E+08
1E+08
5E+07
0
1.01
1.03
1.04
1.00
1.98
3.09
12.0 11.5 11.0 10.5 10.0 9.5 9.0 8.5 8.0 7.5 7.0 6.5 6.0 5.5 5.0 4.5 4.0 3.5 3.0 2.5 2.0 1.5 1.0 0.5 0.0
f1 (ppm)

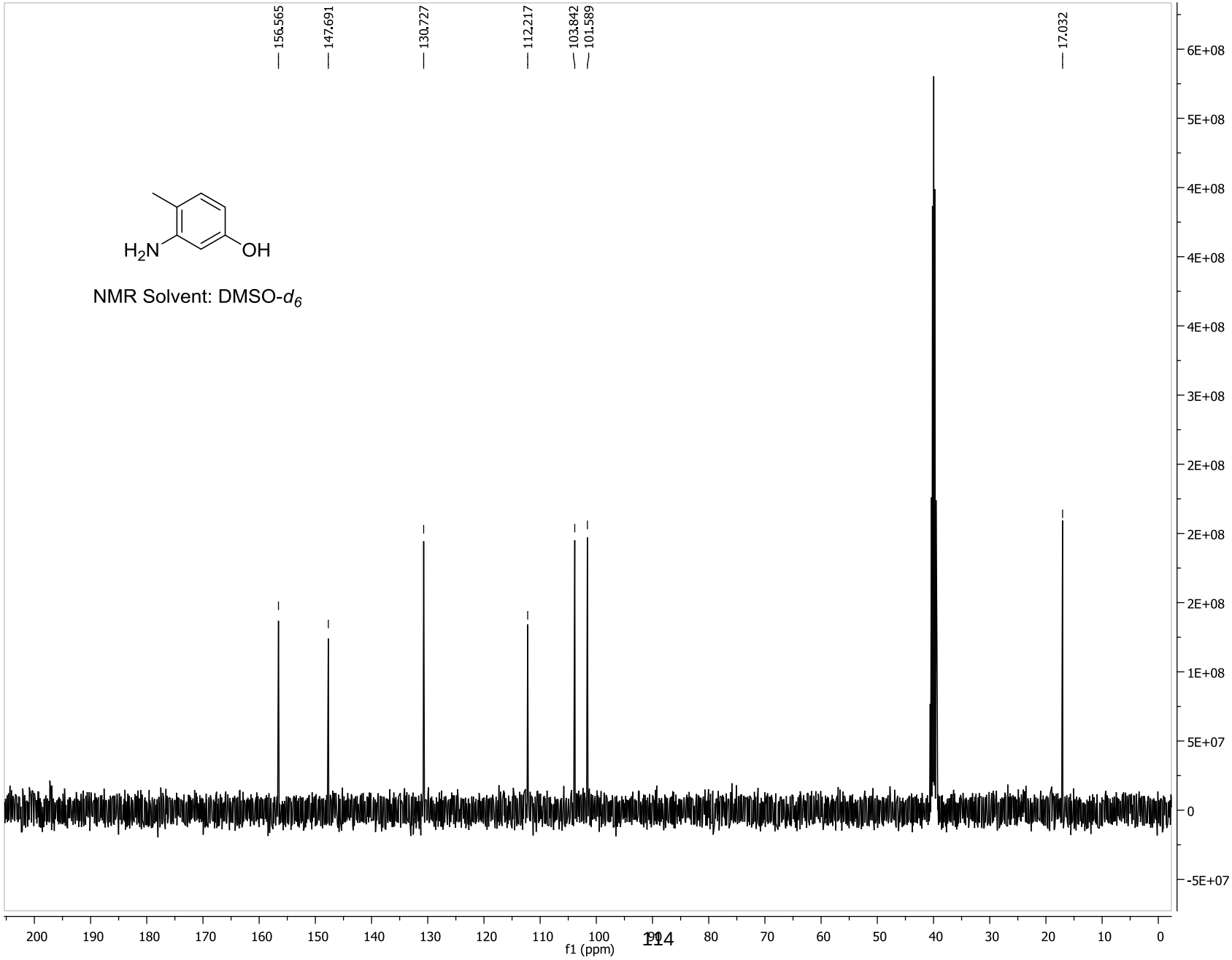
156.565
147.691
130.727
112.217
103.842
101.589
17.032
H2N
OH
NMR Solvent: DMSO-d6
6E+08
5E+08
4E+08
4E+08
4E+08
3E+08
2E+08
2E+08
2E+08
1E+08
5E+07
0
-5E+07
200
190
180
170
160
150
140
130
120
110
100
90
80
70
60
50
40
30
20
10
0
f1 (ppm)

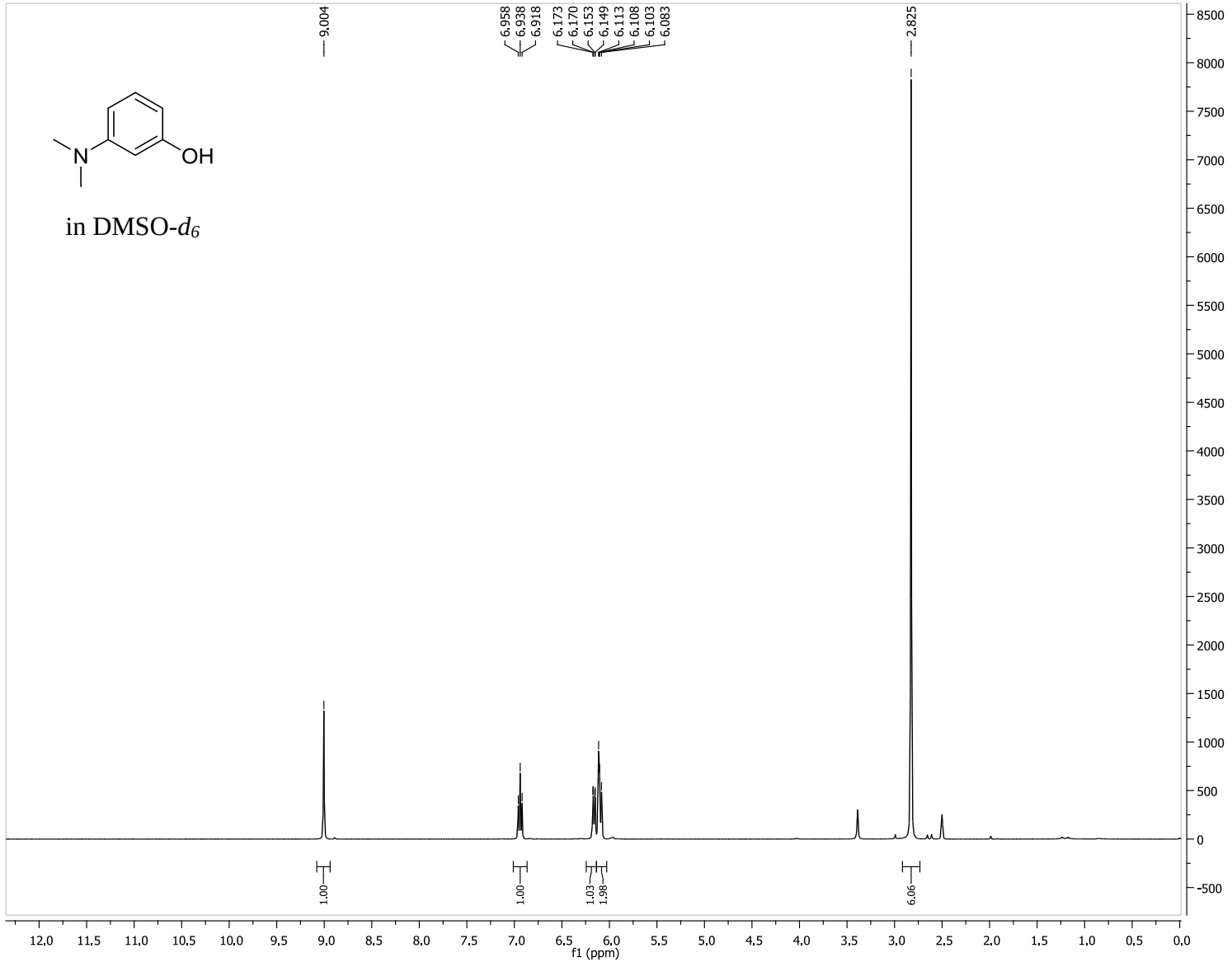
9.004
6.958
6.938
6.918
6.173
6.170
6.153
6.149
6.113
6.108
6.103
6.083
2.825
N
OH
in DMSO-d_6
1.00
1.00
1.03
1.98
6.06
f1 (ppm)

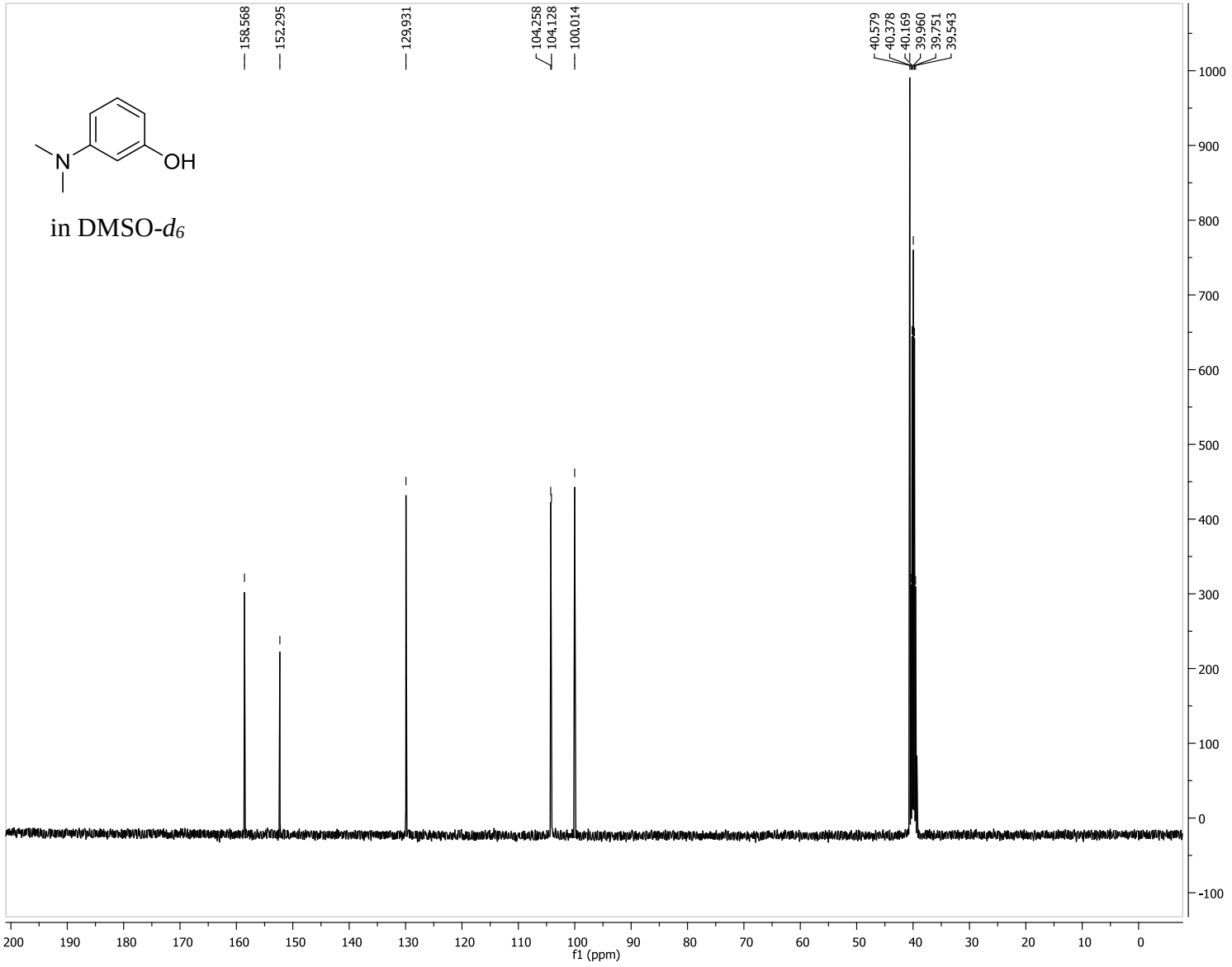
158.568
152.295
129.931
104.258
104.128
100.014
40.579
40.378
40.169
39.960
39.751
39.543
N
OH
in DMSO-d_6
f1 (ppm)

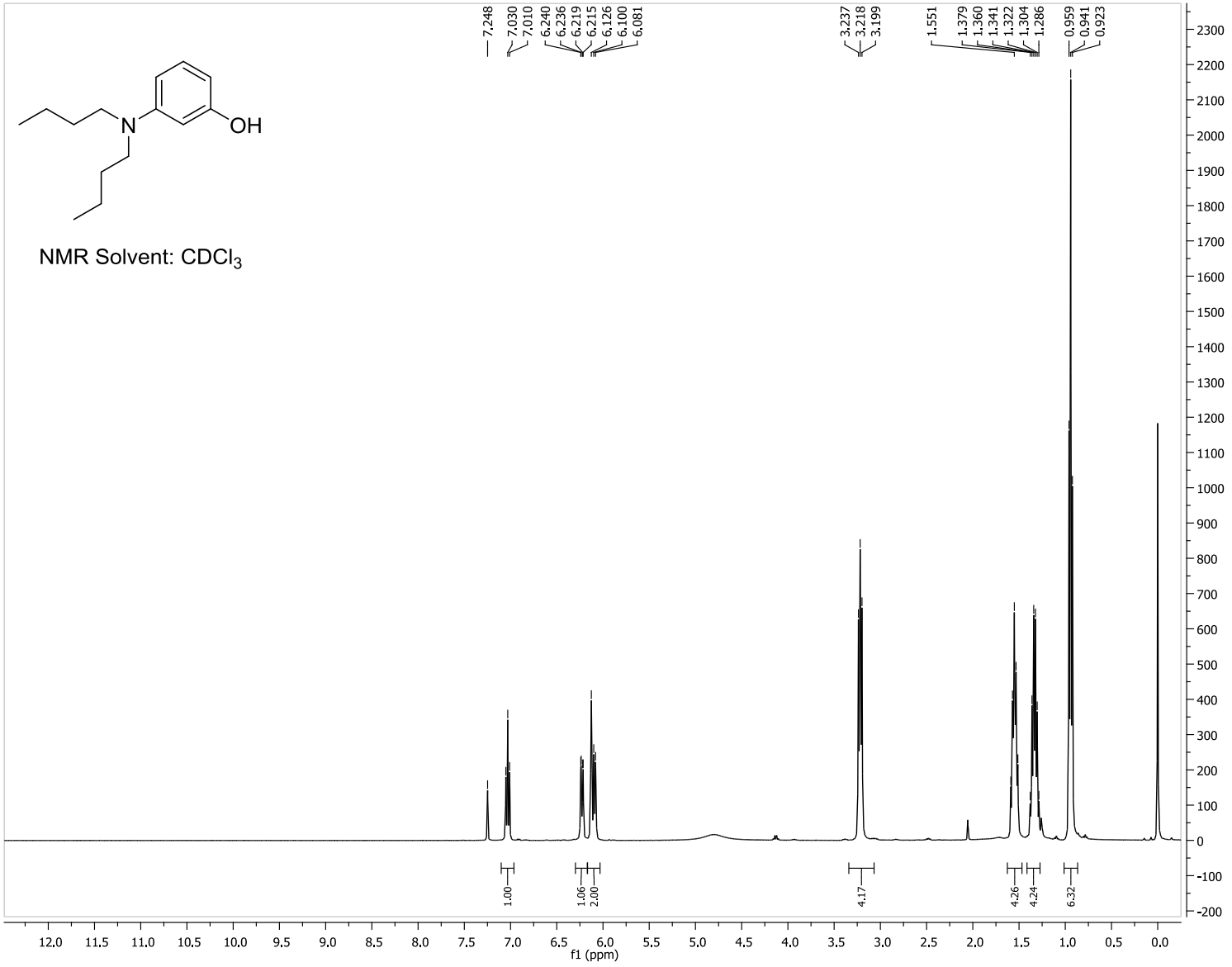
7.248
7.030
7.010
6.240
6.236
6.219
6.215
6.126
6.100
6.081
3.237
3.218
3.199
1.551
1.379
1.360
1.341
1.322
1.304
1.286
0.959
0.941
0.923
N
OH
NMR Solvent: CDCl3
1.00
1.06
2.00
4.17
4.26
4.24
6.32
f1 (ppm)

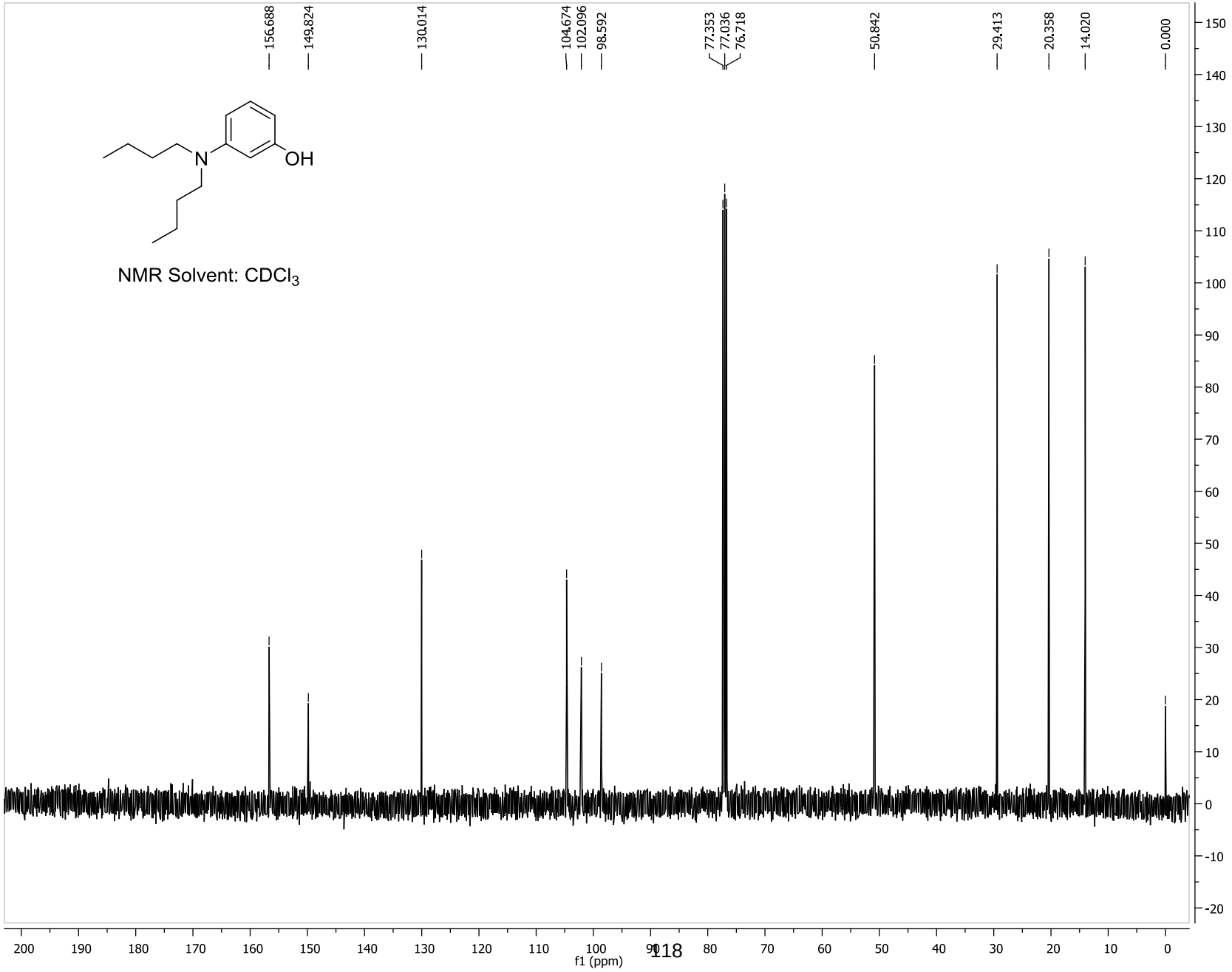
156.688
149.824
130.014
104.674
102.096
98.592
77.353
77.036
76.718
50.842
29.413
20.358
14.020
0.000
N
OH
NMR Solvent: CDCl3
f1 (ppm)

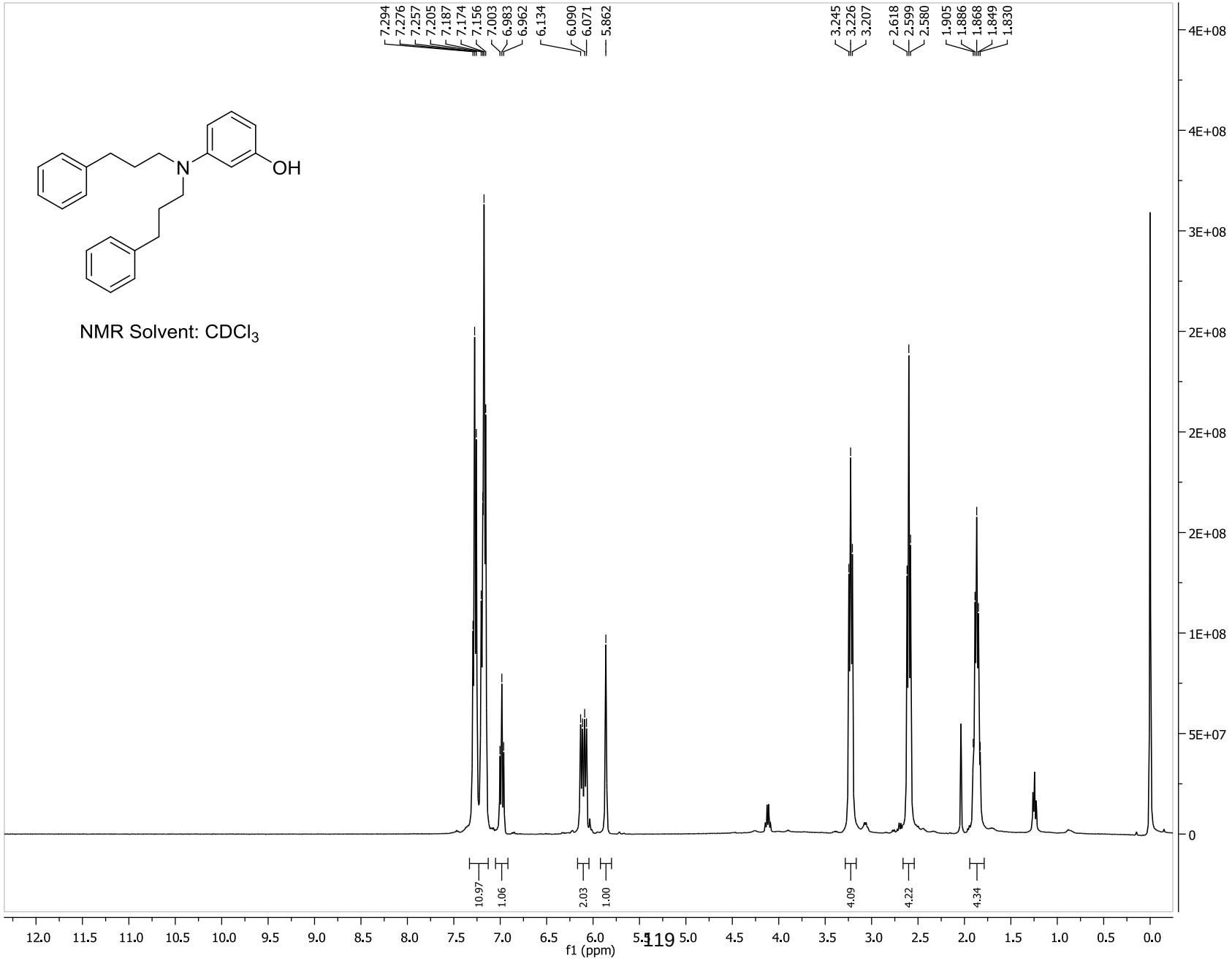
7.294
7.276
7.257
7.205
7.187
7.174
7.156
7.003
6.983
6.962
6.134
6.090
6.071
5.862
3.245
3.226
3.207
2.618
2.599
2.580
1.905
1.886
1.868
1.849
1.830
N
OH
NMR Solvent: CDCl3
4E+08
4E+08
3E+08
2E+08
2E+08
2E+08
1E+08
5E+07
0
10.97
1.06
2.03
1.00
4.09
4.22
4.34
12.0
11.5
11.0
10.5
10.0
9.5
9.0
8.5
8.0
7.5
7.0
6.5
6.0
5.5
5.0
4.5
4.0
3.5
3.0
2.5
2.0
1.5
1.0
0.5
0.0
f1 (ppm)

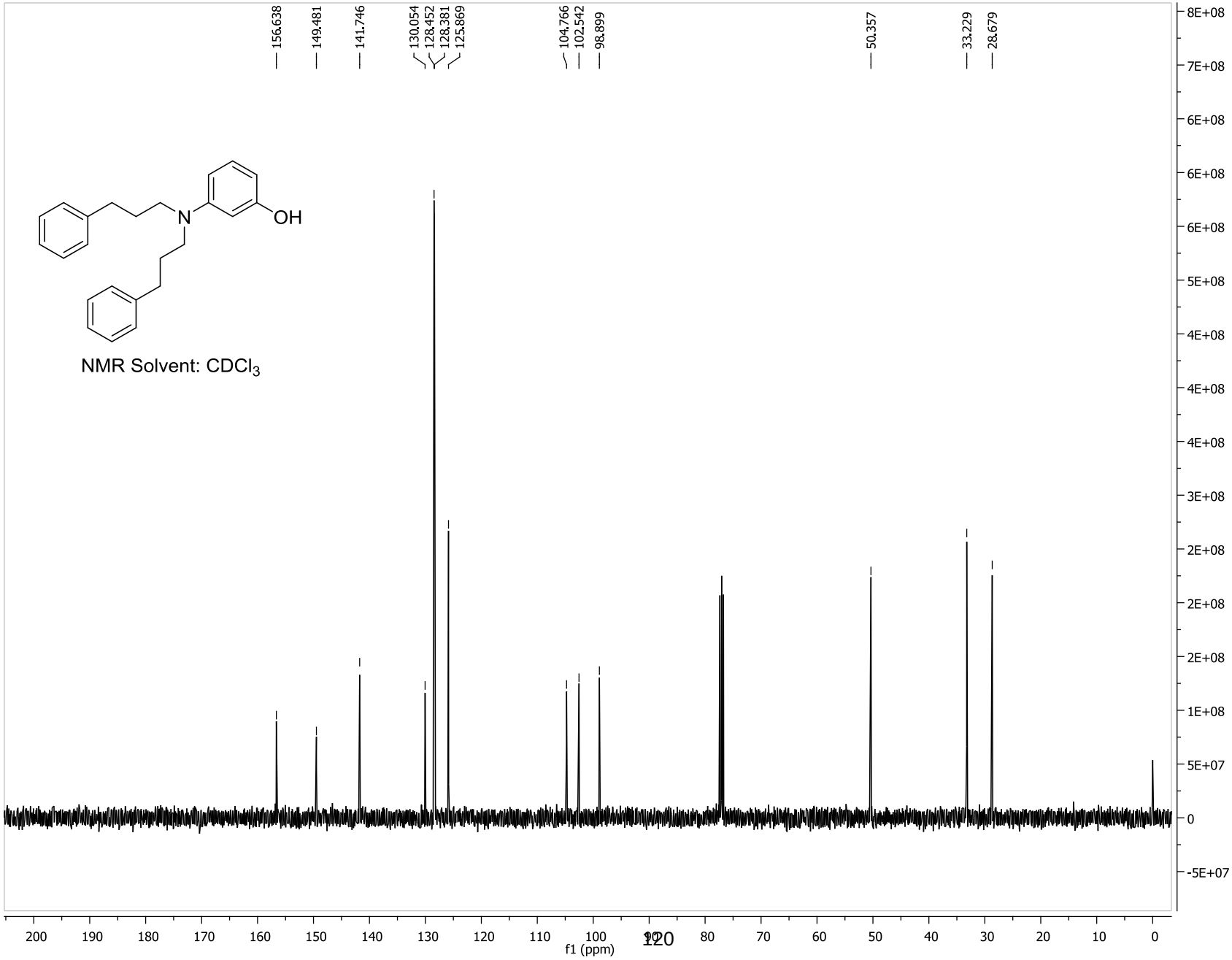
156.638
149.481
141.746
130.054
128.452
128.381
125.869
104.766
102.542
98.899
50.357
33.229
28.679
OH
N
NMR Solvent: CDCl3
8E+08
7E+08
6E+08
6E+08
6E+08
5E+08
4E+08
4E+08
4E+08
3E+08
2E+08
2E+08
2E+08
1E+08
5E+07
0
-5E+07
200
190
180
170
160
150
140
130
120
110
100
90
80
70
60
50
40
30
20
10
0
f1 (ppm)

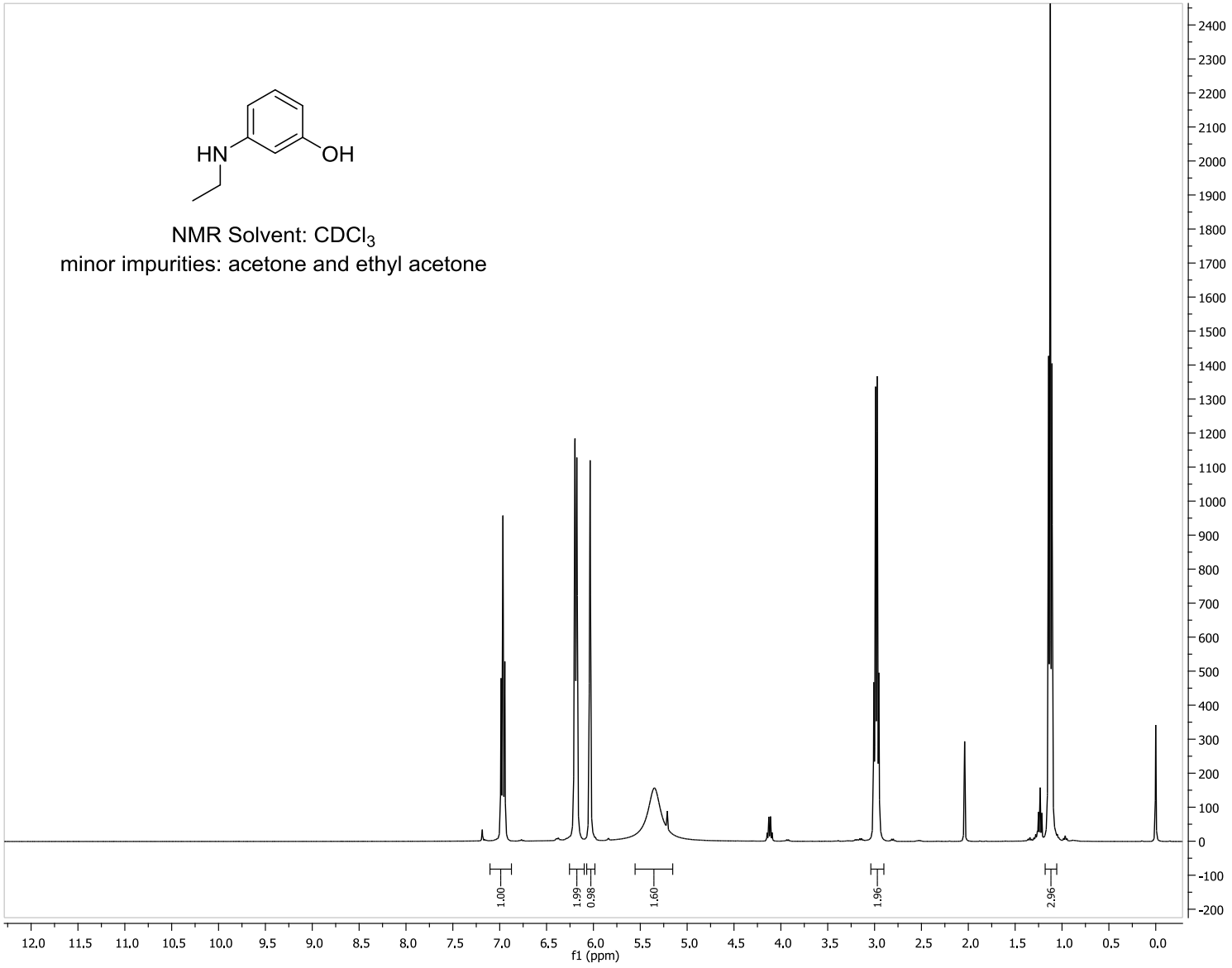
HN
OH
NMR Solvent: CDCl3
minor impurities: acetone and ethyl acetone
1.00
1.99
0.98
1.60
1.96
2.96
f1 (ppm)

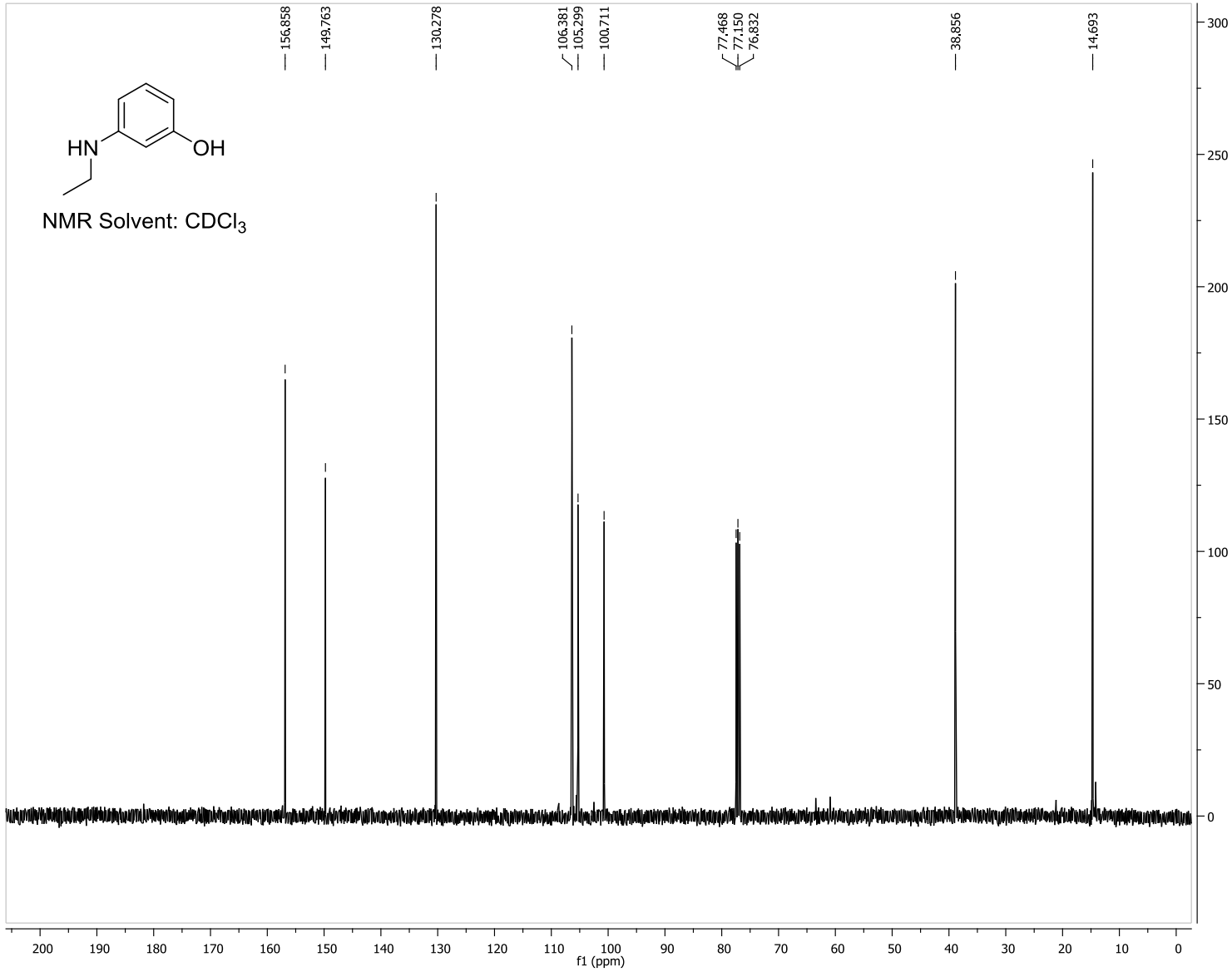
156.858
149.763
130.278
106.381
105.299
100.711
77.468
77.150
76.832
38.856
14.693
HN
OH
NMR Solvent: CDCl3
f1 (ppm)

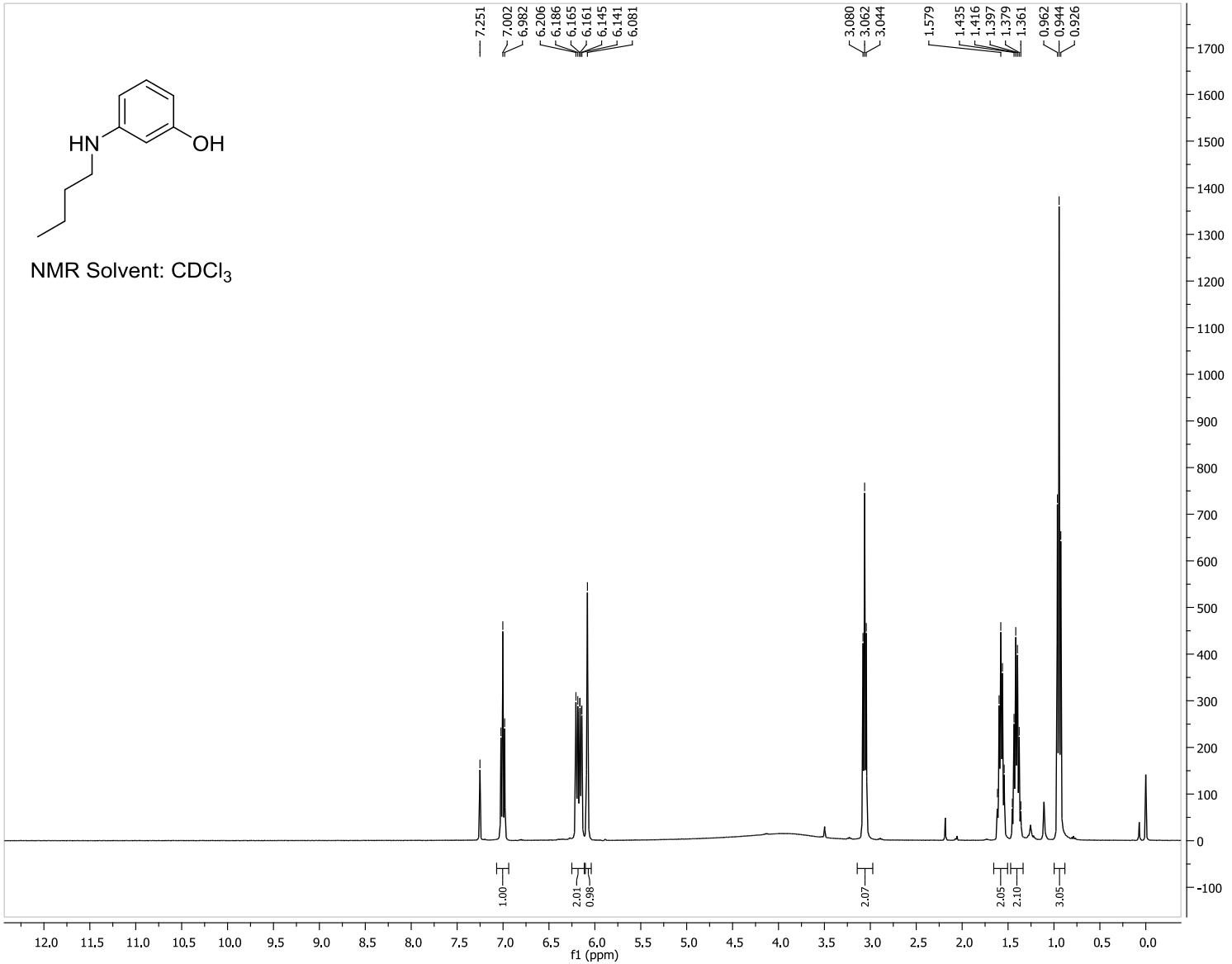
7.251
7.002
6.982
6.206
6.186
6.165
6.161
6.145
6.141
6.081
3.080
3.062
3.044
1.579
1.435
1.416
1.397
1.379
1.361
0.962
0.944
0.926
HN
OH
NMR Solvent: CDCl3
1.00
2.01
0.98
2.07
2.05
2.10
3.05
f1 (ppm)

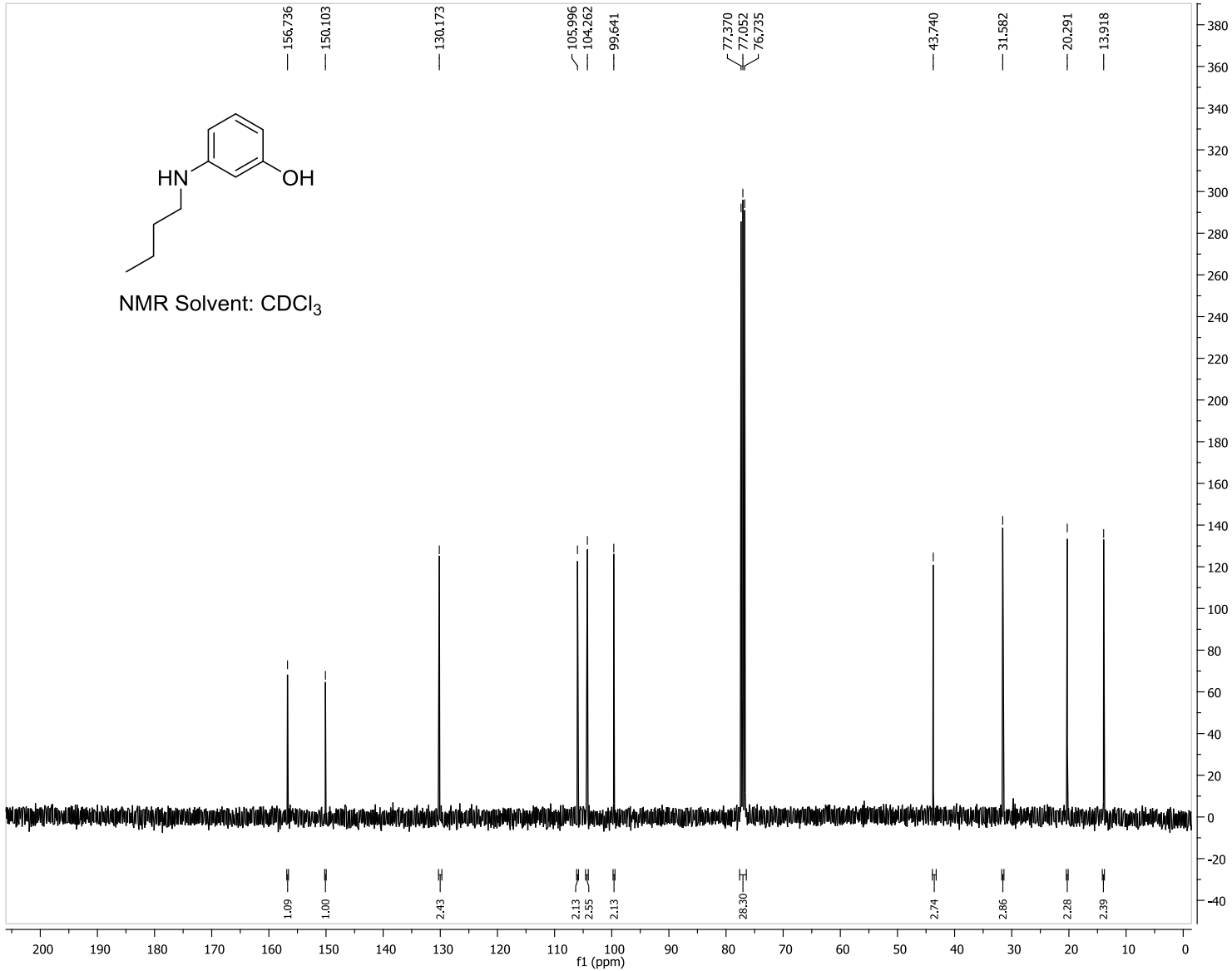
156.736
150.103
130.173
105.996
104.262
99.641
77.370
77.052
76.735
43.740
31.582
20.291
13.918
HN
OH
NMR Solvent: CDCl3
1.09
1.00
2.43
2.13
2.55
2.13
28.30
2.74
2.86
2.28
2.39
f1 (ppm)

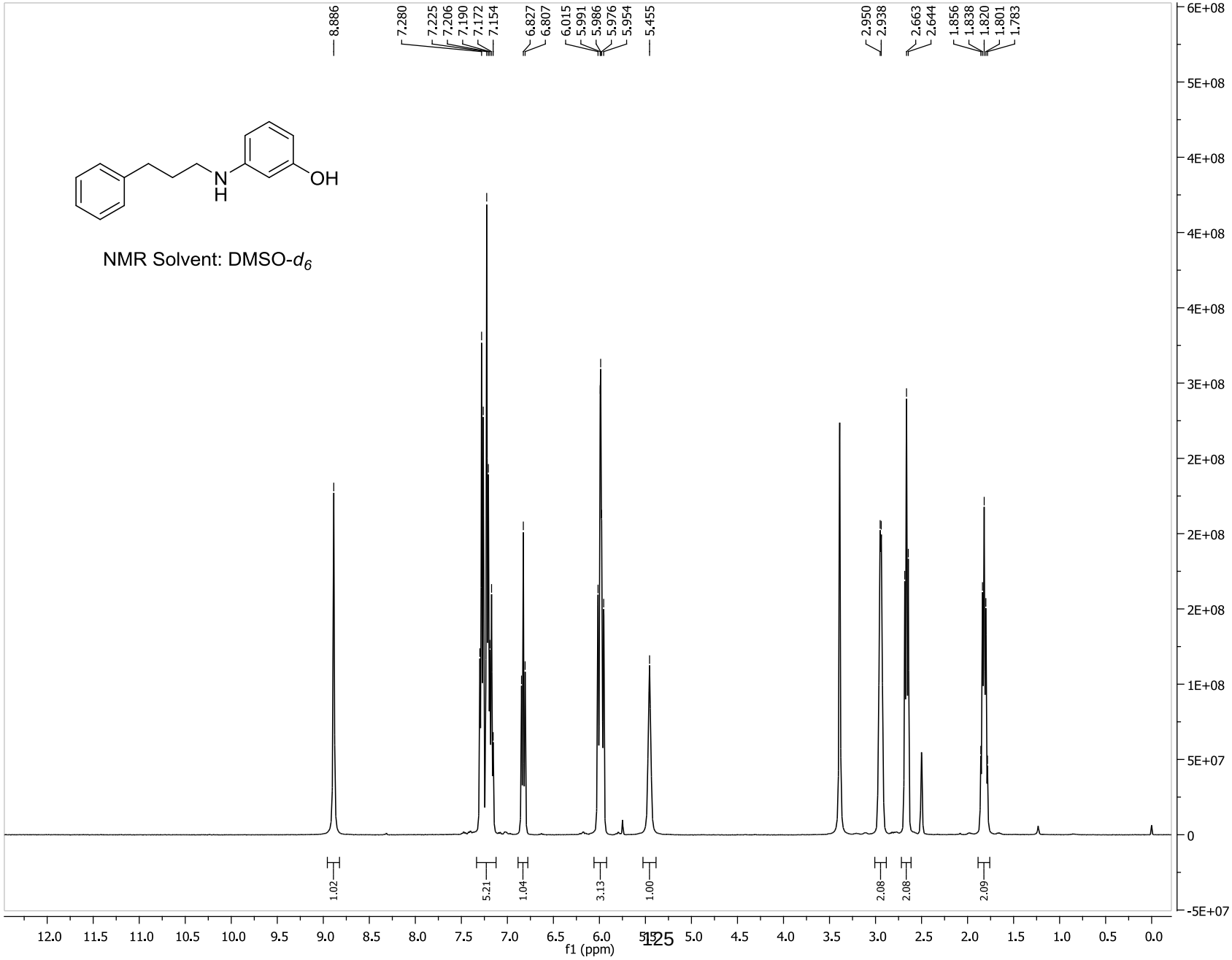
8.886
7.280
7.225
7.206
7.190
7.172
7.154
6.827
6.807
6.015
5.991
5.986
5.976
5.954
5.455
2.950
2.938
2.663
2.644
1.856
1.838
1.820
1.801
1.783
N
H
OH
NMR Solvent: DMSO-d_6
1.02
5.21
1.04
3.13
1.00
2.08
2.08
2.09
f1 (ppm)

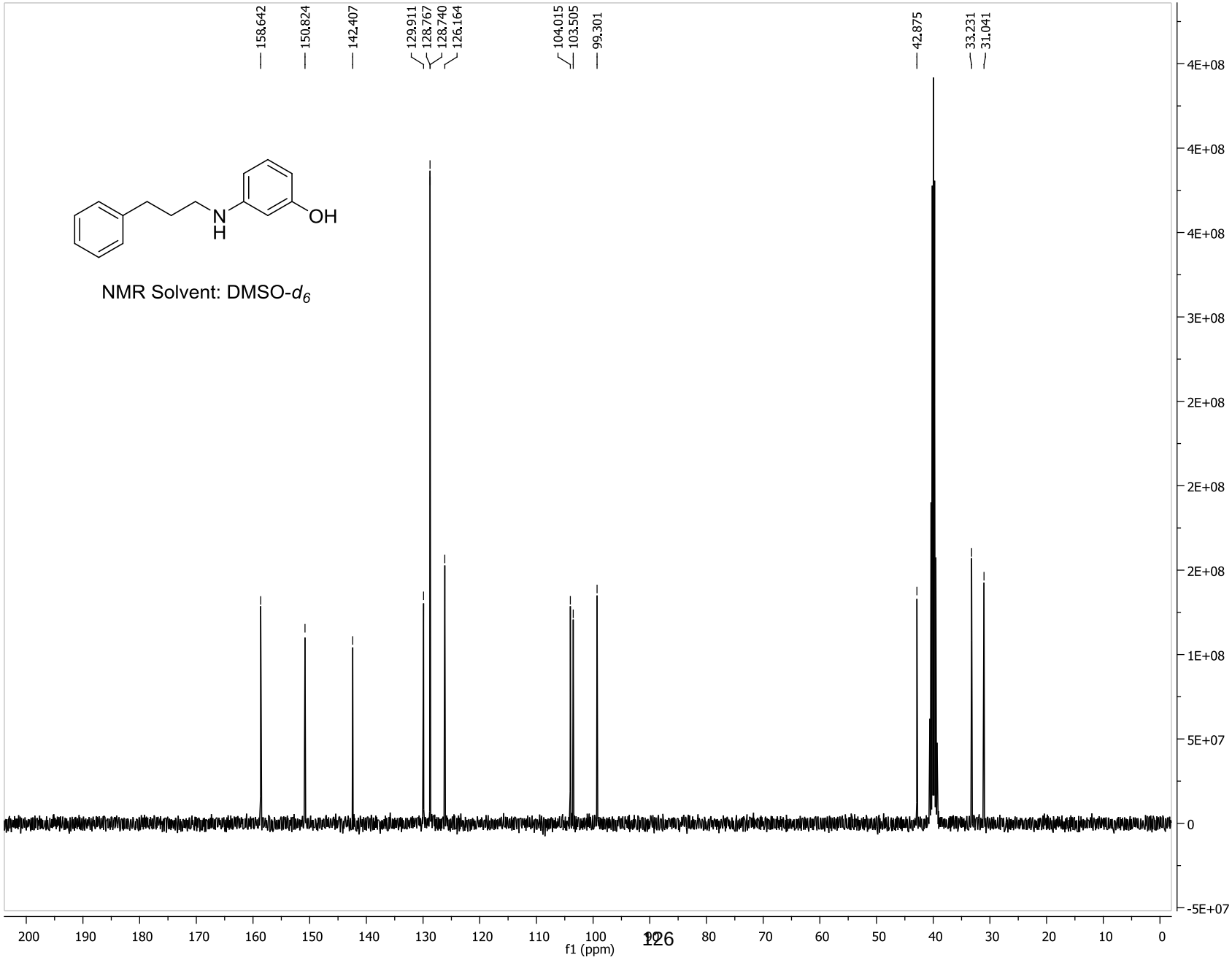
158.642
150.824
142.407
129.911
128.767
128.740
126.164
104.015
103.505
99.301
42.875
33.231
31.041
N
H
OH
NMR Solvent: DMSO-d_6
4E+08
4E+08
4E+08
3E+08
2E+08
2E+08
2E+08
1E+08
5E+07
0
-5E+07
200
190
180
170
160
150
140
130
120
110
100
90
80
70
60
50
40
30
20
10
0
f1 (ppm)

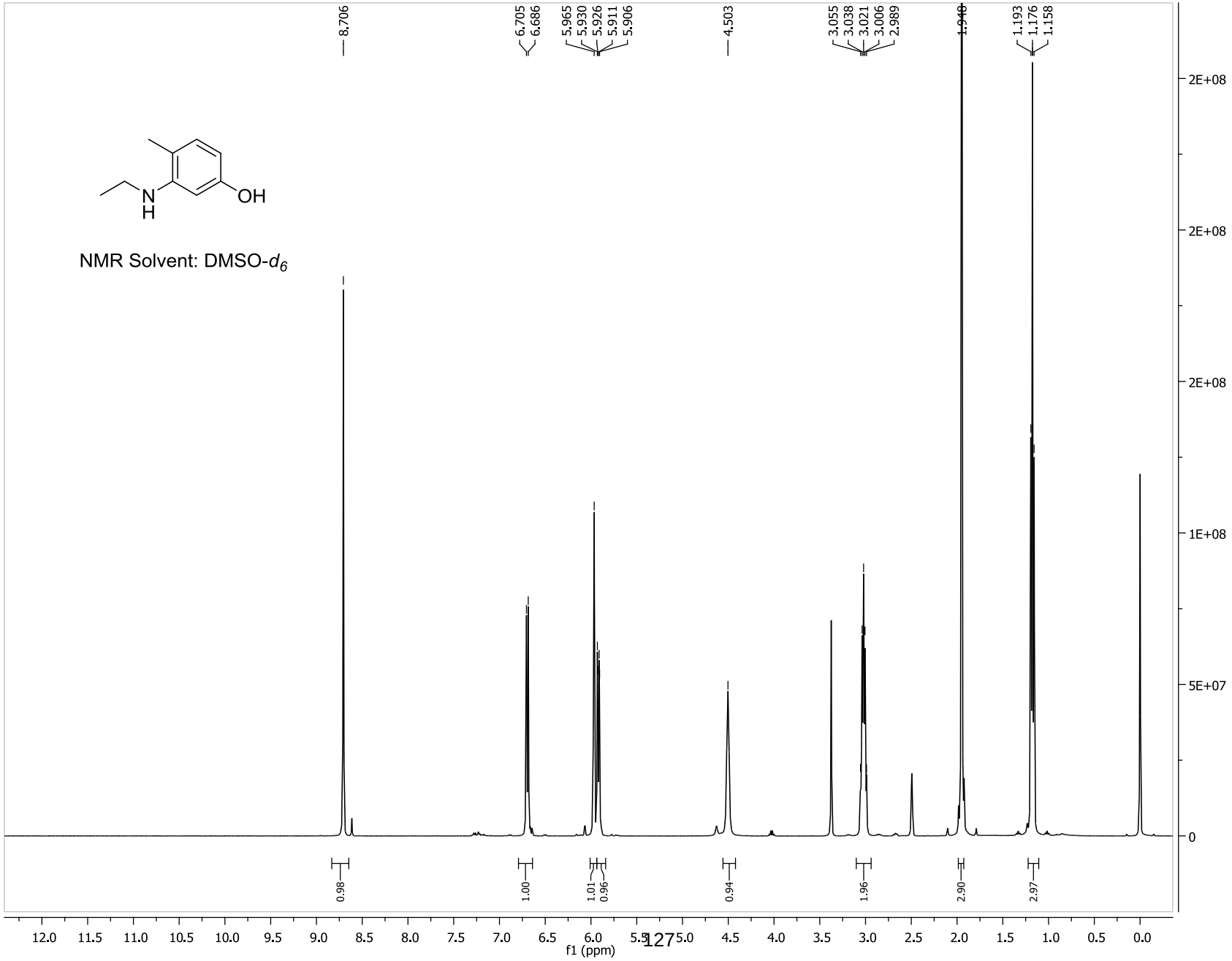
8.706
6.705
6.686
5.965
5.930
5.926
5.911
5.906
4.503
3.055
3.038
3.021
3.006
2.989
1.948
1.193
1.176
1.158
N
H
OH
NMR Solvent: DMSO-d_6
2E+08
2E+08
2E+08
1E+08
5E+07
0
0.98
1.00
1.01
0.96
0.94
1.96
2.90
2.97
12.0 11.5 11.0 10.5 10.0 9.5 9.0 8.5 8.0 7.5 7.0 6.5 6.0 5.5 5.0 4.5 4.0 3.5 3.0 2.5 2.0 1.5 1.0 0.5 0.0
f1 (ppm)

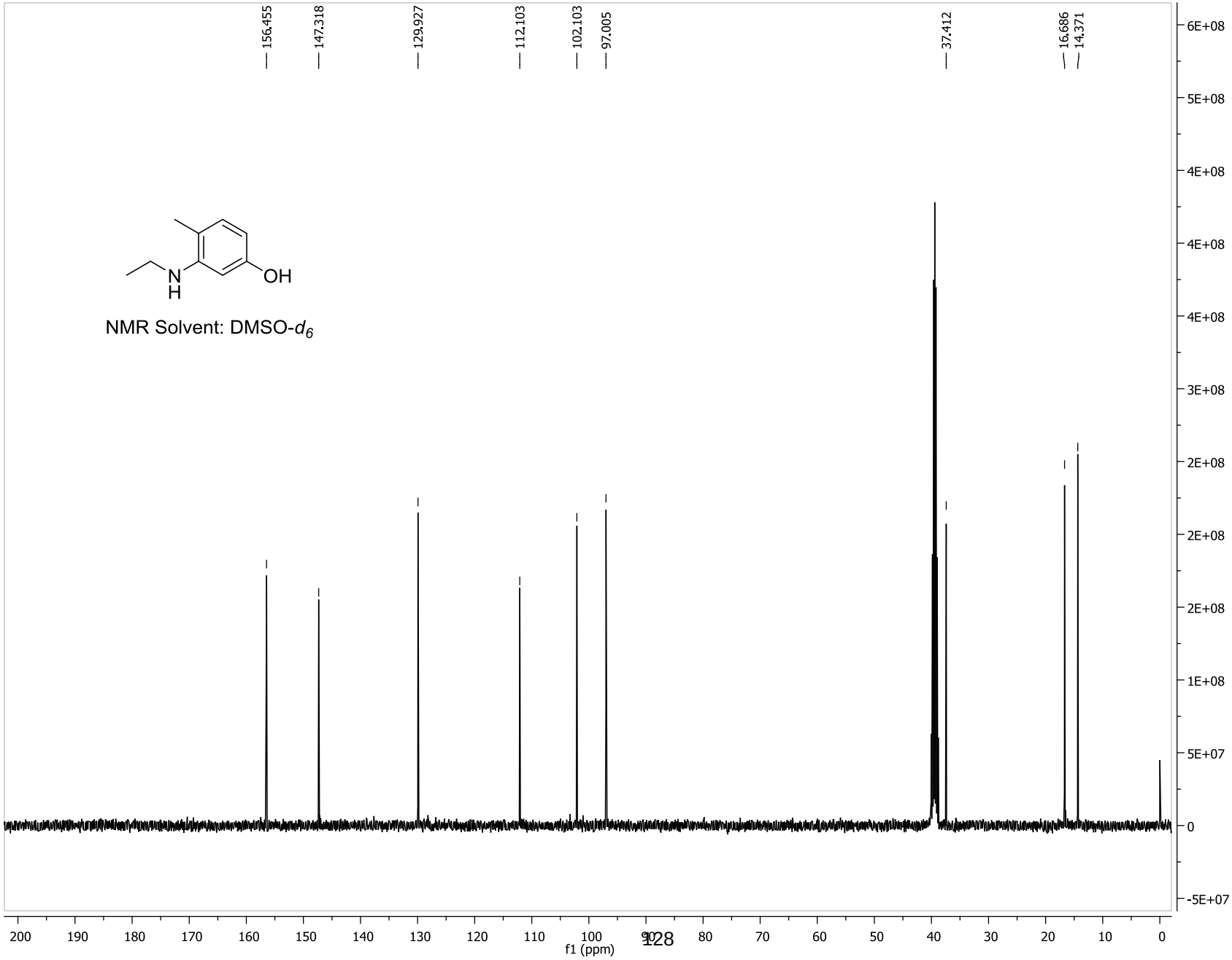
156.455
147.318
129.927
112.103
102.103
97.005
37.412
16.686
14.371
N
H
OH
NMR Solvent: DMSO-d_6
6E+08
5E+08
4E+08
4E+08
4E+08
3E+08
2E+08
2E+08
2E+08
1E+08
5E+07
0
-5E+07
200
190
180
170
160
150
140
130
120
110
100
90
80
70
60
50
40
30
20
10
0
f1 (ppm)

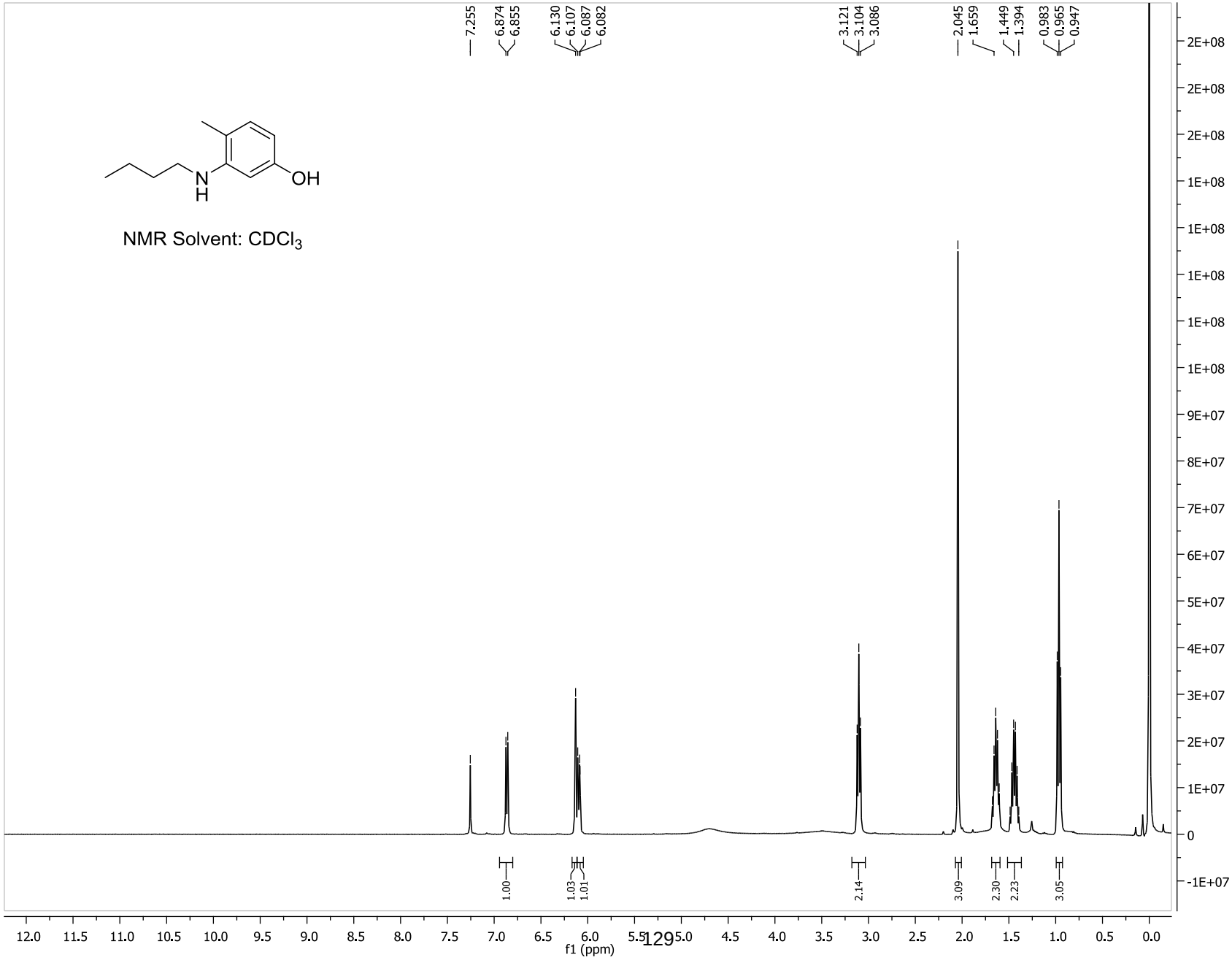
7.255
6.874
6.855
6.130
6.107
6.087
6.082
3.121
3.104
3.086
2.045
1.659
1.449
1.394
0.983
0.965
0.947
N
H
OH
NMR Solvent: CDCl3
1.00
1.03
1.01
2.14
3.09
2.30
2.23
3.05
f1 (ppm)

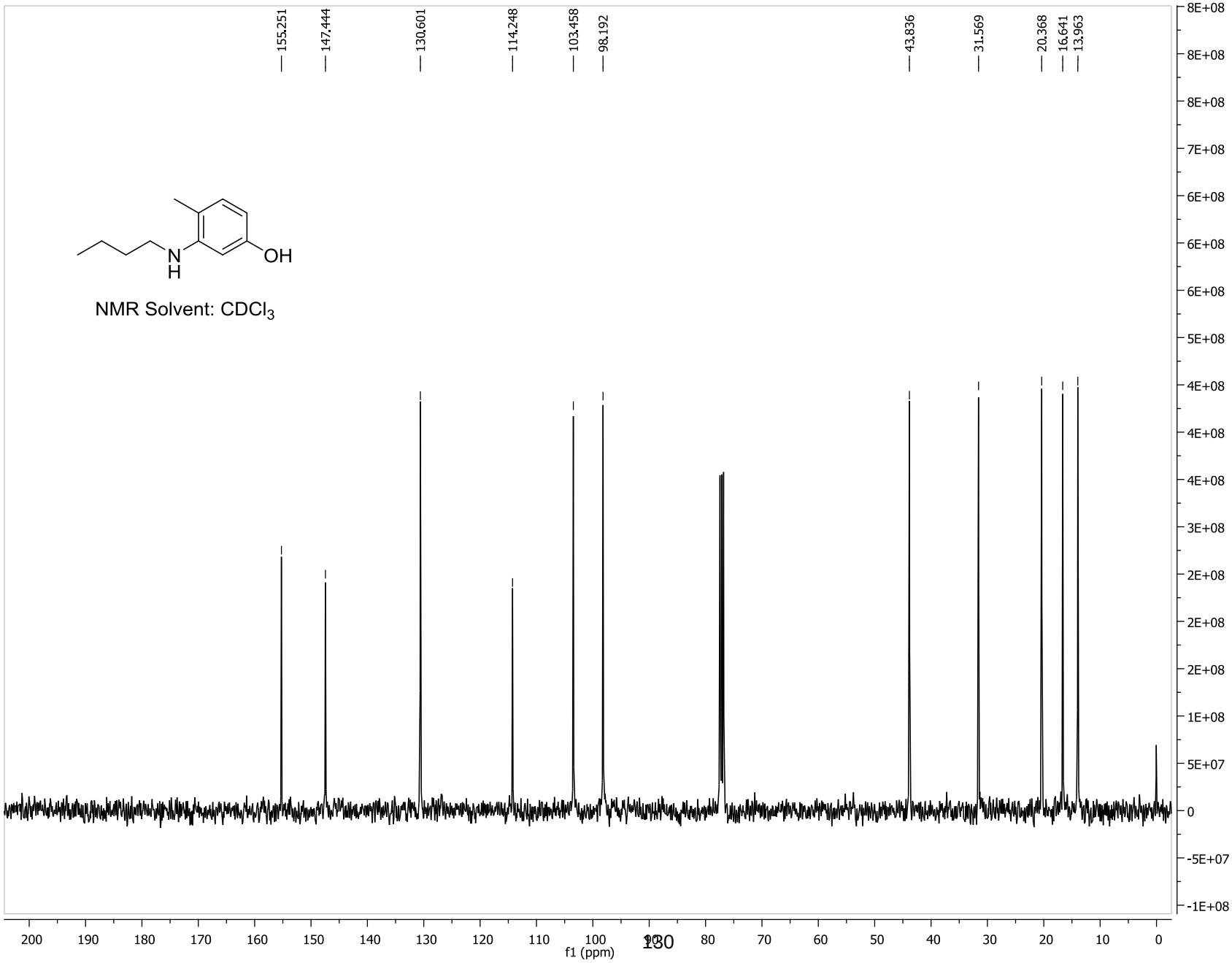
155.251
147.444
130.601
114.248
103.458
98.192
43.836
31.569
20.368
16.641
13.963
N
H
OH
NMR Solvent: CDCl3
f1 (ppm)

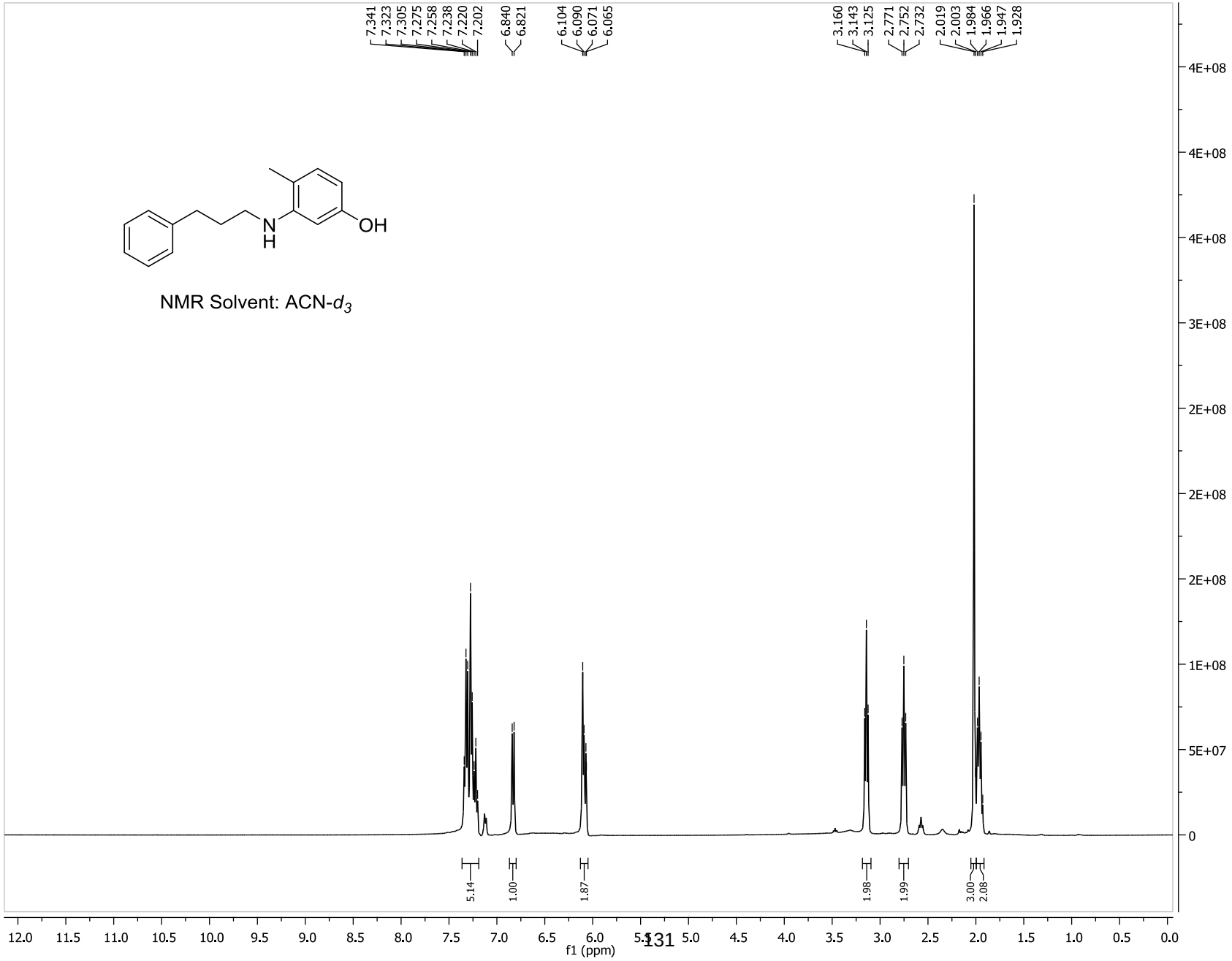
7.341
7.323
7.305
7.275
7.258
7.238
7.220
7.202
6.840
6.821
6.104
6.090
6.071
6.065
3.160
3.143
3.125
2.771
2.752
2.732
2.019
2.003
1.984
1.966
1.947
1.928
N
H
OH
NMR Solvent: ACN-d_3
4E+08
4E+08
4E+08
3E+08
2E+08
2E+08
2E+08
1E+08
5E+07
0
5.14
1.00
1.87
1.98
1.99
3.00
2.08
12.0
11.5
11.0
10.5
10.0
9.5
9.0
8.5
8.0
7.5
7.0
6.5
6.0
5.5
5.0
4.5
4.0
3.5
3.0
2.5
2.0
1.5
1.0
0.5
0.0
f1 (ppm)

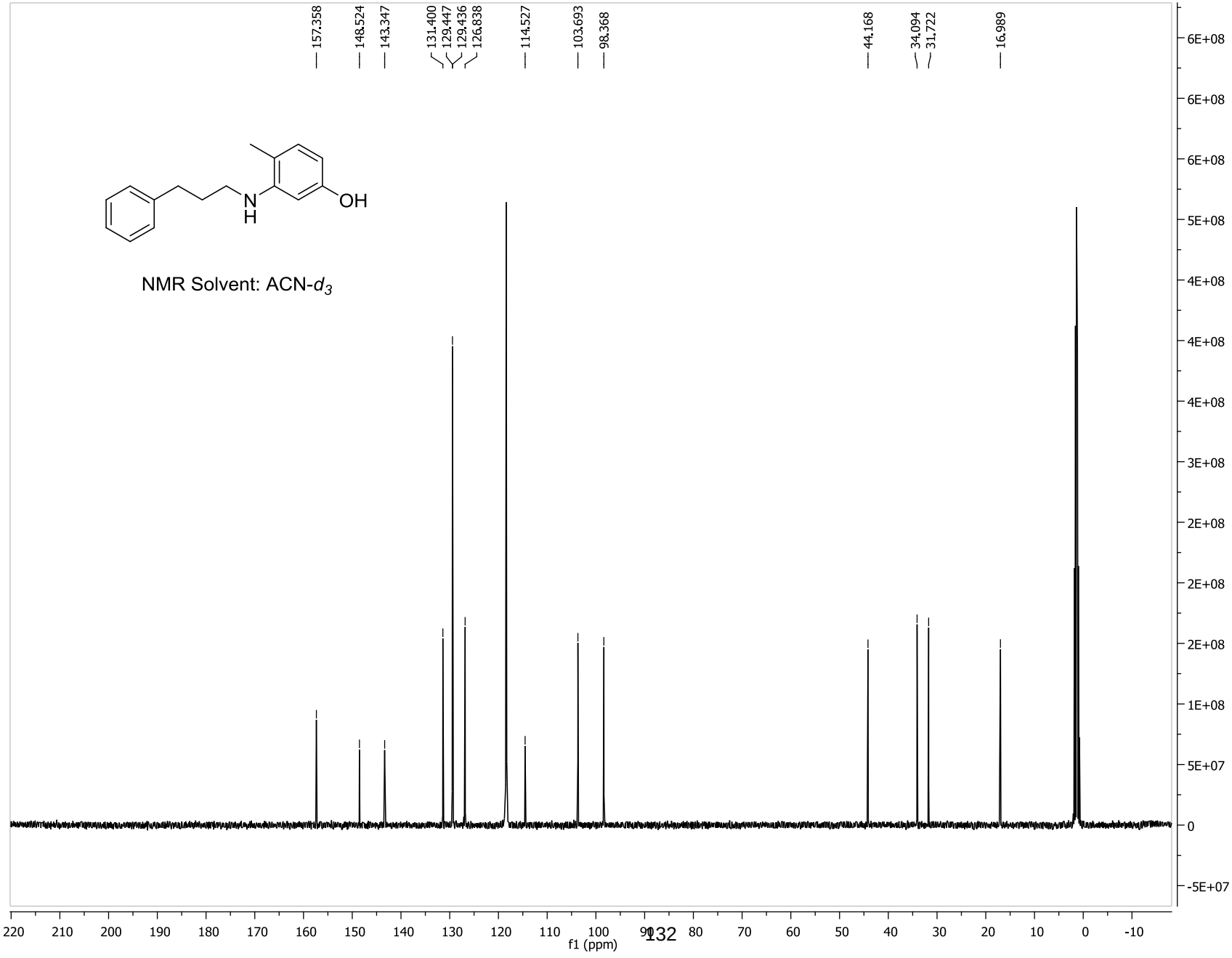
157.358
148.524
143.347
131.400
129.447
129.436
126.838
114.527
103.693
98.368
44.168
34.094
31.722
16.989
OH
N
H
NMR Solvent: ACN-d_3
6E+08
5E+08
4E+08
3E+08
2E+08
1E+08
5E+07
0
-5E+07
220 210 200 190 180 170 160 150 140 130 120 110 100 90 80 70 60 50 40 30 20 10 0 -10
f1 (ppm)

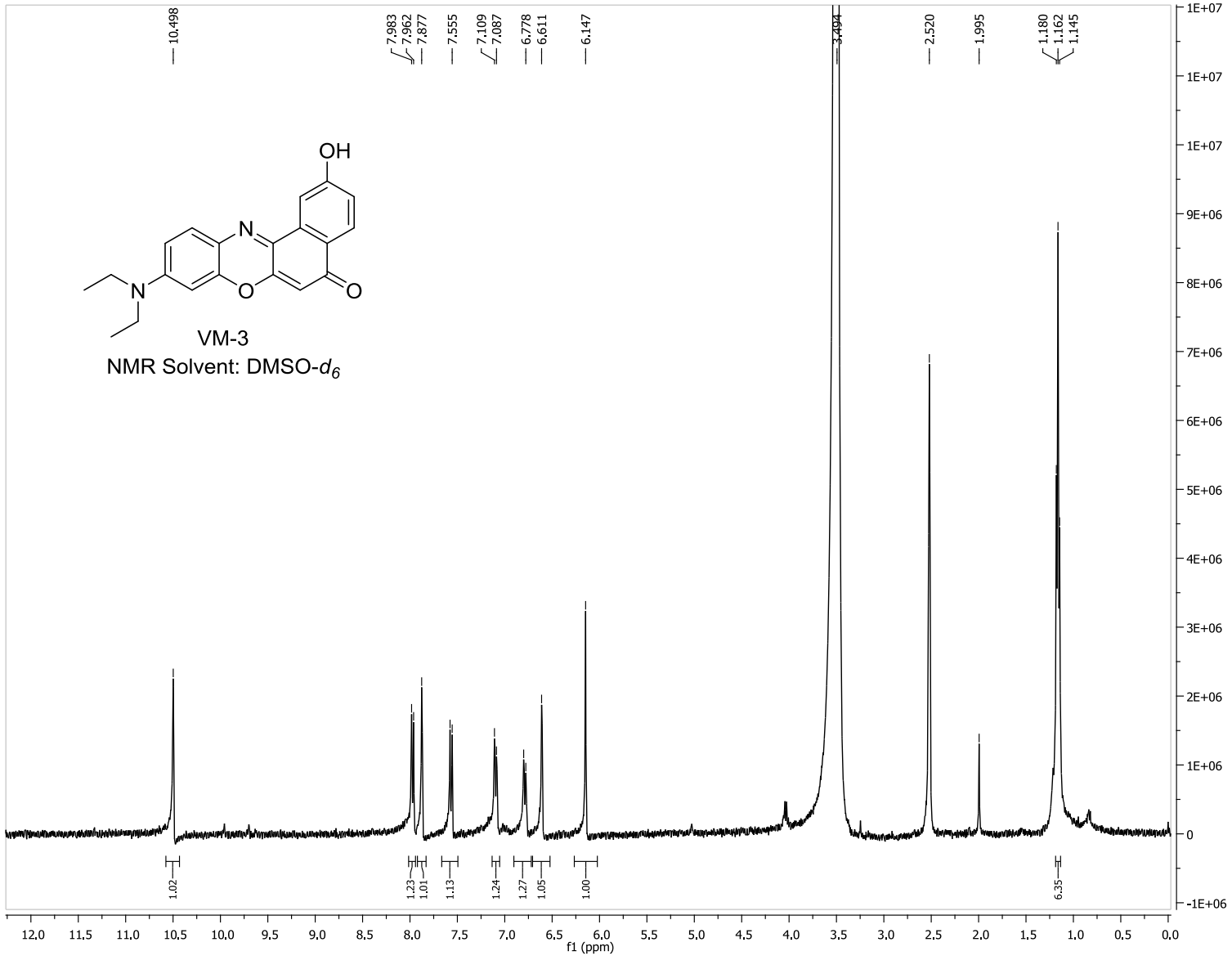
10.498
7.983
7.962
7.877
7.555
7.109
7.087
6.778
6.611
6.147
3.494
2.520
1.995
1.180
1.162
1.145
OH
N
O
N
O
VM-3
NMR Solvent: DMSO-d_6
1.02
1.23
1.01
1.13
1.24
1.27
1.05
1.00
6.35
f1 (ppm)

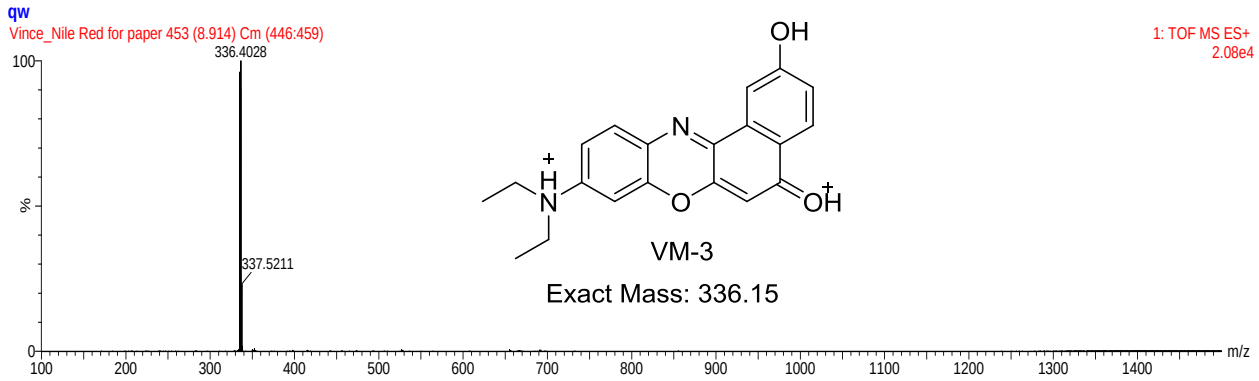
qw
Vince_Nile Red for paper 453 (8.914) Cm (446:459)
1: TOF MS ES+
2.08e4
336.4028
337.5211
%
m/z
VM-3
Exact Mass: 336.15

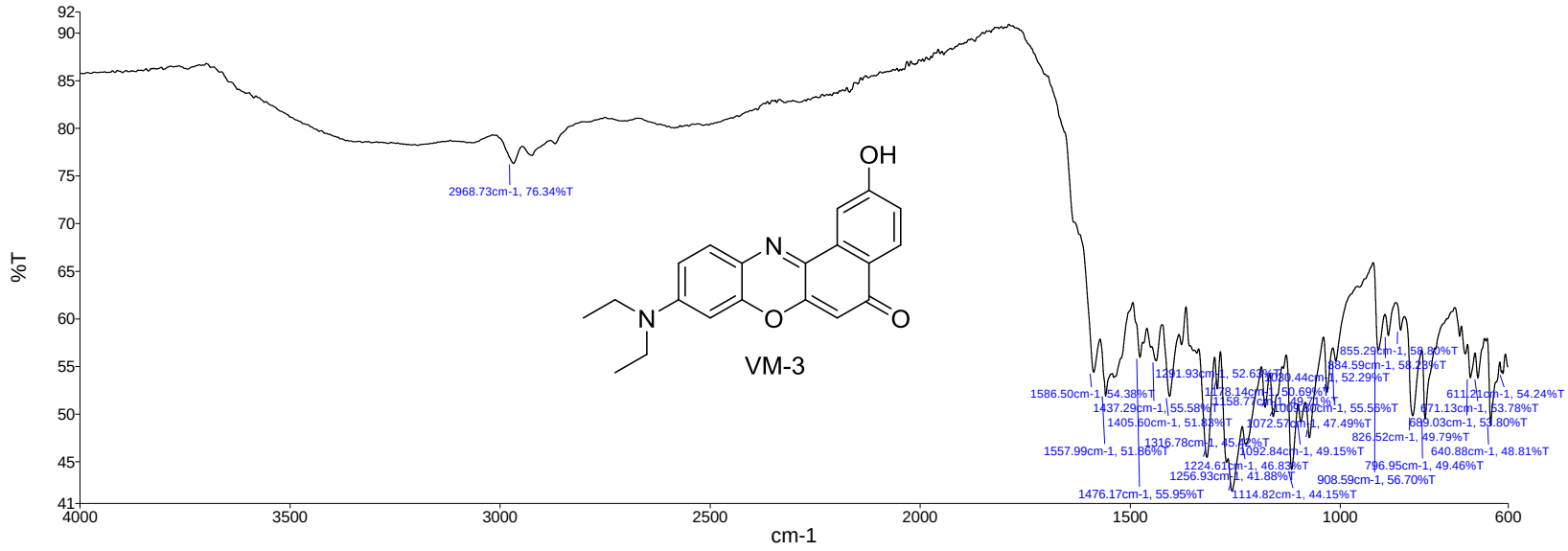
%T
cm-1
2968.73cm-1, 76.34%T
VM-3
1586.50cm-1, 54.38%T
1557.99cm-1, 51.86%T
1476.17cm-1, 55.95%T
1437.29cm-1, 55.58%T
1405.60cm-1, 51.68%T
1316.78cm-1, 45.82%T
1256.93cm-1, 41.88%T
1224.61cm-1, 46.83%T
1114.82cm-1, 44.15%T
1092.84cm-1, 49.15%T
1072.57cm-1, 47.49%T
908.59cm-1, 56.70%T
826.52cm-1, 49.79%T
796.95cm-1, 49.46%T
689.03cm-1, 53.80%T
640.88cm-1, 48.81%T
611.21cm-1, 54.24%T

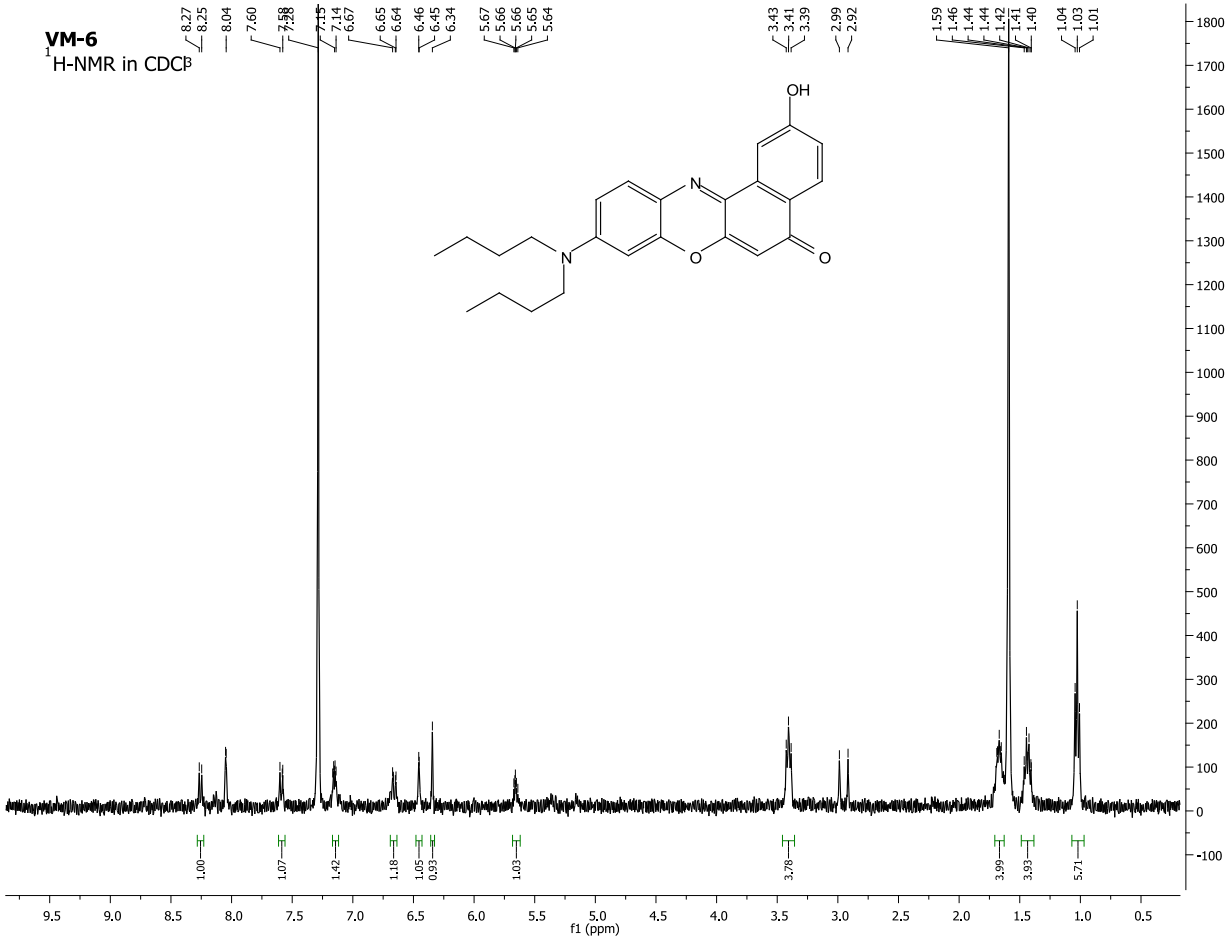
VM-6
1H-NMR in CDCl3
OH
N
O
N
O
f1 (ppm)

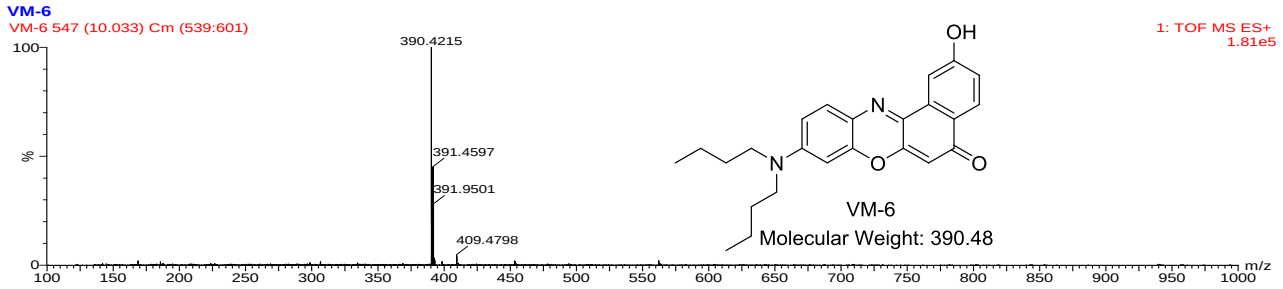
VM-6
VM-6 547 (10.033) Cm (539:601)
1: TOF MS ES+
1.81e5
390.4215
391.4597
391.9501
409.4798
%
m/z
OH
N
O
O
VM-6
Molecular Weight: 390.48

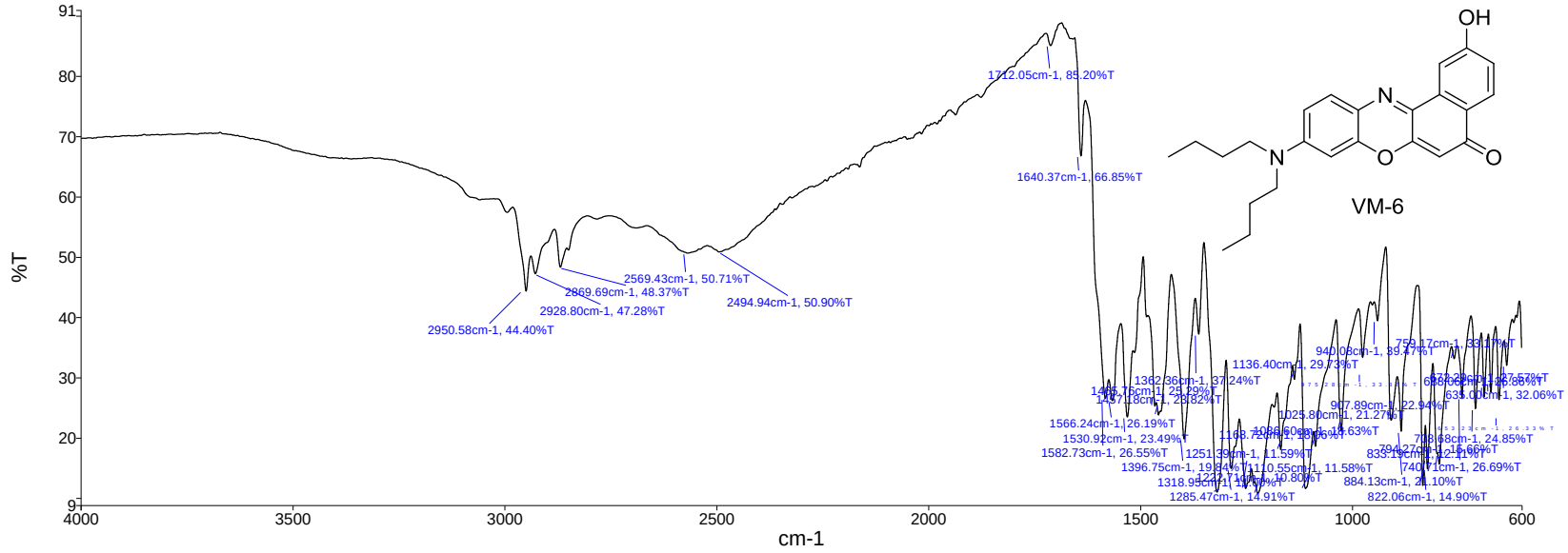
%T
cm-1
1712.05cm-1, 85.20%T
1640.37cm-1, 66.85%T
2950.58cm-1, 44.40%T
2928.80cm-1, 47.28%T
2869.69cm-1, 48.37%T
2569.43cm-1, 50.71%T
2494.94cm-1, 50.90%T
1566.24cm-1, 26.19%T
1530.92cm-1, 23.49%T
1582.73cm-1, 26.55%T
1396.75cm-1, 19.84%T
1318.95cm-1, 19.80%T
1285.47cm-1, 14.91%T
1136.40cm-1, 29.73%T
1362.36cm-1, 37.24%T
1251.39cm-1, 11.59%T
1110.55cm-1, 11.58%T
1025.80cm-1, 21.27%T
907.89cm-1, 22.94%T
884.13cm-1, 20.10%T
822.06cm-1, 14.90%T
740.11cm-1, 26.69%T
728.68cm-1, 24.85%T
633.00cm-1, 32.06%T
OH
N
O
O
VM-6

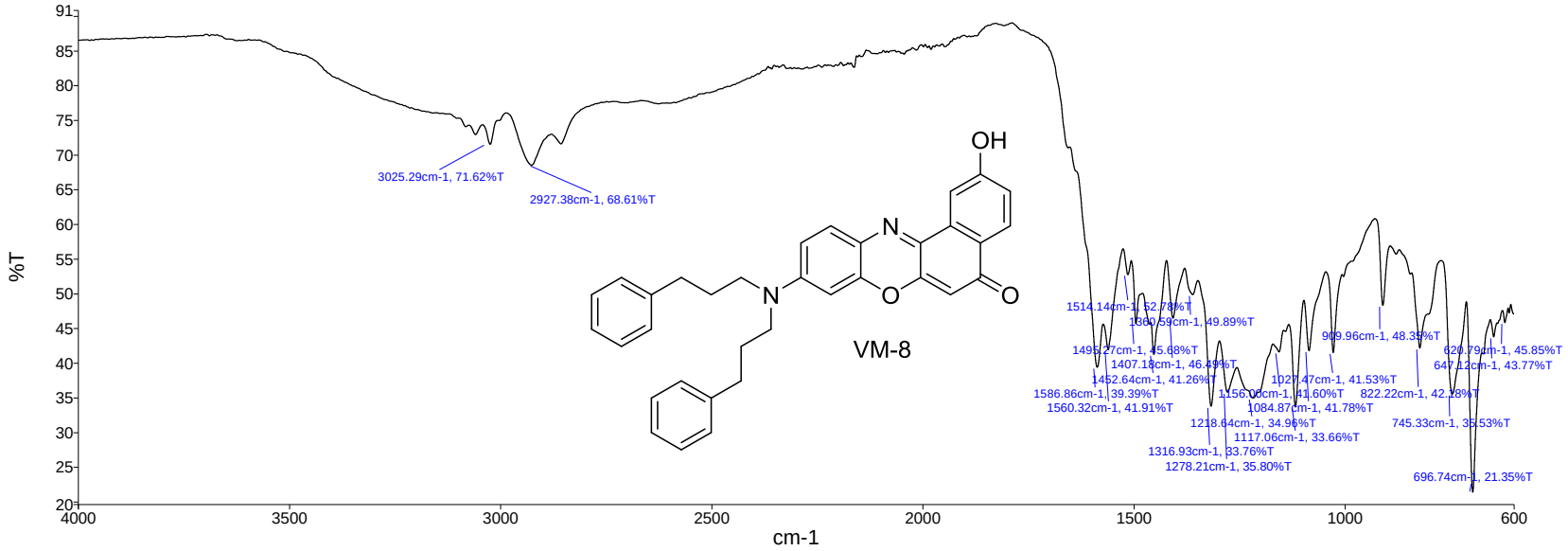
%T
cm-1
3025.29cm-1, 71.62%T
2927.38cm-1, 68.61%T
OH
N
O
O
VM-8
1514.14cm-1, 52.78%T
1495.27cm-1, 45.68%T
1452.64cm-1, 41.26%T
1586.86cm-1, 39.39%T
1560.32cm-1, 41.91%T
1407.18cm-1, 46.49%T
1660.59cm-1, 49.89%T
909.96cm-1, 48.35%T
620.79cm-1, 45.85%T
647.12cm-1, 43.77%T
1027.47cm-1, 41.53%T
1156.08cm-1, 41.60%T
822.22cm-1, 42.78%T
1084.87cm-1, 41.78%T
1218.64cm-1, 34.96%T
745.33cm-1, 35.53%T
1117.06cm-1, 33.66%T
1316.93cm-1, 33.76%T
1278.21cm-1, 35.80%T
696.74cm-1, 21.35%T

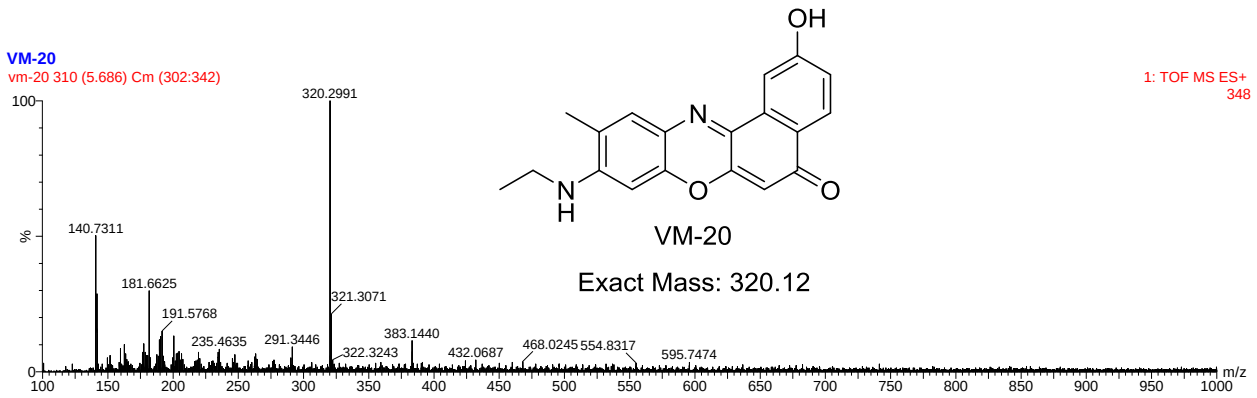
VM-20
vm-20 310 (5.686) Cm (302:342)
1: TOF MS ES+
348
%
m/z
320.2991
140.7311
181.6625
191.5768
235.4635
291.3446
321.3071
322.3243
383.1440
432.0687
468.0245
554.8317
595.7474
OH
N
H
O
O
VM-20
Exact Mass: 320.12

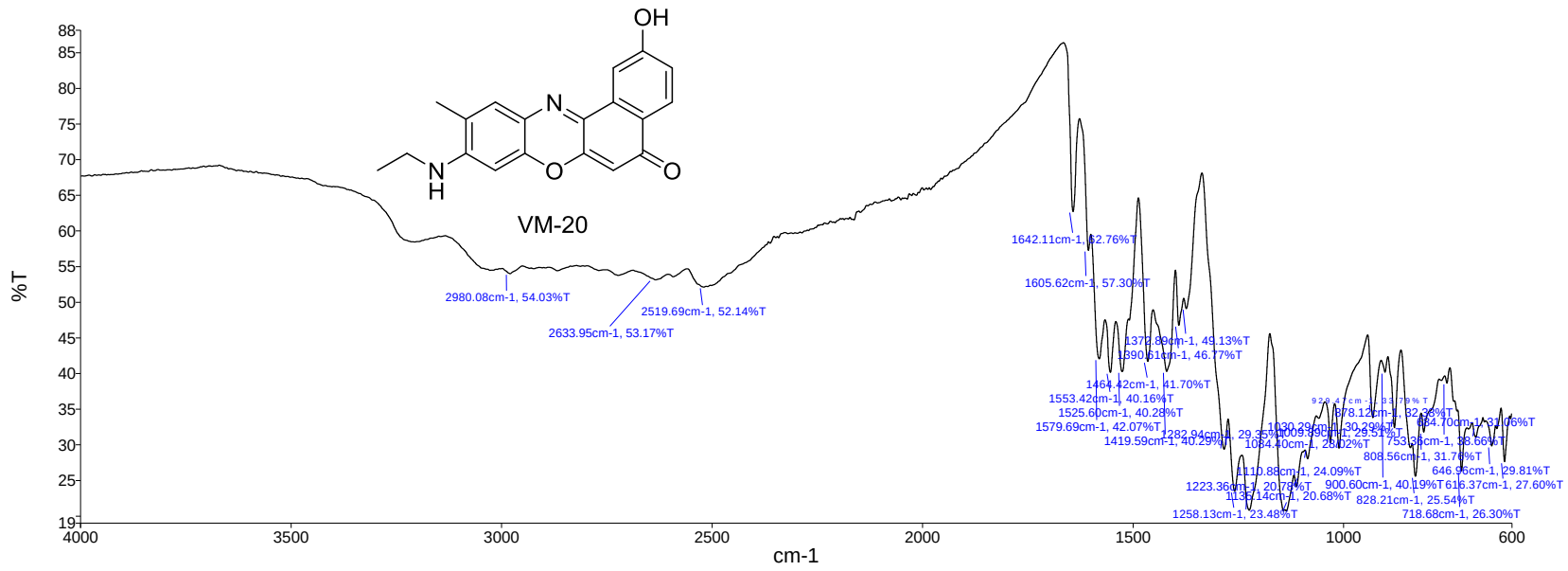
OH
N
N
H
O
O
VM-20
%T
cm-1
2980.08cm-1, 54.03%T
2633.95cm-1, 53.17%T
2519.69cm-1, 52.14%T
1642.11cm-1, 52.76%T
1605.62cm-1, 57.30%T
1464.42cm-1, 41.70%T
1553.42cm-1, 40.16%T
1525.60cm-1, 40.28%T
1579.69cm-1, 42.07%T
1419.59cm-1, 40.29%T
1372.89cm-1, 49.13%T
1390.61cm-1, 46.77%T
1282.94cm-1, 29.35%T
1223.36cm-1, 20.75%T
1258.13cm-1, 23.48%T
1135.14cm-1, 20.68%T
1110.88cm-1, 24.09%T
1084.40cm-1, 29.02%T
1030.29cm-1, 30.29%T
900.60cm-1, 40.19%T
878.12cm-1, 32.36%T
828.21cm-1, 25.54%T
808.56cm-1, 31.74%T
753.38cm-1, 38.56%T
718.68cm-1, 26.30%T
694.70cm-1, 31.06%T
646.96cm-1, 29.81%T
616.37cm-1, 27.60%T

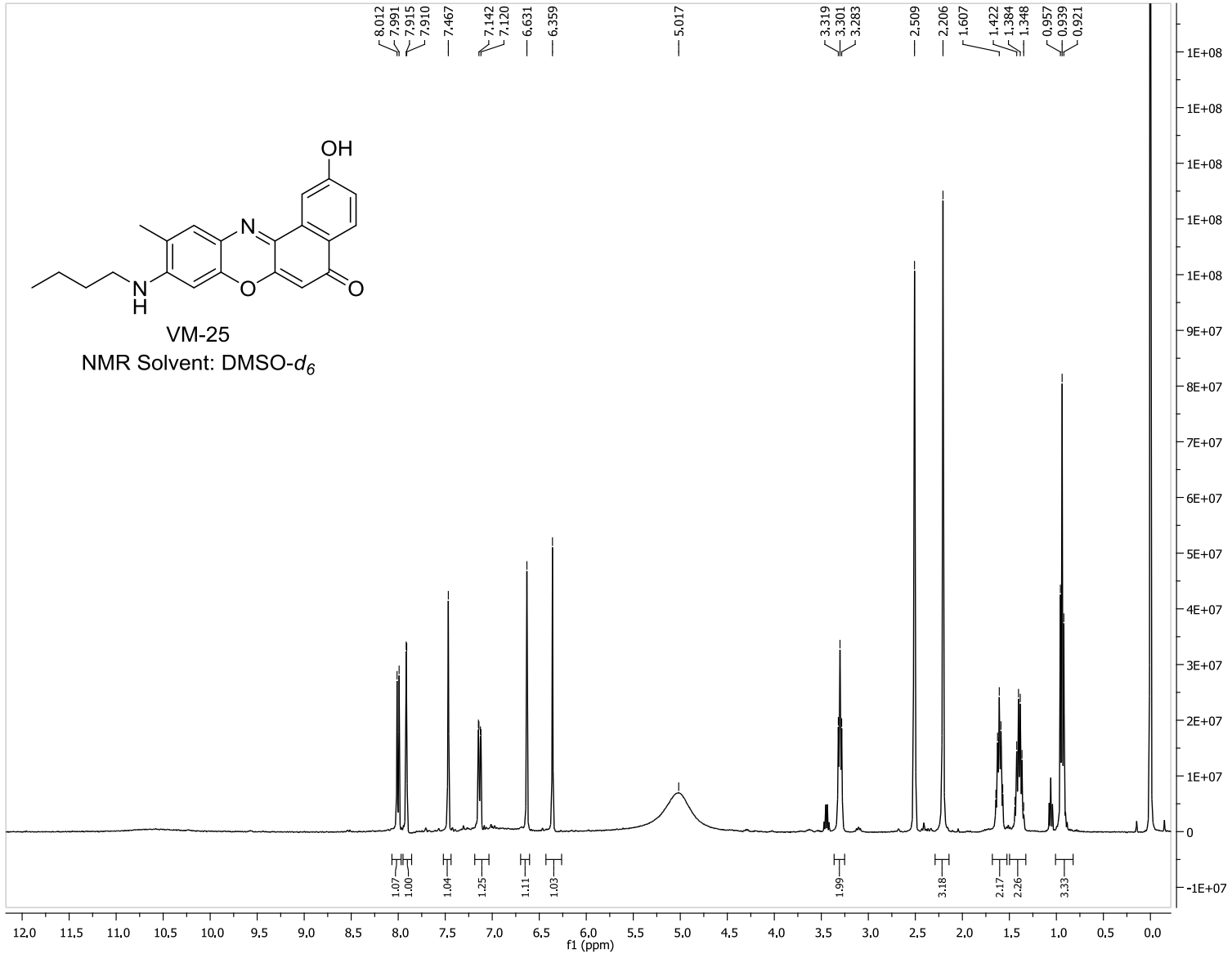
8.012
7.991
7.915
7.910
7.467
7.142
7.120
6.631
6.359
5.017
3.319
3.301
3.283
2.509
2.206
1.607
1.422
1.384
1.348
0.957
0.939
0.921
OH
N
O
O
N
H
VM-25
NMR Solvent: DMSO-d6
1.07
1.00
1.04
1.25
1.11
1.03
1.99
3.18
2.17
2.26
3.33
f1 (ppm)

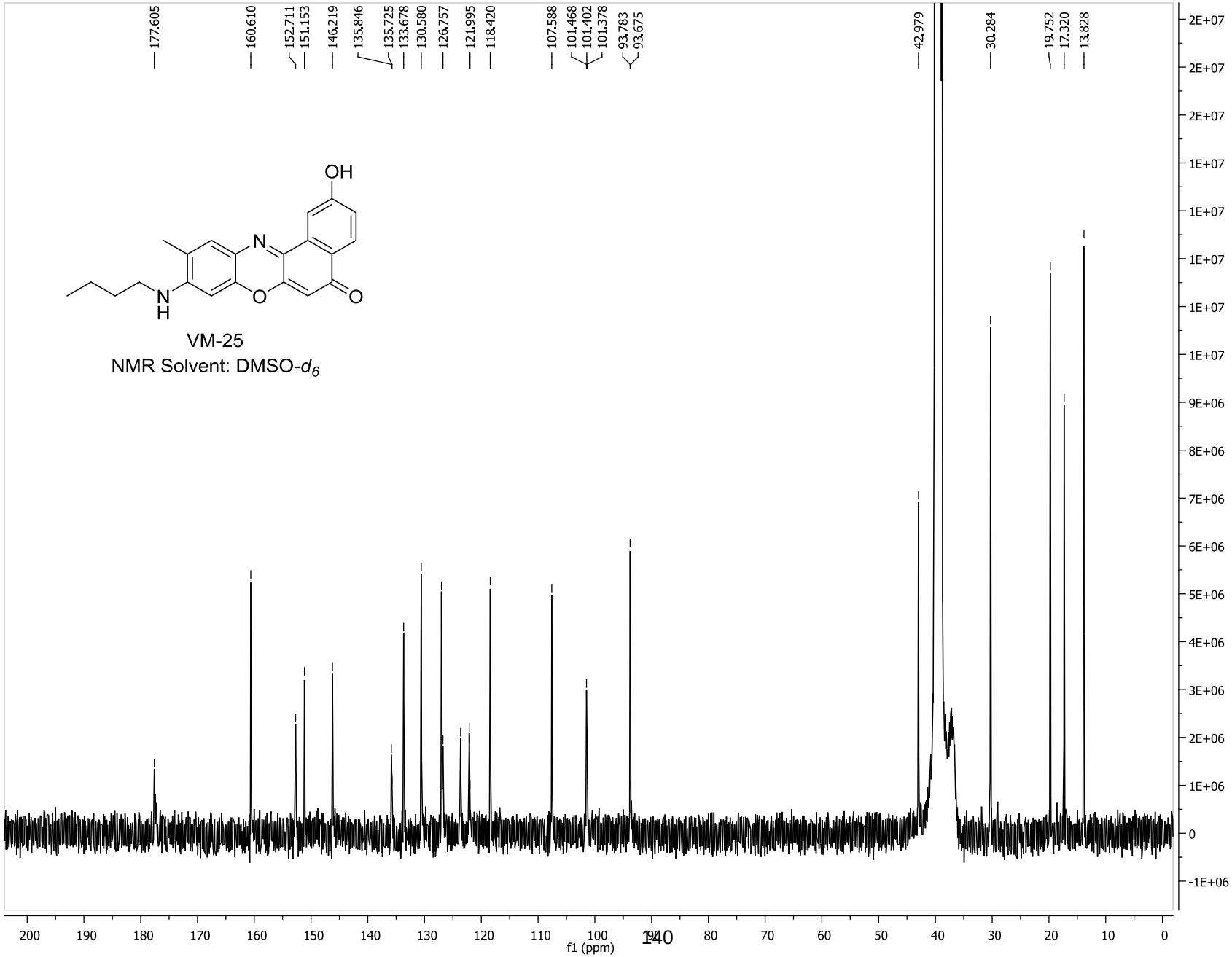
177.605
160.610
152.711
151.153
146.219
135.846
135.725
133.678
130.580
126.757
121.995
118.420
107.588
101.468
101.402
101.378
93.783
93.675
42.979
30.284
19.752
17.320
13.828
OH
N
O
O
N
H
VM-25
NMR Solvent: DMSO-d6
f1 (ppm)

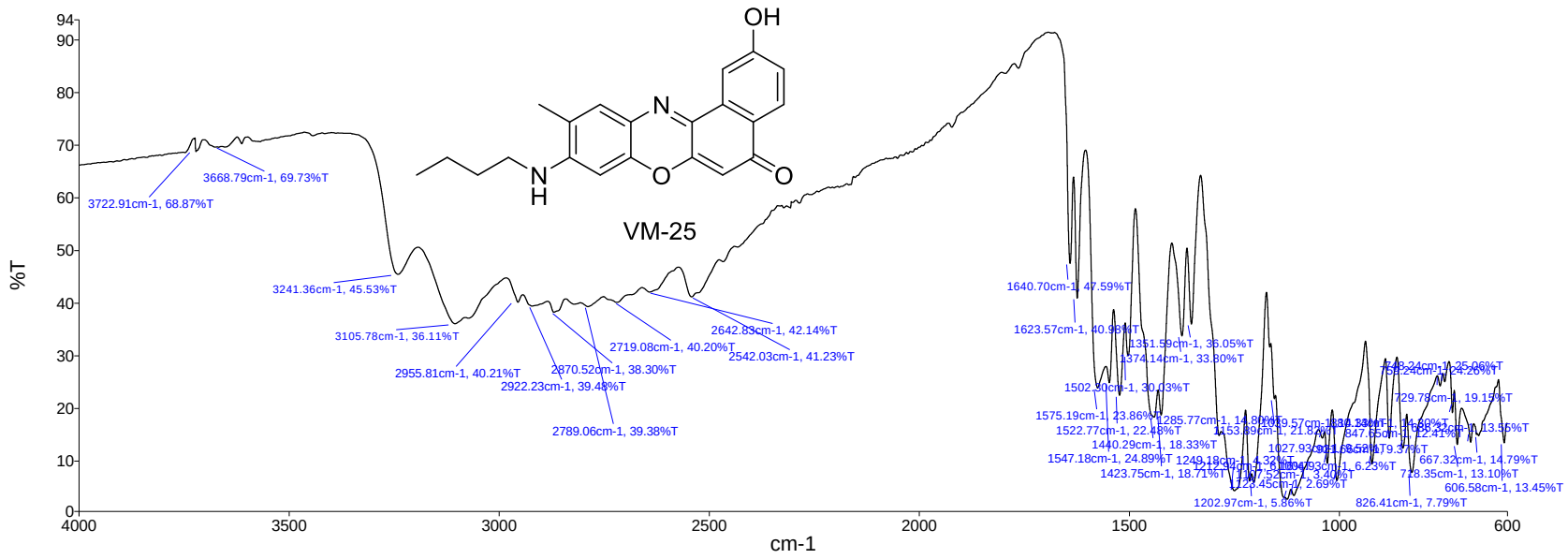
OH
N
O
O
N
H
VM-25
%T
cm-1
3722.91cm-1, 68.87%T
3668.79cm-1, 69.73%T
3241.36cm-1, 45.53%T
3105.78cm-1, 36.11%T
2955.81cm-1, 40.21%T
2922.23cm-1, 39.48%T
2870.52cm-1, 38.30%T
2789.06cm-1, 39.38%T
2719.08cm-1, 40.20%T
2642.83cm-1, 42.14%T
2542.03cm-1, 41.23%T
1640.70cm-1, 47.59%T
1623.57cm-1, 40.98%T
1502.90cm-1, 30.03%T
1575.19cm-1, 23.86%T
1522.77cm-1, 22.48%T
1547.18cm-1, 24.89%T
1440.29cm-1, 18.33%T
1423.75cm-1, 18.71%T
1351.59cm-1, 36.05%T
1374.14cm-1, 33.80%T
1285.77cm-1, 14.80%T
1253.89cm-1, 21.64%T
1249.19cm-1, 5.32%T
1202.97cm-1, 5.86%T
1027.93cm-1, 6.23%T
826.41cm-1, 7.79%T
729.78cm-1, 19.15%T
667.32cm-1, 14.79%T
728.35cm-1, 13.10%T
606.58cm-1, 13.45%T

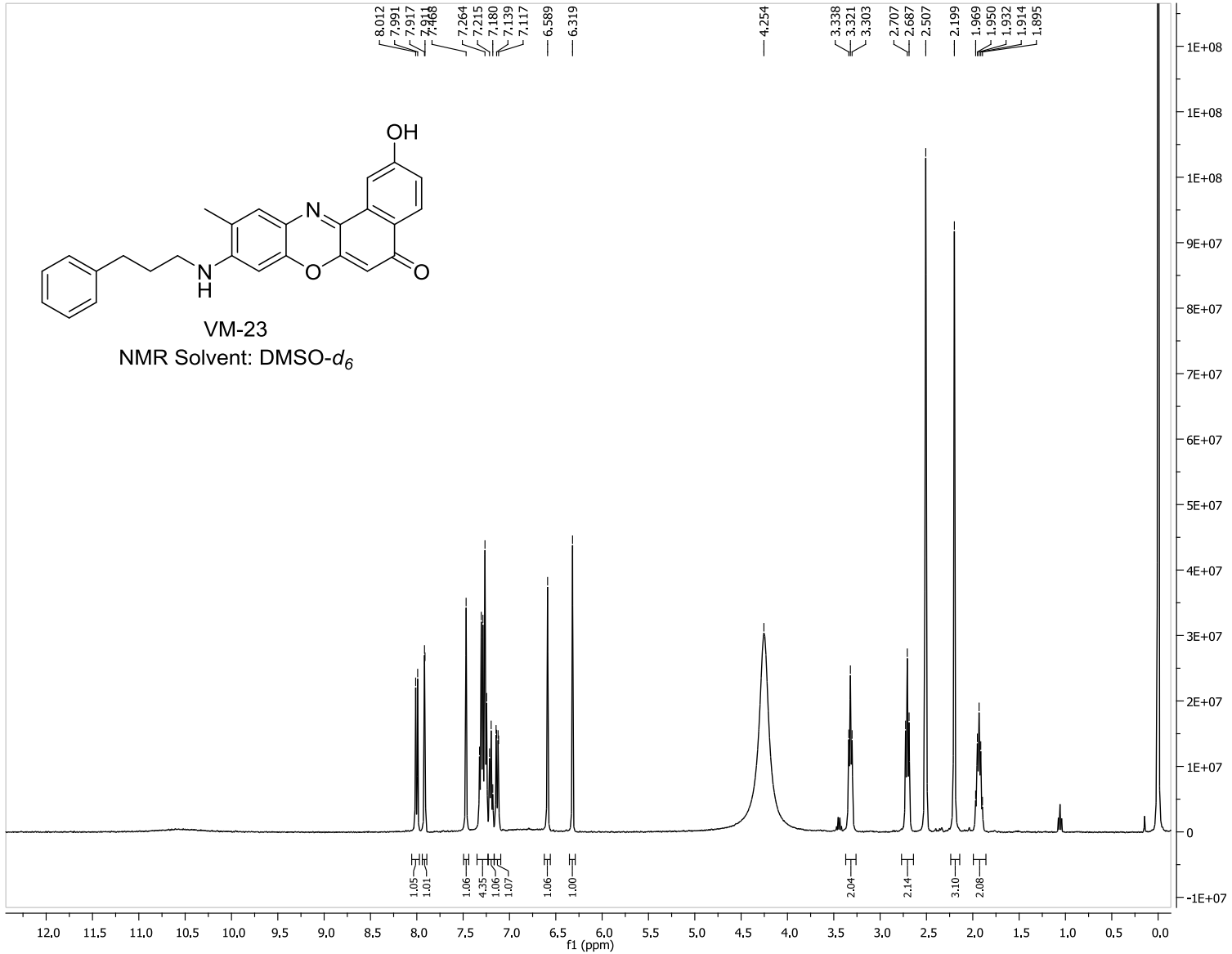
8.012
7.991
7.917
7.264
7.215
7.180
7.139
7.117
6.589
6.319
4.254
3.338
3.321
3.303
2.707
2.687
2.507
2.199
1.969
1.950
1.932
1.914
1.895
OH
N
O
N
H
O
VM-23
NMR Solvent: DMSO-d_6
1.05
1.01
1.06
4.35
1.06
1.07
1.06
1.00
2.04
2.14
3.10
2.08
f1 (ppm)

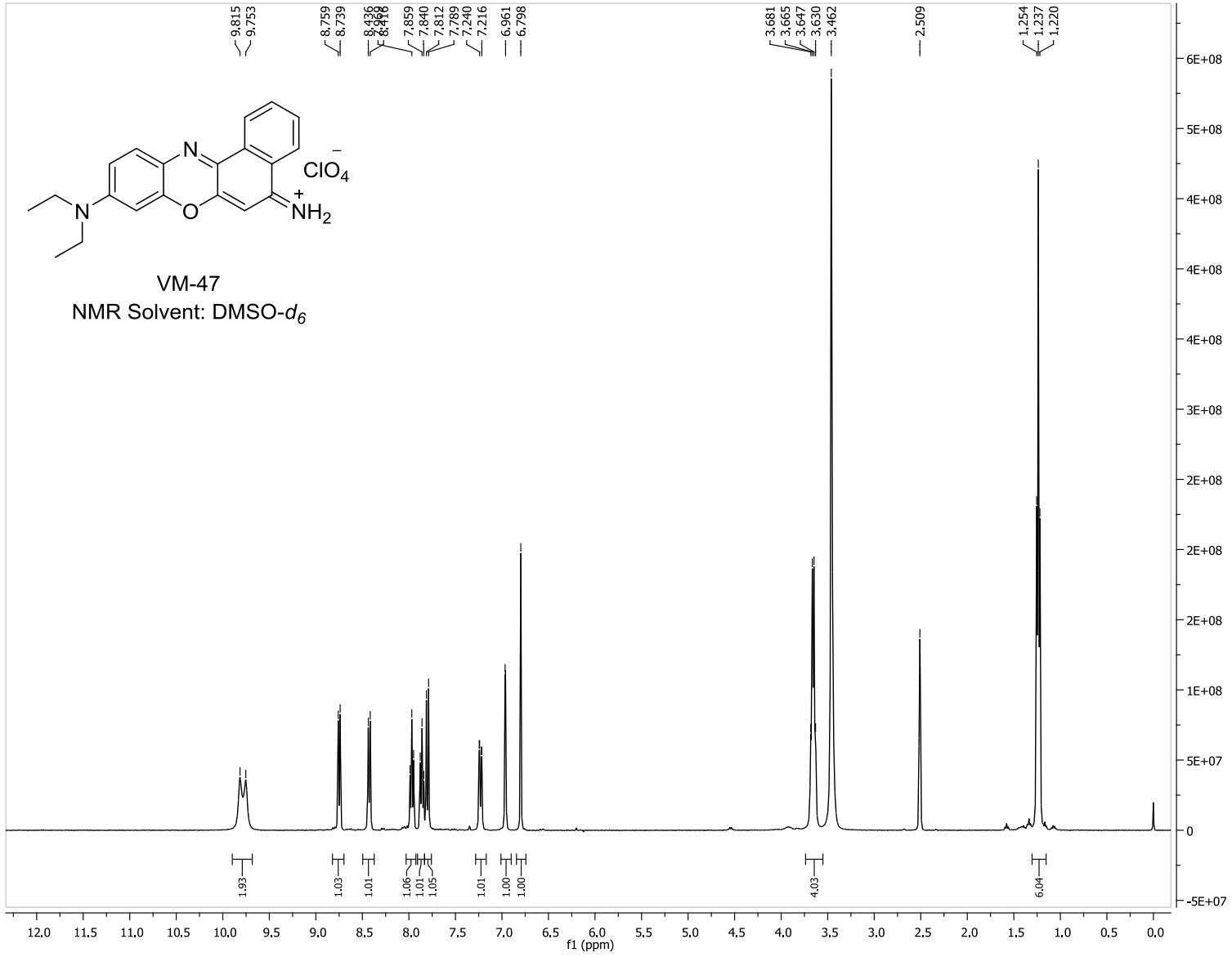
9.815
9.753
8.759
8.739
8.436
8.418
7.859
7.840
7.812
7.789
7.240
7.216
6.961
6.798
3.681
3.665
3.647
3.630
3.462
2.509
1.254
1.237
1.220
N
O
N
ClO4
NH2
VM-47
NMR Solvent: DMSO-d6
1.93
1.03
1.01
1.06
1.01
1.05
1.01
1.00
1.00
4.03
6.04
f1 (ppm)

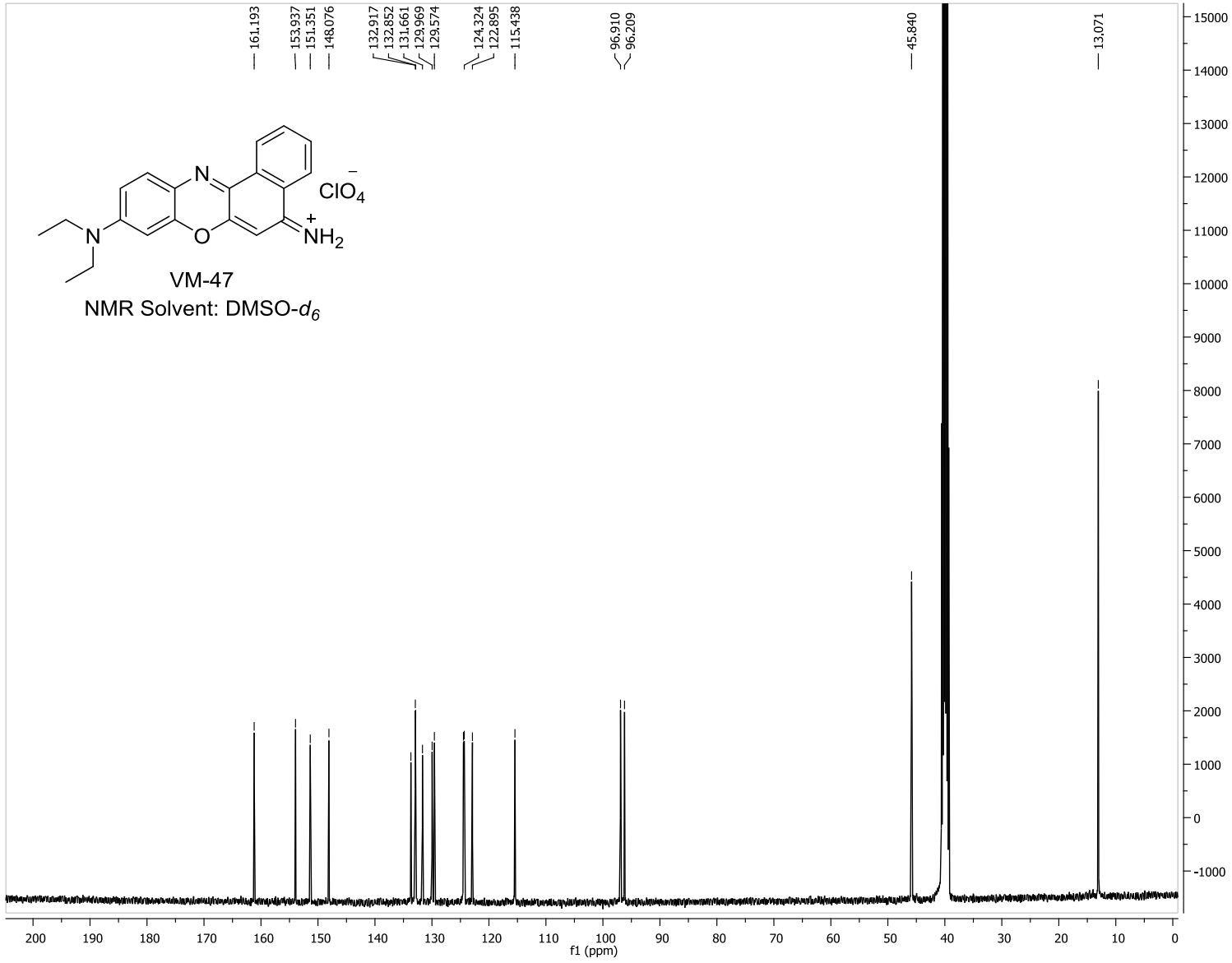
161.193
153.937
151.351
148.076
132.917
132.852
131.661
129.969
129.574
124.324
122.895
115.438
96.910
96.209
45.840
13.071
ClO4
NH2
VM-47
NMR Solvent: DMSO-d6
f1 (ppm)

VM_47_ESIPOS_HENARY_05202015 #220-229 RT: 3.09-3.21 AV: 10 NL: 1.58E9
T: FTMS + p ESI Full ms [100.00-1000.00]

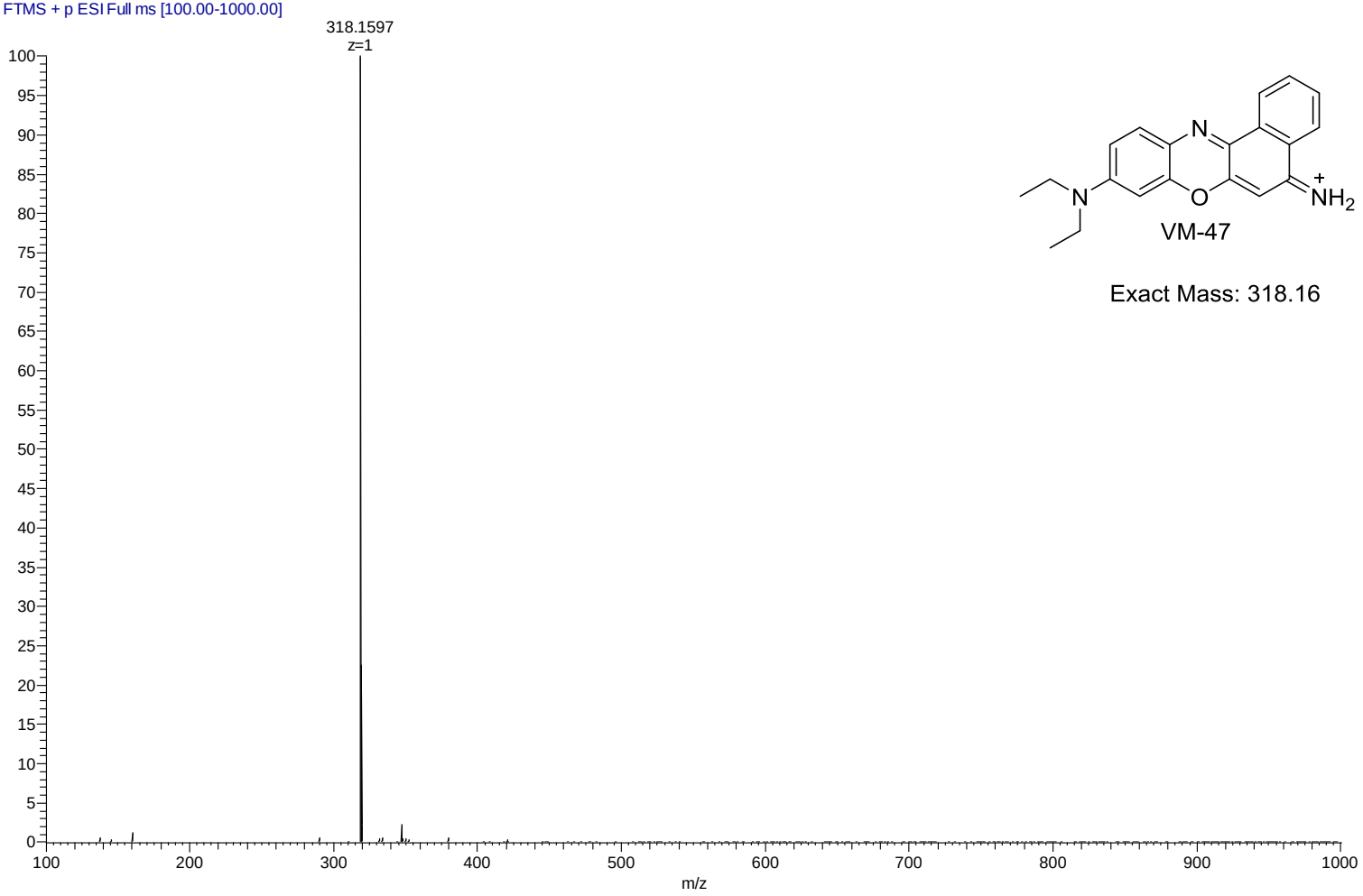

VM-47

Exact Mass: 318.16

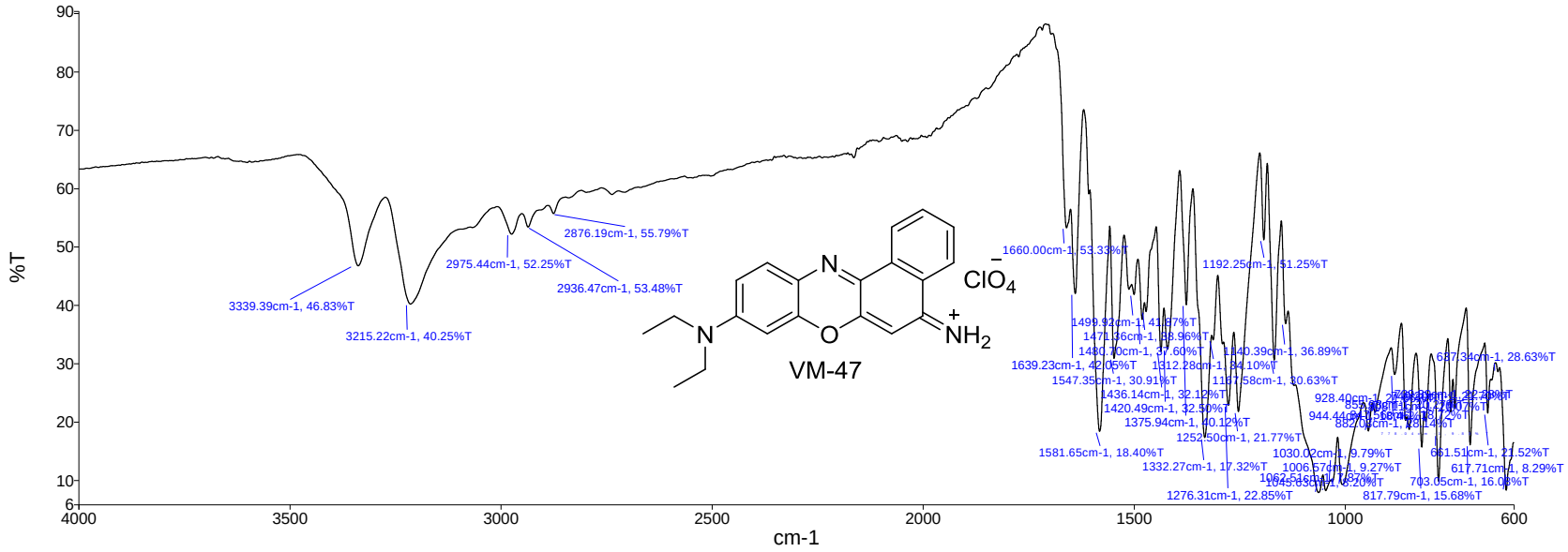
%T
cm-1
3339.39cm-1, 46.83%T
3215.22cm-1, 40.25%T
2975.44cm-1, 52.25%T
2936.47cm-1, 53.48%T
2876.19cm-1, 55.79%T
1660.00cm-1, 53.33%T
1639.23cm-1, 42.05%T
1581.65cm-1, 18.40%T
1547.35cm-1, 30.91%T
1499.92cm-1, 41.87%T
1471.36cm-1, 38.96%T
1436.14cm-1, 32.12%T
1420.49cm-1, 32.50%T
1375.94cm-1, 40.12%T
1332.27cm-1, 17.32%T
1312.28cm-1, 34.10%T
1276.31cm-1, 22.85%T
1252.50cm-1, 21.77%T
1192.25cm-1, 51.25%T
1140.39cm-1, 36.89%T
1117.58cm-1, 30.63%T
1030.02cm-1, 9.79%T
1006.57cm-1, 9.27%T
928.40cm-1
817.79cm-1, 15.68%T
703.05cm-1, 16.08%T
687.34cm-1, 28.63%T
661.51cm-1, 21.52%T
617.71cm-1, 8.29%T
VM-47

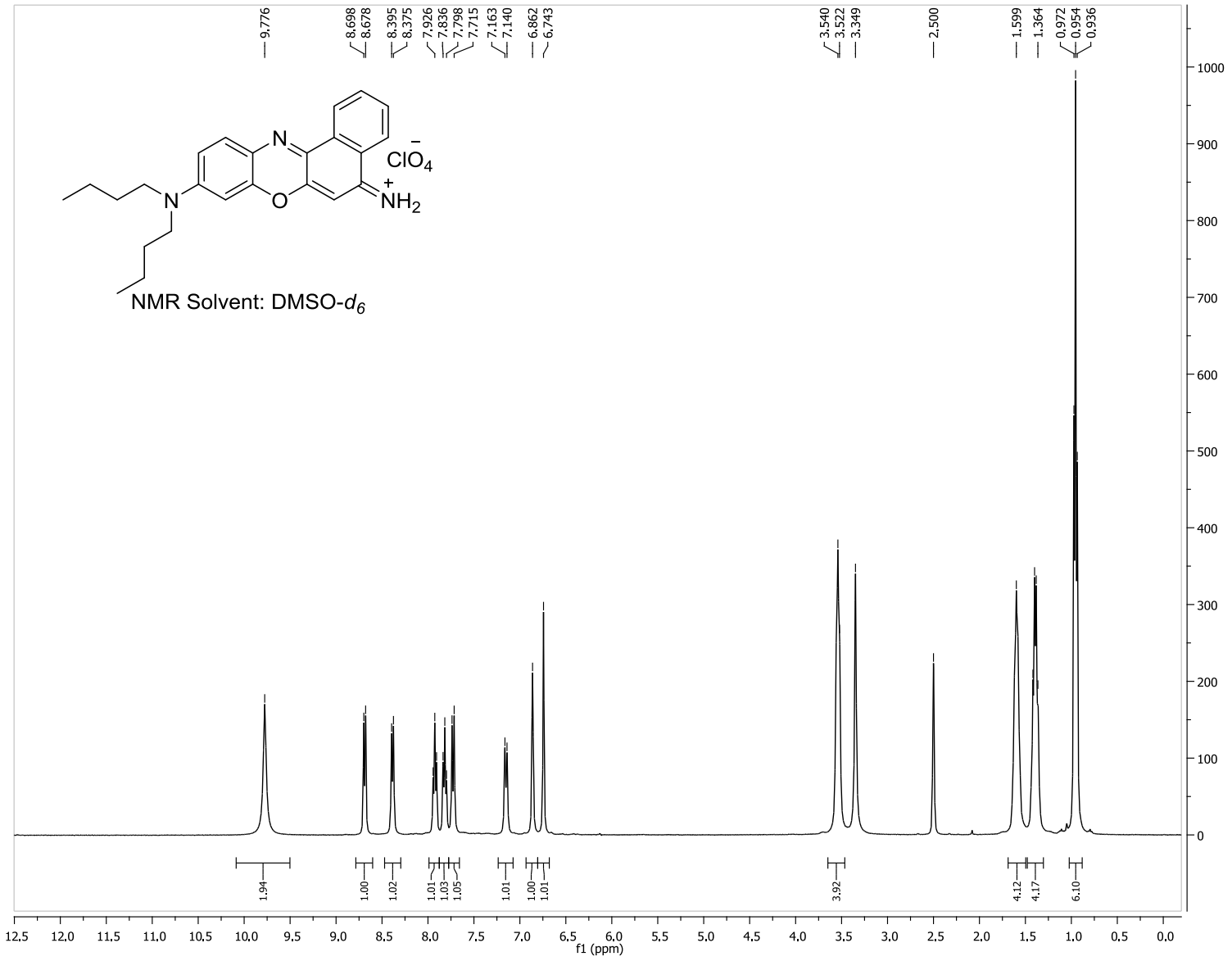
9.776
8.698
8.678
8.395
8.375
7.926
7.836
7.798
7.715
7.163
7.140
6.862
6.743
3.540
3.522
3.349
2.500
1.599
1.364
0.972
0.954
0.936
N
O
N
ClO4
NH2
NMR Solvent: DMSO-d6
1.94
1.00
1.02
1.01
1.03
1.05
1.01
1.00
1.01
3.92
4.12
4.17
6.10
f1 (ppm)

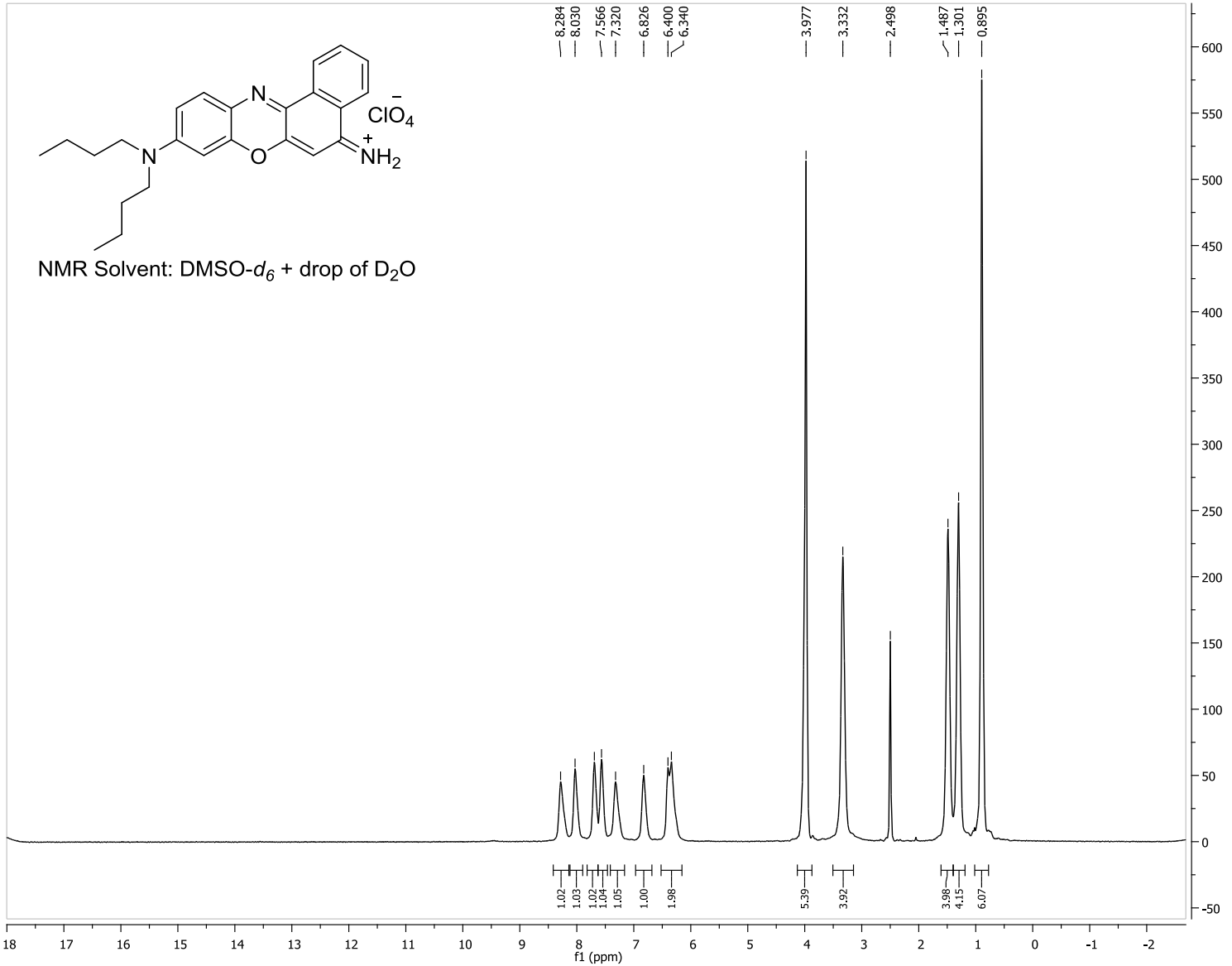
8.284
8.030
7.566
7.320
6.826
6.400
6.340
3.977
3.332
2.498
1.487
1.301
0.895
NMR Solvent: DMSO-d_6 + drop of D_2O
1.02
1.03
1.02
1.04
1.05
1.00
1.98
5.39
3.92
3.98
4.15
6.07
f1 (ppm)

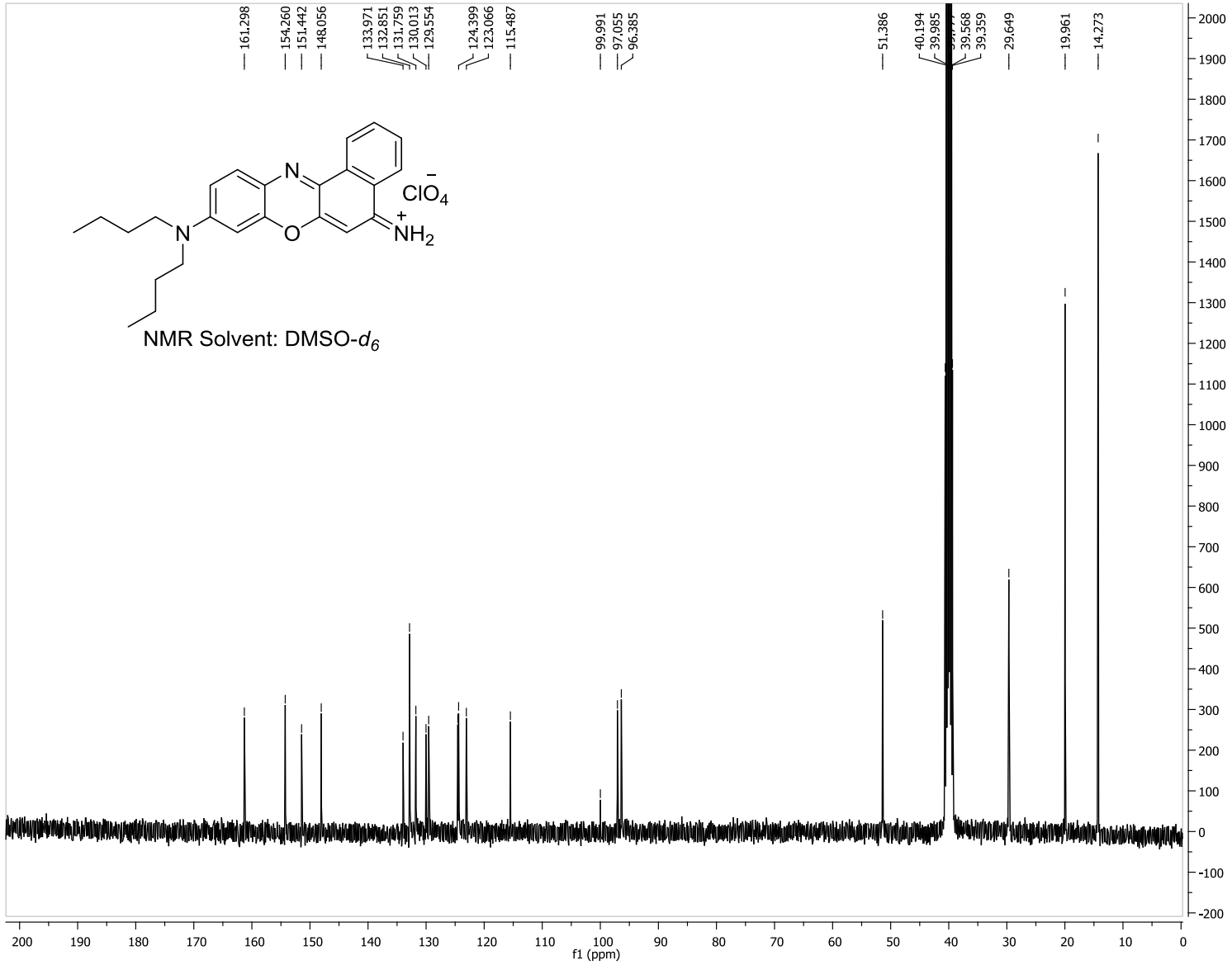
161.298
154.260
151.442
148.056
133.971
132.851
131.759
130.013
129.554
124.399
123.066
115.487
99.991
97.055
96.385
51.386
40.194
39.985
39.568
39.359
29.649
19.961
14.273
N
O
N
ClO4
NH2
NMR Solvent: DMSO-d6
f1 (ppm)

VM_MeOH5_ESIPOS_HENARY_05202015 #217-231 RT: 3.05-3.24 AV: 15 NL: 8.21E7
T: FTMS + p ESI Full ms [100.00-1000.00]

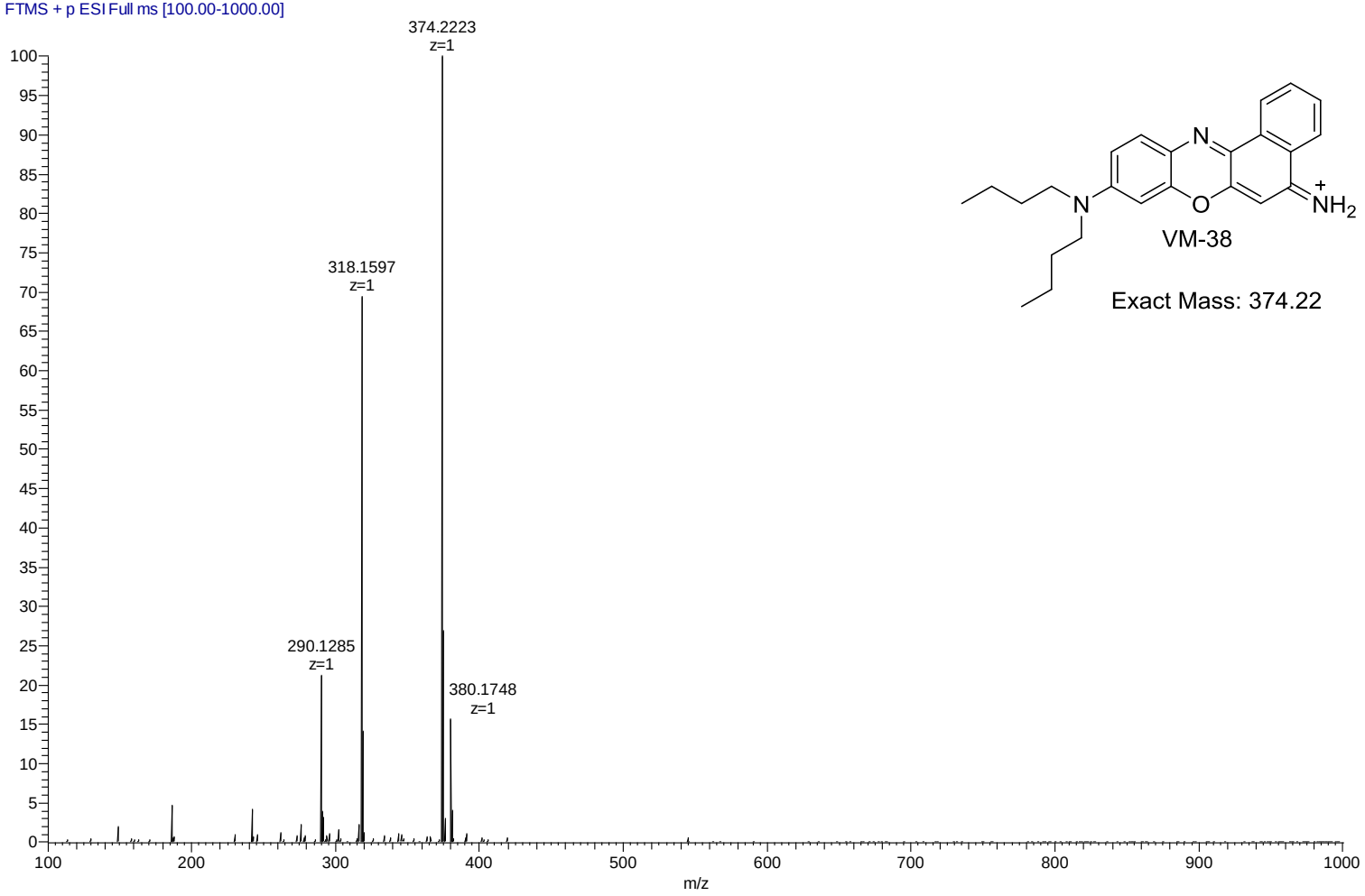

VM-38

Exact Mass: 374.22

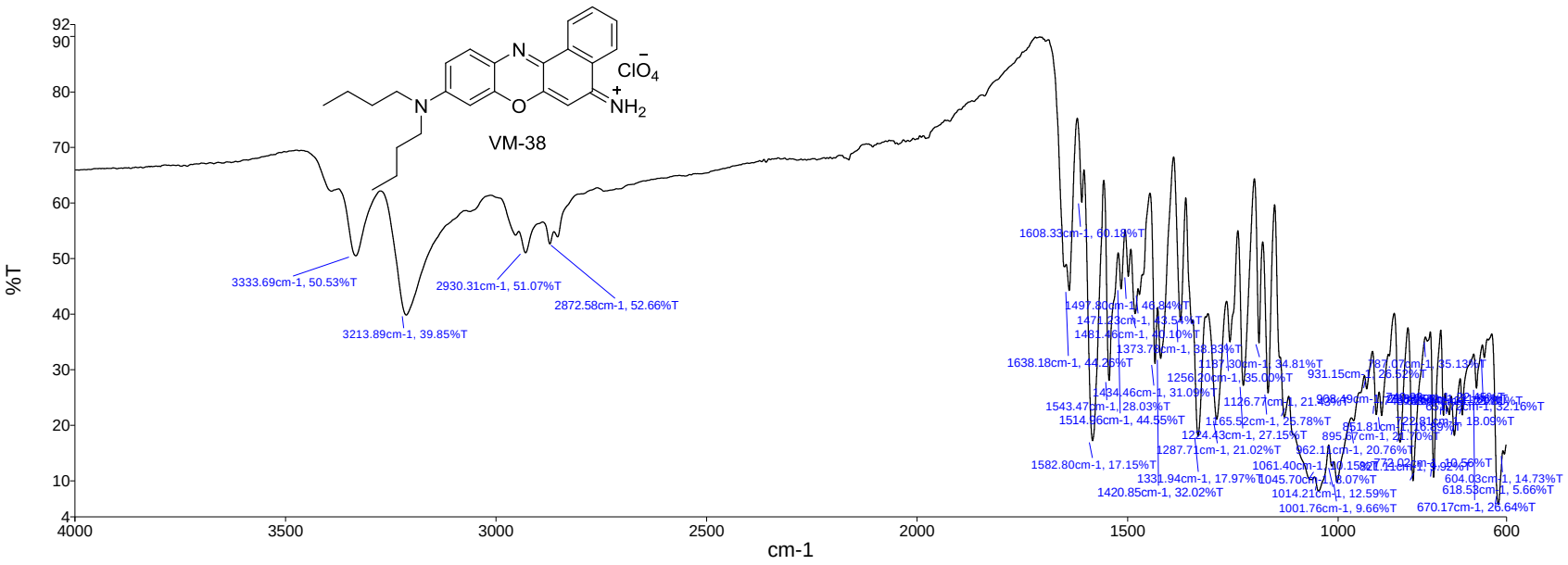
VM-38
%T
cm-1
3333.69cm-1, 50.53%T
3213.89cm-1, 39.85%T
2930.31cm-1, 51.07%T
2872.58cm-1, 52.66%T
1608.33cm-1, 60.18%T
1638.18cm-1, 44.26%T
1582.80cm-1, 17.15%T
1543.47cm-1, 28.03%T
1514.96cm-1, 44.55%T
1497.80cm-1, 46.84%T
1471.23cm-1, 43.51%T
1481.46cm-1, 42.10%T
1373.79cm-1, 38.33%T
1434.46cm-1, 31.09%T
1420.85cm-1, 32.02%T
1331.94cm-1, 17.97%T
1287.71cm-1, 21.02%T
1256.20cm-1, 35.00%T
1224.43cm-1, 27.15%T
1187.30cm-1, 34.81%T
1126.77cm-1, 21.45%T
1165.52cm-1, 25.78%T
1061.40cm-1, 10.15%T
1045.70cm-1, 8.07%T
1014.21cm-1, 12.59%T
1001.76cm-1, 9.66%T
962.14cm-1, 20.76%T
931.15cm-1, 28.52%T
895.67cm-1, 21.70%T
851.81cm-1, 16.95%T
787.07cm-1, 35.13%T
604.03cm-1, 14.73%T
618.53cm-1, 5.66%T
670.17cm-1, 26.64%T

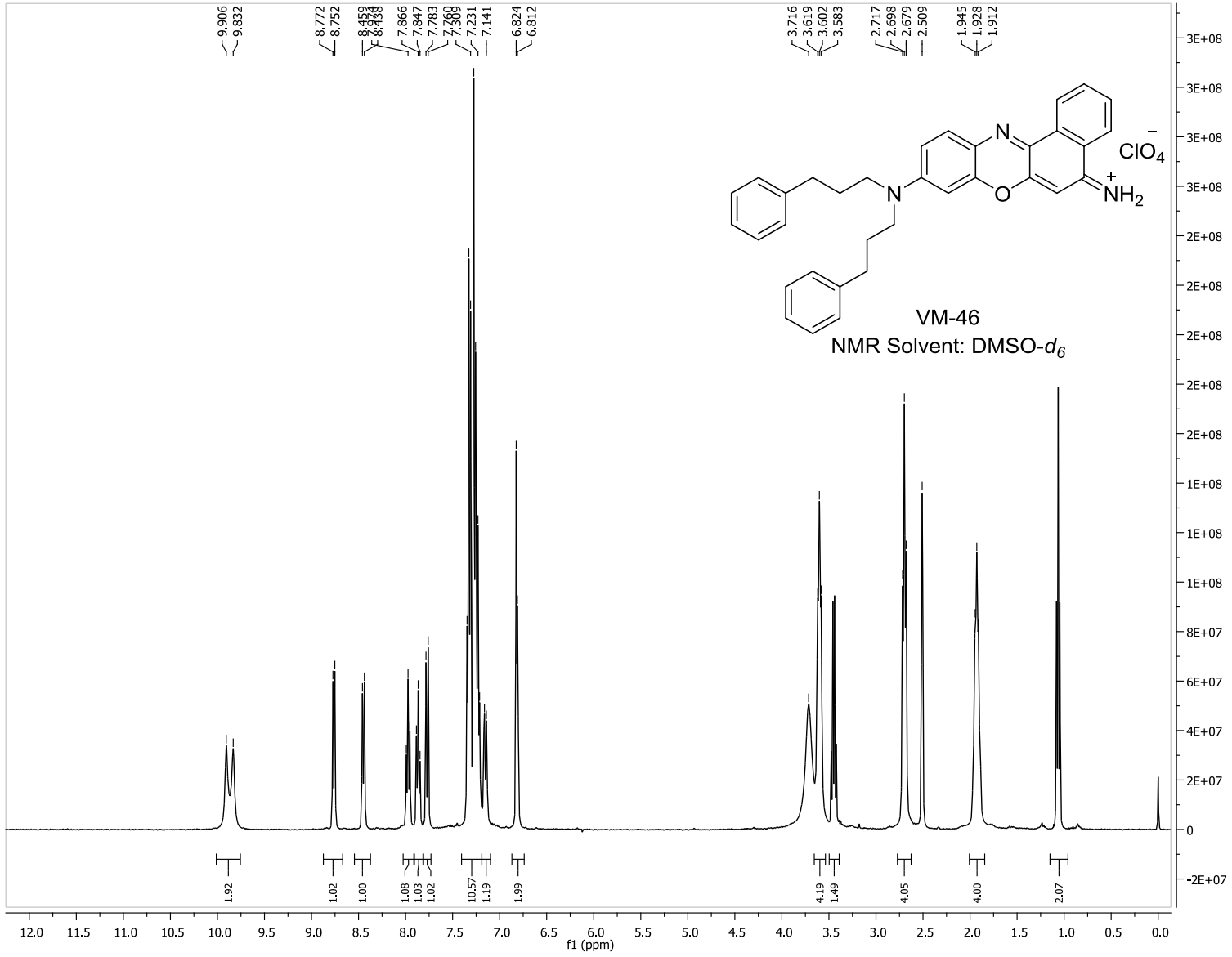
9.906
9.832
8.772
8.752
8.459
8.438
7.866
7.847
7.783
7.360
7.309
7.231
7.141
6.824
6.812
3.716
3.619
3.602
3.583
2.717
2.698
2.679
2.509
1.945
1.928
1.912
N
O
N
ClO4
NH2
VM-46
NMR Solvent: DMSO-d6
1.92
1.02
1.00
1.08
1.03
1.02
10.57
1.19
1.99
4.19
1.49
4.05
4.00
2.07
f1 (ppm)

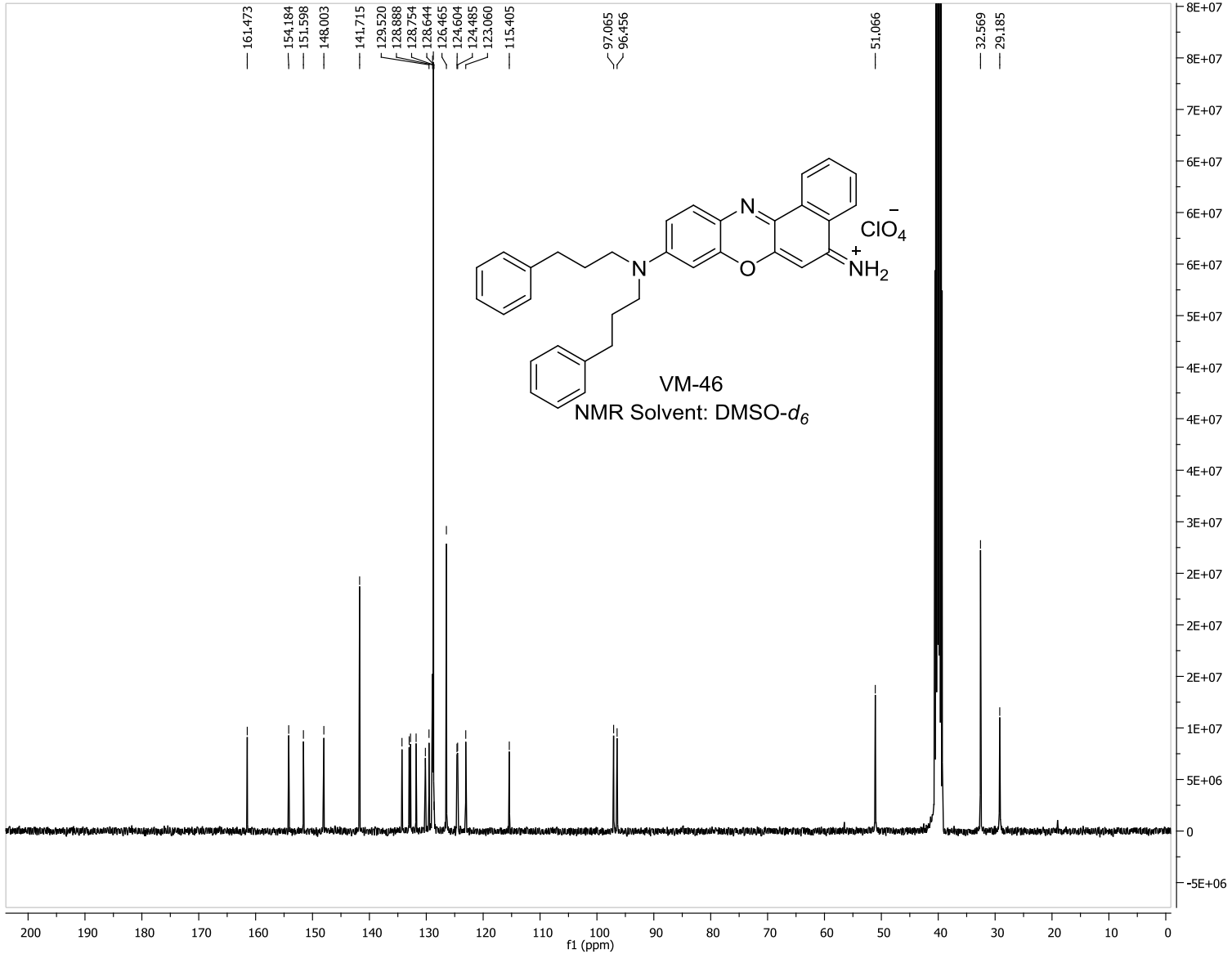
161.473
154.184
151.598
148.003
141.715
129.520
128.888
128.754
128.644
126.465
124.604
124.485
123.060
115.405
97.065
96.456
51.066
32.569
29.185
VM-46
NMR Solvent: DMSO-d6
f1 (ppm)

VM_46_ESIPOS_HENARY_05202015 #213-223 RT: 3.00-3.14 AV: 11 NL: 4.00E8
T: FTMS + p ESI Full ms [100.00-1000.00]

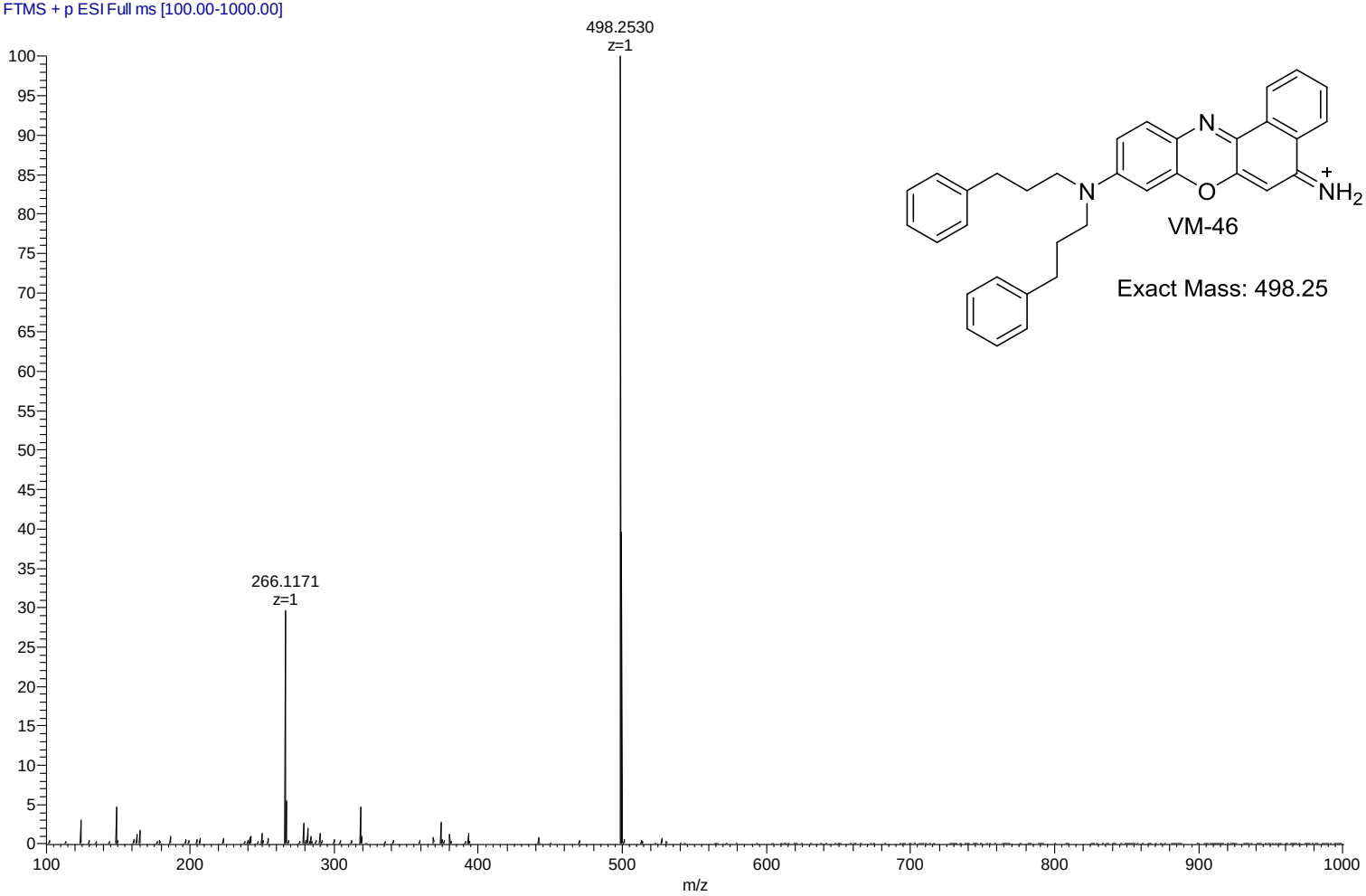

VM-46

Exact Mass: 498.25

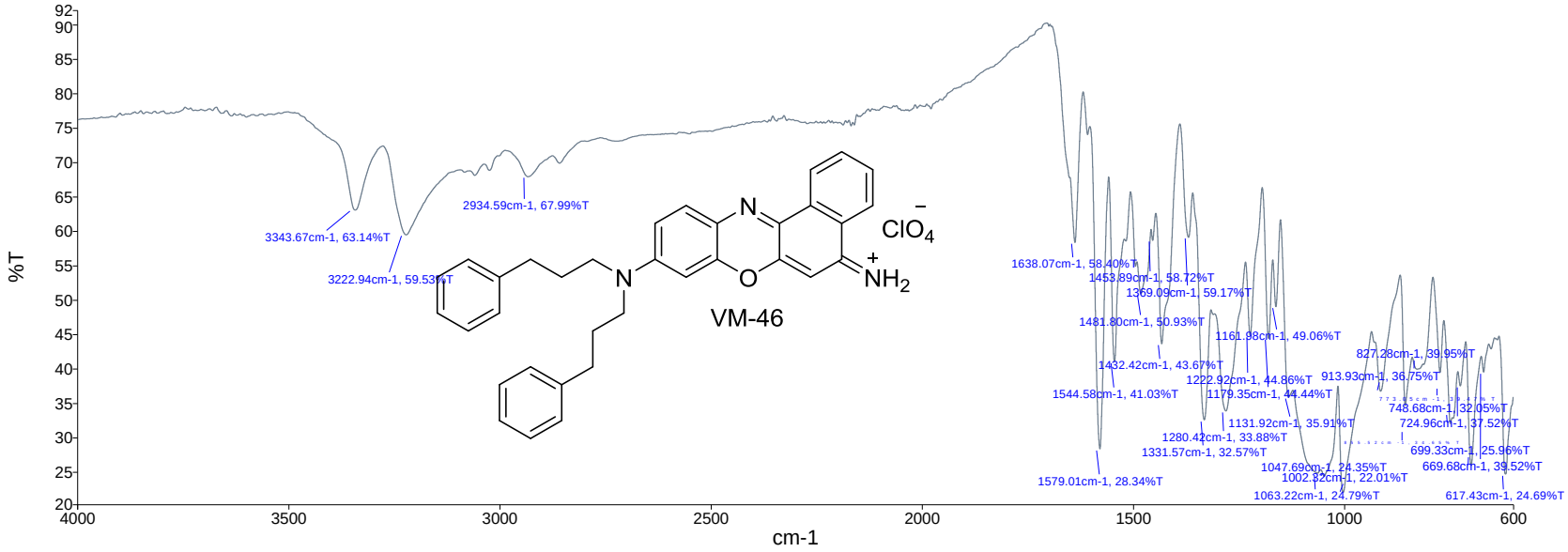
%T
cm-1
3343.67cm-1, 63.14%T
3222.94cm-1, 59.53%T
2934.59cm-1, 67.99%T
1638.07cm-1, 58.40%T
1453.89cm-1, 58.72%T
1369.09cm-1, 59.17%T
1481.80cm-1, 50.93%T
1161.98cm-1, 49.06%T
827.28cm-1, 39.95%T
1432.42cm-1, 43.67%T
913.93cm-1, 36.75%T
1222.92cm-1, 44.86%T
1544.58cm-1, 41.03%T
1179.35cm-1, 44.44%T
748.68cm-1, 32.05%T
1131.92cm-1, 35.91%T
724.96cm-1, 37.52%T
1280.42cm-1, 33.88%T
699.33cm-1, 25.96%T
1331.57cm-1, 32.57%T
669.68cm-1, 39.52%T
1047.69cm-1, 24.35%T
1002.32cm-1, 22.01%T
1579.01cm-1, 28.34%T
1063.22cm-1, 24.79%T
617.43cm-1, 24.69%T
VM-46

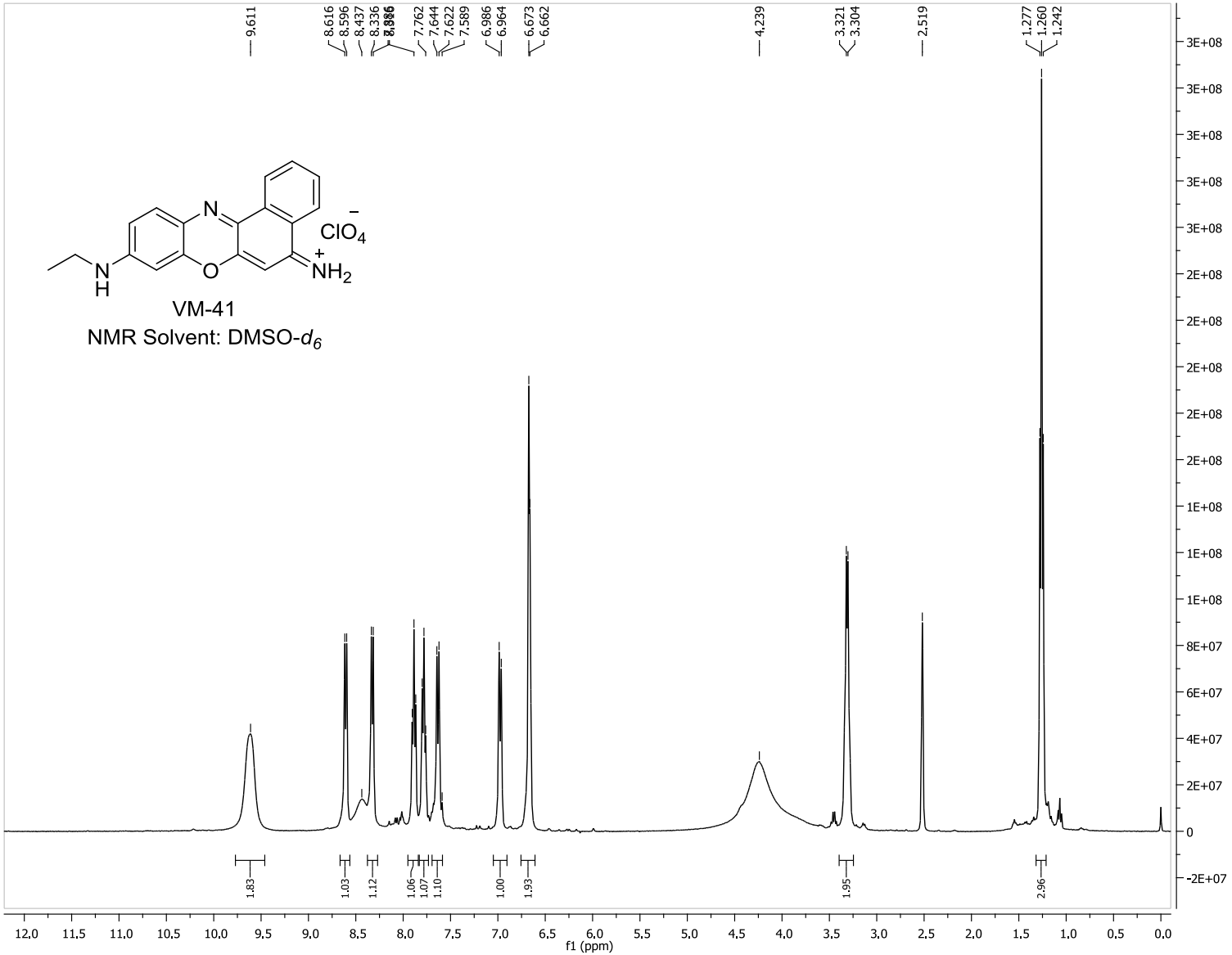
9.611
8.616
8.596
8.437
8.336
7.762
7.644
7.622
7.589
6.986
6.964
6.673
6.662
4.239
3.321
3.304
2.519
1.277
1.260
1.242
ClO4
NH2
VM-41
NMR Solvent: DMSO-d6
1.83
1.03
1.12
1.06
1.07
1.10
1.00
1.93
1.95
2.96
f1 (ppm)

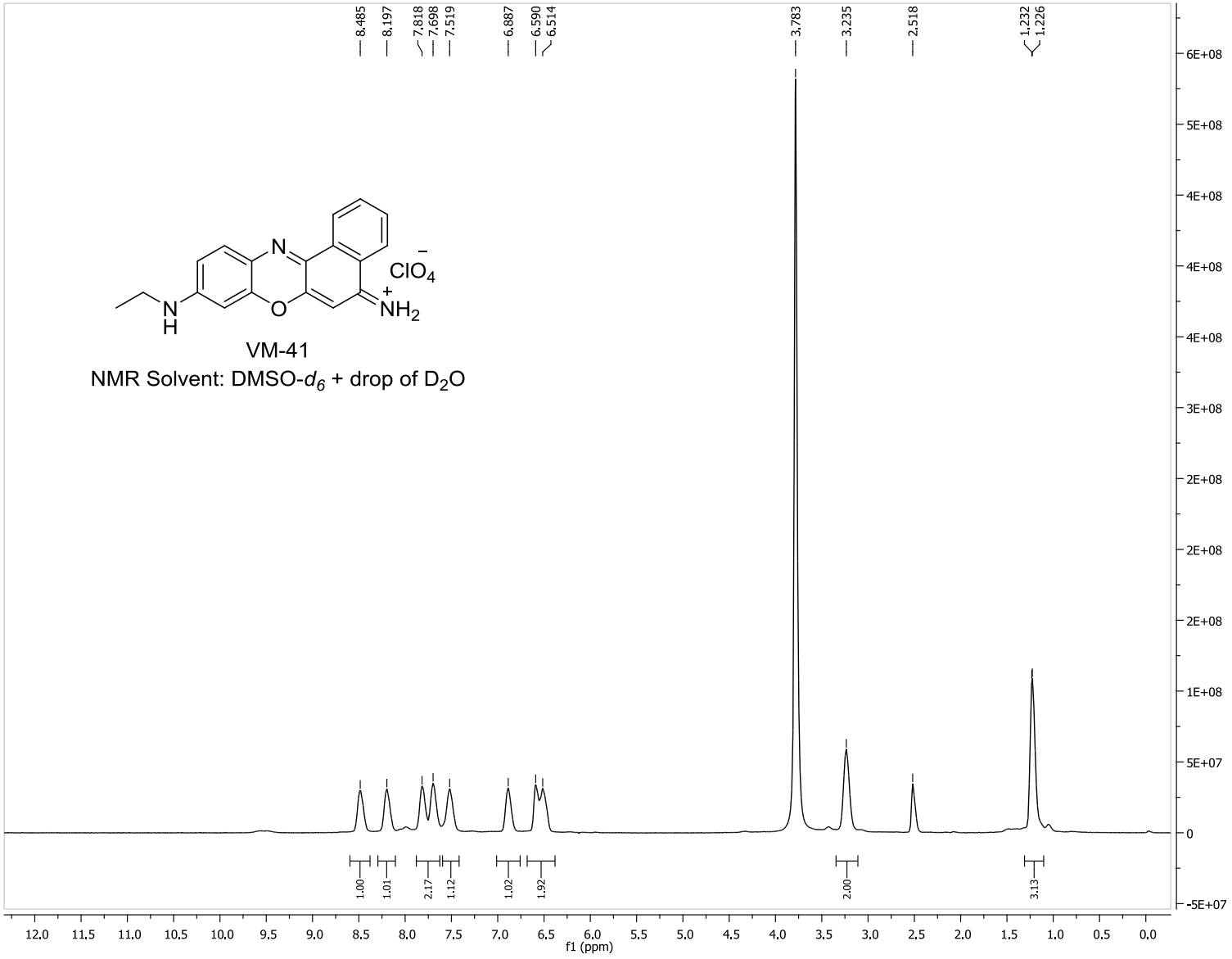
8.485
8.197
7.818
7.698
7.519
6.887
6.590
6.514
3.783
3.235
2.518
1.232
1.226
ClO4
NH2
N
H
O
VM-41
NMR Solvent: DMSO-d6 + drop of D2O
1.00
1.01
2.17
1.12
1.02
1.92
2.00
3.13
f1 (ppm)

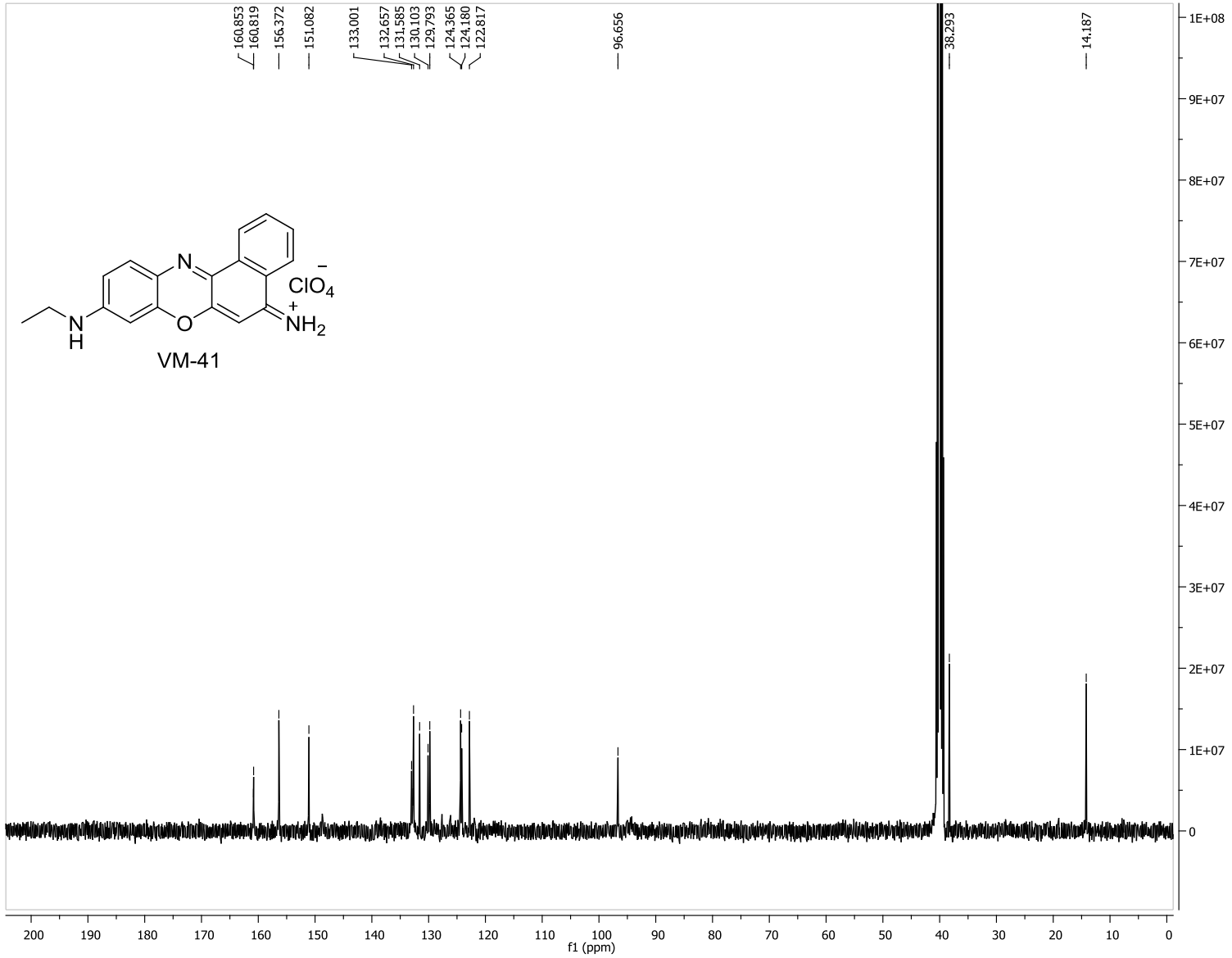
160.853
160.819
156.372
151.082
133.001
132.657
131.585
130.103
129.793
124.365
124.180
122.817
96.656
38.293
14.187
N
ClO4
+
NH2
N
H
O
VM-41
1E+08
9E+07
8E+07
7E+07
6E+07
5E+07
4E+07
3E+07
2E+07
1E+07
0
200
190
180
170
160
150
140
130
120
110
100
90
80
70
60
50
40
30
20
10
0
f1 (ppm)

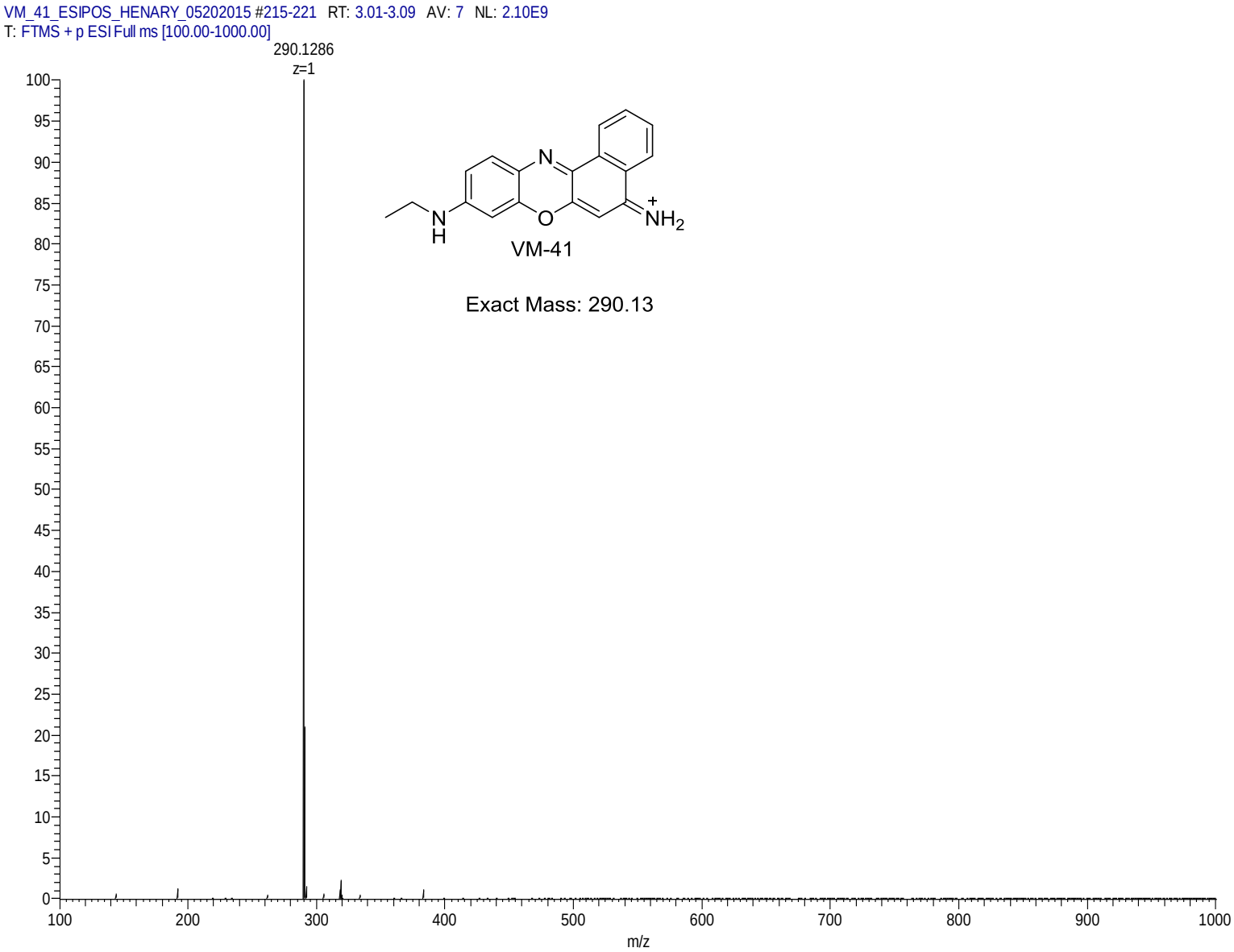
VM_41_ESIPOS_HENARY_05202015 #215-221 RT: 3.01-3.09 AV: 7 NL: 2.10E9
T: FTMS + p ESI Full ms [100.00-1000.00]
290.1286
z=1
VM-41
Exact Mass: 290.13
m/z

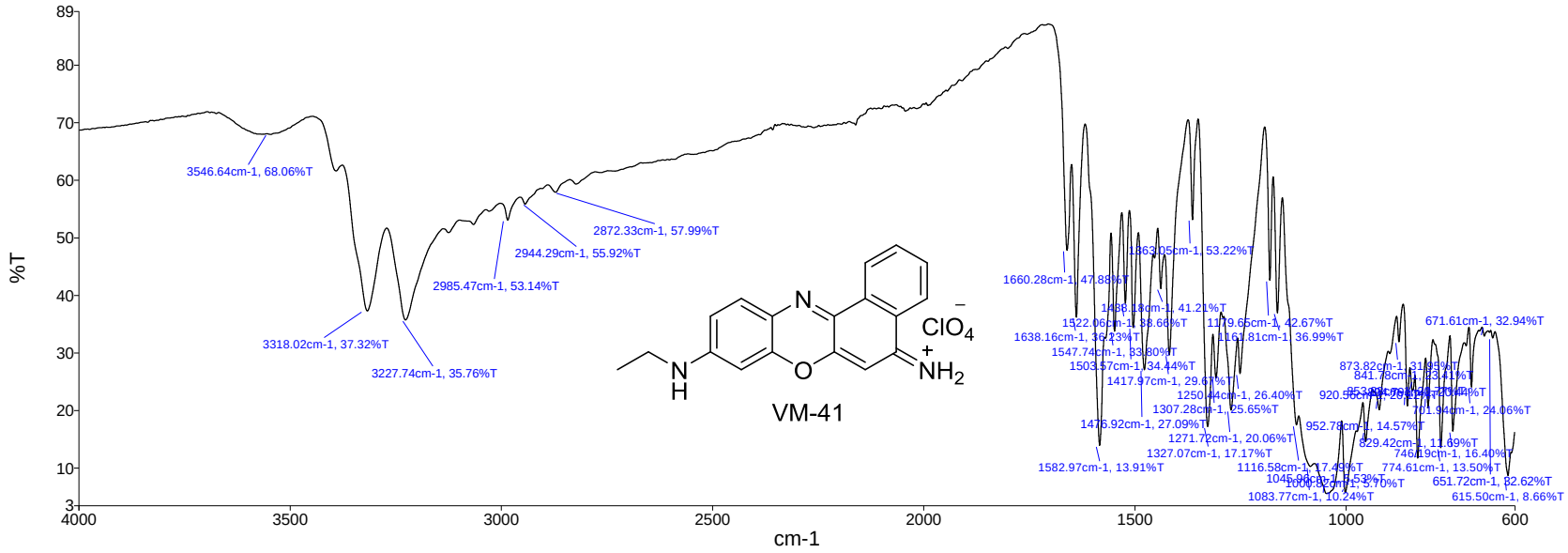
%T
cm-1
3546.64cm-1, 68.06%T
3318.02cm-1, 37.32%T
3227.74cm-1, 35.76%T
2985.47cm-1, 53.14%T
2944.29cm-1, 55.92%T
2872.33cm-1, 57.99%T
1660.28cm-1, 47.88%T
1638.16cm-1, 36.23%T
1582.97cm-1, 13.91%T
1547.74cm-1, 33.80%T
1522.06cm-1, 38.66%T
1503.57cm-1, 34.44%T
1476.92cm-1, 27.09%T
1436.14cm-1, 41.21%T
1417.97cm-1, 29.67%T
1383.05cm-1, 53.22%T
1327.07cm-1, 17.17%T
1307.28cm-1, 25.65%T
1271.72cm-1, 20.06%T
1250.44cm-1, 26.40%T
1179.65cm-1, 42.67%T
1161.81cm-1, 36.99%T
1116.58cm-1, 17.49%T
1083.77cm-1, 10.24%T
1045.94cm-1, 11.53%T
1000.82cm-1, 5.70%T
952.78cm-1, 14.57%T
920.56cm-1, 29.24%T
873.82cm-1, 31.95%T
841.78cm-1, 33.41%T
829.42cm-1, 11.69%T
774.61cm-1, 13.50%T
746.19cm-1, 16.40%T
721.94cm-1, 24.06%T
671.61cm-1, 32.94%T
651.72cm-1, 32.62%T
615.50cm-1, 8.66%T
VM-41

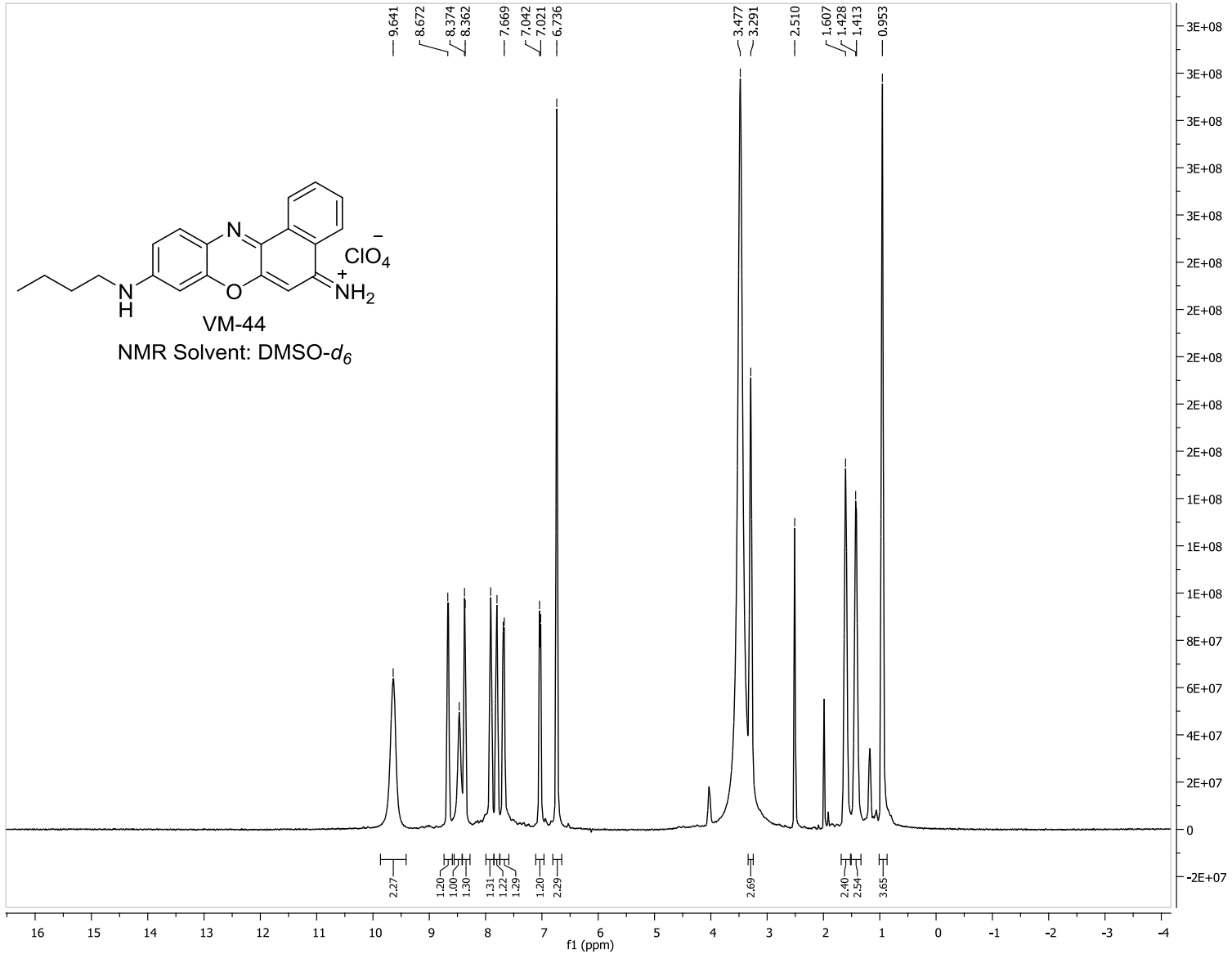
9.641
8.672
8.374
8.362
7.669
7.042
7.021
6.736
3.477
3.291
2.510
1.607
1.428
1.413
0.953
ClO4
NH2
N
H
O
VM-44
NMR Solvent: DMSO-d6
2.27
1.20
1.00
1.30
1.31
1.22
1.29
1.20
2.29
2.69
2.40
2.54
3.65
f1 (ppm)

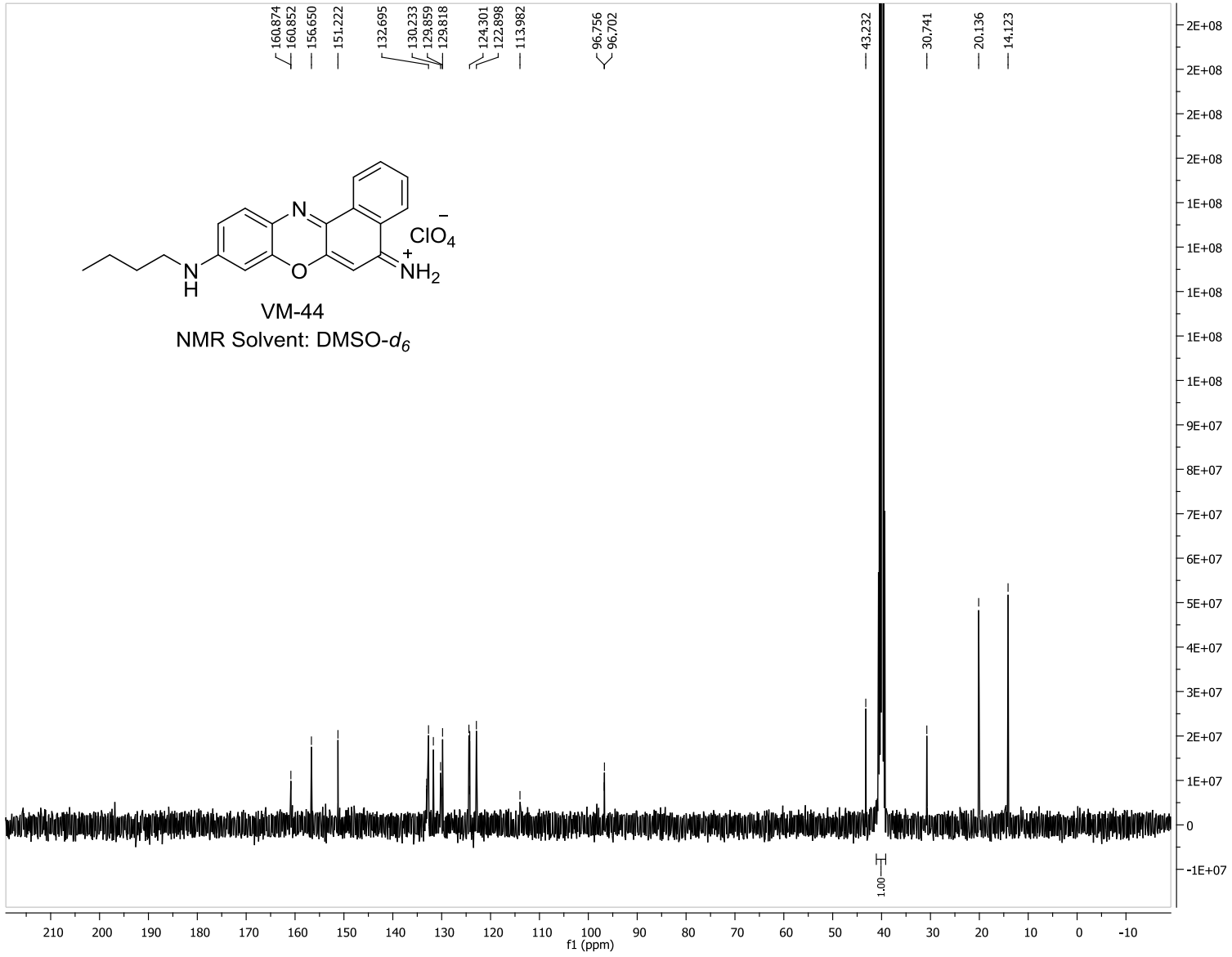
160.874
160.852
156.650
151.222
132.695
130.233
129.859
129.818
124.301
122.898
113.982
96.756
96.702
43.232
30.741
20.136
14.123
N
O
N
H
ClO4
NH2
VM-44
NMR Solvent: DMSO-d6
1.00
f1 (ppm)

VM_44_ESIPOS_HENARY_05202015 #178-184 RT: 2.49-2.57 AV: 7 NL: 1.68E9
T: FTMS + p ESI Full ms [100.00-1000.00]

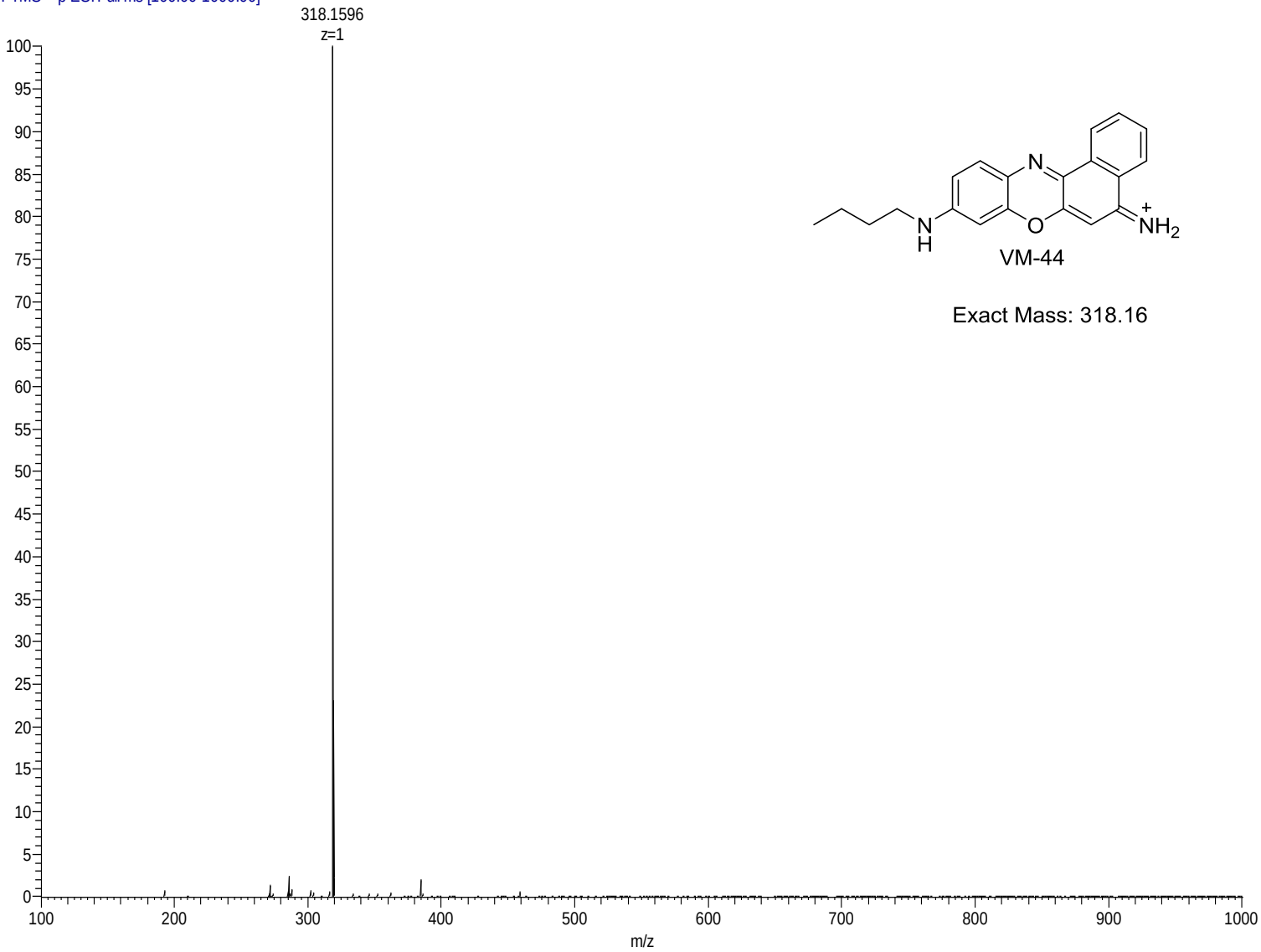

VM-44

Exact Mass: 318.16

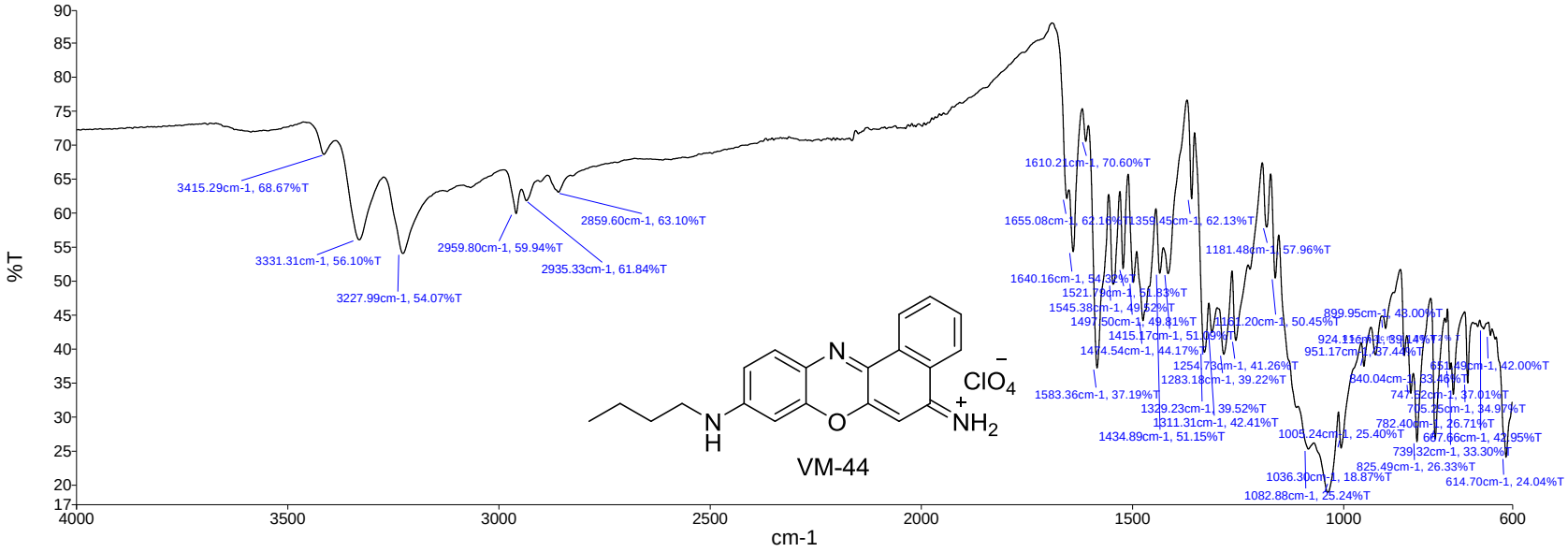
%T
cm-1
3415.29cm-1, 68.67%T
3331.31cm-1, 56.10%T
3227.99cm-1, 54.07%T
2959.80cm-1, 59.94%T
2935.33cm-1, 61.84%T
2859.60cm-1, 63.10%T
1610.21cm-1, 70.60%T
1655.08cm-1, 62.18%T
1640.16cm-1, 54.32%T
1521.79cm-1, 51.83%T
1545.38cm-1, 49.52%T
1497.50cm-1, 49.81%T
1415.17cm-1, 51.09%T
1454.54cm-1, 44.17%T
1583.36cm-1, 37.19%T
1434.89cm-1, 51.15%T
1329.23cm-1, 39.52%T
1311.31cm-1, 42.41%T
1283.18cm-1, 39.22%T
1254.73cm-1, 41.26%T
1359.45cm-1, 62.13%T
1181.48cm-1, 57.96%T
1181.20cm-1, 50.45%T
1005.24cm-1, 25.40%T
1036.30cm-1, 18.87%T
1082.88cm-1, 25.24%T
899.95cm-1, 43.00%T
951.17cm-1, 37.44%T
840.04cm-1, 33.46%T
747.52cm-1, 37.01%T
705.25cm-1, 34.97%T
782.40cm-1, 26.71%T
739.32cm-1, 33.30%T
825.49cm-1, 26.33%T
651.49cm-1, 42.00%T
607.66cm-1, 42.95%T
614.70cm-1, 24.04%T
VM-44

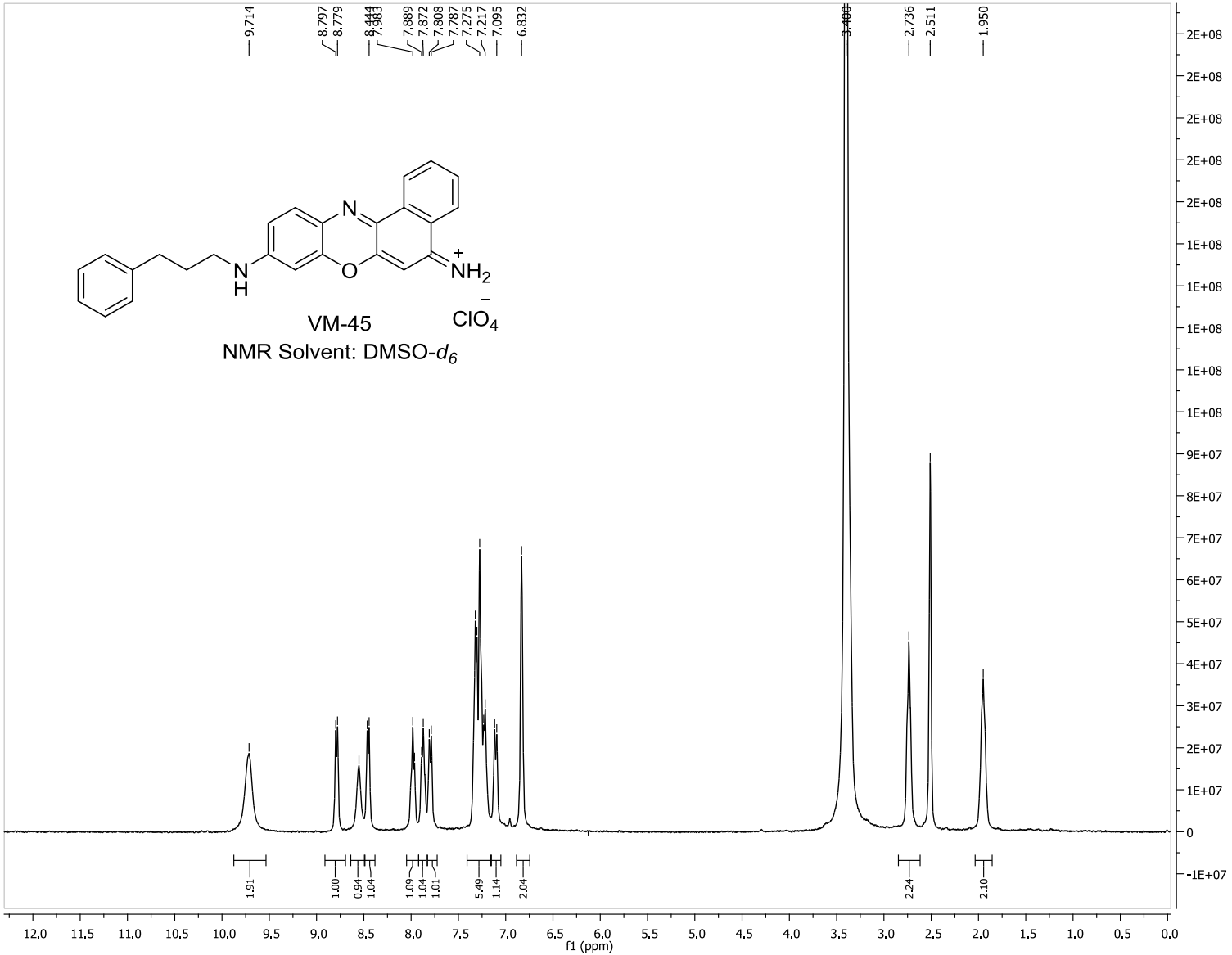
9.714
8.797
8.779
8.444
7.983
7.889
7.872
7.808
7.787
7.275
7.217
7.095
6.832
3.400
2.736
2.511
1.950
N
O
N
H
+
NH2
VM-45
ClO4
NMR Solvent: DMSO-d6
1.91
1.00
0.94
1.04
1.09
1.04
1.01
5.49
1.14
2.04
2.24
2.10
f1 (ppm)

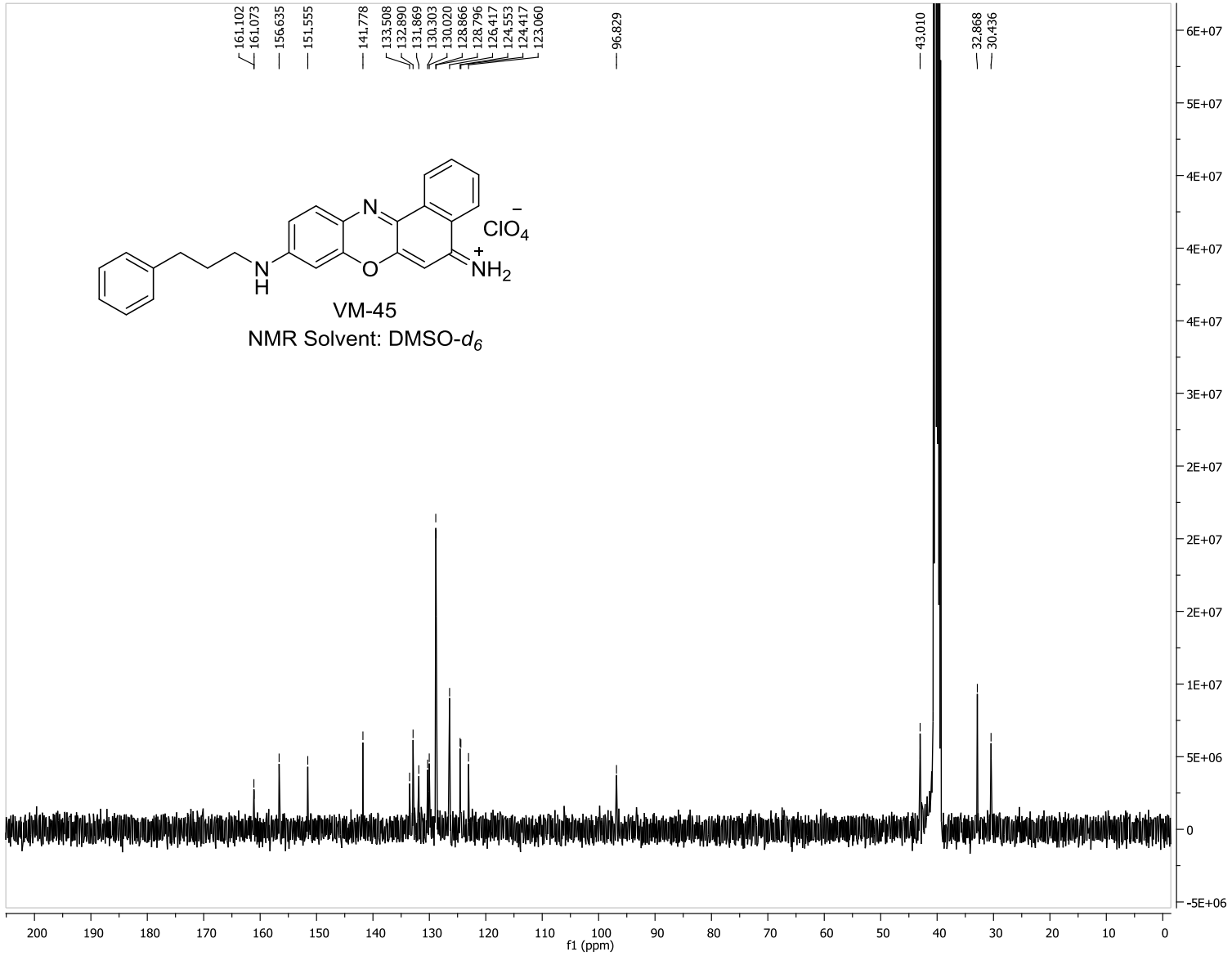
161.102
161.073
156.635
151.555
141.778
133.508
132.890
131.869
130.303
130.020
128.866
128.796
126.417
124.553
124.417
123.060
96.829
43.010
32.868
30.436
N
H
O
N
ClO4
NH2
VM-45
NMR Solvent: DMSO-d6
6E+07
5E+07
4E+07
4E+07
4E+07
3E+07
2E+07
2E+07
2E+07
1E+07
5E+06
0
-5E+06
200
190
180
170
160
150
140
130
120
110
100
90
80
70
60
50
40
30
20
10
0
f1 (ppm)

VM_45_ESIPOS_HENARY_05202015 #216-225 RT: 3.03-3.16 AV: 10 NL: 1.01E9
T: FTMS + p ESI Full ms [100.00-1000.00]

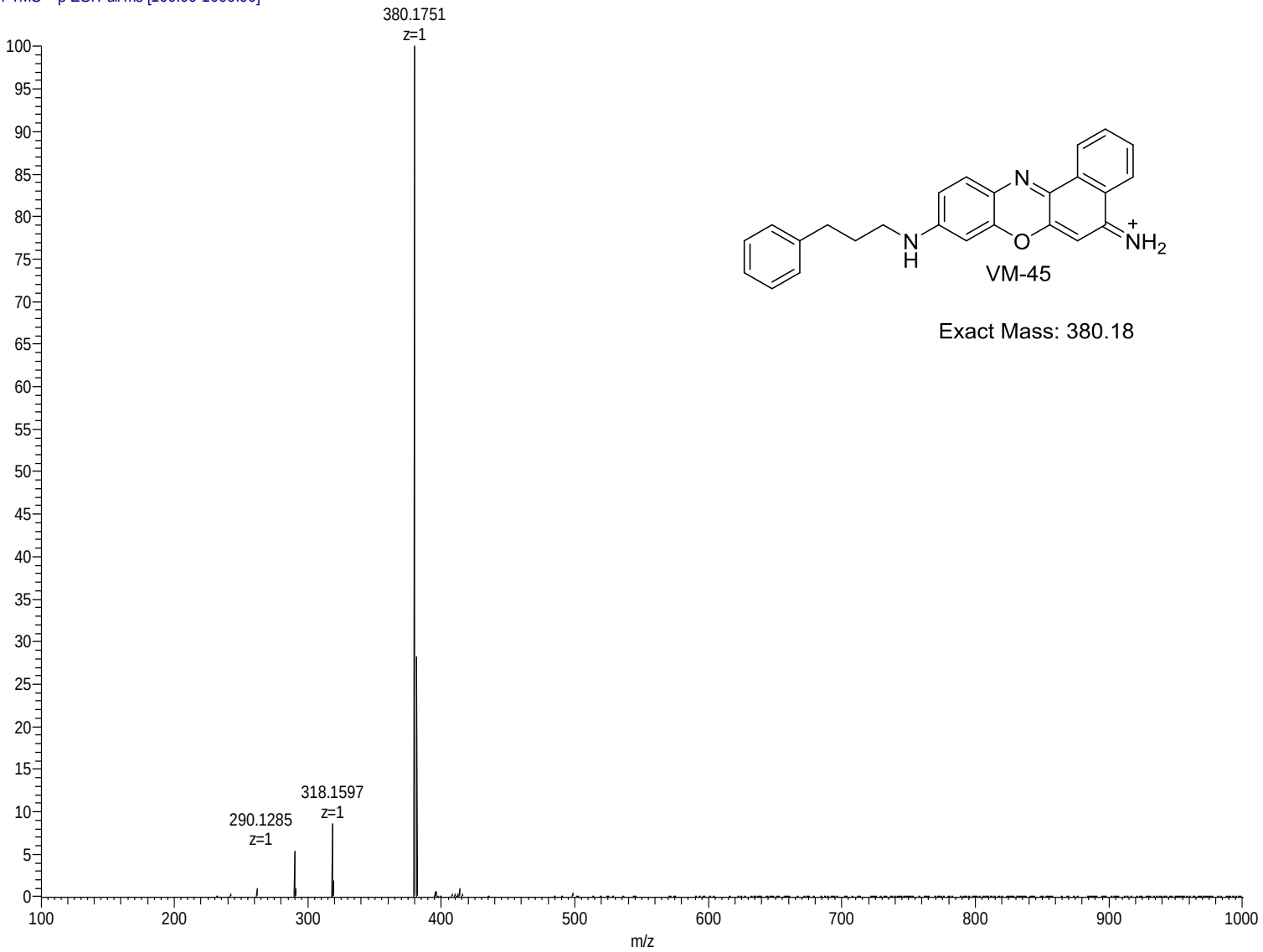

VM-45

Exact Mass: 380.18